

# **GANDOLF Thunderstorm Warning Project**

**Technical Report  
W103**

# **GANDOLF Thunderstorm Warning Project**

Technicla Report W103

C E Pierce and P J Hardaker

Research Contractor:

The Radar R&D Projects Team, The Met. Office

**Further copies of this report are available from:  
Environment Agency R&D Dissemination Centre, c/o  
WRc, Frankland Road, Swindon, Wilts SN5 8YF**



**tel: 01793-865000 fax: 01793-514562 e-mail: [publications@wrcplc.co.uk](mailto:publications@wrcplc.co.uk)**



**Publishing Organisation:**

Environment Agency  
Rio House  
Waterside Drive  
Aztec West  
Almondsbury  
Bristol BS32 4UD

Tel: 01454 624400

Fax: 01454 624409

ISBN:TH-12/97-B-BAFP

© Environment Agency 1997

All rights reserved. No part of this document may be reproduced, stored in a retrieval system, or transmitted, in any form or by any means, electronic, mechanical, photocopying, recording or otherwise without the prior permission of the Environment Agency.

The views expressed in this document are not necessarily those of the Environment Agency. Its officers, servant or agents accept no liability whatsoever for any loss or damage arising from the interpretation or use of the information, or reliance upon views contained herein.

**Dissemination status**

Internal: Released to Regions  
External: Released to the Public Domain

**Statement of use**

This Technical Report summarises the work undertaken over the duration of Project 510 from April 1994 to completion in April 1997. Recipients of the report are to pass comments to the Environment Agency Project Manager.

**Research contractor**

This document was produced under R&D Project 510 by:

Radar R&D Projects Team  
The Met. Office  
London Road  
Bracknell  
Berkshire RG12 2SZ

Tel: 01344 856640 Fax: 01344 854024

**Environment Agency Project Leader**

The Environment Agency's Project Leader for R&D Project 510 was:  
Regional Flood Warning Manager, Thames Region.

Contact address: Flood Warning Centre, The Grange, 97 Crossbrook Street, Waltham Cross,  
HERTS, EN8 8HE. Tel. 01992 645000.

**Amendments**

Any corrections or proposed amendments to this manual should be made through the regional Agency representative on the Water Resources National Abstraction Licensing Group.

R&D Technical Report W103

<b>CONTENTS</b>	<b>Page</b>
<b>LIST OF TABLES</b>	<b>iv</b>
<b>LIST OF FIGURES</b>	<b>iv</b>
<b>GLOSSARY OF TERMS</b>	<b>viii</b>
<b>EXECUTIVE SUMMARY</b>	<b>x</b>
<b>KEY WORDS</b>	<b>xi</b>
<b>1. INTRODUCTION AND BACKGROUND</b>	<b>1</b>
<b>2. OBSERVING AND FORECASTING CONVECTION</b>	<b>5</b>
2.1 Initiation of convection	5
2.2 Use of instability indices derived from radiosonde and numerical model data	5
2.3 Use of satellite data	6
2.4 Use of radar data	6
2.5 Use of extrapolation forecasts	7
2.6 Use of Numerical Weather Prediction (NWP) models	8
2.7 Use of conceptual models	8
2.8 Summary comments	9
<b>3. A DESCRIPTION OF THE GANDOLF SYSTEM</b>	<b>11</b>
3.1 Introduction	11
3.2 A prototype system	11
3.2.1 Overview	11
3.2.2 Level 0: Operator	11
3.2.3 Level 1: Monitor	12
3.2.4 Level 2: Action	12
3.2.5 Level 3: Alert	13
3.2.6 The control panel	13
3.3 Data	14
3.3.1 Overview	14
3.3.2 Data requirements	14
3.3.3 Data acquisition	15
3.3.4 Data correction	16
3.3.5 Data formats	16
3.4 Precipitation forecasts	17
3.4.1 Overview	17
3.4.2 Extrapolation forecasts	17
3.4.3 The Object-Oriented Model	18

	Page
3.4.3.1 The conceptual model of convection	18
3.4.3.2 Running the OOM	18
3.4.3.3 OOM precipitation forecasts	18
3.5 The diagnosis of non-frontal convection	19
3.5.1 Overview	19
3.5.2 Rainfall radar-based precipitation indices	20
3.5.3 Rainfall radar and satellite CTT difference images	20
3.5.4 Rainfall radar and satellite CTT cross correlation vectors	21
3.5.5 Neural network cloud classification	21
3.5.6 MM diagnostic fields	22
3.5.6.1 Convectively Available Potential Energy	22
3.5.6.2 Vorticity	23
3.5.6.3 Convergence	23
3.5.7 Operationally implemented convection diagnostics	23
3.6 Estimation of forecast reliability	24
3.6.1 Overview	24
3.6.2 Cross correlation vectors	24
3.6.3 Helicity ( $H_R$ )	24
3.6.4 Lagrangian decorrelation time, $T_L$	25
3.6.5 Real time model validation statistics	29
3.6.6 Operationally implemented guidance on model performance	29
3.7 Warnings of heavy precipitation	30
3.7.1 Overview	30
3.7.2 Determination of <i>alert status</i>	30
3.7.3 Generation of Warning Messages	31
3.8 Transmissions to Waltham Cross Flood Warning Centre	31
3.8.1 Overview	31
3.8.2 Transmission formats	31
3.8.3 Transmission times	32
<b>4. ASSESSMENT OF SYSTEM PERFORMANCE</b>	<b>33</b>
4.1 Overview of the summer trials	33
4.2 Operational performance of the GANDOLF system	33
4.3 Performance of the WLS	34
4.3.1 Validation of MM precipitation forecasts	34
4.4 Comparative performance of the OOM, LFM, and Nimrod	35
4.4.1 Overview	35
4.4.2 Precipitation forecast validation statistics	36
4.4.3 River catchments used for model validation	39
4.5 OOM, Nimrod, and LFM case studies	40
4.5.1 Overview	40
4.5.2 Summer 1994	40
4.5.2.1 Overview	40
4.5.2.2 Mesoscale Convective System (MCS): 24 June 1994	40
4.5.2.3 Disorganised convection: 10–11 August 1994	41

	Page
4.5.3 Summer 1995	44
4.5.3.1 Overview	44
4.5.4 Summer 1996	44
4.5.4.1 Overview	44
4.5.4.2 Strong convection with strong steering level winds: 23 July 1996	45
4.5.4.3 Strong convection with light steering level winds: 25 August 1996	45
4.5.4.4 Frontal precipitation with embedded convection: 7 June 1996	46
4.5.4.5 All cases of disorganised, non-frontal convection	47
<b>5. SUMMARY AND CONCLUSIONS</b>	<b>51</b>
<b>6. RECOMMENDATIONS</b>	<b>57</b>
<b>7. OPERATIONAL DEVELOPMENT</b>	<b>59</b>
7.1 Standalone mode	59
7.2 Integrated mode	59
<b>8. ACKNOWLEDGEMENTS</b>	<b>61</b>
<b>9. REFERENCES</b>	<b>63</b>
 <b>APPENDICES</b>	
<b>APPENDIX A: THE OBJECT-ORIENTED MODEL</b>	<b>116</b>
A.1 Convective clouds and precipitation	116
A.1.1 Cloud profiles	116
A.1.2 Precipitation profiles	116
A.1.3 Cell stage descriptions	117
A.1.4 Identification	118
A.2 Producing the forecast	120
A.2.1 Overview of forecast process	120
A.2.2 Growth and decay of cells	120
A.2.3 Initiation of new cells	121
<b>APPENDIX B: COMPARATIVE MODEL PERFORMANCE STATISTICS FOR ALL CASES OF NON-FRONTAL CONVECTION DURING THE SUMMER TRIAL OF 1996</b>	
B.1 Explanation of the layout of Tables B.1., B.2., and B.3.	129

## LIST OF TABLES

Page

Table 1.	A summary of instability indices used to infer the likelihood of convective activity.	5
Table 2.	Summary of the data inputs to the GANDOLF system.	15
Table 3.	Contingency table for the WLS <i>alert status</i> .	30
Table 4.	The performance of the Mesoscale Model in forecasting frontal and convective precipitation as a function of lead time (based upon analysis of 114 forecasts).	35
Table 5.	Contingency table for CSI, HR, FAR	36
Table 6.	Error Component Analysis for a range of hypothetical relationships between observed and predicted precipitation fields.	38
Table 7.	River sub-catchments in the Agency's Thames region used for the purposes of OOM validation.	39
Table 8.	OOM forecast errors as a function of lead time on 10–11 August 1994.	42
Table 9.	Days when convective precipitation fell in the Agency's Thames Region.	45
Table A.1.	Values of main attributes used for classifying cell stage.	123
Table B.1.	LFM performance statistics	135
Table B.2.	Nimrod performance statistics	143
Table B.3.	OOM performance statistics	151

## LIST OF FIGURES

Figure 1	The prototype GANDOLF system	67
Figure 2	The GANDOLF control panel	68
Figure 3	An outline of the GANDOLF radar correction scheme (if the data are not processed by Nimrod).	69
Figure 4	Time series of radar images on 24 June 1994 (1745 GMT to 1900 GMT) and parameters derived from them over a rectangular box centred on London. The rapid changes within the box in rainfall area, mean intensity, area average rainfall and maximum rainfall are shown.	70
Figure 5	Variation with time of area averaged rainfall over the rectangular area shown in Figure 4 compared with the modelled hourly accumulated rainfall normalised with respect to the total number of model grid points for a PRE-STORM MCS reported by Tao <i>et al.</i> (1993).	71
Figure 6	One hour radar echo difference field for 1745-1845 GMT, 24 June 1994.	72
Figure 7	One hour radar echo difference field for 1900-1800 GMT, 31 August 1994.	73
Figure 8	Variation of cloud height on 24 June 1994 over the Channel, and for thunderstorms observed in north-east Colorado (Lee <i>et al.</i> , 1991) and Alberta (Chisholm and Renick, 1972).	74
Figure 9	Radar difference field for 2000-1945 GMT, 24 June 1994, showing storm motion vectors.	75
Figure 10	A Neural Network cloud classification showing four classes: clear (blue), dynamic (green), shallow convection (yellow) and deep convection (red).	76

		Page
Figure 11	Lagrangian time autocorrelation functions: frontal cases.	77
Figure 12	Lagrangian time autocorrelation functions: convective cases.	78
Figure 13	Lagrangian decorrelation time ( $T_L$ ) versus CAPE.	79
Figure 14	Lagrangian decorrelation time ( $T_L$ ) versus modified Richardson Number( $CAPE/H_R$ ).	80
Figure 15	Least squares regression of Lagrangian decorrelation time ( $T_L$ ) and Helicity ( $H_R$ ) using both UK data (Rippon <i>et al.</i> , 1995) and Canadian data (Zawadski <i>et al.</i> , 1994).	81
Figure 16	Contour plot of forecast Lagrangian Decorrelation Time ( $T_L$ ) in minutes, 24 June 1994, DT 0600 GMT, VT 1800 GMT.	82
Figure 17	Contour plot of forecast near surface CAPE, 24 June 1994, DT 0600 GMT, VT 1800 GMT.	83
Figure 18	Contour plot of forecast Helicity field for 24 June 1994, DT 0600 GMT, VT 1800 GMT.	84
Figure 19	Critical Success Index (CSI) expressed as a function of model DT and lead time (T+1, T+2, and T+3 hours) on 24 June 1994: a comparison of the performance of FRONTIERS and the OOM.	85
Figure 20	OOM forecast validation: precipitation forecasts for Towncroft Lane, Bromley South and Elmers End Road, 10 August 1994, 2030 GMT–2100 GMT.	86
Figure 21	OOM forecast validation: precipitation forecasts for Langley Road, West Barnes and Wimbledon Common, 10 August 1994, 2000 GMT–2030 GMT.	87
Figure 22	OOM forecast validation: precipitation forecasts for Colindeep Lane, Edmonton Green and Silver Street, 10 August 1994, 2130 GMT–2200 GMT.	88
Figure 23	OOM forecast validation: precipitation forecasts for Towncroft Lane, Bromley South and Elmers End Road, 11 August 1994, 0800 GMT–0900 GMT.	89
Figure 24	OOM forecast mean errors, standard deviation of errors and RMSE for all high rain events, 10-11 August 1994.	90
Figure 25	Surface analysis for 0000 GMT, 23 July 1996.	91
Figure 26(a)	Chenies 2 km surface beam image sequence for the period 0300 GMT to 0420 GMT.	92
Figure 26(b)	Chenies 2 km surface beam image sequence for the period 0430 GMT to 0550 GMT.	93
Figure 26(c)	Chenies 2 km surface beam image sequence for the period 0600 GMT to 0720 GMT.	94
Figure 27(a)	OOM precipitation forecasts for DT 0400 GMT, VT 0410 GMT to 0530 GMT, 23 July 1996.	95
Figure 27(b)	OOM precipitation forecasts for DT 0400 GMT, VT 0540 GMT to 0700 GMT, 23 July 1996.	96
Figure 28	Nimrod precipitation forecast sequence for DT 0400 GMT, 23 July 1996.	97
Figure 29	Surface analysis for 0000 GMT, 25 August 1996.	98

Figure 30(a)	Chenies 2 km surface beam image sequence for the period 1630 GMT to 1750 GMT, 25 August 1996.	99
Figure 30(b)	Chenies 2 km surface beam image sequence for the period 1800 GMT to 1920 GMT, 25 August 1996.	100
Figure 30(c)	Chenies 2 km surface beam image sequence for the period 1930 GMT to 2050 GMT, 25 August 1996.	101
Figure 31(a)	OOM precipitation forecasts for DT 1700 GMT, VT 1710 GMT to 1830 GMT, 25 August 1996.	102
Figure 31(b)	OOM precipitation forecasts for DT 1700 GMT, VT 1840 GMT to 2000 GMT, 25 August 1996.	103
Figure 32(a)	OOM cell forecasts for DT 1700 GMT, VT 1710 GMT to 1830 GMT, 25 August 1996.	104
Figure 32(b)	OOM cell forecasts for DT 1700 GMT, VT 1840 GMT to 2000 GMT, 25 August 1996.	105
Figure 33	Nimrod precipitation forecast sequence for DT 1700 GMT, 25 August 1996.	106
Figure 34	Surface analysis for 0000 GMT, 7 June 1996.	107
Figure 35(a)	Chenies 2 km surface beam image sequence for the period 1630 GMT to 1750 GMT, 7 June 1996.	108
Figure 35(b)	Chenies 2 km surface beam image sequence for the period 1800 GMT to 1920 GMT, 7 June 1996.	109
Figure 35(c)	Chenies 2 km surface beam image sequence for the period 1930 GMT to 2050 GMT, 7 June 1996.	110
Figure 36(a)	OOM cell forecasts for DT 1650 GMT, VT 1700 GMT to 1820 GMT, 7 June 1996.	111
Figure 36(b)	OOM cell forecasts for DT 1650 GMT, VT 1830 GMT to 1950 GMT, 7 June 1996.	112
Figure 37(a)	OOM precipitation forecasts for DT 1650 GMT, VT 1700 GMT to 1820 GMT, 7 June 1996.	113
Figure 37(b)	OOM precipitation forecasts for DT 1650 GMT, VT 1830 GMT to 1950 GMT, 7 June 1996.	114
Figure 38	Nimrod precipitation forecast sequence for DT 1700 GMT, 7 June 1996.	115
Figure 39	Comparative performance of 15 minute accumulation forecasts for the OOM, LFM and Nimrod: Catchment CSI as a function of catchment and forecast lead time.	116
Figure 40	Comparative performance of 15 minute accumulation forecasts for the OOM, LFM and Nimrod: Catchment HR as a function of catchment and forecast lead time.	117
Figure 41	Comparative performance of 15 minute accumulation forecasts for the OOM, LFM and Nimrod: Catchment FAR as a function of catchment and forecast lead time.	118
Figure 42	Comparative performance of 15 minute accumulation forecasts for the OOM, LFM and Nimrod: (Forecast - observed) catchment 15 minute accumulation as a function of catchment and forecast lead time.	119

- Figure 43 Comparative performance of 15 minute accumulation forecasts for the OOM, LFM and Nimrod: MSE of 15 minute accumulation as a function of catchment and forecast lead time. 120
- Figure A.1. Theoretical vertical profile of adiabatic cloud density, without any mixing of ambient air, for a cloud base at 1 km with a temperature of 10°C in an ICAO standard atmosphere environment. The density is plotted in  $\text{g m}^{-3}$  and the ordinates give height in kilometres and temperatures in degrees C. 128
- Figure A.2. Idealised vertical radar reflectivity profiles expressed in  $\text{mm h}^{-1}$  for the cell stages identified in the OOM. CB = cloud base, ML = mid-cloud level, CT = cloud top. The solid line is the profile for developing (d) cells, dotted for young mature (m), dashed for fully mature (M), dash-dotted for early dissipating (E), and dash-double-dotted for dissipating (D). 129
- Figure A.3. Schematic showing the four elevations of the beams available in the Chenies radar. Beam elevations are 0.5, 1.5, 2.5 and 4.0 degrees. The mid-point of each beam is shown as a dashed line and the numbers 1 to 10 indicate levels at which radar rainfall data are determined. 130
- Figure A.4. Diagram showing the change of cell stage at each 10 minute time step of the OOM. Each row of boxes represents a cell stage with each box indicating a possible value for the current cell potential (see text). The arrows show the allowed changes in cell stage. The bold lines indicate when new (daughter) cells are created at the end of a time step. 131
- Figure A.5. Schematic diagram illustrating how the downdraught is modelled in the OOM. The slope of the line AB is estimated by subtracting the cell velocity (steering level wind)  $V_a$  from the outflow velocity at level B,  $V_b$ , and then multiplying this relative velocity by the age of the cell to give the distance L. Level B is at cloud top - 1/3 cloud depth. The downdraught is displaced from the point X directly beneath the middle of the cloud X' by the distance  $X + L$  in the direction pointed to by the shear vector  $V_b - V_a$ . 132
- Figure A.6. Analysis of convective cells at 1800 GMT 24 June 94 using the OOM. A cross indicates a cell in stage d (developing), asterisk - stage m (young mature), triangle - stage M (fully mature), diamond - stage E (early dissipating), square - stage D (dissipating). The big squares are an arbitrary grid used for reference. 133



## GLOSSARY OF TERMS

a,b,c,d	Elements of the contingency table defined in Section 4.4.2
Accum.	Accumulation
ACF	Autocorrelation function ('^' identifies normalised ACF)
ATD	Arrival-Time-Difference
BT	British Telecommunications
C	Storm velocity
CAPE	Convectively Available Potential Energy
CDN	Central Data Network
CFL	Level of Free Convection
CSI	Critical Success Index
CTH	Cloud Top Height
CTT	Cloud Top Temperature
d	Developing (can have cell potential as subscript)
D	Dissipating (can have cell potential as subscript)
DT	Data Time
DWS	Daily Weather Summary
E	Early dissipating (can have cell potential as subscript)
E <sub>L</sub>	Lagrangian persistence error
EA	Environment Agency
ECA	Error Component Analysis
EL	Equilibrium Level
EOT	End Of Transmission
FAR	False Alarm Rate
FRONTIERS	Forecasting Rain Optimised using New Techniques of Interactively Enhanced Radar and Satellite data
FWC	Flood Warning Centre
GANDOLF	Generating Advanced Nowcasts for Deployment in Operational Land-based Flood forecasts
GUI	Graphical User Interface
h	Height
HC	Hand and Conway (1995)
HP	Hewlett-Packard
H <sub>R</sub>	Helicity
HR	Hit Rate
ICAO	International Civil Aviation Authority
IR	Infrared
IRR	Instantaneous Rainfall Rate
l,e	Lagrangian and Eulerian ACFs respectively
L	Length of horizontal displacement between Levels A and B in the convective cloud model
LFM	Local Forecast Model
m	Young mature (can have cell potential as subscript)
m,c	gradient and intercept in the linear relationship $y = mx + c$
M	Mature (can have cell potential as subscript)
MCS	Mesoscale Convective System
MM	Mesoscale Model

MSE	Mean Square Error
NNCC	Neural Network Cloud Classifier
NWP	Numerical Weather prediction
OOM	Object-Oriented Model
p	Pressure
PID	Process Identification Number
POD	Probability Of Detection
$r_{x,y}$	Pearson's product-moment correlation coefficient
R	Rainfall rate
$R_c$	Climatological rainfall rate
$R_d$	Dry air gas constant
RMS	Root Mean Square
S	Spatial area of a rainfall event
$S_{x,y}$	Standard deviation of distributions x and y
SAM	System Administrator
SOT	Start Of Transmission
t	Time
T	Time interval of the event
$T_L$	Lagrangian decorrelation time
$T_*$	Temperature at '*' hPa level (this may be dewpoint 'd')
$T_{vp}, T_{ve}$	Virtual temperature of air parcel and environment respectively
$U_b$	Error components of the difference in means of the forecast and observed events
$U_c$	Error components of covariance of the forecast and observed events
$U_d$	The relative bias of the correlation
$U_r$	The non-linear error in the correlation
$U_v$	Error components of the difference in standard deviations of the forecast and observed events
V	Velocity vector
$V_a$	Cell velocity (steering level wind)
$V_b$	Outflow velocity at Level B within the convective cloud model
$V_H$	Environmental horizontal wind vector
VT	Validation Time
$W_H$	Horizontal vorticity
WLS	Warning Level System
WM	Warning Message
x,y	Position variables; also used to represent the distributions of observed and forecast variables in the calculation of the MSE statistics
$z_{1000-700}$	Atmospheric thickness from 1000 to 700 hPa in decametres
$\alpha, \beta$	Horizontal spatial lags
$\alpha_0, \beta_0$	Horizontal lags that maximise correlation
$\Delta T$	Time interval
$\theta_{w900}$	Wet bulb potential temperature at 900 hPa
$\tau$	Time lag

## EXECUTIVE SUMMARY

This technical report summarises the findings of the GANDOLF Thunderstorm Warning Project – a joint Environment Agency–Met. Office, R&D programme, established to explore ways of improving the short range prediction (up to three hours ahead) of heavy convective precipitation, initially in the Agency’s Thames Region. Section 1 describes the background to the Project. Section 2 examines current methods for observing and forecasting convection. The two following sections describe the research and development work undertaken by the Met. Office over the three year duration of the study. Sections 5 to 7 present the Project results, conclusions and recommendations respectively. Two accompanying final reports, the Project Operations Manual and the Project Record provide additional information on the operation of the prototype GANDOLF nowcasting system and associated software and data archives.

The aims of the Project were two-fold: firstly, to validate an object-oriented (OO) conceptual model of convection devised to improve the prediction of heavy convective precipitation; and secondly, to provide the Thames region of the Agency with objective guidance on the most appropriate choice of radar-based precipitation forecast in a range of weather situations. It was hoped that the work undertaken in these two areas would improve the spatial accuracy and timeliness of flood warnings during periods of non-frontal convection. With this latter goal in mind, the approach adopted in the Project was to develop and trial an automated, convective precipitation nowcasting system – GANDOLF – capable of fulfilling the two aims outlined above.

Existing precipitation forecasts employed for flood prediction by Thames Region come from two sources: the Met. Office’s Nimrod system (the automated replacement for FRONTIERS), and the Institute of Hydrology’s Local Forecast Model (LFM). The associated forecast algorithms utilise linear extrapolation techniques to generate a suite of forecast precipitation fields from an initial, observed field, the latter being derived from C-band radar reflectivity measurements. Whilst this approach has been shown to work satisfactorily for frontal precipitation, its applicability to convective precipitation is limited – the evolution of showery precipitation fields is often markedly non-linear. The object-oriented conceptual model (OOM) of convection developed in the Met. Office by Hand and Conway (1995) was designed specifically to address this problem. It forms the hub of the GANDOLF nowcasting system. Peripheral system components were developed to identify and distinguish airmass convection and frontal weather systems, and to measure and predict the relative performance of object-oriented and extrapolation-based precipitation forecast algorithms.

The performance of 15 minute precipitation accumulation forecasts generated by the OOM, Nimrod and the LFM was assessed over two six month periods spanning the months May to October in 1995 and 1996 (see Section 4). The forecast validation area was restricted to 19 flood prone river sub-catchments in Thames region. When convective precipitation was observed to fall somewhere within a 76 km radius of the Chenies radar, a suite of error statistics were computed for each of the three models over the 19 sub-catchments. Forecast data were then amalgamated to produce average performance statistics over all catchments on an event by event basis, and over all events. The conclusions regarding comparative performance drawn in Sections 4 and 5 of this report are based upon all catchments and all events, since model performance on catchment by catchment and event by event bases proved highly variable.

In terms of forecast accuracy and its implications for flood prediction, the two most important statistical measures of performance are bias and Mean Squared Error. Smoothed over all catchments and all events these statistics were somewhat ambiguous. In terms of MSE, it would appear that Nimrod forecasts are generally more skilful than those of the OOM or LFM at lead times under 75 minutes. However, a significant proportion of this additional skill can be attributed to the effects of resolution: Nimrod forecasts have a 5 km as opposed to 2 km resolution. This tends to remove the largest errors from the sum of the squared forecast errors, hence the lower MSE. The horizontal length scale of individual convective storms (~ 1 km for developing cumulus) favours the use of 2 km rather than 5 km resolution radar data in the quantitative nowcasting of convective precipitation. Since the performance of the LFM was shown to be significantly worse than that of the OOM and Nimrod, chiefly as a result of forecast advection errors, these findings would seem to favour use of the OOM.

Forecast bias statistics show Nimrod and the LFM to have under predicted 15 minute accumulations at all lead times. By contrast, the OOM generally over predicts accumulations at lead times under 75 minutes. Thereafter the bias is negative. In terms of flood prediction, a positive bias may be preferable to a negative bias, since the impact of an unpredicted flood event, is likely to be worse than a false alarm. Furthermore, the loss of information on locally higher rainfall accumulations arising from smoothing of the observed precipitation field (the maximum resolution of Chenies radar imagery is currently 2 km) may be compensated for, at least in part, by a positive bias in the resultant precipitation forecasts.

Considered in isolation, the statistical measures of performance described above would suggest favouring the use of the OOM or Nimrod in convective situations. However, when considered in conjunction with the visual evidence afforded by numerous case studies (see Section 4), it is resolved that, overall, the OOM offers better forecast guidance during episodes of non-frontal, convective precipitation than either Nimrod or the LFM.

Section 7 concludes that the 1995 and 1996 summer trials of the GANDOLF system were largely successful. They have shown the system to be capable of 24 hour, standalone operation. It is recommended that the future of GANDOLF be reviewed following a third summer trial of the system, and subsequent independent evaluation by the Agency. There are two possible scenarios regarding future operational implementation, should this third trial confirm the findings summarised here. The most obvious solution would be to bring the existing system into full operational use with minimal modification. The alternative is to incorporate the various system components into an upgraded version of Nimrod. This latter option has the advantage of maintaining a single system for Met. Office quantitative forecast provision to the Agency.

## **KEY WORDS**

Rainfall radar; Precipitation forecasting; Convection; Thunderstorm warning; GANDOLF



# 1. INTRODUCTION AND BACKGROUND

The prediction of convective storms and other, related, severe local weather phenomena has long posed difficulties for the weather forecaster. Whilst the mechanisms underpinning the release of convective instability, and the development of convective precipitation are now reasonably well understood in quantitative terms, reliable, deterministic predictions of convective cell initiation and subsequent behaviour have remained largely beyond the capabilities of meteorologists.

This state of affairs might appear somewhat paradoxical. However, one must consider the important fact that the lowest few kilometres of the atmosphere are frequently in a finely balanced state of conditional static instability. Consequently, the smallest of local variations in the physical condition of the atmospheric boundary layer, or that of the underlying Earth's surface, can trigger the release of substantial quantities of Convectively Available Potential Energy (CAPE) in a relatively short space of time.

For example, on showery days during the summer months, it is often observed that certain geographical locations (e.g. south facing hill slopes) are favoured over others for initiating convection. Once the latent CAPE in the atmosphere is released in these areas, the development of convective storms can be extremely rapid: the growth of a mature *cumulonimbus* from an apparently benign *cumulus* cloud can take as little as thirty minutes.

The precipitation accompanying these convective storms poses significant problems for flood forecasters. Whilst intensities often exceed  $10 \text{ mm hr}^{-1}$  (values of more than  $30 \text{ mm hr}^{-1}$  are not uncommon over periods of minutes), the spatial and temporal extents of the precipitation are typically very limited – a few square kilometres and about one hour. The difficulties entailed in providing timely flood warnings for such events are exacerbated in urbanised or semi-urbanised areas where the catchment characteristics give rise to very rapid rainfall-runoff responses.

This problem is of particular concern to the Thames Region of the Agency whose responsibilities for flood warning cover river catchments in the vicinity of London. In common with other regions of the Agency, Thames Region employs computer models of catchment water balance that make forecasts of river discharge, given predictions of precipitation accumulation. Herein lies the heart of the problem: obtaining accurate precipitation forecasts.

To date, Thames Region have employed various rainfall radar, extrapolation-based precipitation nowcasts for this purpose, for example, those produced by the FRONTIERS and Nimrod systems at the Met. Office. These have proven their worth in forecasting frontal precipitation, but have, at times, demonstrated serious deficiencies in their treatment of convective precipitation. Thus, results from several Agency–Met. Office collaborative studies (FOAG, 1992, 1993) led to the conclusion that the ability of FRONTIERS to “accurately forecast rainfall in ... convective events ... is generally poor”.

The temporal and spatial characteristics of convection pose rigorous demands on any would-be convective precipitation forecasting system. In the light of the preceding discussion, it is apparent that extrapolation-based predictions of convective precipitation are deficient in several respects. Firstly, they are generally of insufficient spatial and temporal resolution to

identify individual convective cells. Secondly, they are unable to simulate in a physically realistic fashion, the growth and decay of these cells.

The other routine source of precipitation forecasts issued by the Met. Office are Numerical Weather Prediction (NWP) models. Such models make deterministic forecasts of future physical states of the atmosphere using a set of fundamental equations called the Primitive Equations. Whilst NWP has markedly improved the accuracy of short and medium range weather forecasts during the last three decades, it has serious limitations with regard to the prediction of small scale weather phenomena.

NWP models such as the Met. Office's Unified Model, represent the atmosphere as a three dimensional lattice of grid points. The spacing of these grid points limits the scale of atmospheric disturbances that can be resolved explicitly. Even, the finest resolution, operational NWP models (e.g. the Met. Office's Mesoscale Model) cannot adequately represent disturbances with a horizontal length scale much less than 50 km, and are not designed to do so. Sub-grid scale phenomena like convection are treated in a statistical fashion using parameterization schemes. Such treatment is inadequate for the purposes of flood forecasting.

The need to find an alternative, yet objective approach to the prediction of convective rainfall became increasingly apparent in the late 1980s and early 1990s, following a number of serious floods caused by summer thunderstorms (e.g. 8 May 1988, 22 September 1992, 11 August 1994). This experience led the Agency and the Met. Office to establish a joint research and development programme to address the problem. Since its initiation in 1994, this Thunderstorm Warning Project has explored the predictive skills of an Object-Oriented conceptual Model (OOM) of convection (Hand and Conway, 1995).

With the advent of such a model, an additional problem has arisen for the Agency, namely, the selection of the most suitable forecast (extrapolation or OOM) in any given weather situation. Such a decision is not easily made, especially in the high pressure environment of the Flood Warning Centre (FWC), where time is limited. The choice of forecast must be based upon a full and reasoned evaluation of the prevailing weather conditions, and a knowledge of how well each forecast performs under those conditions.

For this reason, the approach adopted in the Thunderstorm Warning Project has been to deploy the OOM within an experimental, automated system called GANDOLF (Generating Advanced Nowcasts for the Deployment of Operational Land-based Flood forecasts). This system is capable of identifying and distinguishing frontal and convective precipitation, and of making an informed and objective decision as to which precipitation model should be used, given the prevailing weather conditions.

The aims of the Thunderstorm Warning Project have therefore been two fold:

- the validation of a model designed specifically to forecast non-frontal convective precipitation (the OOM);
- to provide informed and objective guidance as to which of a range precipitation forecasts (extrapolation or object-oriented) should be used in any given weather situation.

This final Technical Report for the Thunderstorm Warning Project presents the findings of the work undertaken in these two areas, together with exploratory research and development in other related areas.





## 2. OBSERVING AND FORECASTING CONVECTION

### 2.1 Initiation of convection

As pointed out by Doswell (1982, 1985) and others, there are two main mechanisms for the initiation of thunderstorms, namely, convective instability (meaning conditional or latent static instability in this instance), and mesoscale convergence leading to the release of potential instability. The latter may result from:

- sea-breeze convergence;
- convective outflow boundaries (e.g. colliding gust fronts);
- upslope flow or thermal effects on slopes;
- dryline convergence (only occurring in a limited number of locations with conditions similar to the southern USA) or other boundary layer convergence.

Whilst Doswell *et al.* (1996) describe an “ingredients-based method” for the prediction of convective activity, Collier and Lilley (1994) have summarised data analysis-based methods for forecasting convection. Some of these are discussed below.

### 2.2 Use of instability indices derived from radiosonde and numerical model data

A range of instability indices have been tested by Collier and Lilley (1994). These include the Boyden Index (Boyden, 1963), the K Index (George, 1960), the Rackliff Index (Rackliff, 1962) and the Convectively Available Potential Energy (CAPE). The first three indices employ indirect means to infer the extent of any latent static instability in the atmosphere. The last, CAPE, which is not strictly an index, affords a direct estimate of instability, and is commonly calculated from radiosonde ascents using a thermodynamic diagram such as the Tephigram.

Table 1 summarises how these instability indices are used to indicate the probability of convective activity. Single index-based forecasts of convection have been shown to be the most reliable (Collier and Lilley, 1994). However, it should be borne in mind that none of these methods attempt to account for the mechanisms which may facilitate or hinder the release of the instability they identify. Consequently, they should not be used in isolation to infer the probability of convection occurring.

**Table 1. A summary of instability indices used to infer the likelihood of convective activity.**

Index	Condition for convective activity
K	$T_{850} - T_{500} + T_{d850} - T_{700} + T_{d700} \geq 20$
Rackliff	$\theta_{w900} - T_{500} \geq 30$
Boyden	$z_{1000-700} - T_{700} - 200 \geq 94$
CAPE	+ve for free convection, -ve for forced convection

In Table 1,  $T$  denotes temperature, where the subscript identifies the pressure level in hecto-pascals (hPa); a 'd' denotes that the temperature is a dew-point value.  $\theta_{w900}$  is the parcel, wet-bulb potential temperature at 900 hPa, and  $z_{1000-700}$  is the thickness in decametres between the 1000 and 700 hPa.

### 2.3 Use of satellite data

Although observations from current, operational meteorological satellites cannot provide reliable estimates of atmospheric instability, they can be used to identify favourable convective precursor conditions (e.g. high near surface humidity), and also to monitor the severity and extent of any existing convective activity (e.g. from estimates of Cloud Top Temperature). Both geostationary and sun-synchronous satellite imagery have their uses in these respects.

For the purposes of monitoring the temporal changes in a convectively unstable atmosphere, the half-hourly or hourly, stationary image sequences supplied by geostationary satellites are most valuable. Both visible and infrared (IR) pictures can be utilised to monitor the behaviour of organised convective systems associated with mesoscale convergence (Purdom, 1982). Cloud Top Temperatures (CTTs) derived from IR data are particularly useful in this context, since they afford some indication of the severity of the convection.

The object-oriented convective precipitation model or OOM discussed in Section 3.4.3 employs Meteosat derived CTTs, in conjunction with Mesoscale Model 3-D temperature forecasts, to estimate convective cloud top heights (see Appendix A). Unfortunately, problems with parallax and poor resolution prevent accurate determination of CTTs for individual convective cells. A single temperature is derived for each satellite image pixel (about 7 km<sup>2</sup> at 50 °N in the case of Meteosat) and this will reflect not only the temperature of the cloud tops, but also that of the land surface in areas of cloud free air.

In addition to measuring the thermal properties of the atmosphere, satellite radiometers observing at slightly longer wavelengths than the thermal IR can return information on water vapour in the atmosphere. Observations in the split IR channels (wavelengths of 11 µm and 12 µm) may be used to estimate the humidity of the lower troposphere. Elevated, near surface concentrations of water vapour commonly precede the outbreak of convective showers. For example, in the south-east of England, summer thunderstorms are often associated with the so called Spanish Plume: a warm, humid (high wet-bulb potential temperature), low level air current originating over northern Spain.

### 2.4 Use of radar data

The ability of satellite imagery to identify the early stages of convective activity is severely limited by its temporal and spatial resolution. The time between the initiation of the first convective thermals and the development of a fully mature cumulo-nimbus may be as little as 30 minutes. Since current operational geostationary satellites can only supply visible and IR images on 30 minute or 60 minute cycles, they cannot hope to monitor the minute to minute changes in the extent and severity of convective activity. In addition, the spatial resolution of geostationary imagery is such that only quite extensive (a few square kilometres) areas of

cloud can be identified with any degree of certainty. Individual, immature cumulus clouds are unresolvable.

Here ground-based radar systems can demonstrate their worth. High powered radar may be used to recognise convective thermals in the boundary layer prior to the development of cloud and precipitation (see for example, Harrold and Browning, 1971). Once precipitation is falling, rainfall radar systems can be used to elucidate the three dimensional structure of precipitation rates. Such systems require the definition of reflectivity thresholds above which the back-scattered radar signal can be assumed to be almost entirely from hydrometeors. Knight and Miller (1993) suggest that the threshold for S-band radar (10 cm) is 10 dBZ, for C-band radar (5 cm) 0 dBZ and for X-band (3 cm) 10 dBZ.

The structure and temporal evolution of non-frontal convective precipitation fields are quite different to those of frontal precipitation. These differences can be elucidated in rainfall radar data with the aid of simple statistical measures such as precipitation area and area averaged rainfall rate. For example, the movement of a Mesoscale Convective System (MCS) into a given target area is characterised by a rapid rise in area average rainfall. This rise is typically much greater than that observed in association with frontal activity. The more common, disorganised, non-frontal convective precipitation can also distinguished from that of frontal origin in a similar fashion. In this case, the former tends to exhibit higher mean rainfall rates and smaller total precipitation areas.

## **2.5 Use of extrapolation forecasts**

Extrapolation techniques are widely used in the preparation of weather forecasts for up to six hours ahead (nowcasts). Underpinning this approach is the assumption that the macroscale features of a meteorological field, for example, precipitation, will be conserved in the near future. Thus, it should be possible to nowcast future states of the observed field by advecting it in the direction of its propagation.

Since the introduction of a C-band rainfall radar network in the UK such techniques have been employed by the Met. Office in semi (FRONTIERS) and fully (Nimrod) automated precipitation nowcasting systems. In the FRONTIERS system (recently replaced by Nimrod) the forecast scheme used cross-correlation vectors to advect contiguous areas of precipitation identified in the radar network rainfall analyses. At times when the advection directions or speeds were shown to be in error, the system allowed manual corrective action to be taken. In the currently operational Nimrod system, this is not permitted. Instead, the forecast scheme compares the accuracy of forecasts produced by a range of plausible advection vectors, derived from a combination of cross-correlation techniques, echo centroid tracking and Mesoscale Model wind forecasts. It then selects those extrapolation vectors which are likely to minimise the forecast error.

Collaborative validation studies of FRONTIERS by the Met. Office and the Agency have demonstrated problems with extrapolation-based nowcasts of convective precipitation (FOAG, 1992, 1993). In view of the temporal and spatial complexities of convection these findings are not at all surprising. The failings of FRONTIERS in this respect, and to a lesser extent, its successor Nimrod, can be attributed to two factors. First, and most fundamentally, the evolution of convective cells is highly non-linear, and any forecast scheme that relies purely upon advection of observations will rapidly lose skill. Secondly, the existing

spatial (5 km) and temporal resolutions (15 minutes) of the radar network data are inadequate for distinguishing the structure of individual, precipitating cells, or for monitoring their growth and decay.

The resolution deficiencies in the UK rainfall radar network are currently being addressed. However, it is likely to be some years before data of a resolution sufficient to deal with the problems of localised flood prediction and urban hydrology become available.

## **2.6 Use of Numerical Weather Prediction (NWP) models**

During the last three decades computer-based NWP models have greatly improved the accuracy of short and medium range weather forecasts. The Met. Office run a suite of such models collectively known as the Unified Model (UM). In these, the state of atmosphere is represented at discrete points in space. These points are arranged on a regular, three dimensional grid, and each *grid point* is deemed to be representative of the *parcel* of air surrounding it. Forecasts of future states of the atmosphere in each parcel are made by solving a set of partial differential equations at each grid point. These so-called Primitive equations comprehensively describe the dynamical and thermodynamical macroscale behaviour of the Earth's troposphere.

Model grid point spacing and forecast time step (the time interval between successive solutions of the Primitive equations) pose a limit on the temporal and spatial scales of atmospheric disturbances that can be resolved explicitly. Currently, the finest resolution, operational NWP models have a horizontal grid length of approximately 10 km and a forecast time step of about one minute. In the case of the Met. Office's Mesoscale Model (hereafter referred to as the MM), these attributes have the values 16.8 km and 90 seconds respectively. Typical horizontal length scales for disorganised convective turbulence range from a few metres to a few kilometres. Consequently, convection remains a sub-grid scale phenomenon in all operational, grid point-based NWP models. Its effects must instead be accounted for in a statistical fashion using parameterisation schemes. Such treatment is inadequate for the purposes of localised flood prediction.

Although not available for routine operational use, much higher resolution mesoscale NWP models, capable of resolving organised convection, do exist. The Joint Centre for Mesoscale Modelling (JCMM) in Reading is involved in their development and validation. However, the demands made by such models on computer processing power, and the weather observing network are likely to restrict their use to non-operational applications for some time to come.

## **2.7 Use of conceptual models**

Whilst the deterministic approach to weather forecasting adopted in NWP works well for synoptic scale weather systems, and can be applied with some skill to mesoscale weather phenomena, its application to the prediction of sub-mesoscale processes such as disorganised convection is fraught with problems. There is a significant chaotic component to atmospheric motions at this scale. Consequently, very detailed and accurate measurements of atmospheric state are required if forecast errors are not to swamp the predictive skill of the model. The routine collection of such measurements over large areas is neither practicable nor financially viable.

Conceptual models (see Browning, 1990), capable of encapsulating the structure and behaviour of sub-mesoscale phenomena, whilst avoiding an explicit treatment of their physics, may provide an alternative way forward. Hand and Conway (1995) have developed such a model for the prediction of convective precipitation. This adopts an Object-Oriented (hereafter referred to as OO) approach to the treatment of convection in which rainfall radar data are used, in combination with satellite derived CTTs, to recognise and classify discrete convective cell objects. This Object-Oriented Model (OOM) is described in detail in Appendix A. As discussed in the introduction, its validation has been one of the primary aims of the Thunderstorm Warning Project.

## **2.8 Summary comments**

This chapter has briefly reviewed a range of methods for identifying and forecasting convection. Each of these has its own problems and deficiencies, some of which have been discussed in the preceding sub-sections. Evidently, the diagnosis of convection using a single source of observations, or its prediction using one forecast algorithm may be less reliable than an approach which attempts to exploit the benefits of a range of observational and modelling techniques. This philosophy underpins the design of the GANDOLF system.

For example, the diagnosis of convection in GANDOLF is based upon a combination of MM forecast diagnostic fields (e.g. CAPE and convergence), a real time, satellite-derived Neural Network Cloud Classification (hereafter referred to as the NNCC) and current weather observations. Similarly, the prediction of convective precipitation involves a conceptual model of convection (the OOM after Hand and Conway, 1995) and extrapolation techniques which use MM wind forecasts. These and other components of the GANDOLF system are discussed in Section 3.



### **3. A DESCRIPTION OF THE GANDOLF SYSTEM**

#### **3.1 Introduction**

Components of the GANDOLF system have been discussed in earlier Thunderstorm Warning Project Interim and Progress Reports. The aim here is to present a coherent, non-technical and up-to-date description of GANDOLF, structured to reflect both the primary functions of the System and the various research and developmental problems that have been addressed during the course of the project. As such, this Section is intended to compliment the more detailed and technical approach adopted in the Project Operations Manual.

#### **3.2 A prototype system**

##### **3.2.1 Overview**

A schematic flow diagram of the prototype GANDOLF system is shown in Figure 1. Its hierarchical structure reflects the requirement for an automated system capable of modifying its response in accordance with changes in the prevailing weather conditions. As with any operational system the final design represents a compromise, arrived at by an iterative process of balancing the desire for optimal system performance against the practical restraints imposed by an operational working environment.

GANDOLF has been implemented on a Hewlett-Packard 712/80 series UNIX workstation at the Met. Office HQ in Bracknell. The System is linked to a Central Data Network (CDN) for access to near real time weather observations from radar, satellite and NWP sources. A dedicated telecommunications link between GANDOLF and a computer system running at the Agency's Flood Warning Centre at Waltham Cross allows the uninterrupted transmission of heavy rainfall warning messages (Section 3.7 and Ops. Man., 4.8), convective precipitation forecasts (Section 3.4.3 and Appendix A) and information on model performance (Section 3.6.6).

GANDOLF has been coded using a combination of the following programming languages: UNIX shell script, FORTRAN 77, FORTRAN 90 and PV-WAVE. It is important to stress that the System is standalone, and its robust design enables it to operate with one or more missing data sources, the proviso being that radar actuals are always available. As eluded to above, System operation is modified in accordance with observed changes in the weather within the *GANDOLF domain* (NG 120 – 1095 km E; -310 – 665 km N). There are three distinct levels of automated operation: Monitor, Action and Alert; and one manual level, Operator, concerned with start-up and shutdown of the System. Each of these is discussed below.

##### **3.2.2 Level 0: Operator**

Operator comprises the manual operations involved in start-up and shutdown of the GANDOLF system. Two special UNIX scripts are employed for this purpose (see Ops. Man., Sections 3.2–3.3). The start-up process involves the initiation of numerous data gathering scripts. This is achieved in a staggered fashion so that full Monitor functionality is only attained after about 20 minutes. Such an approach is designed to minimise the risk of System



overload. For similar reasons, shutdown of the System proceeds in a staggered fashion from the highest operational level (Level 3: Alert) downwards. Consequently, System functionality is lost in the following order: Alert, Action, Monitor.

### 3.2.3 Level 1: Monitor

Monitor is GANDOLF's lowest level of standalone operation. Its primary function is the coordination of remote data gathering, to ensure that the System always has access to the most recent weather observations and forecasts.

The primary, external source of data is the Nimrod nowcasting system. Nimrod routinely transfers radar composite analyses and forecasts, MM predicted fields of temperature, pressure, wind and precipitation, and Meteosat visible (VIS) and infrared (IR) imagery to the System (see the Project Operations Manual, Sections 4.2–4). In addition, the Met. Office's satellite processing system, Autosat-3, also supplies Meteosat VIS and IR data in near real time. In conjunction with a pre-trained neural network-based cloud classifier, these Autosat-3 imagery enable GANDOLF to distinguish between convective and dynamically forced cloud systems (see Section 3.5.5 and Op. Man., Section 4.7). The resulting classification is used in combination with various convection diagnosis algorithms to determine when it is appropriate to run the OOM.

GANDOLF defines a geographical area called the *Operational domain* or *GANDOLF domain* which is routinely examined for evidence of precipitation. If precipitation is detected anywhere within this rectangle then all System data are automatically archived. In addition, if precipitation is identified within range of the Chenies radar (the *Chenies domain*: NG 290 – 710 km E; -10 – 410 km N), GANDOLF triggers the start-up of the second, standalone level of operation: Action.

### 3.2.4 Level 2: Action

The second level of standalone operation is primarily concerned the running and validation of the OOM. When precipitation is observed to fall anywhere within a 210 km radius of the Chenies radar – the *Chenies domain* – the OOM is run on a ten minute cycle until the precipitation stops. Each model run generates a maximum of 18 ten minute Instantaneous Rainfall Rate (IRR) precipitation forecasts, and three, hourly accumulation forecasts. Estimates of 15 minute accumulations used by Thames Region's flood prediction models are derived from the ten minute IRRs (see Section 3.4.2.3).

The validation of OOM precipitation forecasts is undertaken in near real time after each OOM run. This permits the generation of a time series of OOM performance indices (see Op. Man., Section 5.6) that can be used by Thames Region, together with other performance criteria, to assess the value of the forecasts they are receiving (see Section 3.6). Level 2: Action is responsible for generating coded messages containing these performance indicators (see Op. Man., Section 6.5). When the OOM forecasts convective precipitation in the *Thames Domain* (NG 380 – 580 km E; 120 – 280 km N), GANDOLF initiates the third and highest, standalone level of operation: Alert.

### 3.2.5 Level 3: Alert

When the GANDOLF system attains operational Level 3: Alert, the latest OOM precipitation forecast sequence is sent to Thames Region's Flood Warning Centre (FWC) at Waltham Cross via the dedicated communications link described in Section 3.2.1 (Waltham Cross FWC is responsible for issuing flood warnings in the London area). Typically, each such transmission comprises 18 ten minute IRR and 12 fifteen minute accumulation forecasts (see Ops. Man., Section 6.4). Verification statistics are also sent when observed ten minute IRR and 15 minute accumulations (derived from Chenies actuals) are available (see Ops. Man., Section 6.5).

The Waltham Cross FWC also receives heavy precipitation Warning Messages (WMs) generated by the GANDOLF Warning Level System (WLS). These transmissions are independent of Level 3: Alert, since they are sent routinely, regardless of whether precipitation is forecast in the *Thames Domain* or not (Sections 3.7 and Ops. Man., Section 4.8). During periods of dry weather, the transmission of WMs ensures the integrity of the telecommunications link with the Met. Office. When it is raining, the relaying of precipitation forecasts, validation statistics, and WMs to Waltham Cross is managed so that only one transmission attempts to use the communications link at any given time.

### 3.2.6 The control panel

Orderly operation of the GANDOLF system involves the coordination of a large number of different processes, including data gathering and reformatting, the running and validation of the OOM, and the transmission of warnings, precipitation forecasts and validation statistics to Waltham Cross FWC. These are monitored most easily using some form of Graphical User Interface (GUI). The GANDOLF *control panel* affords such a facility. Figure 2 shows the control panel as it would appear to the System operator.

At the top of the panel are a series of buttons. These are linked to information on the current operational status of the GANDOLF system. The *GANDOLF* button displays a brief summary of the GANDOLF project and its aims. The *Help* button enables the operator to examine the Project Operations Manual on-line. Two pictures are displayed in the top panel. These are the latest Meteosat IR and Nimrod radar composite images.

The *Operations* panel displays details concerning the current operational status of the System. From left to right are the *current time*, the GANDOLF *run time* (hours and minutes since System start-up), the operational status of the System, the level of standalone operation (*Monitor*, *Action*, or *Alert*), the data archive mode (*Delete / Archive*), and the GANDOLF start-up (*Go / Stop*) button.

The *Inputs* panel displays information on the current data inputs to GANDOLF. A suite of UNIX processes control the gathering of data from various remote computer systems (Ops. Man., Sections 4.1.2.2–8). They can be started or stopped manually by clicking on the *Control* buttons. The Process IDentification number (PID) for each process and the validation time of the latest data are shown beneath. The latest Data Times (DTs) for each data source are also displayed. The settings on the *Display* buttons determine whether or not data are displayed upon input to the System.

The *Models* panel has a similar format to the *Inputs* panel. The UNIX processes controlling the handling of Nimrod forecasts and the running of the OOM can be started or stopped manually by a mouse click on the relevant *Control* button. Under normal operating conditions the GANDOLF System will determine which processes should run and which should not at any given time. However, the inclusion of manual override buttons affords an extra degree of flexibility in the way the System is managed. Movie loops of the latest model forecast sequences can be displayed automatically as soon as they are available by setting the *Movie* loops buttons to *YES*.

The *Diagnostics* panel allows the operator to control which of a range diagnostic tools are used when assessing the risk and severity of convection and heavy convective precipitation. Helicity (Section 3.6.3) and CAPE (Section 3.5.6.1) are used to determine the Lagrangian decorrelation time,  $T_L$  (Section 3.6.4). Convergence (Section 3.5.6.3) and Vorticity (Section 3.5.6.2) are calculated because they afford some means of assessing the risk of the release of convective instability. The last tool, labelled as *NNCC*, refers to the Neural Network Cloud Classifier (Section 3.5.5). This is designed to identify and distinguish convective and dynamically forced cloud systems. The classification of cloud within the *Thames Domain*, together with other diagnostics, permits the System to decide when to run the OOM (see Ops. Man., Sections 4.7, 4.8.4 and 5.2).

The *Advisory* panel displays current information on precipitation forecasts and warnings issued to Waltham Cross FWC. The *Warning* button displays either *YES* or *NO*, depending on whether a warning is in effect or not. The *Level* display shows the current *alert status* (Section 3.7.2). The buttons, *Send IRR* and *Send Accum*, control the transmission of IRR and accumulation forecasts. The *Trans Status* display changes from *Stopped* to *Transmit* when data transfers are in progress.

If the *Exit* button is clicked during system operation, an orderly shutdown sequence is initiated which kills all system processes from the top level (Level 3: Alert) downwards.

### 3.3 Data

#### 3.3.1 Overview

The GANDOLF system receives a wide range of near real time observational data and NWP forecast products. These are used for two main purposes: running a conceptual model of convection (the OOM); and diagnosing the current weather type (dynamic or convective). These inputs to the System must be co-ordinated so that data are received in an orderly fashion and within strict time margins. The timeliness of real time data inputs is critical if the data are to be pre-processed sufficiently quickly to permit their operational use. Sections 3.3.2–4 address these issues.

#### 3.3.2 Data requirements

Table 2 summarises the current data requirements of the GANDOLF system. Data are obtained from various operational and database computer systems within the Met. Office. These systems are interconnected by the Central Data Network (CDN).

**Table 2 Summary of the data inputs to the GANDOLF system.**

Data source	Data type	Spatial resolution	When available
Mesoscale Model data from Nimrod and COSMOS.	Forecast fields of temperature, precipitation, humidity, surface pressure, wind to T+18 or T+30.	16.8 km	Four times daily.
Geostationary satellite: Meteosat data from Nimrod and Autosat-3.	Infrared, Visible	Best resolutions are: IR: 5 km VIS: 2.5 km	Half hourly at 0000 UTC, 0030 UTC etc.
Multi-site radar network data from Nimrod.	Actuals	5 km	Every 15 minutes at 0000 UTC, 0015 UTC etc.
	Hourly IRR forecasts to T+6.	5 km	Every 30 minutes at 0000 UTC, 0030 UTC etc.
	15 min. accum. forecasts to T+3.	5 km	Every 30 minutes at 0000 UTC, 0030 UTC etc.
Chenies single site, multi-beam, 2 km radar data from RADARNET	Raw actuals	2 km	Every 5 minutes at 0,5,10, .. , 55 minutes past each hour.
Surface and upper air weather data from the COSMOS Synoptic Data Bank.	Coded observations.	Point observations.	Every hour.

### 3.3.3 Data acquisition

As shown in Table 2, data are received from a range of sources, the most important of which is the Nimrod system. Data collection in GANDOLF is co-ordinated by a suite of Level 1: Monitor, UNIX scripts (see Ops. Man., Section 4.1.2.2–8). These are designed to search for input data at regular intervals and on a continuous cycle. The timing of inputs received from Nimrod, RADARNET, and Autosat-3 are controlled by automated scripts on the host systems. Data held on the COSMOS system are actively retrieved by GANDOLF when required.

The timeliness of data receipt is very important, particularly for multiple beam, single site radar observations and Meteosat IR imagery used by the OOM. The latter is run on a ten minute cycle for the Data Times (DTs), 0, 10, .., 50 minutes past each hour. Multiple beam radar data must be received within two minutes of collection, if each model run and the

subsequent processing and transmission of forecasts are to be completed within the allotted time of eight minutes. Meteosat IR imagery used by the OOM for runs on the hour and half hour (DTs 0 and 30 minutes) are not received by GANDOLF until about four minutes after the registered DT. This delays model execution until approximately five and 35 minutes past each hour.

#### **3.3.4 Data correction**

Observations from radar and satellite systems must be quality controlled before they can be used for operational purposes. For example, Meteosat imagery are corrected for parallax error, and this is the responsibility of the host systems (Autosat-3 and Nimrod). The radar imagery received by GANDOLF are not pre-processed. Consequently, they must be corrected for the effects of clutter, anaprop and bright-band before they are used by the System.

The GANDOLF radar correction scheme is outlined in Figure 3. This has yet to be fully implemented operationally. However, a clutter removal scheme proposed by Collier *et al.* (1995) has been coded in PV-WAVE ready for incorporation into Level 1: Monitor. The routines devised by Hardaker and Auer (1995) for hail decontamination are relatively easy to implement, but will not be incorporated into the prototype system unless it undergoes further trials, or a period of full operational use. This is also the case for the bright-band detection and correction algorithm proposed by Hardaker *et al.* (1995). If GANDOLF is ultimately integrated into Nimrod, then the radar data will be quality controlled in the same way that current Nimrod products are processed.

#### **3.3.5 Data formats**

GANDOLF was originally coded to use radar and satellite products from the FRONTIERS system. On 15 December 1995, this semi-automated operational rainfall radar system was replaced with a fully automated version, Nimrod (Golding, 1997). Extensive modifications to GANDOLF were required to allow for this change in data source.

The original prototype GANDOLF system received MM data in an ASCII format from the Met. Office's COSMOS system. This was a particularly inefficient operation, owing to the sizes of the files transferred over the CDN (each file was of the order of 50 Mb). The current System receives MM data fields, radar and satellite imagery directly from Nimrod in Nimrod format. The latter is a binary format compatible with the OOM. Consequently, the transition from FRONTIERS to Nimrod has simplified certain operations within GANDOLF.

At the present time, GANDOLF does not use Nimrod quality controlled single site, multiple beam, radar actuals. Instead, it receives the raw, 8-bit encoded radar data from the RADARNET system. These are converted to Nimrod format prior to their use by the System.

Whilst the format of data inputs to the GANDOLF system is standardised to that of Nimrod, output formats vary according to the final destination of the data. All data destined for Waltham Cross FWC are output in Type 2 radar format (see Section 3.8 and Ops. Man., Section 6.2). Data archived for validation purposes are stored in Nimrod, or PV-WAVE binary formats.

## 3.4 Precipitation forecasts

### 3.4.1 Overview

The conceptual model of convective precipitation, known as the OOM, forms the centre piece of the GANDOLF system. In addition to precipitation forecasts produced by this model, Thames Region also routinely use products generated by the Met. Office's Nimrod system and the Institute of Hydrology's Local Forecast Model (LFM). In Sections 3.4.2–3, these three precipitation nowcasting models are briefly reviewed.

Unlike Nimrod and the LFM, the OOM is designed specifically for the prediction of non-frontal convective precipitation. Consequently, the GANDOLF system must be capable of accurately diagnosing non-frontal convection if the model is to produce valid forecasts. Section 3.5 explores various means of identifying non-frontal convection from current weather observations.

One of the principle design requirements of the GANDOLF system, outlined in the Introduction, was the provision of guidance on the choice of model forecast. Given the prevailing weather conditions, Thames Region need to know which of the precipitation forecasts at their disposal (OOM, Nimrod and LFM) is likely to produce the most reliable estimates of river discharge. Methods of estimating forecast reliability and the provision of guidance are reviewed in Section 3.6.

### 3.4.2 Extrapolation forecasts

Existing rainfall radar-based precipitation forecasts employed operationally by Thames Region are generating from radar analyses using various extrapolation techniques. Underpinning such an approach is the assumption that significant features of a precipitation field are conserved, at least in the short range. Thus, it should be possible to nowcast future states of the field by advecting it in the direction of its propagation.

In the Nimrod system the extrapolation scheme involves a combination of cross-correlation techniques, echo centroid tracking and steering vectors derived from MM wind fields. These have been described by Golding (1997). Nimrod uses 5 km resolution, Met. Office radar network analyses as its starting point. In contrast, the Institute of Hydrology's LFM is designed to run on 2 km, single site radar data from the Chenies radar. Here, the extrapolation scheme is based upon the use of cross correlation vectors. In addition, the initial, observed rainfall intensities are weighted towards field mean intensities as the forecast lead time increases. The methodology is based upon the work of Austin and Bellon (1974). A full description of the LFM can be found in Moore *et al.* (1991).

In common with the LFM, the OOM uses a Chenies 2 km radar image as its starting point. It also employs MM wind vectors to advect discrete, contiguous areas of precipitation as is the case in Nimrod extrapolation scheme. However, unlike either of the two models described above, the OOM attempts to simulate, in a physically realistic fashion, the growth or decay of the precipitation field over time.

### 3.4.3 The Object-Oriented Model

#### 3.4.3.1 *The conceptual model of convection*<sup>1</sup>

The OOM, developed by Hand and Conway (1995), is based upon a detailed and physically realistic conceptual model of a convective cell, such as might develop in convectively unstable airmasses in mid-latitudes. It utilises single site multiple beam radar data, satellite derived Cloud Top Temperatures (CTTs) and various MM forecast fields to detect and classify precipitating convective cells. In the model, each cell is represented by a cell object. This object possesses a set of attributes which describe the vigour of the cell, its depth, CTT, rainfall rate and so on. These attributes are used to assign each cell to one of five developmental stages. Together, these stages describe the typical life cycle of a convective cloud, from birth to dissipation.

The OOM forecast scheme employs representative steering level wind vectors from the MM to move cell objects forward in space. As a model forecast proceeds, cells are allowed to evolve according to the idealised life cycle mentioned above. The forecast time step is ten minutes, and at every step a development potential is calculated for each cell. This determines the form of the remainder of its life cycle, and therefore the amount of precipitation it will produce.

The diagnosed development potential can take one of six numerical values representing a spectrum of convective instability from weak to strong. When a certain development potential is reached mature cells are permitted to generate new, daughter cells. In this way, the OOM is able to simulate the non-linear growth of convective precipitation that is often observed to accompany non-frontal convection.

#### 3.4.3.2 *Running the OOM*

During periods when precipitation is observed to fall somewhere in the *Chenies domain* (NG 290–710 km E; -10–410 km N) the GANDOLF system runs the OOM on a ten minute cycle (Ops. man, Section 5.2). At the beginning of each cycle, the System checks the availability of Nimrod-formatted MM fields, multiple beam, single site Chenies radar data, and Meteosat IR imagery if the DT is on the hour or half hour. If these inputs are present, the OOM executable is run. Model run times vary from as little as one minute to five minutes, depending on the quantity of precipitation present in the *Chenies domain* and the extent of any other System processing. After the completion of each model run, the System converts OOM 10 minute IRR and 15 minute accumulation forecasts from Nimrod format to Type 2 radar format, prior to their transmission to Waltham Cross FWC (Ops. Man., Sections 5.4 and 6.4).

#### 3.4.3.3 *OOM precipitation forecasts*

Every OOM run generates 18 ten minute IRRs, and three 60 minute accumulations for lead times up to T+3 hours. The flood prediction models used by Thames Region require the input of 15 minute rainfall accumulation forecasts. After each OOM run, the GANDOLF system must therefore estimate a sequence of 15 minute accumulations from the OOM's ten minute

---

<sup>1</sup> For a comprehensive description of the OOM see Appendix A.

IRRs. This requires some form of integration scheme. A range of plausible integration methods exist, and at first glance it is unclear which, if any, is likely to be the more accurate.

To illustrate the problem, one can consider the various ways in which forecasts of IRR for 1400 GMT and 1410 GMT, might be combined to estimate the accumulation for the period 1400 GMT to 1415 GMT. If the IRR is measured in  $\text{mm hr}^{-1}$ , two obvious solutions are:

$$Accum_{1400-1415} = \frac{1}{6} IRR_{1400} + \frac{1}{12} IRR_{1410} \quad (1),$$

and:

$$Accum_{1400-1415} = \frac{1}{12} IRR_{1400} + \frac{1}{6} IRR_{1410} \quad (2).$$

Both (1) and (2) make the assumption that an instantaneous forecast of rain rate is representative of the five or ten minute mean rain rate encompassing the validation time of the forecast. Hence, the equivalent accumulation is simply one twelfth or one sixth of the predicted hourly rate. For example, in (1), the forecast IRR for 1400 GMT is deemed to be equivalent to the mean IRR between 1400 GMT and 1410 GMT. Similarly, the forecast IRR for 1410 GMT is assumed to be a good approximation of the mean IRR between 1410 GMT and 1415 GMT.

The two schemes presented in (1) and (2) differ only in the relative contribution each IRR forecast makes to the overall accumulation. Common sense would suggest that the accuracy of accumulations predicted in this way should be independent of the integration scheme used, given large enough data samples. This is because variations of actual rainfall rate over the period of accumulation should be essentially random. It is evident however, that when radar actuals are used as truth, the integration method used for estimating observed accumulations must be similar to that used for the forecasts.

During the summer trials, predicted 15 minute accumulations were derived as shown in (1). Their observed counterparts were estimated from five minute Chenies radar actuals using the following scheme:

$$Accum_{1400-1415} = \frac{1}{12} (IRR_{1400} + IRR_{1405} + IRR_{1410}) \quad (3).$$

Here it should be noted that Thames Region received IRR forecasts from the GANDOLF system during the 1996 summer trial. Accumulation forecasts were generated by Agency software on the computer system at Waltham Cross FWC.

### 3.5 The diagnosis of non-frontal convection

#### 3.5.1 Overview

From the outset of the Project, emphasis was placed upon the need for guidance concerning the use of OOM forecasts in favour of those issued by the existing operational systems:



Nimrod and the LFM. Early exploratory work looked at the use of a variety of algorithms capable of diagnosing non-frontal convection, including:

- rainfall radar-based precipitation indices (Section 3.5.2);
- rainfall radar and CTT difference images (Section 3.5.3);
- rainfall radar and CTT cross correlation vectors (Section 3.5.4);
- a Neural Network Cloud Classifier or NNCC (Section 3.5.5);
- MM diagnostic fields of CAPE, vorticity and convergence (Section 3.5.6.1–3).

The work undertaken in each of these area is described below.

### **3.5.2 Rainfall radar-based precipitation indices**

Time series of precipitation area and area average rainfall rate were compiled for a rectangular area centred on Thames Region (the *Thames Domain*: NG 380–580 km E; 120–280 km N). Figure 4 shows such a time series spanning a six hour period. These data can be compared with characteristic times series for particular precipitation types. For example, on the 24 June 1994, a Mesoscale Convective System developed over the Channel Islands and moved north-eastwards across the south-east of England (see Section 4.5.2.1). The area average rainfall on this occasion exhibited an increase, typical of MCS cases described in the literature. This similarity was confirmed by a comparison with the MCS criteria defined by Browning and Hill (1984). Figure 5 compares the changes observed on the 24 June 1994 with those reported by Tao *et al.* (1993). There is a clear consensus on the temporal variations in area average rain that typically accompany MCSs. Similar techniques can be employed with satellite data (see Section 3.5.3 below). It should be noted that the data used in these radar studies were corrected for the effects of hail attenuation.

### **3.5.3 Rainfall radar and satellite CTT difference images**

The changes in rainfall rate or CTT over a period of time can be examined by subtracting a radar or satellite image observed at time,  $t$ , from one observed at time  $t-\Delta T$ . The resultant difference image will exhibit areas of negative rain rate or CTT associated with decreases in these variables over the time interval,  $\Delta T$ ; and areas of positive rain rate or CTT where there have been increases in rain rate or CTT over the same period. Figures 6 and 7 show rainfall radar based difference images for two convective events observed during the summer of 1994. Significant variations in convective rain rate and CTT commonly occur over time intervals of as little as ten or 15 minutes. In contrast, frontal precipitation fields tend to exhibit a much slower temporal evolution. Consequently, the routine examination of difference images may provide another means of diagnosing convection.

Figure 8 compares the temporal changes in thunderstorm cloud top height, observed over the UK (24 June 1994) with those from north-east Colorado and Alberta in the USA. The rates of growth are very similar in all cases.

#### 3.5.4 Rainfall radar and CTT cross correlation vectors

Rainfall radar or CTT difference images such as those shown in Figures 6 and 7 may be used to derive cross correlation vectors representing the motions of individual storms. These *development* vectors are a product of both the movement of the IRR or CTT field and its growth or decay. A series of such vectors can be computed from the same data by using a range of IRR or CTT thresholds. During periods of non-frontal convection, the vector series for a given storm will often exhibit variations with increasing IRR or CTT threshold: vectors at high thresholds typically show a different orientation to those at low thresholds. This behaviour arises from the mismatching of storms observed at the two times,  $t$  and  $t+\Delta T$ . These mismatches are a consequence of rapid changes in storm IRRs or CTTs. Such behaviour is unique to non-frontal convection. Figure 9 shows an example of development vectors obtained from a radar difference image on 24 June 1994. The method used to determine rain rate development vectors is summarised below. A similar approach can be used to generate CTT development vectors.

- Estimation of a typical size for the convective objects in the image pair. These objects are assumed to be square for simplicities sake.
- Smoothing the difference image so as to enhance features of convective object size.
- Finding a local maximum IRR in the image associate with a particular convective cell.
- Searching for a minimum IRR within a sphere (centred on the maximum) whose radius is proportional to the nearest MM predicted steering level wind speed.
- Repeating the above steps for all other IRR maxima in the image, above a defined threshold.

If the vectors so derived are seen to vary with increasing threshold IRR then non-frontal convection is diagnosed.

#### 3.5.5 Neural network cloud classification

Early in 1996, the Satellite Image Applications Group in the Met. Office undertook a study of pattern recognition techniques, the aim being to find an optimal method for the objective classification of convective and dynamically forced cloud systems in satellite imagery (Pankiewicz, 1995). This study demonstrated the potential for improving on existing methods of identifying non-frontal convection.

In the context of cloud classification, artificial neural networks have the advantage that they can exploit the sorts of information that a human analyst might use when classifying features in a satellite picture. For example, apart from considering the spatial variations in pixel brightness and shape, size and scale context (the relationship between a given feature and other features of different scales) can be utilised to distinguish cloud type. Furthermore, once coded, trained neural networks are quick and efficient to run, a factor of particular importance in the context of operational implementation.

A detailed explanation of the multi-layered perceptron artificial neural network (hereafter referred as the Neural Network Cloud Classifier or NNCC) implemented in GANDOLF is beyond the scope of this report. However, a full explanation of its theoretical basis can be found in Pankiewicz (1995). What is important to emphasise here is that such a technique can provide GANDOLF with a means of identifying non-frontal convective activity, prior to the onset of convective precipitation. This represents a significant improvement over the diagnostic methods outlined above in Sections 3.5.2–4.

The NNCC has been trained to identify and distinguish four categories of cloud using half-hourly, simultaneous, collocated Meteosat infrared and visible images. The four categories are Dynamic (frontal), Shallow Convection, Deep Convection, and Clear (no cloud). In addition, where the NNCC is unable to identify an image pixel unambiguously, it may allocate a Unclassified class. The output from the NNCC is a data array of the same size and resolution as the original satellite images. However, in the place of pixel brightness values are numeric codes representing the categories described above. An example of a classified image is shown in Figure 10.

### 3.5.6 MM diagnostic fields

A range of diagnostic fields can be derived from MM predicted prognostic fields of temperature, humidity, pressure, and wind. Those of relevance to the diagnosis of convection are explained below.

#### 3.5.6.1 Convectively Available Potential Energy (CAPE)

CAPE is defined as the quantity of potential energy available for the generation of convection. The growth of large ‘reservoirs’ of CAPE is a pre-requisite for the realisation of strong convection (see for example, Emmanuel, 1994). CAPE is defined as follows:

$$CAPE = R_d \int_{CFL}^{EL} (T_{vp} - T_{ve}) d \ln p \quad (1),$$

where  $R_d$  is the gas constant for dry air ( $287 \text{ J kg}^{-1} \text{ K}^{-1}$ ),  $T_{vp}$  and  $T_{ve}$  are the virtual absolute temperatures (K) of the air parcel and the environment respectively,  $p$  is the pressure in hPa, CFL is the level of free convection, and EL is the equilibrium level.

The CFL is defined as the height above which a rising parcel of air will develop a positive buoyancy, enabling it to rise in the absence of external forcing. The equilibrium level is located at the point of neutral static stability above the CFL.

Weisman and Klemp (1982) used CAPE to distinguish precipitation events by precipitation type (i.e. convective and non-convective). In other studies, Zawadzki and Rô (1978) employed CAPE to stratify precipitation events by rain rate.

### 3.5.6.2 Vorticity

Vorticity is a three dimensional property concerned with rotary motion in fluids. As regards such motion in the atmosphere, the primary concern is with horizontal vorticity (i.e. that about the local vertical). The local, relative, horizontal vorticity is defined as:

$$W_H = \nabla \times V \quad (3),$$

where  $V$  is the velocity vector.  $W_H$  arises from a combination of horizontal curvature and shear motions.

Synoptic and mesoscale scale weather disturbances are associated with organised rotary motions that have length scales ranging from tens to thousands of kilometres. By contrast, the characteristic length scales of rotary motion associated with non-frontal convection are orders of magnitude smaller and cannot be resolved by NWP models. Vorticity computed from NWP predicted wind fields can therefore be used to diagnose the presence of dynamically-forced weather systems.

### 3.5.6.3 Convergence

Convergence of the horizontal wind field, defined as:

$$C = -\text{div}_H V = -\left(\frac{\partial u}{\partial x} + \frac{\partial v}{\partial y}\right) \quad (4),$$

occurs on a wide range of spatial scales, but the length scales of organised convergence associated with frontogenesis are orders of magnitude greater than those associated with convective updraughts. Consequently, convergence diagnosed from MM wind fields can be used in conjunction with other diagnostics, to identify dynamically forced, frontal weather systems.

## 3.5.7 Operationally implemented convection diagnostics

The convection diagnosis algorithms implemented in the operational version of GANDOLF are those described in Sections 3.5.5, 3.5.6.1 and 3.5.6.3. The methods outlined in Sections 3.5.2-4 proved of limited worth because they can only be used when precipitation is falling. A diagnosis of the current *weather type* (see Ops. Man., Section 4.8.4) is required prior to the onset of precipitation. For this reason, the NNCC described by Pankiewicz (1995) forms the hub of the operational, convection diagnosis software.

The NNCC is used to classify the cloud type in each pixel of paired, half hourly, Meteosat IR and VIS images. The number of pixels falling into each of the four categories, *deep convection*, *shallow convection*, *dynamic*, and *clear*, is computed for the *Thames Domain*. These numbers are then used in conjunction with MM derived diagnostic fields of CAPE, and convergence to determine whether the current weather situation is convective or frontal (dynamic). It is important to note that the classifier is limited in its operational use to day-light hours. During the hours of darkness, MM precipitation type is used as a substitute to determine the current *weather type*.

When GANDOLF is running operationally, this *weather type* classification serves two purposes. Firstly, it enables selective running of the OOM when the prevailing weather conditions are appropriate. Secondly, it is used by the WLS to generate WMs. These WMs contain an *alert status* (see Ops. Man., Section 4.8.5) which reflects the nature of any forecast precipitation. Thus, when dynamic precipitation is expected the *alert status* is a letter: **A-H**, but when non-frontal convective precipitation is predicted, the *alert status* is a number in the range **1-9**. The GANDOLF WLS is briefly described in Section 3.7 (for additional detail refer to Ops. Man., Section 4.8).

## 3.6 Estimation of forecast reliability

### 3.6.1 Overview

With the trial operational implementation of the OOM, Thames Region have three precipitation forecasts at their disposal. Although the OOM is specifically designed for the prediction of non-frontal convective precipitation, it does not necessarily follow that it will out-perform the extrapolation forecasts of the LFM or Nimrod during convective episodes. Consequently, some guidance on the relative reliability of the three models is required.

Work done by Lilley (1986) and others has demonstrated a correlation between Helicity (Section 3.6.3) and the longevity of individual convective cells. The latter is likely to have an influence on the useful range of extrapolation-based precipitation forecasts, since the more rapid the growth and decay of precipitating cells, the more quickly will an extrapolation of an observed precipitation field diverge from the truth. The computation of Helicity and related parameters from MM wind forecasts offers a means of estimating the time beyond which extrapolation forecasts cease to possess significant predictive skill.

This section examines a range of potential solutions to the problem of determining the relative performance of OO and extrapolation-based precipitation forecasts.

### 3.6.2 Cross correlation vectors

As described in Section 3.5.4 time sequential pairs of thresholded IRR images may be used to derive a series of cross correlation vectors for each distinct convective cell in a precipitation field. The vectors so derived are a product of both storm motion and of cell growth and decay. The variation of vector direction with changing threshold IRR is an indirect measure of rates of change in the precipitation field. This technique may be used to derive a crude estimate of the longevity of individual cells, and thus the maximum useful temporal range of an extrapolation forecast. There are, however, other theoretically-based methods of estimating this limit of predictability which can be applied in a predictive, as well as analytical mode.

### 3.6.3 Helicity ( $H_R$ )

Helicity ( $H_R$ ) has been defined by Lilly (1986) as:

$$H_R = \int_0^h (V_H - C) \cdot W_H dh \quad (5),$$

where  $V_H$  is the environmental, horizontal wind,  $C$  is the storm velocity,  $W_H$  is the local relative horizontal vorticity, and  $h$  is height. The Helicity,  $H_R$ , is proportional to the area swept by the vector  $V_H - C$  through the layer extending from the surface to the height,  $h$ . Since Helicity has units of energy it can be interpreted as a measure of wind shear energy that includes the directional shear. A positive value of Helicity implies cyclonic rotation, and a negative value, anti-cyclonic rotation.

Studies by Lilly and others (Lilly, 1986; Davies-Jones *et al.*, 1990; Woodall, 1990; Leftwich, 1990) have considered the use of Helicity in interpreting the behaviour of convective storms. Lilly (1986) conjectured that “supercell” thunderstorms owe their stability, longevity and apparent predictability to high values of Helicity. More recently, Leftwich (1990) has published evidence suggesting that the relationship between the magnitude of Helicity and storm severity is non-linear. Such findings have important implications for the forecasting of convective precipitation.

To compute the Helicity, an approximation to the integral given in (5) must be derived using analytical geometry. This approximation takes the form:

$$H_R = \sum_{n=0}^{N-1} \left[ (U_{n+1} - C_x)(V_n - C_y) - (U_n - C_x)(V_{n+1} - C_y) \right] \quad (6),$$

where  $C$  is the storm’s translation velocity, and  $(U_n, V_n)$  for  $n = 0$  to  $N-1$  are the observed winds at selected discrete altitudes within the storm. The storm’s translation velocity,  $C$ , is approximated by the wind at 700 hPa.

#### 3.6.4 Lagrangian decorrelation time, $T_L$

Zawadzki *et al.* (1994) have studied the predictability of radar derived precipitation patterns using a Lagrangian persistence extrapolation technique. This involves the translation of observed precipitation objects using motion vectors calculated by cross correlating pairs of time sequential radar images. The aim of their work was to test the findings of Bellon and Austin (1984), namely that, for a duration of up to (and including) three hours, linear extrapolation-based prediction of precipitation patterns is valid. In doing so they discovered that the useful range of precipitation forecasts produce by Lagrangian persistence varied with the prevailing weather conditions. They were able to relate this variability to fluctuations in certain numerical model diagnostics, including CAPE and Helicity ( $H_R$ ).

The Lagrangian persistence forecast method evolved from a consideration of the Lagrangian autocorrelation function (ACF). An autocorrelation function describes the way in which a function is correlated with itself (this can account for both spatial and temporal correlation). According to Bendat and Piersol (1966), such a function will contain two variables for each single variable in the original function. In the case of rainfall, there are four spatial and two temporal variables, since IRR is a function of position ( $x, y$ ) and time ( $t$ ).

Zawadzki (1973) noted that precipitation was a non-stationary and non-homogeneous process and so he looked at variations in IRR in terms of a “space ACF” and a “time ACF”. He made use of two major assumptions consistent with non-homogeneity and non-stationarity:

- the “time ACF” is defined over a time period longer than the duration of the storm;

- the “space ACF” is defined over an area large enough to contain the storm for the duration of its life.

The Lagrangian time ACF has been the focus of research in this Project. As the name implies, such a parameter is defined in a Lagrangian frame of reference (i.e. moving with the storm), and is therefore assumed to be independent of storm motion. It provides an estimate of the time beyond which a persistence-based extrapolation forecast ceases to possess any predictive skill. A derivation of the Lagrangian time ACF is presented below.

The autocorrelation function (ACF) of a rainfall rate,  $R(x, y, t)$  can be defined as follows:

$$A_{ST}(\alpha, \beta, \tau) = \overline{\langle R(x, y, t) R(x + \alpha, y + \beta, t + \tau) \rangle} \quad (7),$$

where  $\alpha$  and  $\beta$  are the two horizontal spatial lags and  $\tau$  is the time lag. The angular brackets denote the mean over an area  $S$ , which is large enough to contain the entire storm. The overbar denotes the mean over the time interval of the event,  $T$ . This must be longer than the storm duration.

The ACF is normalised ( $\hat{ACF}$ ) thus:

$$\hat{ACF}(\alpha, \beta, \tau) = \frac{A_{ST}(\alpha, \beta, \tau)}{\langle R^2 \rangle} \quad (8),$$

where  $\langle R^2 \rangle$  is the mean-square value of  $R(x, y, t)$  over both  $S$  and  $T$ .

The normalised Lagrangian time ACF is defined as follows:

$$l(\tau) = \hat{ACF}(\alpha_0, \beta_0, \tau) \quad (9),$$

where  $\alpha_0$  and  $\beta_0$  are the horizontal lags which maximise the cross-correlation between radar images separated by a time interval  $\tau$ . These will determine the pattern speed for the forecast by Lagrangian persistence. It should be noted the values in (9) are normalised to between 0 and 1.

According to Lorenz (1969), the “range of predictability” of a Lagrangian persistent forecast is the time interval within which the errors in prediction do not exceed some pre-chosen magnitude. This upper bound on predictability must be greater than the size of typical observational errors, but less than the size of the difference between randomly chosen states of the system.

The error threshold for the Lagrangian persistence model is obtained as follows. From Zawadzki *et al.* (1994), one can write:

$$E_L = 2\sqrt{\langle R^2 \rangle} [1 - l(\tau)] \quad (10),$$

where  $E_L$  is the Lagrangian persistence error,  $l(\tau)$  is the Lagrangian time ACF,  $\langle R \rangle$  is the forecast rainfall, and  $\tau$  is the time interval between the radar images used. Rearranging gives:

$$l(\tau) = 1 - \frac{E_L}{2\langle R^2 \rangle} \quad (11).$$

One can define the temporal skill threshold,  $T_L$ , as the time beyond which the Lagrangian persistence forecast error is greater than the observed climatological error in IRR. If  $\langle R_c \rangle$  denotes the mean climatological error, then:

$$l(T_L) = 1 - \frac{E_L}{2\langle R_c^2 \rangle} \quad (12).$$

Atkinson and Smithson (1976) give the annual mean rainfall rate ( $\langle R_c \rangle$ ) for Camden Square, London as  $1.3 \text{ mm h}^{-1}$ . The root mean square log (RMSL) error of persistence forecasts of six hourly rainfall totals (FOAG, 1992) is 0.56 mm. Taking this value of RMSL,

$$E_L = \frac{1}{6} [10^{0.56}]^2 = 2.19 \quad (13).$$

Therefore:

$$l(T_L) = 1 - \frac{2.19}{2 \times 1.3^2} = 0.35 \quad (14).$$

(14) defines the error threshold. The parameter,  $T_L$ , represents the maximum forecast time lag or lead time for which the skill of the Lagrangian persistence model exceeds that of the climatological value.

Between May 1994 and July 1995 a total of ten precipitation events were examined using time sequences of 15 minute radar composite analyses. Of these events, four were frontal, five were convective, and one was frontal with embedded convection. In each case the maximum lead time for which  $l(T_L) \geq 0.35$  was established (Rippon, 1995). Figures 11 and 12 illustrate the Lagrangian time ACFs for each study event.

Following the example of Zawadzki *et al.* (1994) an attempt was made to establish a relationship between the Lagrangian decorrelation time,  $T_L$ , for each precipitation event and certain numerical model diagnostics. The latter included CAPE and Helicity ( $H_R$ ), derived from MM forecasts of temperature, humidity and wind.

Zawadzki *et al.* (1994) derived the following relationship between  $T_L$  and CAPE:

$$T_L = 30 + 7.9 \ln(\text{CAPE}) \quad (15),$$

for which they found a correlation coefficient of 0.61 (at the 5% significance level). This indicates that about 37% of the variance in  $T_L$  could be explained by the variability in CAPE.



Such a result is broadly in line with the studies of Zawadzki and Rô (1978), who found a similar level of correlation between CAPE and rain rate.

Of the cases studied by Zawadzki *et al.* (1994), approximately 50% had CAPE values in excess of  $1000 \text{ J kg}^{-1}$ . In the UK study conducted by Rippon *et al.* (1995), CAPE values of this magnitude were only observed on three occasions. This would appear to explain the closer fit of (15) when considering a subset of the ten UK precipitation events for which CAPE was highest (see Figure 13).

Zawadzki *et al.* (1994) also derived the following relationship between the modified Richardson number and  $T_L$ :

$$T_L = 114 - 1.3 \frac{CAPE}{H_R} \quad (16),$$

where  $CAPE/H_R$  is the modified Richardson number. The latter is used as a measure of the stability of boundary layer flows. The correlation of  $T_L$  with the modified Richardson number was found to be as high as 0.92 (significant at the 5% confidence limit).

When formulating this relationship Zawadzki *et al.* (1994) considered only those events for which  $CAPE \geq 850 \text{ J kg}^{-1}$ . In the UK case study all events were used. It can be seen from Figure 14 that, for values of  $CAPE/H_R > 10 \text{ J kg}^{-1}$ , the regression equation is a close fit. For those points which are described closely by (16),  $CAPE \geq 500 \text{ J kg}^{-1}$ , very much in agreement with Zawadzki *et al.* (1994). The results from the UK study are consistent with the conclusions of Weisman and Klemp (1982). They found that an increase in the ratio of convective energy to shear energy led to a decrease in cell longevity.

Zawadzki *et al.* (1994) did not examine any precipitation events associated with negative values of  $H_R$ , whereas in the UK study there were two such cases. Negative  $H_R$ , as opposed to the more common positive  $H_R$ , indicates anti-cyclonic rotation. In thunderstorms, either should be equally likely, assuming that they are sub-mesoscale and short-lived.

Somewhat surprisingly, Zawadzki *et al.* (1994) found no significant linear correlation between  $T_L$  and  $H_R$  alone, despite the fact that research by Lilly (1986) and others suggests that one should expect to find a relationship between the persistence of precipitation and  $H_R$ . For an idealised flow where wind and vorticity are always co-linear, it can be shown that the vorticity equation becomes linear (Lilly, 1986). The linearity of wind and vorticity causes the energy cascade between different scales of atmospheric turbulence to be blocked. As a consequence each scale of motion may then evolve independently. The hypothesis formulated by Lilly (1986) was “.. given that Helicity measures the colinearity of  $V_H$  and  $W_H$  in a highly helical atmospheric flow, precipitating cells may benefit from a restricted energy cascade and exhibit an enhanced longevity.”.

The plot of  $T_L$  versus  $H_R$  in Figure 15 exhibits a strong correlation between the two variables, particularly for the UK convective events studied. The following regression equation was found by merging the results from Canadian and UK studies:

$$T_L = 50 + 0.6 H_R \quad (17).$$

The associated correlation coefficient of 0.97 was significant at the 1% level. In the UK study, frontal precipitation events also showed a linear correlation between  $T_L$  and  $H_R$ , but subsequent regression analysis did not demonstrate any statistical significance. This suggests that while (17) can be usefully applied to convective precipitation events, this is not so in frontal situations. Figure 16 shows a MM derived forecast field of  $T_L$  over the UK. Corresponding fields of CAPE and  $H_R$  are shown in Figures 17 and 18 respectively. Figure 16 was generated from a  $H_R$  field using (17).

From the UK case study data described here, it would appear that Helicity alone is a more effective predictor of  $T_L$  than the ratio of CAPE and  $H_R$  proposed by Zawadzki *et al.* (1994). However, there may be other numerical model diagnostics capable of providing useful guidance on the predictability extrapolation-based precipitation forecasts. These might include geostrophic vorticity, the vertical distribution of temperature advection, and the wind shear energy (Moncrieff and Green, 1972).

### 3.6.5 Real time model validation statistics

The ability to estimate fields of Lagrangian decorrelation time,  $T_L$ , from MM derived fields of Helicity and CAPE allows the GANDOLF system to advise the Thames Region staff on the probable useful range of extrapolation forecasts during episodes of non-frontal convection. However, such an approach cannot be employed for frontal precipitation events since no clear relationship between  $T_L$  and either CAPE or Helicity has been demonstrated on these occasions.

One alternative means of assessing the relative performance of the OOM, and extrapolation-based models involves the near real time validation of precipitation forecasts against radar actuals. Software incorporated into Level 2: Action of GANDOLF, allows the System to compare the performance of the OOM and Nimrod in near real time. The resulting performance statistics can be sent to Waltham Cross FWC in a Type 2 radar formatted *verification block* (Ops. Man, Section 6.5). This approach has the advantage that it provides actual and not predicted measures of comparative model performance.

### 3.6.6 Operationally implemented guidance on model performance

The guidance on comparative model performance, issued to Waltham Cross FWC by the prototype operational GANDOLF system, is based upon the two approaches described in Sections 3.6.4 and 3.6.5. During periods of non-frontal convective precipitation, it is recommended that Waltham Cross FWC use the Lagrangian decorrelation time,  $T_L$ , (sent in Type 2 *header blocks*) as an estimate of the maximum useful range of their extrapolation-based precipitation forecasts. In addition, they may compare the near real time performance statistics for the OOM and Nimrod (sent in Type 2 formatted *verification blocks*). These will highlight potential sources of forecast error, perhaps most significantly, that due to inaccurate extrapolation vectors (these may be MM wind vectors or cross correlation vectors). During episodes of frontal precipitation, OOM forecasts are not available, and there is therefore no requirement for forecast guidance.

## 3.7 Warnings of heavy precipitation: the Warning Level System (WLS)

### 3.7.1 Overview

The GANDOLF WLS is required to issue warnings of impending precipitation in the *Thames Domain*. These warnings take the form of five minute, coded text messages, referred to as Warning Messages (WMs). They are transmitted to the Waltham Cross FWC at 0, 5, 10, .. , 55 minutes past each hour. Each WM comprises two or three parts: a date-time stamp, an *alert status*, and an Expected Time of Arrival (ETA) for forecast precipitation (optional). A full technical explanation of the GANDOLF WLS can be found in the Project Operations Manual, Section 4.8. The descriptions provided in Sections 3.7.2–3 provide a brief summary of the salient features.

### 3.7.2 Determination of *alert status*

The WLS *alert status* can either be a number (0–9) or a letter (A–H). Its value depends on three things: whether precipitation is convective or dynamic, the forecast depth of accumulation, and the forecast lead time. The differentiation between convective and dynamic precipitation is designed to indicate when the OOM model is in use. The OOM was developed specifically for the prediction of non-frontal convective precipitation and therefore only runs when the *alert status* is a number between 1 and 9 (an *alert status* of 0 means “No warning”). Table 3 shows a simplified contingency table used by the WLS to compute the *alert status*.

**Table 3** Contingency table for the WLS *alert status*.

Weather type	Forecast lead time / minutes	Forecast accumulated precipitation in one hour / mm	WLS alert status or WLC
1 (dynamic) or 3 (dyn.+conv.)	> 180	0.0	0
		< 4.0	A
		4.0 - 8.0	B
		8.0 - 16.0	C
		16.0 - 32.0	D
	<= 180	0.0	0
		< 4.0	E
		4.0 - 8.0	F
		8.0 - 16.0	G
		16.0 - 32.0	H
2 (convective)	> 180	0.0	0
		< 4.0	1
		4.0 - 8.0	2
		8.0 - 16.0	3
		16.0 - 32.0	4
	<= 180	0.0	0
		< 4.0	5
		4.0 - 8.0	6
		8.0 - 16.0	7
		16.0 - 32.0	8
		> 32.0	9

### 3.7.3 Generation of Warning Messages

A WM is composed of two or three parts depending on the current weather situation (see Ops. Man., Section 4.1.2.9). The first two parts, a date-time stamp and an *alert status* (WLC), are always present. The third part, an ETA for forecast precipitation, is only appended to the message string when precipitation is forecast or observed in the *Thames Domain*. Some examples of message format are presented below.

When precipitation is forecast but not observed, the WM takes the following form:

**GANDOLF warning at 29.09.96 10:55:06 GMT. Alert status is 1. Precipitation expected by 1600 GMT.**

When precipitation is forecast and observed in the *Thames Domain*, the message time stamp and the ETA are identical (to the nearest minute). In this instance, the forecast maximum accumulation used to determine the *alert status* will come from the forecast whose Validation Time (VT) is nearest to the current time:

**GANDOLF warning at 29.09.96 10:55:06 GMT. Alert status is 5. Precipitation expected by 1055 GMT.**

When precipitation is neither observed nor forecast, the message comprises two parts instead of three, and simply serves to confirm that no warning is in effect. In addition, message transmission during dry interludes indicates error free operation of both the GANDOLF system and the telecommunications link with the Waltham Cross computer system:

**GANDOLF warning at 29.09.96 10:55:06 GMT. Alert status is 0.**

## 3.8 Transmissions to Waltham Cross Flood Warning Centre

### 3.8.1 Overview

At the beginning of September 1995, British Telecom installed a dedicated, Modem controlled electronic link between the computer system at the Waltham Cross FWC, and the GANDOLF workstation at the Met. Office in Bracknell. The modems were set up to permit uni-directional data transmission from the Met. Office to Waltham Cross at 9600 bps. The first successful test transmissions were completed in November of the same year.

During the GANDOLF operational trial in the summer of 1996, WMs, OOM precipitation forecasts, and comparative model validation statistics were routinely sent to Waltham Cross FWC. The transmission format used was that employed by the Met. Office for all asynchronous radar data transmissions. Section 3.8.2 summarises this Type 2 radar format. A comprehensive description of the formats used for *data*, *header*, *alert* and *verification blocks* can be found in Appendix B of the Project Operations Manual.

### 3.8.2 Transmission formats

All transmissions to the Waltham Cross FWC follow closely the Type 2 radar data format described in the Met. Office's Weather Radar Group report No.3, version 3.1. This format is normally used for 2 km resolution, asynchronous five minute, single site radar data.

Type 2 transmissions comprise the following components:

- a Start Of Transmission (SOT) block;
- a header block;
- data blocks;
- an End Of Transmission (EOT) block.

Here, a block is defined as a string of 532 bytes or characters. SOTs serve to alert the receiving computer to the impending transmission of useful data, whilst EOTs act as end of transmission markers. A header block contains all the information necessary for the unambiguous interpretation of the data contained in the following data blocks. In the GANDOLF system, *alert* and *verification* blocks may also follow a header block. Alert blocks contain WMs generated by the WLS, and verification blocks, coded validation statistics for Nimrod and the OOM.

### 3.8.3 Transmission times

The dedicated BT telecommunications link between the GANDOLF system and the Waltham Cross FWC's computer currently operates at a line speed of 9600 bps (less than the originally intended 19200 bps). Consequently, the transmission time for a GANDOLF WM comprising 532 bytes is close to 0.5 seconds. It follows that the transmission time for a single Type 2 formatted IRR or accumulation forecast, containing one header block and 16 data blocks ( $532 \times 17$  bytes), is approximately 7.5 seconds.

Each OOM run cycle produces 19 IRR forecasts (including the instantiation), and twelve 15 minute accumulation forecasts. Assuming a transmission rate of one forecast every eight seconds, the cumulative transmission time per OOM run cycle is 248 seconds. Given that this cycle is ten minutes in length (600 seconds), the transmission of two five minute WMs, a full compliment of OOM forecasts and validation statistics (one or two blocks) can be achieved well within the allotted time.

## **4. ASSESSMENT OF SYSTEM PERFORMANCE**

### **4.1 Overview of the summer trials**

Trials of the prototype GANDOLF system were conducted over the summers of 1995 and 1996. The summer of 1995 was particularly dry, with a low incidence of non-frontal convection in the south-east of England. Only three convective precipitation events were observed during the trial period, two of which were associated with frontal or trough activity. By contrast, the summer of 1996 was an active one, with over 20 days of non-frontal convection, and a handful of days with convection enhanced frontal precipitation. In addition to these trial events, several archived case studies were used to make retrospective runs of the OOM. One of these involved organised convection associated with a Mesoscale Convective System (24 June 1994), the other, a particularly active case of non-frontal convection (10–11 August 1994) which caused localised flooding in central London.

During each operational trial, the Waltham Cross FWC routinely received WMs, and OOM IRR forecast sequences from the GANDOLF system. The WMs were displayed on a monitor in the FWC. They were employed in conjunction with precipitation forecasts from Nimrod and the LFM to assess the flood risk for various river sub-catchments in the vicinity of London. OOM IRR forecasts provided additional qualitative guidance: they were routinely displayed on a monitor for visual examination by FWC duty officers.

The aims of the summer trials were two fold:

- to assess the reliability of the prototype GANDOLF system and its components;
- to compare the performance of the OOM, Nimrod and LFM.

Each of these is considered in the following Sections.

### **4.2 Operational performance of the GANDOLF system**

The structure and basic functions of the GANDOLF system were discussed in Section 3. System components associated with each of the three levels of standalone operation were developed and tested in isolation, in response to specific design requirements. The subsequent integration of these components into a single operational system involved the temporal co-ordination of various interdependent System operations in such a way as to optimise System performance in terms of speed and reliability.

The first trial of the prototype GANDOLF system during the summer of 1995 brought to light certain weaknesses in System design. For example, the amount of processing necessary to reformat MM fields from an ASCII format to an OOM compatible format led to problems with the management of system resources on the HP 712/80 workstation. Subsequent recoding of GANDOLF to cater for receipt of Nimrod formatted MM fields solved this problem.

During periods of heavy, organised convective precipitation on the 7 June 1996, the OOM was observed to crash on numerous occasions, apparently as a result of memory allocation failure in one of the FORTRAN 90 modules. Subsequent attempts to reproduce the error with

retrospective model runs were unsuccessful. Consequently, this bug in the OOM software remains to be identified and corrected. It should be emphasised however, that whatever the exact cause of the problem, it does not appear to affect model performance routinely.

### 4.3 Performance of the WLS

During the course of the summer 1996 trial, Agency staff noted several flaws in the behaviour of the GANDOLF WLS. At times, the warning levels issued were seen to fluctuate up and down in response to uncorrected anaprop and clutter echoes in the Chenies radar images. In addition, warnings for forecast lead times in the range three to 24 hours were shown to significantly exceed those for lead times between zero and three hours. As a result, a marked downward step in *alert status* was often observed at T+3 hours. The problem proved to be associated with the use of Mesoscale Model (MM) precipitation forecasts for the generation of longer range (three to 24 hour) precipitation warnings. Subsequently, WLS performance was improved by introducing Nimrod-based warnings for lead times spanning the range T+3 to T+6 hours.

#### 4.3.1 Validation of MM precipitation forecasts

MM precipitation forecasts form the basis of heavy precipitation warnings issued for lead times beyond 6 hours and out to 30 hours. It is therefore appropriate to present some case study validation statistics for these forecasts. The validation period spanned approximately one month, from 28 September 1995 to 31 October 1995. Convective precipitation occurred on ten days during this time interval, with thunderstorms being recorded in the Daily Weather Summaries (DWSs) on three of these days.

Currently, there are four MM runs per day, at 0000, 0600, 1200 and 1800 GMT. For each forecast, the occurrence of convective or frontal precipitation in the area monitored by the Chenies and Channel Islands radars was noted. The maximum accumulation of precipitation forecast in this area during the 6 hour period ending at each validation time was also recorded. Performance was assessed by comparing forecast accumulations with actual accumulations (in the periods 2100 to 0900 GMT and 0900 to 2100 GMT) extracted from the DWSs. Only data for those days on which the MM forecast convective precipitation are included in the statistical analysis presented below. Nineteen days worth of model predictions were examined in this way.

Table 4 shows the number of MM forecasts falling into convective and frontal precipitation categories for all lead times. On some occasions the MM forecast frontal precipitation when convective precipitation occurred. On others, frontal precipitation occurred when none was forecast. Over the validation period, the former error was noted in 26 forecasts, and the latter in four forecasts. The total number of forecasts analysed was 114.

Table 4 summarises the performance of the MM as a function of forecast lead time, using three separate performance indicators: the Critical Success Index (CSI), Probability Of Detection (POD), and False Alarm Rate (FAR). These indices were discussed in Section 4.4.2. Given the limited size of the data sample, no definite conclusions regarding MM performance can be drawn. Nonetheless, it is interesting to note that T+18 hour forecasts appear to be the most accurate. In fact, forecast accuracy increases from T+6 to T+18, and thereafter decreases. The FAR is particularly large at T+6, due perhaps to model 'spin-up'

problems. Assuming that this measured performance is a general representation of MM behaviour, the implications are that forecasts of convective precipitation are only useful between T+18 and T+24.

**Table 4 The performance of the Mesoscale Model in forecasting frontal and convective precipitation as a function of lead time (based upon analysis of 114 forecasts).**

Lead time	T+6	T+12	T+18	T+24	T+30	T+36
Frontal	14 from 19	8 from 12	13 from 13	13 from 14	9 from 15	7 from 12
Convective	1 from 2	5 from 7	5 from 6	3 from 5	1 from 2	3 from 7
CSI	0.14	0.45	0.86	0.5	0.12	0.25
POD	0.50	0.71	0.83	0.60	0.50	0.43
FAR	0.83	0.44	0.00	0.25	0.86	0.63

The implications of this study are that heavy convective precipitation warnings from the MM for lead times between 3 and 18 hours ahead are likely to be unreliable. Warnings of heavy frontal precipitation may be similarly affected. At the present time, there are no alternatives to the detailed, short range weather forecast guidance provided by the MM.

## 4.4 Comparative performance of the OOM, LFM and Nimrod

### 4.4.1 Overview

The primary aim of the summer trials was a comparison of the performance of OOM precipitation forecasts with those of Nimrod and the LFM. Forecast precipitation accumulations over specified catchments are employed by the Agency to make predictions of river discharge. The latter form the basis of the flood warnings issued to the public. The two existing precipitation nowcasting systems employed by Thames Region – Nimrod and the LFM – generate 15 minute accumulation forecasts. The OOM was originally designed to produce ten minute IRR and 60 minute accumulation forecasts. Consequently, an integration scheme was required to estimate OOM 15 minute accumulations from the existing IRR predictions. This scheme was described in Section 3.4.3.3.

For the duration of both summer trials, all OOM and Nimrod forecasts of convective precipitation were archived, together with observed 15 minute accumulations derived from sequences of Chenies IRR actuals (Section 3.4.3.3). Rain gauge measurements of accumulation were also available for the purposes of forecast validation. However, owing to the difficulties incumbent in estimating total catchment accumulations from these point observations, and the limited time available for the validation exercise, it was decided that radar-based observations of accumulation would be used as ground truth. This approach had the additional advantage of permitting near real time validation of the models.

Precipitation forecasts produced by the LFM were not available to the GANDOLF system during the course of the summer trials. Instead, all the relevant case data were supplied to the Met. Office on a TK70 VAX compatible tape at the end of the summer 1996 trial. Thus, although the performance of Nimrod and the OOM could be evaluated on-line (Ops. Man., Section 5.6.2), that of the LFM was determined off-line at the end of the trials.



#### 4.4.2 Precipitation forecast validation statistics

In assessing the performance of a model designed to predict temporal changes in a three dimensional field, one must consider both the spatial and temporal accuracy of its forecasts. An examination of time synchronous observed and predicted fields will highlight the extent of any spatial discrepancies. However, these are likely to reflect, at least in part, the effects of timing errors in the forecasts. Thus, even when the area and intensity of a precipitation field are forecast well, a small error in the predicted direction or speed of its movement will heavily affect the measured spatial performance. In practice, it is therefore very difficult to isolate and quantify the temporal and spatial components of forecast error.

The approach to forecast assessment adopted here involves the use of a range of statistical tools to ascertain the degree of spatial correspondence between time synchronous observed and predicted precipitation fields. This approach is repeated over the full range of model lead times, so that some indication of the time dependency of model performance is obtained. Visual inspection of simultaneous fields, together with a comparison of collocated observed and forecast steering level winds afford some means of identifying the primary sources of model error.

The performance statistics employed to assess model performance in Section 4.5.4.5 can be categorised into two groups. First, there are those that are purely spatial. These include the Hit Rate (HR), False Alarm Rate (FAR), and Critical Success Index (CSI). Second, there are statistics that also consider the magnitude of the discrepancy between collocated, observed and forecast values. These include Root Mean Squared Error (RMSE) and the Mean Squared Error (MSE). In the context of evaluating the accuracy of predicted catchment accumulations, the MSE is more sensitive to large absolute discrepancies between forecast and observed accumulations than the RMSE.

Computation of the CSI, HR, and FAR requires the definition of a contingency table to represent all possible combinations of observed and forecast behaviour. Using a rain / no rain boundary condition, four contingencies: a, b, c, and d, can be defined. These are described in Table 5.

**Table 5 Contingency table for CSI, HR, FAR**

Contingency	
a	Number of cases where precipitation did not occur and was not forecast to occur.
b	Number of cases where precipitation occurred that was forecast to occur.
c	Number of cases where precipitation occurred that was not forecast.
d	Number of cases where precipitation did not occur but was forecast.

A similar set of contingencies may be described for other boundary conditions. For example, one could choose to examine the spatial performance of predictions of rainfall accumulation  $\geq 4 \text{ mm hr}^{-1}$ . Regardless of this choice of rain rate or accumulation threshold, the HR, FAR and CSI are given as:

$$HR = \frac{b}{b + c} \quad (18),$$

$$FAR = \frac{d}{b + d} \quad (19),$$

$$CSI = \frac{b}{b + c + d} \quad (20).$$

In the GANDOLF validation software, HR, FAR, and CSI statistics were computed using an IRR threshold of 0.125 mm hr<sup>-1</sup> and an accumulation threshold of 0.2 mm hr<sup>-1</sup>.

Spatial performance can also be evaluated with the Mean Squared Error (MSE):

$$MSE_{xy} = \frac{\sum_{i=1}^n (x_i - y_i)^2}{n} \quad (21),$$

where the variables x and y represent collocated observed and forecast values respectively. The MSE provides a measure of the magnitude of the error between x and y. Its merit can be demonstrated by envisaging a situation in which the spatial extent of a precipitation field has been forecast well (high CSI, high HR, and low FAR), but its corresponding distribution of rain rates or accumulations has been poorly predicted (high MSE). In these circumstances the interpretation of the MSE in conjunction with the CSI, HR and FAR will pin-point the specific failings of the forecast.

Error Component Analysis (ECA) may permit one to go a step further, and elucidate the linear and non-linear contributions to the forecast error given by the MSE. Thiel (1971) has shown that the MSE can be broken down into three components that arise from:

- a difference in the means of forecast and observed data,  $U_b$ ;
- a difference in the standard deviations of forecast and observed data,  $U_v$ ;
- the incomplete covariation,  $U_c$ .

$U_b$ ,  $U_v$  and  $U_c$  are given by the following formulae:

$$U_b = (\bar{x} - \bar{y})^2 \quad (22),$$

$$U_v = (s_x - s_y)^2 \quad (23),$$

$$U_c = 2(1 - r_{xy}) \cdot s_x s_y \quad (24),$$

where  $r_{xy}$  is Pearson's product-moment correlation coefficient, and  $s_x$  and  $s_y$  are the standard deviations of observed and forecast data respectively. The MSE can be expressed as:

$$MSE = U_b + U_v + U_c \quad (25).$$

Thus, each of the terms,  $U_b$ ,  $U_v$  and  $U_c$  may be presented in relative terms by dividing through by the MSE.

If the relationship between forecast and observed variables is assumed to be predominantly linear (it can be argued that this is true for a short range precipitation forecast derived by some form of extrapolation from an initial, observed field), it is possible to obtain two alternative MSE components representing the errors arising from relative bias ( $U_r$ ) and from what is called disturbance ( $U_d$ ). These can be expressed in the following terms:

$$U_r = (s_x - r_{xy}s_y)^2 \quad (26),$$

$$U_d = (1 - r_{xy}^2)s_y^2 \quad (27).$$

If viewed in the context of simple linear regression ( $y = mx + c$ ),  $U_b$  is a measure of that portion of the MSE arising from the constant,  $c$ . Similarly,  $U_r$  is a measure of the contribution arising as a consequence of the coefficient,  $m$ , being unequal to one. Since the sum of the  $U_b$  and  $U_r$  terms gives the fraction of the MSE that can be explained by fitting the optimal linear correction, the remainder,  $U_d$ , can be interpreted as the non-linear error component. The sum of  $U_d$  and  $U_r$  is equivalent to the sum of  $U_v$  and  $U_c$  and so the MSE is also equal to the sum of  $U_b$ ,  $U_r$  and  $U_d$ .

One can envisage a range of hypothetical situations that demonstrate the relative importance of the error components,  $U_b$ ,  $U_r$  and  $U_d$ . These are summarised in Table 6.

**Table 6 Error Component Analysis for a range of hypothetical relationships between observed and predicted precipitation fields.**

Relationship between observed (obs) and forecast (for) fields	MSE	$U_b$ contribution	$U_r$ contribution	$U_d$ contribution
for = obs	zero	no	no	no
for = obs + c	non-zero	yes	no	no
$\overline{for} = \overline{obs}$ but $s_{for} \neq s_{obs}$	non-zero	no	yes	no
for = obs $\times$ m	non-zero	yes	yes	no
for = obs <sup>2.5</sup>	non-zero	yes	yes	yes

When forecast and observed fields are identical, it is self evident that all error components will be zero. However, if one envisages an artificial scenario in which each forecast rain rate or accumulation is equal to its corresponding observed value plus some constant,  $c$ , then the MSE is solely attributable to the absolute bias,  $U_b$  (a difference between the means of the two variables).

If instead each forecast value equates to some fixed multiple of the observed value both the absolute ( $U_b$ ) and relative ( $U_r$ ) biases contribute to the MSE. A somewhat less obvious condition arises when forecast and observed fields differ in such a way that their means remain constant, but their standard deviations differ. In this instance, it is the relative bias alone that accounts for the MSE.

Of course, in the real world, the error in a forecast of precipitation rate or accumulation is likely to comprise all three error components:  $U_b$ ,  $U_r$ , and  $U_d$ . The disturbance  $U_d$  represents that portion of the error that is non-linear. Forecast timing errors tend to be non-linear in nature and thus will make a contribution to  $U_d$ . At a more fundamental level, the processes involved in the development and decay of convective precipitation are also highly non-linear. Consequently, one would expect  $U_d$  to make a significant contribution to forecast error, particularly at longer lead times when the effects of any timing errors will be magnified.

#### 4.4.3 River catchments used for model validation

Rather than validate model performance over an arbitrarily defined area or areas within the *Chenies domain*, Thames Region requested that the Met. Office assess the performance of the OOM, LFM and Nimrod over 19 river sub-catchments within the *Thames Domain*. These sub-catchments are listed in Table 7. Many of them are urbanised or semi-urbanised, and therefore contain water courses that respond rapidly to intense rainfall.

**Table 7 River sub-catchments in the Agency's Thames region used for the purposes of OOM validation.**

Catchment number	Catchment name	Area / km <sup>2</sup>	Size / 2 km pixels
0	All sub-catchments	650.0	281
1	Mimmshall Brook	53.4	21
2	Towncroft Lane, Orpington	6.2	4
3	Elmers End Road	7.2	6
4	Longley Road Recorder	22.2	11
5	West Barnes Lane	18.4	11
6	Wimbledon Common	42.8	18
7	Yeading West	19.6	13
8	Yeading East	9.6	6
9	Colindeep Lane	32.8	15
10	Chipping Ongar	67.4	22
11	Sewardstone Road	38.2	16
12	Luton Hoo	77	28
13	Gypsy Lane	26.4	12
14	Albany Park	44.0	17
15	Edmonton Green	24.8	14
16	Silver Street	48.6	23
17	Bretons Park	52.6	19
18	Gaynes Park	52.8	20
19	Bromley South Recorder	6.0	5

Unfortunately, there is a fundamental problem with validating the predictions of the OOM, LFM and Nimrod over small catchment areas: as the catchment size decreases, so the number of forecasts must be increased to provide a large enough data sample (effectively, the number of model runs multiplied by the size of the catchment area in pixels) with which to demonstrate statistically significant behaviour. Thus, for the same number of model runs, the model performance assessed over a large catchment area will be statistically more reliable than one measured over a small catchment area. If the catchment size is reduced to a point where it is less than the resolution of the forecast field (in this case 4 km<sup>2</sup>) the measurement of model performance becomes indeterminate since the location of a given forecast pixel (2 km pixel for precipitation forecasts) cannot be known with sufficient precision ( $\pm \sqrt{2}$  km for precipitation forecasts).

In the light of the above problem, it is worth noting that some of the smaller sub-catchments listed in Table 7 (e.g. Bromley South Recorder, and Towncroft Lane, Orpington) are of a size approaching the resolution of the precipitation forecasts. For this reason, the figures and discussion in Section 4.5.4.5 are largely based upon statistics compiled for “All sub-catchments” – an artificial catchment incorporating the 19 sub-catchments listed in the Table.

## **4.5 OOM, Nimrod and LFM case studies**

### **4.5.1 Overview**

As mentioned in Section 4.4.2, there are two, quite different approaches commonly used to assess the performance of precipitation forecasts. One involves a qualitative description and comparison of time synchronous observed and predicted precipitation fields. The other employs a range of statistical tools to arrive at a quantitative measure of forecast performance. Each approach has its advantages and disadvantages, and neither should be used in isolation if one is to gain a true picture of model behaviour. In the following sub-sections therefore, both approaches are employed to elucidate the strengths and weaknesses of the OOM, LFM and Nimrod.

### **4.5.2 Summer 1994**

#### *4.5.2.1 Overview*

During the first year of the Thunderstorm Warning Project there were a number of significant convective events that occurred in Thames Region prior to the full development of the GANDOLF system. Rather than exclude these important cases from the validation exercise, the System was designed to run in both real time and archive modes, thereby allowing the OOM to be run on archived data. The performance of the OOM during two such events is examined here.

The first event is an example of organised severe convection associated with a MCS (24 June 1994); the second is a case of disorganised, non-frontal convection that caused flooding in central London (10-11 August 1994). The performance of the OOM on these two occasions was reviewed in earlier Project Interim and Progress Reports. The validation statistics presented in Sections 4.5.2.2 and 4.5.2.3 below differ somewhat from those described in Section 4.5.2.5, for the reason that they were produced by staff in the Forecast Research division of the Met. Office. Precipitation forecasts from the FRONTIERS and the LFM were unavailable in both cases. Consequently, a comparison of OOM performance with that of FRONTIERS and the LFM is not possible.

#### *4.5.2.2 Mesoscale Convective System (MCS): 24 June 1994*

During the evening of 24 June 1994 a Mesoscale Convective System (MCS) moved north-eastward across south-east England. It exhibited many of the features noted by Browning and Hill (1984) in their study of an MCS over the UK. The origin of the system was traced to a convergence zone that formed over the Channel Islands and Brittany early in the afternoon. Scattered convective cells, first observed over the Channel Islands between 12Z and 13Z, subsequently merged into a vigorous, organised, rapidly expanding cluster of cumulo-nimbus clouds. By early evening this MCS had moved into south-east England whence it continued its

steady north-eastward progress across East Anglia and out over the North Sea. The strength of the convection and the change of the wind direction with height indicated that the case would be a good test for the OO forecast scheme.

Figures 16, 17 and 18 show T+12 hour predictions of  $T_L$ , CAPE, and  $H_R$  from the 0600 GMT run of the MM on the 24 June 1994. CAPE values of more than  $1000 \text{ J Kg}^{-1}$  were diagnosed for the south-east of England, indicating the potential severity of any realised convection. Helicity values associated with the centre of the MCS (to the south of the Isle of Wight at 1800 GMT) were predicted to be about  $50 \text{ m}^2\text{s}^{-2}$ , suggesting significant vertical wind shear. Lagrangian decorrelation times ( $T_L$ ) of approximately 114 minutes (using (16)) were predicted for the same area.

As described in Section 3.6.4, the ratio of CAPE to helicity has been shown to be correlated with the longevity of individual convective cells. Consequently, an empirical relationship may be derived between CAPE/helicity and  $T_L$  (the relationship between  $T_L$  and  $H_R$  was not explored in this case study). This can be employed to estimate the maximum useful range of an extrapolation-based precipitation forecast, such as that produced by FRONTIERS. The validity of such a technique appears to be borne out by the performance statistics presented in Figure 19.

Figure 19 compares the spatial performance of precipitation forecasts made by FRONTIERS and the OOM over a four hour period on the 24 June 1994. The three graphs summarise model performance (in terms of CSI) as a function of forecast lead time, and data time. From the MM predicted value of  $T_L$  given above, one would expect the maximum useful range of FRONTIERS precipitation forecasts to be a little under two hours. If the OOM is able to model the growth of new convective cells effectively, one should expect to find it outperforming FRONTIERS beyond two hours. These two expectations are largely confirmed by the statistics presented.

Considered in isolation, Figure 19 might give a misleading impression of OOM performance. It is important to recognise that the development of large areas of well organised convection, such as occurred on 24 June 1994, is a rare event. In more typical convective rainfall situations, where the convection is less well organised and shorter lived, the benefits of an OO scheme are more obvious. With its high temporal resolution (ten minutes), the OOM can simulate the growth and decay of individual convective cells. This capability is beyond the scope of FRONTIERS, both owing to its inability to grow or decay areas of rainfall, and its poor temporal resolution.

#### *4.5.2.3 Disorganised convective: 10-11 August 1994*

The disorganised convective activity which led to localised flooding in London on 10 and 11 August 1994, is more typical of the sort of scenario that the OOM was designed to address. On both days, an almost stagnant, convectively unstable air mass lay over the south-east of the England. Owing to the lightness of the steering level winds, convective cells tended to move very slowly and erratically, making this occasion a particularly challenging one for the OOM. Locally very intense rain rates and significant accumulations were observed during the evening of 10 August 1994 and the following morning. Thus, model runs for the periods 1800 to 2200 GMT on 10 August 1994, and 0600 to 1000 GMT on the 11 August 1994 are considered

below. The catchments chosen for the purposes of model validation are those summarised in Table 7.

Within each of the periods of interest, observed half-hourly rainfall totals were calculated for each sub-catchment, from Chenies 5 minute, 2 km, surface beam radar data. These were compared with those independently calculated by Thames Region and agreed within the limits of rounding error. Measurable rain fell in all of the sub-catchments at some time during the study periods. However, there was a large degree of variability between catchments, with some receiving considerably more than others.

OOM performance was assessed on a catchment by catchment basis, using a combination of mean and root mean square error statistics. Table 8 summarises the performance of the OOM's half hourly predicted accumulations over all catchments as a function of lead time. The lead time minutes refer to the start of an accumulation period. For example, a T+10 minute prediction for the period 2000 to 2030 GMT refers to the OOM forecast made from data at 1950 GMT.

**Table 8 OOM forecast errors as a function of lead time on 10–11 August 1994**

Lead time (in minutes)	Mean error (in mm)	Root Mean Square Error (in mm)
0	-0.03	0.93
10	-0.03	1.03
20	-0.02	1.44
30	0.01	1.36
40	-0.03	1.30
50	0.08	1.88
60	-0.03	1.53
70	-0.03	1.43
80	-0.06	1.73
90	-0.05	1.60
100	-0.07	1.51
110	-0.10	1.45
120	-0.02	1.54
130	-0.12	1.57
140	-0.10	1.53
150	-0.07	1.55

The Mean Error column in Table 8 indicates no significant bias in the OOM forecasts. However, one must be careful when interpreting such a result, because the calculations include many correct forecasts of no or very small amounts of rain in the catchments. More important is the variation in RMSE with lead time. This increases quickly up to T+20. Thereafter it fluctuates between 1.36 and 1.88, until the end of forecast period when there is a tendency for the error to settle at around 1.55.

Local maxima of RMSE are evident at lead times of T+20, T+50 and T+80. One possible explanation for this stems from the behaviour of the conceptual model. The first daughter cells start to produce new areas of precipitation at T+20. Thirty minutes later, at T+50, these daughter cells are assumed to have evolved into mature storms which can, in turn, produce more daughters. This cycle is repeated by T+80. The increase in RMSE at T+20, T+50 and

T+80 may point to a need to improve the treatment of daughter cells. After T+80, cells analysed at T+0 are starting to disappear, thus compensating for any new development. This may explain the levelling out of the RMSE. At T+0 and T+10 the RMSE is very similar. This suggests that, on average, forecasts are going to deteriorate beyond T+10, but may retain some usefulness out to T+150.

The main requirement of the OOM is to provide timely and accurate warnings of high rainfall accumulations. In order to examine such occurrences, and to make the verification as objective as possible, the half-hourly accumulations for each catchment for each day were examined. Those with highest values in excess of 5 mm/2 km square were identified as high rainfall periods. The figure of 5 mm/2 km square was chosen as a threshold because hourly accumulations exceeding 10 mm/2 km square are considered by Thames Region to be liable to produce an emergency. On 10 August 1994, half hourly accumulations of 10 mm were exceeded in catchments 2, 5, and 17. Overall, 12 periods of high rainfall were identified for verification. Catchments 10, 16 and 17 only received high rainfall on 10 August. The southern catchments were affected on 11 August.

Individual half-hourly rainfall accumulation forecasts for each of the 12 periods are shown in Figures 20 to 23. The observed accumulation has been plotted as a dashed line for comparison. All of these forecasts under-predicted the amount of rain, though by varying amounts. They also show a tendency towards decreasing accuracy with increasing lead time, although in several cases some of the longer range forecasts were more accurate than those made earlier, for example, Elmers End Road in Figure 20 and Bromley South in Figure 23. Some forecasts maintain small errors out to relatively long lead times. For example, the forecasts for West Barnes in Figure 21 were quite accurate out to T+50. However, the accuracy of other forecasts fell off quickly beyond T+10, notably for Towncroft Lane and Bromley South in Figure 20. The forecasts for Edmonton Green and Silver Street (in Figure 22) were consistently poor, even at T+0.

The errors of all the forecasts have been summarised in Figure 24. The graphs show that the mean error increases with lead time up to T+80 after which it remains fairly constant. Beyond T+20 the standard deviation of error varies little. Consequently, the RMSE reflects the distribution of mean errors. These show a steady increase from T+0 to T+80, but little change thereafter out to T+150. These results are substantially different from those presented earlier (all forecasts in all catchments).

The tendency is to under predict the rainfall by increasing amounts at longer ranges. The levelling out of the graphs beyond T+80 must be treated with caution. The average observed accumulation was 8.23 mm/2 km square and so the mean error can never fall below the -8.23 ordinate in this sample. However, what one can say is that by T+80, forecasts are almost as bad as is possible. Hence, their usefulness in terms of catchment specific rainfall predictions is extremely doubtful at lead times beyond T+80.

The value of the OOM forecasts discussed above depends to a great extent on expectation and how the rainfall predictions compare with others produced by different methods (e.g. Nimrod, LFM). In the absence of forecasts from other models, the following rule of thumb should be used as a guide. If one is seeking to predict occasions when the rainfall accumulation will exceed 5 mm/2 km square, then one should be looking for RMSEs that are at least less than 5 mm/2 km square. In this case study, only forecasts with lead times in the range T+0 to T+20



satisfied the aforementioned criterion. However, forecasts up to T+80 may provide some useful tendencies.

### **4.5.3 Summer 1995**

#### *4.5.3.1 Overview*

The summer of 1995 was a particular dry one. In all, three convective events were examined: 10 July 1995, and 26-27 July 1995. Only one of these cases was truly suitable for assessing OOM performance (27 July 1995); the others were associated with frontal or trough activity. For this reason, the results from this first operational trial of the GANDOLF system are not discussed separately here. However, the 27 July 1995 event has been included in the average performance statistics discussed in Section 4.5.4.5

### **4.5.4 Summer 1996**

#### *4.5.4.1 Overview*

In marked contrast to the summer of 1995, the incidence of convective activity in the south-east of England during the following summer was high. Non-frontal convective precipitation fell somewhere in Thames Region on 29 days during the five month trial. Four of these days were of particular concern to the Agency because they produced significant accumulations in flood prone, urbanised or semi-urbanised catchments. A complete list of event dates is shown in Table 9.

The statistics used to validate model performance over the summer of 1996 have been described in Section 4.4.2. They are more comprehensive than those used to assess forecast accuracy in earlier case studies (see Sections 4.5.2 and 4.5.3). On each day with convective precipitation, OOM, LFM, and Nimrod 15 minute accumulation forecasts were used in conjunction with time synchronous, radar-based estimates of observed 15 minute accumulation, to generate performance statistics for the twenty catchments listed in Table 7. In addition, average performance statistics for each event, and over all non-frontal convective days have been calculated (see Section 4.5.4.5).

Preliminary assessment of comparative model performance over the summer of 1996 was based upon three of the four special interest cases mentioned above. These were 7 June, 23 July, and 25 August 1996. A discursive account of the performance of the OOM and Nimrod on these dates is reproduced here in Sections 4.5.4.2-4. Their inclusion in this final technical report is intended to afford the reader with specific examples of comparative model performance in a range of different convective situations. The weaknesses and strengths of each model can then be highlighted.

In addition to these cases studies, average statistical performance of the OOM, LFM and Nimrod over all non-frontal convective events is discussed in Section 4.5.4.5.

**Table 9 Days when convective precipitation fell in the Agency's Thames region**

Dates
20-21 May 1996
7, 22 June 1996
1-2, 4-8, 22-24, 28-29 July 1996
1, 7, 10-12, 20, 22-28 August 1996

*4.5.4.2 Strong convection with strong steering level winds: 23 July 1996*

Figure 25 shows the surface synoptic situation for 0000 GMT on 23 July 1996. In the early hours of the morning, a thundery trough moved northwards across the English Channel into southern England. A cold front lying to the west of Wales was almost stationary, maintaining a warm, humid southerly flow across England and Wales. The synoptic situation has some superficial similarities to that of 7 June 1996 (Section 4.5.4.4). However, in this instance the presence of a well defined trough and consequent convergence triggered the widespread development of heavy convective showers.

The extent of the convective precipitation can be seen in the sequence of Chenies actuals in Figures 26. The precipitation field seems to have little apparent macroscale structure to it, except perhaps over Kent where a band of heavier rain aligned south-west to north-east can be discerned.

The OOM run for 0400 GMT on 23 July 1996 is shown in Figure 27. There is a marked tendency for the model to instantiate a large number of dissipating cells. This is indicated by the ubiquity of low precipitation intensity (blue) squares at lead times up to T+70 minutes. At longer lead times the area of low intensity ( $< 1 \text{ mm h}^{-1}$ ) precipitation appears to shrink, whilst that of high intensity ( $> 4 \text{ mm h}^{-1}$ ) precipitation increases somewhat.

A comparison between actual and predicted precipitation fields reveals that the OOM over develops the precipitation observed over Wiltshire and Gloucestershire. However, the more organised precipitation affecting Kent is moved away too quickly. The quality of the forecast at longer lead times is therefore rather poor. Again, a contributing factor was the over prediction of MM steering level wind speeds.

A very different picture emerges from the Nimrod run for the same Data Time (DT). Figure 28 clearly demonstrates the loss of detail that is the result of using 5 km resolution radar data. There is also a noticeable tendency for the model to reduce maximum precipitation intensities with increasing lead time. This behaviour may be realistic under certain meteorological conditions, but was not so in this case. As regards the shape of observed and predicted precipitation fields, Nimrod clearly fails to forecast the heavier rain over Norfolk that is apparent in the Chenies actual for 0700 GMT.

*4.5.4.3 Strong convection with light steering winds: 25 August 1996*

The surface synoptic situation for the 0000 GMT on 25 August 1996 is shown in Figure 29. It is quite different to that of the other two cases studies examined in Sections 4.5.4.2 and 4.5.4.4. On 25 August 1996 a low pressure centred just to the north-east of the Scottish mainland was feeding a cool, maritime polar air mass across the UK. Apparently disorganised

outbreaks of showery precipitation developed throughout the day, but tended to become heavier during the afternoon.

Figure 30 shows a sequence of Chenies 2 km actuals for the period 1630 GMT to 2050 GMT on 25 August 1996. As was the case on the 23 July 1996, there appears to be little overall structure to the precipitation field. Nonetheless, closer scrutiny of the image sequence does reveal that the location of some of the heavier showers seems to coincide with the high ground of the Chilterns and the Dorset downs. One particular band of showers aligned south-west to north-east along the Chilterns is seen to maintain its shape as it moves slowly eastward.

An OOM run for 1700 GMT on 25 August 1996 is displayed in Figure 31. The precipitation forecast sequence reveals the tendency observed in previous examples for the model to instantiate a significant number of dissipating cells. This is indicated by the extent of the blue ( $< 1 \text{ mm h}^{-1}$ ) squares in forecasts for lead times between T+10 minutes and T+70 minutes, and is confirmed by comparing Figure 31 with the cell stage forecasts in Figure 32.

Beyond T+70 minutes the area of predicted precipitation appears to shrink dramatically. This change coincides with the dissolution of the majority of the instantiated dissipating cells. The remaining cells are mostly young mature and mature convective cells with the potential for daughter cell development. The predicted precipitation fields for lead times between T+80 and T+180 demonstrate a pulsating behaviour. This seems to arise because the cells in the OOM forecast have synchronised life cycles. The end result of this is a simultaneous transition of cell stage and therefore of rainfall intensity. Clearly such behaviour is not realistic, and it would seem that the OOM instantiation and forecast algorithms are at fault.

A visual examination of the observed precipitation fields for the period 1700 GMT to 2000 GMT on 25 August 1996 does reveal a tendency for the area of rainfall to decrease, but not to the extent suggested by the OOM forecast. Towards the end of the period, the precipitation appears to become confined to three main areas. The OOM predicts the position of the rain on the Suffolk-Norfolk border quite well, but the heavy rain near the south coast is omitted altogether. This area developed after 1700 GMT and thus could not be forecast by the model.

The Nimrod forecast sequence for 1700 GMT on 25 August 1996 is markedly different to that of the OOM (see Figure 33). The loss of detail in the 5 km data is apparent when compared with the 2 km observed precipitation fields (Figure 30). Nimrod has a marked tendency to over predict the area of precipitation whilst under predicting the maximum precipitation rates. This bias increases with increasing lead time so that, by T+3 hours, the aerial extent of the forecast precipitation field significantly exceeds that observed.

#### *4.5.4.4 Frontal precipitation with embedded convection: 7 June 1996*

Figure 34 shows the surface synoptic situation for 0000 GMT on 7 June 1996. A cold front lying across south-west England and west Wales developed a wave and this delayed its eastward movement. At the surface, a warm, moist south to south-westerly flow affected central and southern England. The midday radiosonde ascent from Herstmonceaux showed this near surface air to be capped by a shallow temperature inversion, above which the atmosphere was potentially unstable up to the tropopause. This scenario is quite typical of those which lead to the outbreak summer thunderstorms in the south-east of England.

During the late afternoon on 7 June, scattered convective showers developed to the north and north-west of London. These grew rapidly, forming significant multi-cellular storms as they tracked north-north-eastwards at a speed of approximately  $13 \text{ m s}^{-1}$ . This is seen clearly in the Chenies surface beam radar imagery for the period 1630 GMT to 2050 GMT (Figure 35).

The OOM cell and precipitation forecasts for the DT 1650 GMT (Figures 36 and 37 respectively), identified a number of dissipating cells in the vicinity of Luton, and over the Chilterns to the south-west. At least some of these cells appear to have been associated with uncorrected anaprop and clutter. It is evident however that only a selection of the instantiated cells were analysed as having the potential for daughter cell development. Comparison of the observed and predicted precipitation fields in Figures 34 and 37 suggests that the OOM was able to distinguish between genuine and spurious dissipating cells. Those that were genuine went on to develop daughter cells, which in turn formed mature storms.

Although the model simulates the development of this pre-frontal convective precipitation quite well, its northward movement was too fast owing to the over prediction of steering level wind speeds by the MM. A comparison between observed and forecast 700 hPa winds revealed a discrepancy of about  $7 \text{ m s}^{-1}$ .

As regards the larger area of precipitation associated with the frontal wave, the spatial accuracy of the OOM forecasts deteriorates rapidly because the model cannot see precipitation beyond the range of the Chenies radar. Nimrod does not suffer from this deficiency, and therefore its spatial coverage is better at long lead times. The OOM also exhibits a tendency to mis-classify the stages of convective cells embedded in frontal systems. For this reason, its precipitation forecasts cannot be relied upon in these situations.

Figure 38 shows a Nimrod precipitation forecast for the DT 1700 GMT on 7 June 1996. The most noteworthy characteristic of this image sequence is the complete absence of precipitation in the London area. Nimrod was unable to decipher the first precipitation echoes apparent in the Chenies 2 km surface beam at 1650 GMT, presumably because the mean precipitation rate in the relevant 5 km pixel was below the minimum threshold ( $1/32 \text{ mm h}^{-1}$ ).

#### *4.5.4.5 All cases of disorganised, non-frontal convection*

Appendix B presents statistical summaries of the performance of OOM, LFM and Nimrod 15 minute accumulation forecasts over all non-frontal convective events observed during the summer of 1996. Two distinct approaches to the statistical assessment of forecast accuracy have been adopted. In the first, performance was measured at 2 km pixel resolution over each of the twenty catchments listed in Table 7. Here, the mean performance for a particular catchment, for a given lead time, is an average over all catchment pixels and all model runs. In the second approach, forecast accuracy was measured at catchment resolution, by comparing observed and predicted total accumulations for each catchment. The first approach was intended to elucidate model skill in predicting the fine structure of convective precipitation fields. The purpose of the second approach is to investigate the ability of each model to forecast catchment total accumulations over a 15 minute period.

When comparing model performance at the resolution of individual forecast pixels ( $4 \text{ km}^2$ ) the issue of statistical significance is particularly relevant. Scrutiny of the 2 km performance statistics presented in Appendix B shows the standard deviations of CSI, HR, FAR and MSE

statistics presented in Appendix B shows the standard deviations of CSI, HR, FAR and MSE to be of similar magnitude to the mean values for each sub-catchment. It is apparent that any differences between the magnitudes of the intra-sample (the variation in performance of a single model) and inter-sample (the variation in performance between the different models) variances are very small. Consequently, it is not possible to demonstrate a statistically significant difference between the performance of the models, even when average performance over a large number of events is considered.

The above conclusion does not imply that the prediction of catchment total accumulations over small areas is beyond the capability of the models. The effect of summing 2 km accumulations over an entire catchment is to smooth out some of the high resolution “noise” in the precipitation fields. Appendix B also presents summary performance statistics for the three models at catchment resolution, for each catchment, for each model lead time. The statistics computed include observed (O) and forecast (F) catchment total accumulation (expressed as a mean depth over the catchment area), the bias in forecast catchment total accumulation (F-O), and its standard deviation (SD (F-O)), catchment CSI, HR, FAR, MSE,  $U_b$ ,  $U_r$ , and  $U_d$ .

Bearing in mind the definitions of CSI, HR and FAR given in Section 4.4.2, the calculation of these indices at catchment resolution might be expected to yield the following results. For large catchments (i.e. “All sub-catchments”) the FAR is likely to be very low, or zero. In other words, there are likely to be few or no cases where precipitation was forecast somewhere in a large catchment, and not observed somewhere in it. Consequently, the corresponding HR and CSI should be high. As catchment size decreases one should expect the FAR to rise, since errors in model forecast advection speed and direction have a larger impact at smaller scales. These trends are clearly observed in Figures 39-41. The FAR for “All sub-catchments” is zero at all lead times, but for “Towncroft lane, Orpington” and “Chipping Ongar, Cripsey brook sub-catchment” it is greater than zero. In the latter cases the corresponding CSI and HR are lower.

The above observations provide an objective means of identifying a lower limit to catchment size, beyond which forecasts possess little or no spatial predictive skill. To identify this lower limit, one must first select a performance threshold below which forecast skill is assumed to be negligible. Considering CSI, which is the most rigorous of the spatial performance indices described above, a plausible threshold might be 0.3. When applied to the CSI performance statistics in Figure 39, this suggests that both Nimrod and the OOM possess significant predictive skill out to two hours, even over small catchments such as “Towncroft Lane, Orpington”. The LFM fares much less well. Over the largest sub-catchments such as “Chipping Ongar, Cripsey Brook sub-catchment” the model possesses very limited predictive skill, even at T+15 minutes. The same story is repeated for the smaller sub-catchments. This poor spatial predictive skill is largely due to forecast advection errors.

Figures 42 and 43 summarise model performance in terms of the bias and MSE of predicted catchment total accumulations. On each graph in Figure 42, a fourth bar has been added to indicate mean observed catchment accumulation at each lead time. This permits a comparison between observed accumulation and the magnitude of the bias. From the Figure it should be apparent that over all events the mean 15 minute accumulation is quite small - about 0.1 mm. Although there were some significant accumulations over individual catchments on a few occasions, these larger values are swamped by the much smaller accumulations more typically

observed. A comparison of the bias statistics for the three models reveals some important differences between them. The OOM has a tendency to over predict total accumulation at lead times less than 90 minutes. By contrast, both Nimrod and the LFM consistently under predict catchment accumulations over the same period.

Under certain conditions, the OOM has been shown to generate unrealistic numbers of Mature or Young Mature convective cells that follow time synchronised life cycles. Such behaviour may account for the systematic over prediction of accumulations in certain catchments. The under prediction of precipitation accumulations by the LFM appears to be a consequence of large errors in the advection scheme, although smoothing of the forecast precipitation fields at longer lead times is also likely to be a contributing factor. Nimrod's tendency towards under prediction can be attributed to excessive smoothing of both radar analyses and forecasts.

The MSE of catchment total accumulation is perhaps the single most important measure of model performance for the Agency. Over "All sub-catchments" in Figure 43 the LFM performs least well. The MSE for the OOM fluctuates on a half hourly cycle, elucidating problems with synchronised cell stages described earlier. Nimrod marginally out-performs the OOM at short lead times. This may be because Nimrod uses smoothed 5 km resolution radar analyses as its starting point. Such smoothing has the effect of reducing the magnitude of the largest errors between forecast and observed accumulations.

Worth a brief mention here are the relative magnitudes of the 2 km MSE components:  $U_b$ ,  $U_r$ , and  $U_d$ . A cursory examination of Appendix B reveals that the non-linear error component,  $U_d$ , makes the largest contribution to the MSE in all three models. A large non-linear error component is to be expected in a forecast of something as spatially and temporally complex as an evolving precipitation field.  $U_r$  is the next largest error component for the OOM and LFM, with  $U_b$  tending to account for the smallest fraction of the MSE. In the case of Nimrod, the relative contributions of  $U_r$  and  $U_b$  are reversed. This difference reflects differences in the way the forecast schemes of the three models modify the initial, observed convective precipitation fields with increasingly lead time.



## 5. SUMMARY AND CONCLUSIONS

Convective precipitation is of particular concern to flood forecasters, especially in urban areas where rapid surface run-off can cause flash flooding. There are two reasons for this concern. Firstly, a significant proportion of serious fluvial flood events are partly or solely a consequence of convection, whether it be in the form of showers, Mesoscale Convective Systems (MCSs) or embedded convection within frontal systems. Secondly, the spatial and temporal characteristics of convection make the deterministic prediction of convective precipitation extremely difficult. The Numerical Weather Prediction (NWP) models used in daily weather forecasting are of limited value in this context. Such models are unable to resolve convection explicitly. They must therefore resort to a statistical treatment of convective processes, which in the main, is inadequate for the purposes of flood prediction.

The current approach to fluvial flood forecasting adopted by the Agency's Thames Region relies upon precipitation forecasts produced by two rainfall radar-based nowcasting systems: the Met. Office's Nimrod system (the automated replacement for FRONTIERS), and the Institute of Hydrology's Local Forecast Model (LFM). The forecast precipitation fields thus produced are fed into computer models of catchment water balance. The latter make predictions of river discharge, and these form an integral part of Thames Region's flood warning service.

Over a number of years of operational use, Thames Region have noted certain deficiencies in the way FRONTIERS/Nimrod and the LFM handle convective precipitation. For example, the Nimrod system, with its spatial resolution of 5 km, is often unable to identify the peak rainfall intensities associated with individual convective cells. In addition, its poor temporal resolution means that it can often miss the early stages of developing thunderstorms. To some extent, the LFM avoids these problems by utilising 2 km resolution radar data and a 15 minute run cycle. However, both systems suffer from one fundamental weakness in the way they generate their forecasts.

The forecast algorithms employed by Nimrod and the LFM make use of linear extrapolation techniques, for example, cross correlation and echo centroid tracking, to predict the movement of precipitation "objects" observed in the radar analyses. Whilst such techniques can produce reliable precipitation forecasts in situations where the intensity and spatial extent of an observed precipitation field are more or less constant over time (e.g. in some frontal precipitation events), they are unable to cope with the rapid growth and decay of precipitation commonly observed in convectively unstable airmasses. What is required in these circumstances is a forecast scheme capable of predicting changes in precipitation area and intensity, as well as position.

Just such a scheme has been developed by Hand and Conway (1995) in the Met. Office. This Object-Oriented (OO) approach utilises a conceptual model of convection, in conjunction with multiple beam rainfall radar observations, and satellite derived Cloud Top Temperatures (CTTs), to identify and classify individual convective cells into one of five developmental stages. Together, these stages represent the typical life cycle of a convective cell, from birth to dissipation. Associated with each stage are pre-defined rainfall rates. The OO forecast algorithm generates a sequence of predicted precipitation fields by simultaneously advecting and evolving each identified convective cell and its accompanying precipitation, according to



this life cycle. In this way it is able to simulate, in a physically realistic fashion, changes in the size, intensity, and position of observed, convective precipitation “objects”.

With the advent of a working model based upon this OO procedure (Hand, 1995), the problem for flood forecasters in Thames Region becomes one of deciding which precipitation forecast (extrapolation or OO) should be used in any given weather situation. Such a decision is not easily made, especially in the high pressure environment of the Flood Warning Centre (FWC). It must be based upon a full and reasoned evaluation of the prevailing weather conditions, and a knowledge of how well each forecast performs under those conditions. The Thunderstorm Warning Project was initiated with the aim of developing an automated nowcasting and decision making system (GANDOLF: Generating Advanced Nowcasts for Deployment in Operational Land-based Flood forecasts) capable of performing this task.

The two fundamental design requirements of this GANDOLF system were:

- to run the Object-Oriented Model (OOM) during episodes of non-frontal convection;
- to provide Thames Region with guidance on the probable accuracy of the OOM and extrapolation forecasts.

The first of these requirements involved the development of tools capable of distinguishing convective and frontal precipitation. A range of plausible algorithms were investigated, including spatial and temporal precipitation indices, rainfall radar and CTT difference images, a Neural Network Cloud Classifier (NNCC), and a range of Mesoscale Model (MM) derived diagnostic fields. The most reliable of these algorithms proved to be one combining the output from the NNCC with MM diagnosed near surface Convectively Available Potential Energy (CAPE) and convergence. The resultant weather type diagnosis algorithm was incorporated into GANDOLF’s Warning Level System (WLS).

The WLS is responsible for issuing 5 minute warnings of heavy precipitation to Thames Region’s FWC at Waltham Cross. The aim of this sub-system is to provide guidance on the probable maximum hourly accumulation to be expected anywhere within Thames Region within the next 24 hours. The system combines the forecast information from three separate models: the MM, Nimrod and the OOM. When more than one forecast is available, the WLS decides which model is likely to be the most reliable. It uses the current weather type diagnosis algorithm described above to make this decision. The warnings issued by the System contain a coded *alert status* whose value is a function of the predicted maximum accumulation, the precipitation type (frontal or convective), and the forecast lead time.

Prior to the operational implementation of the OOM within GANDOLF, various automated data gathering and processing routines had to be coded and tested. These were completed by April 1995, permitting the first Summer trial of the OOM to commence early in May of the same year. Once underway, the emphasis of the Project switched to the provision of guidance on the reliability of the precipitation forecasts received by Thames Region. To this end, the predictability of convective rainfall radar patterns was explored using a Lagrangian persistence extrapolation technique. The aim of this work was to estimate the lead time beyond which extrapolation-based convective precipitation forecasts cease to possess significant predictive skill.

Following the approach developed by Zawadski *et al.* (1994), the Lagrangian decorrelation time ( $T_L$ ) was determined for a range of convective precipitation events (Rippon, 1995). A relationship was then established between  $T_L$  and two meteorological parameters: the modified Richardson number ( $CAPE/H_R$ ) and helicity ( $H_R$ ). These relationships were employed, in conjunction with MM derived  $CAPE/H_R$  and  $H_R$  diagnostics, to make predictions of  $T_L$  and thus to estimate the probable maximum useful range of FRONTIERS extrapolation forecasts. These  $T_L$  predictions were validated by comparing them with Mean Square Error (MSE) statistics for FRONTIERS.

The routine calculation of predicted values of  $T_L$  for the Thames Region was implemented in the GANDOLF system in June 1995. A single, representative forecast decorrelation time (in minutes) was determined for each hour of the day from MM derived hourly helicity forecasts. During periods of convection, it was intended that Agency staff treat the  $T_L$  prediction received in each OOM forecast transmission as a guide to the maximum useful range of FRONTIERS/Nimrod precipitation forecasts. For lead times beyond  $T_L$  it was recommended that the Agency use OOM forecasts in their flood prediction models. For lead times less than  $T_L$  the guidance provided by a combination of FRONTIERS/Nimrod, and the OOM was deemed more appropriate.

Although the efficacy of this forecast selection technique was confirmed in a number of case studies involving severe convection (see Rippon, 1995 and Section 4.5.2.2), this was not always the case for weak convective events. For this reason, the final operational solution to objective forecast selection in GANDOLF was to combine the use of  $T_L$  with real time validation statistics from the OOM and FRONTIERS/Nimrod. The latter comprise MSEs of 15 minute, catchment accumulations. These may be used to monitor the relative performance of extrapolation and OO models in near real time. They also afford a means of validating the accuracy of the hourly  $T_L$  forecasts produced by GANDOLF.

During the summer trials of 1995 and 1996, all convective precipitation forecasts produced by the OOM, FRONTIERS/Nimrod and LFM were archived. In addition, two previously archived events from the summer of 1994 were also considered. The summer of 1995 was largely dry, and produced insufficient data to allow a comparison of model performance. However, more than 20 days with convective precipitation were recorded the following summer, and this more than compensated for the lack of data in the first trial. Model validation was based upon a comparison of observed and forecast 15 minute accumulations. The former were derived by integrating sequences of Chenies single site, 5 minute radar actuals. Validation statistics were calculated for each model for each event. These were then combined to give an idea of average model performance over all convective events.

Model performance was assessed at two resolutions: 2 km pixel and sub-catchment resolution. In the former case, the predictive skill of all three of the models was shown to be highly variable and therefore indistinguishable in statistical terms. The validation statistics generated from the sub-catchment total accumulation forecasts were of more interest: the use of catchment totals has the effect of removing much of the noise observed in the 2 km accumulation statistics.

A comparison of sub-catchment CSI, HR and FAR for the three models (Figures 39–41) confirms the expectation that the spatial performance of all three models should decline with decreasing catchment area. However, the CSI scores for catchments such as “Towncroft lane,

Orpington” would seem to indicate that, over areas as little as 6 km<sup>2</sup>, the OOM and Nimrod still possess significant spatial predictive skill for lead times beyond one hour. This is not the case for the LFM, whose performance is generally poor at spatial resolutions of less than 100 km<sup>2</sup>.

In terms of flood prediction, the two most important measures of performance for the Agency are the bias and MSE of forecast 15 minute accumulations. The comparative performance statistics computed over “All sub-catchments” (an artificial catchment representing the amalgamation of all 19 sub-catchments) demonstrate that the LFM and Nimrod tend to under predict catchment total accumulations at all lead times. This characteristic can be attributed to the behaviour of the forecast algorithms employed by the two models. Both have a tendency to smooth forecast precipitation fields with increasing lead time. By contrast, the OOM tends to over predict accumulations at lead times up to about 75 minutes. Thereafter, the bias is generally negative.

Evidently, both negative and positive biases in predicted accumulation totals are undesirable. However, as regards the relevance of these results to flood warning, a positive bias may be preferable to a negative bias, since the impact of an unpredicted flood event, is likely to be worse than a false alarm. Furthermore, the loss of information on locally higher rainfall accumulations arising from 2 km smoothing of the precipitation field may be compensated for, at least in part, by a positive bias in a 2 km resolution forecast.

The results for catchment total MSE tell a somewhat different story to that described above for the CSI, HR and FAR. Over individual sub-catchments, the magnitudes of the MSE’s for each model vary widely with lead time. These fluctuations reflect the dominance of one or two events in the performance statistics, and are therefore unsuitable for the purposes of generalisation. However, over “All subcatchments”, where the effects of individual events are smoothed out, the LFM is shown to perform least well of the three models, in line with its poorer spatial performance discussed earlier. Of the remaining two models, Nimrod appears to perform best over lead times out to about 75 minutes. At longer range, this pattern is reversed.

The most likely explanation for Nimrod’s superior MSE performance in the short range is resolution related. The use of 5 km resolution, as opposed to 2 km resolution radar data, will have the effect of removing extreme values from the spectrum of observed and forecast catchment accumulations. As a result, the magnitudes of the largest MSEs for a 5 km resolution forecast will be smaller than for an equivalent 2 km resolution forecast.

Another possible explanation for the result described above may lie with the behaviour of the OOM. In the very short range, attempts by the OO forecast scheme to model the growth and decay of precipitation associated with individual convective cells may be less reliable than a straight forward extrapolation forecast. Whether the OO scheme can demonstrate additional predictive skill in convective situations is critically dependent on the model’s ability to classify cell stage correctly. Where cell instantiations are in error, the OOM may perform less well than an extrapolation forecast.

Evidence for mis-classification of convective cell stage can be found in the OOM catchment total MSE statistics. These show a tendency for the MSE to oscillate on a 30 minute cycle, as result of synchronised changes in convective cell life cycle. This oscillation is unrealistic and

stems from a problem with the instantiation of developing cells: specifically the determination of cell potential.

One of the principle aims of the Thunderstorm Warning Project has been the evaluation of the relative performance of extrapolation-based and OO precipitation nowcasting algorithms, the goal being to establish unequivocally whether the OOM possesses superior predictive skill during periods of non-frontal convective precipitation. Considered in isolation, the performance statistics summarised above, do not provide conclusive evidence to justify favouring the use of the OO algorithm at such times. For example, the sub-catchment MSE statistics would appear to favour the use of Nimrod. Nonetheless, when these quantitative findings are viewed in combination with the qualitative, graphical evidence from key, case study events, it is reasonable to conclude that the OOM will generally provide superior guidance to that of Nimrod and the LFM.

The reasons for this conclusion are summarised below.

- The OOM possesses superior spatial and temporal resolution to that of Nimrod (2 km versus 5 km spatial resolution; 10 minute versus 30 minute run cycle) and superior temporal resolution to that of the LFM (10 minute versus 15 minute run cycle). It can therefore provide more reliable early warnings of impending heavy convective precipitation, regardless of the magnitude of subsequent errors in the forecast guidance. Whilst the LFM possesses comparable spatial resolution it does not possess the ability to model the growth of existing precipitation areas in a physically realistic fashion, or to develop new areas of precipitation (daughter cell development).
- In terms of spatial predictive skill (sub-catchment CSI, HR, and FAR), OOM performance is generally superior or comparable to that of the LFM and Nimrod for lead times out to about 60 minutes (see “All sub-catchments”, Figure 39-41). Although its performance at longer lead times tends to fall off quite rapidly, this characteristic does not impact on its value as a short range, early warning and nowcasting system.
- In terms of 15 minute sub-catchment total accumulations, OOM forecasts demonstrate comparable performance in terms of MSE (see “All sub-catchments” in Figure 43), whilst generally affording a positive as opposed to a negative bias (Figure 42) at lead times out to about 75 minutes. Beyond T+75 minutes, the performance of the OOM does not appear to deteriorate quite as rapidly as that of Nimrod or the LFM. Indeed, there is evidence that in certain, rare cases of organised mesoscale convection, the OO scheme is capable of outperforming extrapolation forecasts at lead times out to T+3 hours.



## 6. RECOMMENDATIONS

The summer trials of 1995 and 1996 trial have shown the GANDOLF system to be capable of 24 hour, standalone operation. In addition, the case study events and performance statistics presented in Section 4 suggest that, in the short range (up to T+75 minutes), Object-Oriented Model (OOM) performance is generally equivalent or superior to that of the Local Forecast Model (LFM) and Nimrod during periods of non-frontal convection. Nonetheless, the System was not without fault, and a re-structuring and rationalisation of code would be advisable if GANDOLF is to be used on a routine operational basis. Some examples of System inefficiency are given below.

- When the OOM was coded little thought was paid to the sizes of the output files generated. At present, the model generates 18 Instantaneous Rain Rate (IRR) precipitation forecasts, 12 accumulation forecasts, one cell instantiation and 18 cell forecasts each time it is run. The files containing cell information are currently output as ASCII text. As a result they occupy more hard disk space than is necessary.
- In the current GANDOLF system, Mesoscale Model (MM) diagnostic fields such as vorticity are computed twice, once for the Warning Level System (WLS) and once for the OOM. This is clearly inefficient. The most sensible solution would be to compute all MM diagnostics in Level 1 of GANDOLF. These would then be accessible to both the WLS and OOM when required.
- GANDOLF comprises software modules written in four different programming languages: PV-WAVE, FORTRAN 77, FORTRAN 90 and UNIX. The communications and data gathering software are coded in UNIX shell script. FORTRAN 77 and FORTRAN 90 are used for the OOM, and for the data reformatting software. PV-WAVE has been employed for the implementation of the WLS and other experimental components of GANDOLF, the reason being that it is quick to write. It also provides a visualisation capability that is of great value during the development phase of a project.

The performance and robustness of the GANDOLF system would undoubtedly be improved if the above-mentioned inefficiencies and complications were addressed. It is recommended that these changes be undertaken prior to any full operational implementation of the system.

The summer trials have demonstrated scope for improving:

- the life cycle model;
- the determination of cell potential;
- the thresholds of convergence and relative vorticity required for new cell development.

In addition, System performance could be enhanced by the implementation of new conceptual models to represent different precipitation profiles more precisely. Further benefits might be obtained by combining this approach with stochastic forecasting methods.

Improved vertical resolution from volume scan data and additional information from polarisation diversity data offer an enhanced capability to identify and distinguish convective cell stages. Such information could also aid in the development of more detailed conceptual models. The use of Doppler radar data offers the potential for improving forecast accuracy, and reducing the dependency of the OOM forecast algorithm on output from the Met. Office's Unified Model. Doppler and polarisation diversity data may also permit the generation of new GANDOLF products with commercial potential.

GANDOLF is currently undergoing another six month trial (May to October, 1997). This should allow Thames Region to further inspect the various outputs from the System, and conduct their own validation of its performance. The future of GANDOLF will depend upon this final assessment.

Should Thames Region wish to continue receiving OOM forecast products, the following issues must be considered prior to the implementation of an operational service:

- the deliverables required and their use in flood prediction;
- the restructuring of System code to improve performance;
- the mode of System operation (standalone or integrated in Nimrod);
- the costs involved in the above.

It is recommended that each of these topics be examined jointly by the Met. Office and the Agency in November 1997.

## **7. OPERATIONAL DEVELOPMENT**

The flexibility of GANDOLF allows the system to be developed for operations in either a standalone mode, operating for a specific radar(s), or as part of a wider nowcasting system, such as Nimrod, as a convective forecast product. The relative benefits are presented below.

### **7.1 Standalone Mode**

At present the prototype operational system is connected to the Met Office's Central Data Network (CDN). Through this connection GANDOLF can receive all Met. Office observational data and NWP model fields. The latter are used extensively by the OOM forecast algorithm. With an alternative source to the Met. Office NWP output, the GANDOLF system could potentially be run directly from a single radar. Doppler and polarisation diversity measurements offer such a capability. However, given the current functionality of the UK radar network, the predictive capabilities of a standalone system would probably be very limited in most convective weather situations.

The development of the GANDOLF system to operate in a standalone mode would require Doppler radar data and information from satellite observations. The OOM would then need to be adapted accordingly. Satellite data are readily available through PDUS receiver systems, and most present day radars have a Doppler capability. The ability of GANDOLF to operate independent of NWP fields would need to be demonstrated and evaluated before such a standalone system could be put forward for operational use. If the system was shown to afford sufficient forecast skill, then there could be an international market for its commercial development, enabling the recovery of the initial financial investment. The commercial potential of such a system may in itself provide sufficient impetus for the development of a standalone version of GANDOLF, independently of any integrated approach.

### **7.2 Integrated Mode**

Integrating GANDOLF into the Nimrod system has numerous advantages over the standalone approach. It would:

- ensure that Nimrod quality control procedures are applied to the radar data;
- allow access to synoptic observations, satellite data and MM fields directly;
- permit the generation of OOM forecasts on any or all of the radars in the network.

For operational use in Nimrod, GANDOLF would have to be integrated into the Nimrod operational cycle from its current development platform.





## **8. ACKNOWLEDGEMENTS**

A debt of gratitude is owed to Professor Chris Collier, Director of the Telford Institute of Environmental Systems at the University of Salford. Professor Collier initiated the Project, and on leaving the Met. Office, has continued to play an active role in helping guide this study. Thanks are also due to the team at Thames Region, in particular Martin Crees for his support throughout the project, and to Will Hand and Ewan Archibald from the Met. Office for their significant contributions to this work. We are grateful to the Thunderstorm Warning Project Steering Group including Chris Haggett (Agency Project Manager, Thames Region), Martin Crees (Thames Region), Jenny Soggee (Thames Region), Nicky Bailey (Thames Region), Bryony May (Anglian Region), Mike Knowles (North West Region), Tim Harrison (Midlands Region), Dan Cadman (Welsh Region) and Chris Collier (University of Salford).



## 9. REFERENCES

- Atkinson, B.W. and Smithson, R.A. 1976. "Precipitation", in *The Climate of the British Isles*, Chandler, T.J. and Gregory, S. (Ed), Longman (London), 163-182.
- Austin, G.L. and Bellon, A. 1974. The use of digital weather records for short-term precipitation forecasting. *Quart. J. Roy. Met. Soc.*, **100**, 658-664.
- Ballard, S.P., R. Robinson, R. T. H. Barnes, S. Jackson and S. Woltering, 1993: Development and performance of the new mesoscale model. *Meteorological Office, Forecasting Research Division Tech. Rep. No.40*, 67 pp. (Available from the National Meteorological Library, Bracknell, Berkshire, RG12 2SZ, UK.)
- Bellon, A. and Austin, G.L. 1984. The accuracy of short-term rainfall forecasts, *J. Hydrol.*, **70**, 35-49.
- Bendat, J.S. and Piersol, A.G. 1966. *Measurements and Analysis of Random Data*. Wiley, New York. Chapter 9.
- Bennetts, D., E. McCallum and J. R. Grant, 1986: Cumulonimbus clouds, an introductory review. *Meteor. Mag.*, **115**, 242-256.
- Brown, R., G. P. Sargent, P. D. Newcomb, J. Cheung-Lee and P. M. Brown, 1991: Development of the FRONTIERS precipitation nowcasting system to use mesoscale model products. *Proc. Int. Conf. on Radar Meteorology*, Paris, Amer. Meteor. Soc., 79-82.
- Browning, K.A. 1990. "Organization and internal structure of synoptic and mesoscale precipitation systems in midlatitudes", Chapter 26a in *Radar in Meteorology*, editor D. Atlas, publ. Amer. Met. Soc., Boston, 433-460.
- Browning, K.A. and Hill, F.F. 1984. Structure and evolution of a Mesoscale Convective System near the British Isles. *Quart. J. Roy. Met. Soc.*, **110**, 897-913.
- Cheng, M. and Brown, R. 1993. Estimation of area-average rainfall for frontal rain using the threshold method. *Quart. J. Roy. Met. Soc.*, **119**, 825-844.
- Chisholm, A.J. and Renick, J.H. 1972. The kinematics of multi-cell and supercell Alberta hail storms. Alberta Hail Studies, 1972, Res. Council of Alberta Hail Studies Rep. No. 72-2, 24-31.
- Coad, P., and E. Yourdon, 1991a: Object-oriented Analysis. Yourdon Press/Prentice Hall, 255 pp. : Englewood Cliffs, NJ.
- Collier, C.G., Lilley R.B.E. 1994. Forecasting thunderstorm initiation in north-west Europe using thermodynamic indices, satellite and radar data. *Met. Apps.*, **1**, 75-84.
- Collier, C.G., Hardaker, P.J., Pierce, C.E., Rippon, J., Cluckie, I.D. and Han, D. 1995. The use of life-cycle models of convective systems in forecasting heavy rainfall. *Proc. 3<sup>rd</sup> Inter. Symp. on Hydrol. Appl. of Weather Radar*, São Paulo, Brazil, 477-487.

- Conway B.J., 1992: Current developments in very short range weather forecasting. Appendix 5 of Report of the Meeting of the CAS Group of Rapporteurs on Short Range Weather prediction Research, PWPR No. 1, WMO/TD No. 479, 33pp.
- Conway, B.J., Browning K.A. 1988. Weather forecasting by interactive analysis of radar and satellite imagery. *Phil. Trans. R. Soc.*, London, **A324**, 299-315.
- Cullen, M.J.P. 1993. The unified forecast/climate model. *Met. Mag.*, **122**, No 1449, 81-94.
- Davies-Jones, R., Burgess, D. and Foster M. 1990. Test of Helicity as a tornado forecast parameter, *Prepr. 16<sup>th</sup> Conf. Severe Local Storms*, Alberta, Amer. Met. Soc., 588-592.
- Doswell, C.A. III. 1982. The Operational Meteorology of Convective Weather, Volume I: Operational Mesoanalysis NOAA Tech. Memo. NWS NSSFC-5.
- Doswell, C.A. III. 1985. The Operational Meteorology of Convective Weather, Volume II: Storm Scale Analysis, NOAA, Tech. Memo ERL ESG-15, 240pp.
- Doswell, C.A. III, Brooks, H.E. and Maddox, R.A. 1996. Flash flood forecasting: an ingredients-based methodology. *Wea. and Forecasting*, **11**, 560-581.
- Emanuel, K.A. 1994. *Atmospheric Convection*, OUP, New York, 580pp.
- FOAG. 1992. Evaluation of FRONTIERS Forecast Precipitation Accumulation Final Report. March, Met. Office/NRA.
- FOAG. 1993. FRONTIER' Evaluation of Radar-Based Rainfall and River Flow Forecasts, April 1992 to March 1993. Met. Office/NRA, 122pp.
- Golding, B. 1997. Nimrod: a system for generating automatic very-short-range forecasts. To appear in *Met. Apps.*
- Hand, W.H. and Conway, B.J. 1995. An object-oriented approach to nowcasting showers. *Wea. and Forecasting*, **10**, 327-341.
- Hand, W.H. 1996. A technique for nowcasting heavy showers and thunderstorms. *Met. Apps.*, **3**, 31-41.
- Hardaker, P.J. and Auer, A.H. Jr. 1995. The separation of rain and hail using single polarisation radar echoes and IR cloud top temperature. *Met. Apps.*, **1**, 201-204.
- Hardaker, P.J., Holt, A.R. and Collier, C.G. 1995. A melting-layer model and its use in correcting for the bright band in single-polarization radar echoes. *Quart. J. Roy. Met. Soc.*, **121**, 495-525.
- Harrold, T.W. and Browning K.A. 1971. Identification of preferred areas of shower development by means of high power radar. *Quart. J. Roy. Met. Soc.*, **97**, 330-339.

- Henry S.G. 1995. Evaluation of automated, short-term thunderstorm forecast rules. *Proc. 6<sup>th</sup> Conf. on Aviation Weather Systems.*, Dallas, Texas, Amer. Meteor. Soc., Jan., 83-88.
- Kessler E. 1975. On the condensed water mass in rising air. *Pure Appl. Geophys.*, **113**, 971-981.
- Knight, C.A. and Miller L.J. 1993. First radar echoes from cumulus clouds. *Bull. Amer. Met. Soc.*, **74**, No. 2, 179-188.
- Kummerow, C., Hakkarinen, I.M., Pierce, H.F. and Weinman, J.A. (1991). "Determination of precipitation profiles from airborne passive microwave radiometric measurements", *J. Atmos. Ocean. Tech.*, **8**, 148-158.
- Lee, B.D., Farley, R.D. and Hjelmfelt, M.R. 1991. A numerical case study of convection initiation along colliding convergence boundaries in north-east Colorado. *J. Atmos. Sci.*, **48**, 2350-2366.
- Leftwich, P.W. Jr. 1990. On the use of Helicity in operational assessment of severe local storm potential. *Prepr. 16<sup>th</sup> Conf. Severe Local Storms*, Alberta, Amer. Met. Soc., 306-310.
- Lilly, D.K. 1986. The structure, energetics and propagation of rotating convective storms. Part II: helicity and storm stabilization. *J. Atmos. Sci.*, **43**, 126-140.
- Lorenz, E.N. 1969. The predictability of a flow which possesses many scales of motions. *Tellus*, **21**, 289-307.
- Mahoney W.P., 1988: Gust front characteristics and the kinematics associated with interacting thunderstorms and outflows. *Mon. Wea. Rev.*, **116**, No 6, 1474-1491.
- Mason, B. J. 1971. *The Physics of Clouds (2<sup>nd</sup> ed.)*. Oxford University Press., 671pp.
- Moncrieff, M.W. and Green, J.S.A. 1972. The propagation and transfer properties of steady convective overturning in shear. *Quart. J. Roy. Met. Soc.*, **98**, 336-352.
- Moore, R.J., Hotchkiss, D.S., Kones, D.A. and Black, K.B. 1991 (updated November 1992). London Weather Radar Local Rainfall Forecasting Study, Report to NRA Thames Region, NERC, Institute of Hydrology, 129pp.
- NDG WP8. Nowcasting Development Group Working Paper number 8, "Unformatted transfer of data between a VAX and a SUN workstation" by D Goddard.
- NDG WP26. Nowcasting Development Group Working Paper number 26, "The NDG header format for image and model data files" by W.H. Hand.
- NERC. 1975. Flood studies report. Natural Environment Research Council, Department of Environment, London, Five Volumes.
- Pamment, J.A. 1990. Automated calculation of atmospheric instability indices and other thermodynamic variables, Nowcast. Dev. Group, Tech. Note 15, Met. Office, 44 pp.

Pamment, J.A. and Conway, B.J. 1997. Objective identification of echoes due to anomalous propagation in weather radar data. To appear in *J. Atmos. Ocean. Tech.*

Pankiewicz, G.S. 1995. Pattern recognition techniques for the identification of cloud and cloud systems. *Met Apps.*, **2**, 257-271.

Pierce, C.E., Collier, C.G., Hardaker, P.J. and Rippon, J. (1996). Thunderstorm warning (GANDOLF project): Interim Report. Jan., Met. Office, Bracknell, 61pp.

Purdom, J.F.W. 1982. "Subjective interpretations of Geostationary satellite data for nowcasting", in Nowcasting, editor K.A. Browning, publ. Academic Press, 149-166.

Rippon, J. 1995. Estimating limits of forecast lead-times in an operational flood forecast system. MSc Thesis, Dept. of Geog., Univ. of Birmingham, Sept., 84pp.

Tao, W-K, Simpson J., Sui, C-H., Ferrier, B., Long, S., Scala, J., Chou, M-O. and Pickering, K. 1993. Heating, moisture and water budgets of tropical and mid-latitude squall lines: comparisons and sensitivity to longwave radiation. *J. Atmos. Sci.*, **50**, No. 5, 673-690.

Thiel, H. 1971. Applied econometric forecasting. *Studies in Mathematical and Managerial Economics*, **4**, 26-36.

TN26. FRONTIERS development group, Technical Note number 26, "Satellite Parallax" by M. Cheng.

Weisman, M.L. and Klemp, J.B. 1982. The dependence of numerically simulated convective storms on vertical wind shear and buoyancy. *Mon. Wea. Rev.*, **110**, 504-520.

Wilson, J. W., and C. K. Mueller, 1993: Nowcasts of thunderstorm initiation and evolution. *Wea. Forecasting*, **8**, 113-131.

Woodall, G.R. 1990. Qualitative forecasting of tornadic activity using storm-relative environmental Helicity. *Prepr. 16<sup>th</sup> Conf. Severe Local Storms*, Alberta, Amer. Met. Soc., 311-315.

Young, K.C. 1993. *Microphysical processes in clouds*. New York: Oxford University Press., 427pp.

Young, M.V., 1995: Severe thunderstorms over southeast England on 24 June 1994: A forecasting perspective. *Due to be published in Weather*.

Zawadzki, I. 1973. Statistical properties of precipitation patterns. *J. App. Met.*, **12**, 459-472.

Zawadzki, I. and Rô, C.U. 1978. Correlations between maximum rate of precipitation and mesoscale parameters. *J. Appl. Meteor.*, **17**, 1327-1334.

Zawadzki, I., Morneau, J. and Laprise, R. 1994. Predictability of precipitation patterns: An operational approach. *J. App. Met.*, **33**, 1562-1571.

The prototype GANDOLF system

### LEVEL 1 : Monitor

- Data gathering and processing
- Retrieve data at regular intervals
- Calculate various convection diagnostics
- Identify areas of precipitation in Chenies radar

### LEVEL 2: Action

- Generation & analysis of convective precipitation forecasts
- Determine whether precipitation is associated with non-frontal convection ?
- Apply the relevant forecast
- Assess the movement of precipitation
- Determine current precipitation warning level

### LEVEL 3: Alert

- Dissemination of data to Thames Flood Control Centre
- Send coded warnings, Object Oriented convective precipitation forecasts, and verification data

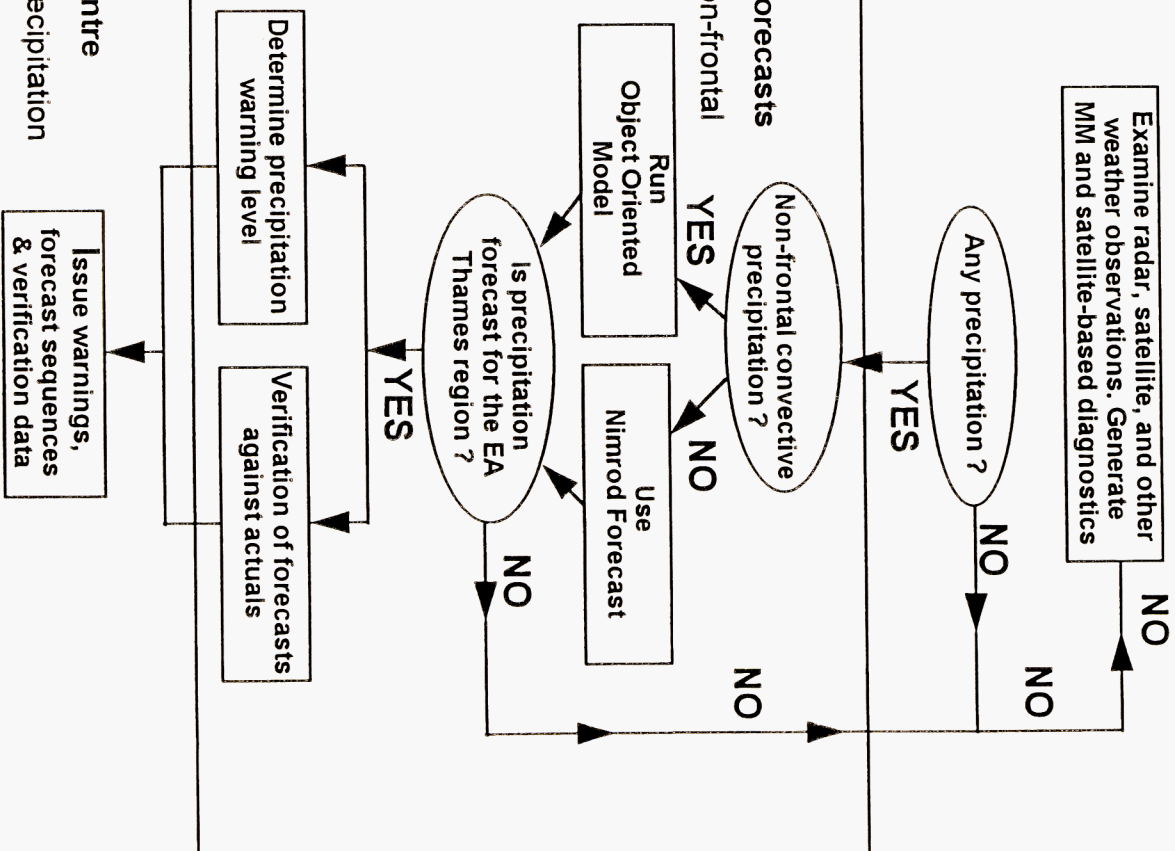







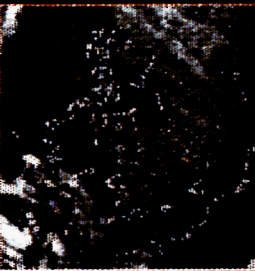
Figure 2 The GANDOLF control panel


**Gandolf Control Panel**











Exit

Help

Operations

Fri 8 Dec 10:42:50 UTC
02:43:55
Status: Running
Level: Winter
Go

Inputs

	Mesoscale	Frontiers Act	Cheries	Meteosat IR	Observations	Sferics
Control	<span style="background-color: green; color: white; padding: 2px 5px;">Go</span>	<span style="background-color: green; color: white; padding: 2px 5px;">Go</span>	<span style="background-color: red; color: white; padding: 2px 5px;">Stop</span>	<span style="background-color: green; color: white; padding: 2px 5px;">Go</span>	<span style="background-color: red; color: white; padding: 2px 5px;">Stop</span>	<span style="background-color: red; color: white; padding: 2px 5px;">Stop</span>
Process ID	4007	7059	None	6698	None	None
Latest	0000 UTC	1015 UTC	None	1030 UTC	None	None
Display	<span style="background-color: black; color: white; padding: 2px 5px;"></span>	<span style="background-color: black; color: white; padding: 2px 5px;"></span>	<span style="background-color: black; color: white; padding: 2px 5px;"></span>	<span style="background-color: black; color: white; padding: 2px 5px;"></span>	<span style="background-color: black; color: white; padding: 2px 5px;"></span>	<span style="background-color: black; color: white; padding: 2px 5px;"></span>

Models

	Object Orient	Frontiers
Control	<span style="background-color: red; color: white; padding: 2px 5px;">Stop</span>	<span style="background-color: red; color: white; padding: 2px 5px;">Stop</span>
Process ID	None	None
Latest	None	None
Display	<span style="background-color: black; color: white; padding: 2px 5px;"></span>	<span style="background-color: black; color: white; padding: 2px 5px;"></span>

Movie Loops

	Actuals	Forecasts
Frontiers	<span style="background-color: black; color: white; padding: 2px 5px;"></span>	<span style="background-color: black; color: white; padding: 2px 5px;"></span>
Meteosat	<span style="background-color: black; color: white; padding: 2px 5px;"></span>	<span style="background-color: black; color: white; padding: 2px 5px;">OOP</span>

Diagnostics

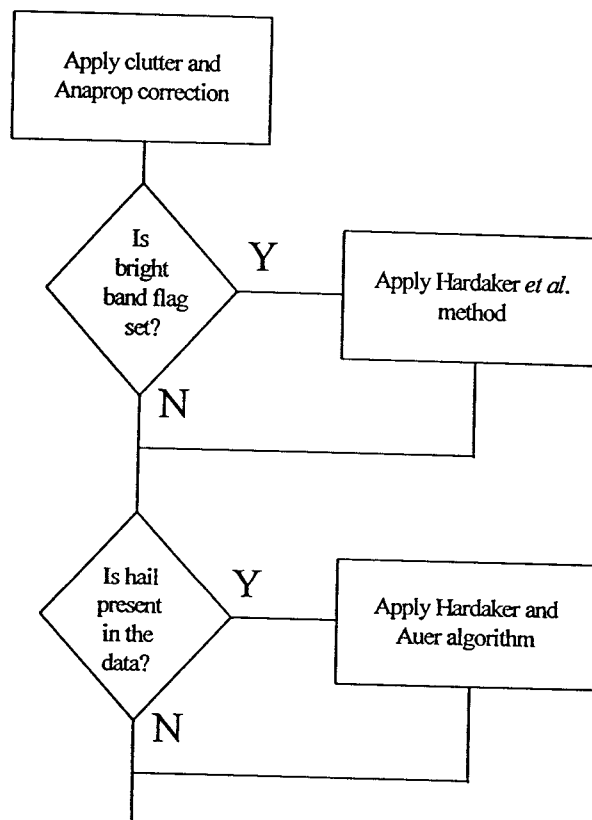
	Cape	Helicity	TL	Convergence	Vorticity	NNCC
Calculate	<span style="background-color: black; color: white; padding: 2px 5px;"></span>	<span style="background-color: black; color: white; padding: 2px 5px;"></span>	<span style="background-color: black; color: white; padding: 2px 5px;"></span>	<span style="background-color: black; color: white; padding: 2px 5px;"></span>	<span style="background-color: black; color: white; padding: 2px 5px;"></span>	<span style="background-color: black; color: white; padding: 2px 5px;"></span>
Display	<span style="background-color: black; color: white; padding: 2px 5px;"></span>	<span style="background-color: black; color: white; padding: 2px 5px;"></span>	<span style="background-color: black; color: white; padding: 2px 5px;"></span>	<span style="background-color: black; color: white; padding: 2px 5px;"></span>	<span style="background-color: black; color: white; padding: 2px 5px;"></span>	<span style="background-color: black; color: white; padding: 2px 5px;"></span>

Advisory

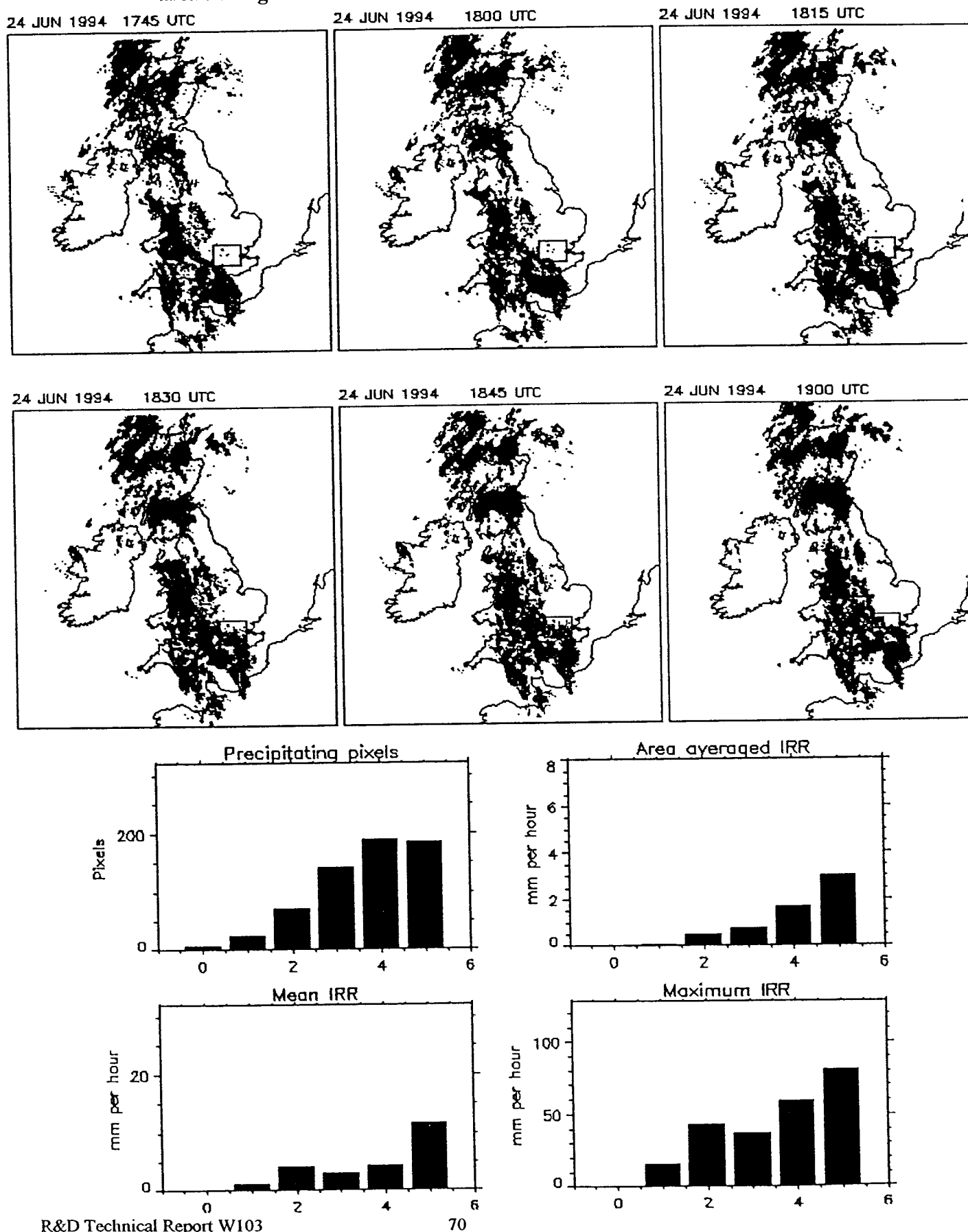
Warning	Level	Send IRR	Send Accum	Trans Status
<span style="background-color: red; color: white; padding: 2px 5px;">No</span>	<span style="background-color: black; color: white; padding: 2px 5px;">None</span>	<span style="background-color: black; color: white; padding: 2px 5px;">No</span>	<span style="background-color: red; color: white; padding: 2px 5px;">No</span>	<span style="background-color: red; color: white; padding: 2px 5px;">Stopped</span>



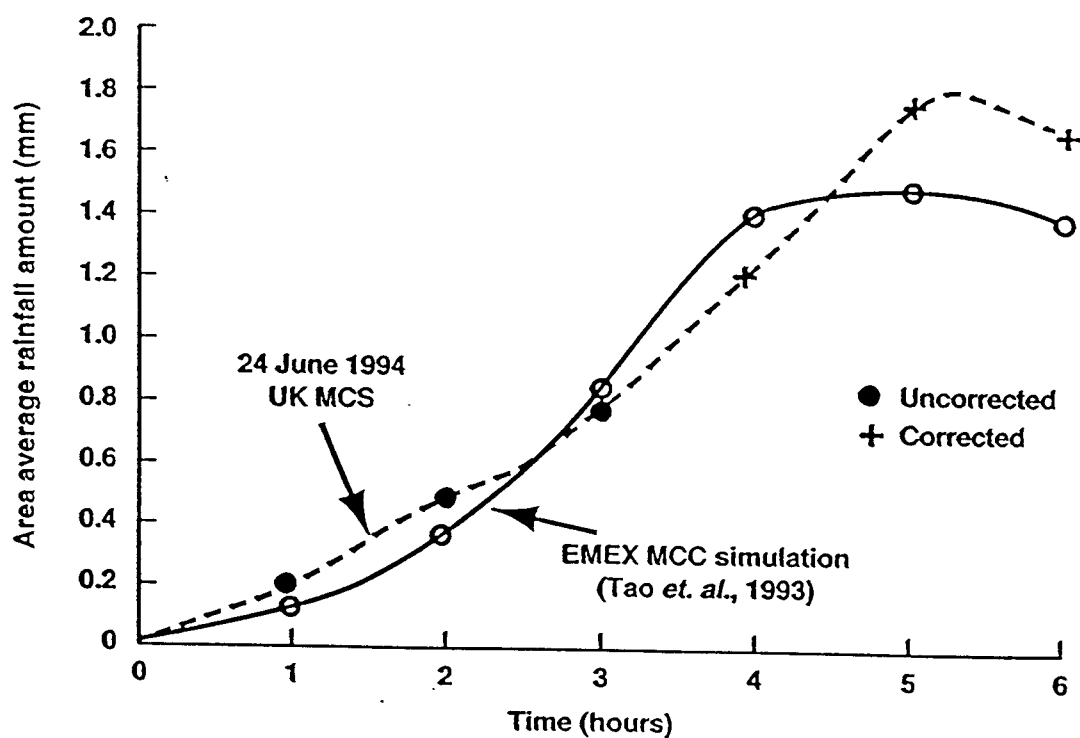
**Figure 3** An outline of the GANDOLF radar correction scheme (if the data are not processed by Nimrod).



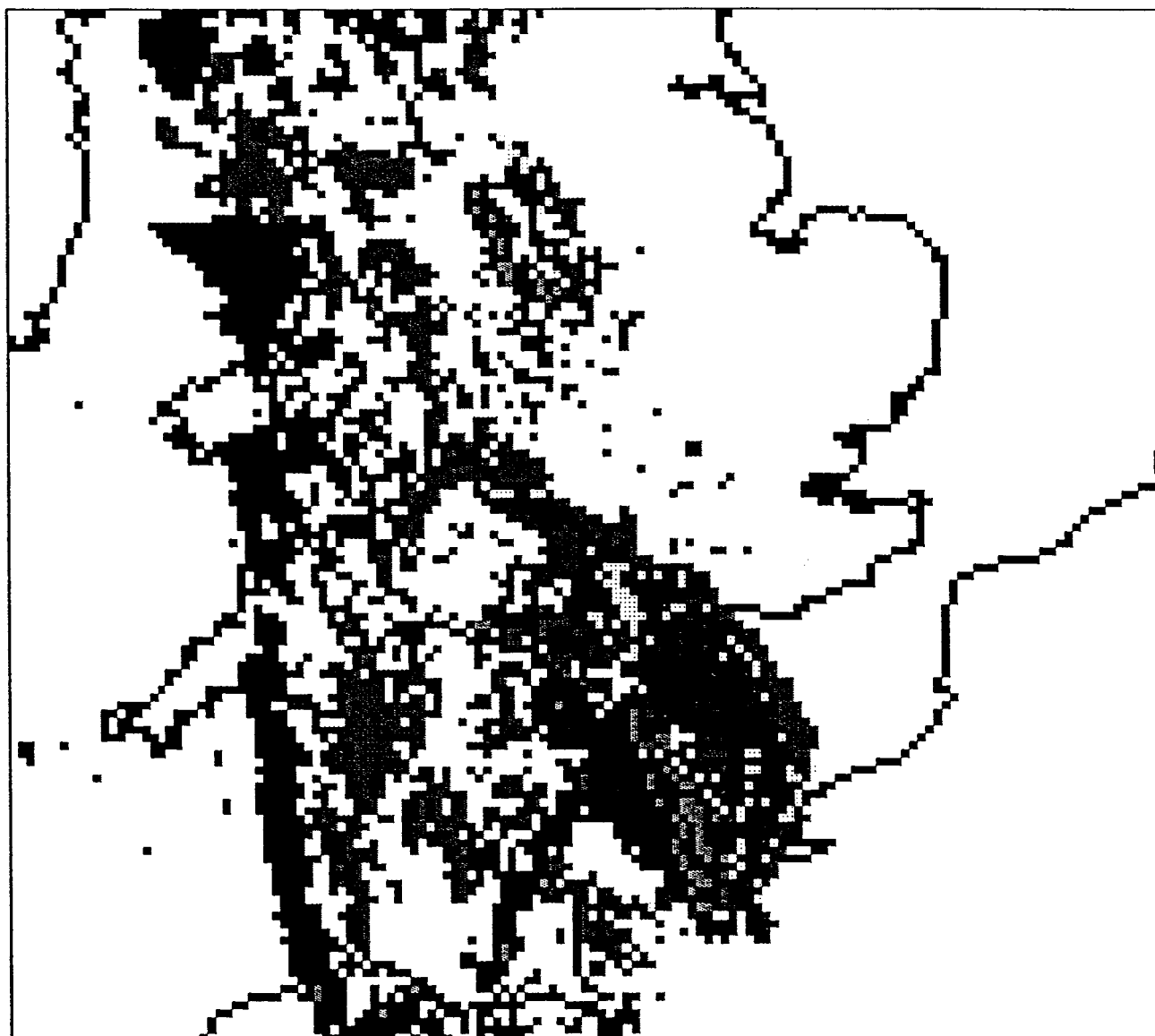
**Figure 4** Time series of radar images on 24 June 1994 (1745 GMT to 1900 GMT) and parameters derived from them over a rectangular box centred on London. The rapid changes within the box in rainfall area, mean intensity, area average rainfall and maximum rainfall are shown.















**Figure 5** Variation with time of area averaged rainfall over the rectangular area shown in Figure 4 compared with the modelled hourly accumulated rainfall normalised with respect to the total number of model grid points for a PRE-STORM MCS reported by Tao *et al.* (1993).

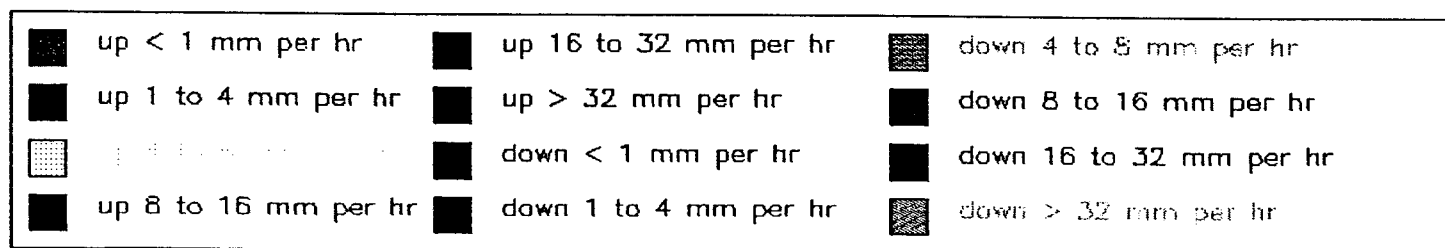
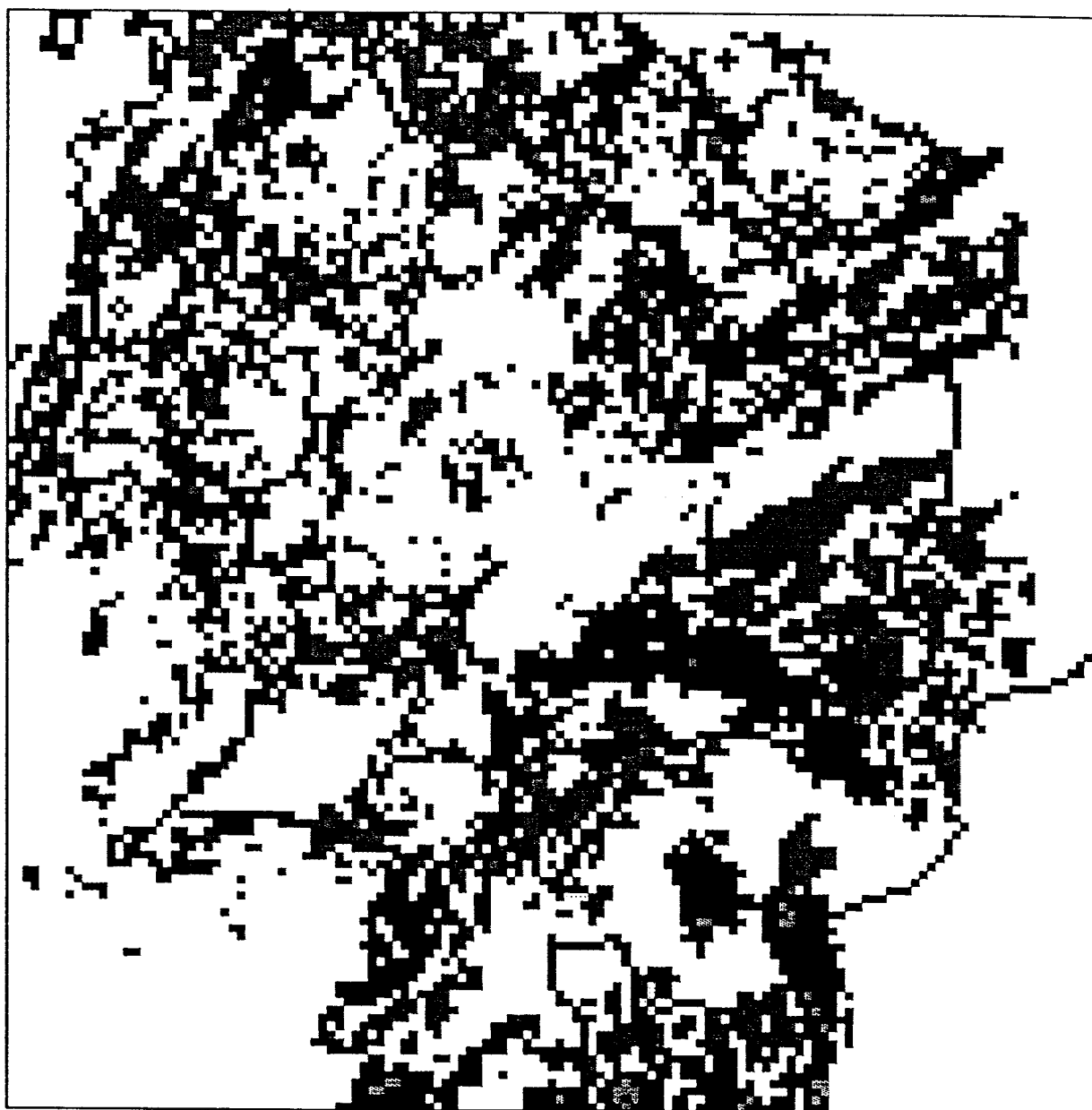


**Figure 6**      **One hour radar echo difference field for 1745-1645 GMT, 24 June 1994.**

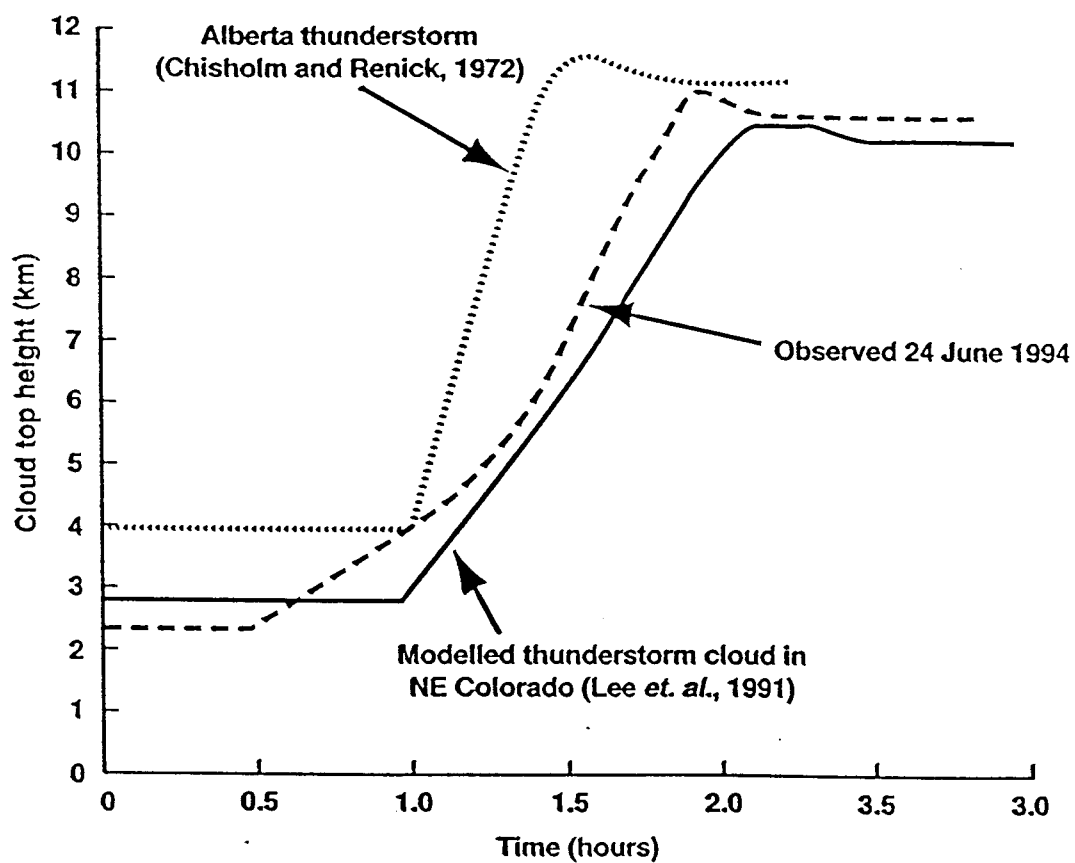


	up < 1 mm per hr		up 16 to 32 mm per hr		down 4 to 8 mm per hr
	up 1 to 4 mm per hr		up > 32 mm per hr		down 8 to 16 mm per hr
	up 4 to 8 mm per hr		down < 1 mm per hr		down 16 to 32 mm per hr
	up 8 to 16 mm per hr		down 1 to 4 mm per hr		down > 32 mm per hr

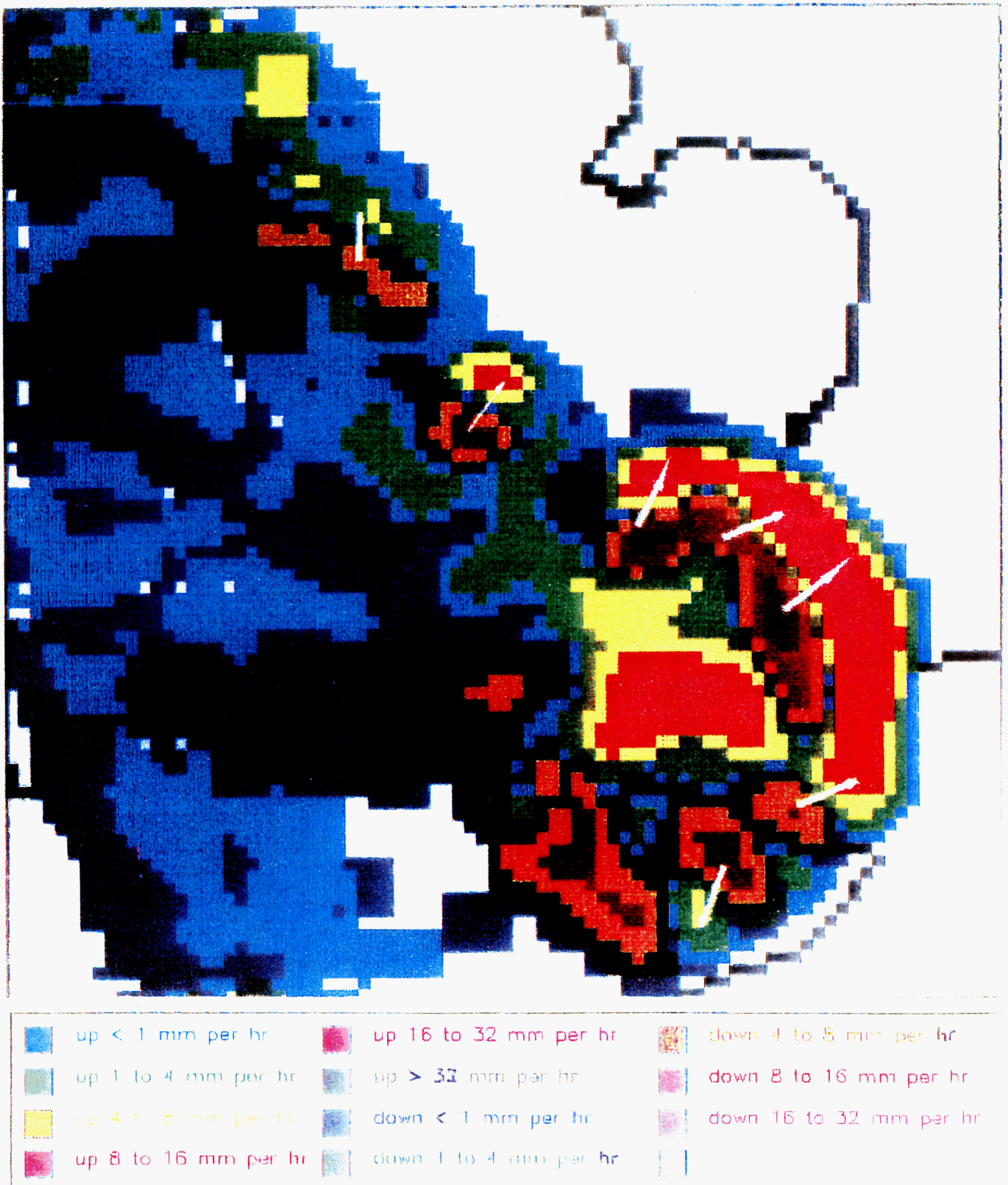
**Figure 7**      **One hour radar echo difference field for 1900-1800 GMT, 31 August 1994.**



**Figure 8** Variation of cloud height on 24 June 1994 over the Channel, and for thunderstorms observed in north-east Colorado (Lee *et al.*, 1991) and Alberta (Chisholm and Renick, 1972).



**Figure 9** Radar difference field for 2000-1945 GMT, 24 June 1994, showing storm motion vectors.





**Figure 10**     **A Neural Network cloud classification showing four classes: clear (blue), dynamic (green), shallow convection (yellow) and deep convection (red).**

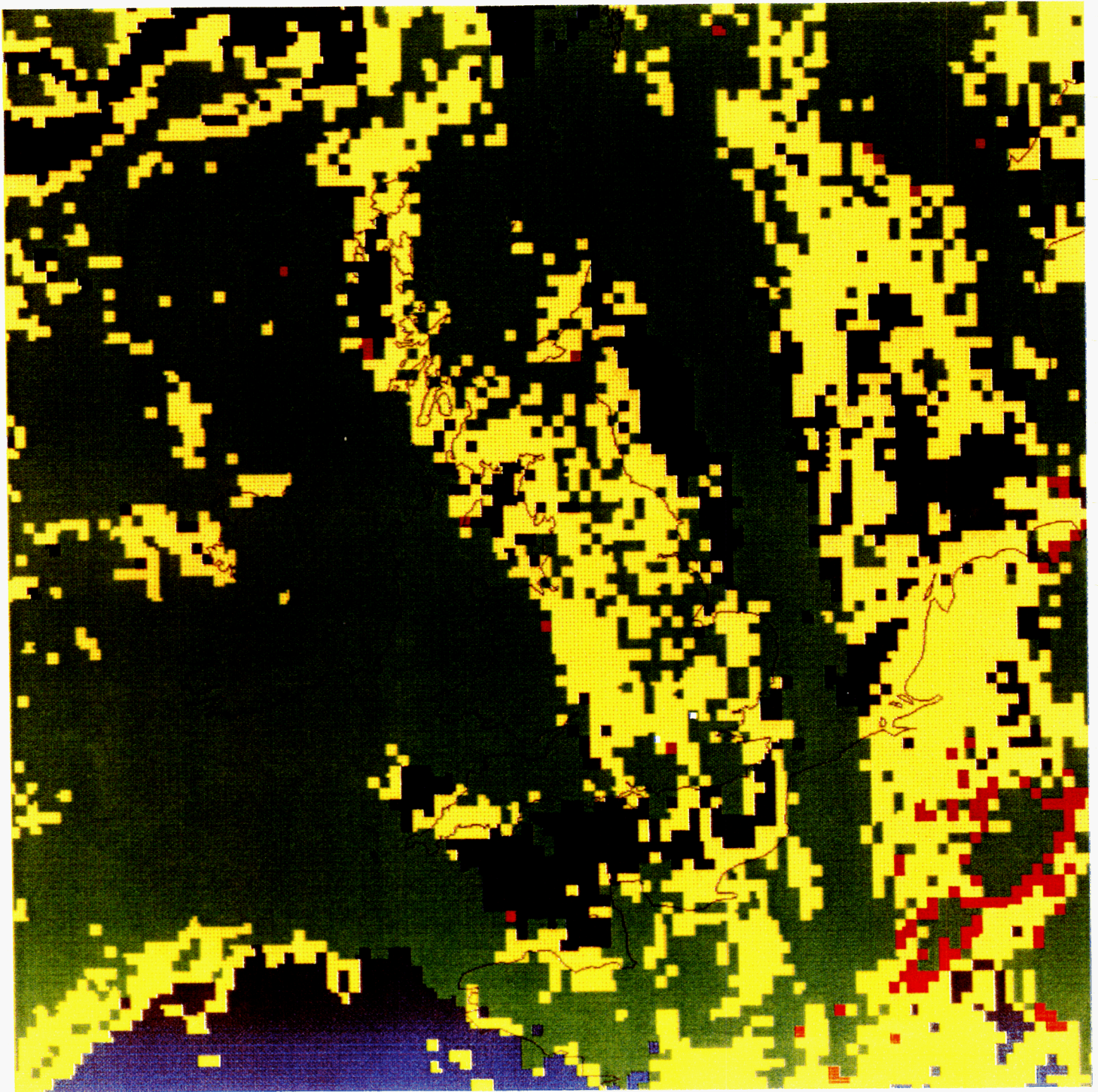


Figure 11 Lagrangian time autocorrelation functions: frontal cases.

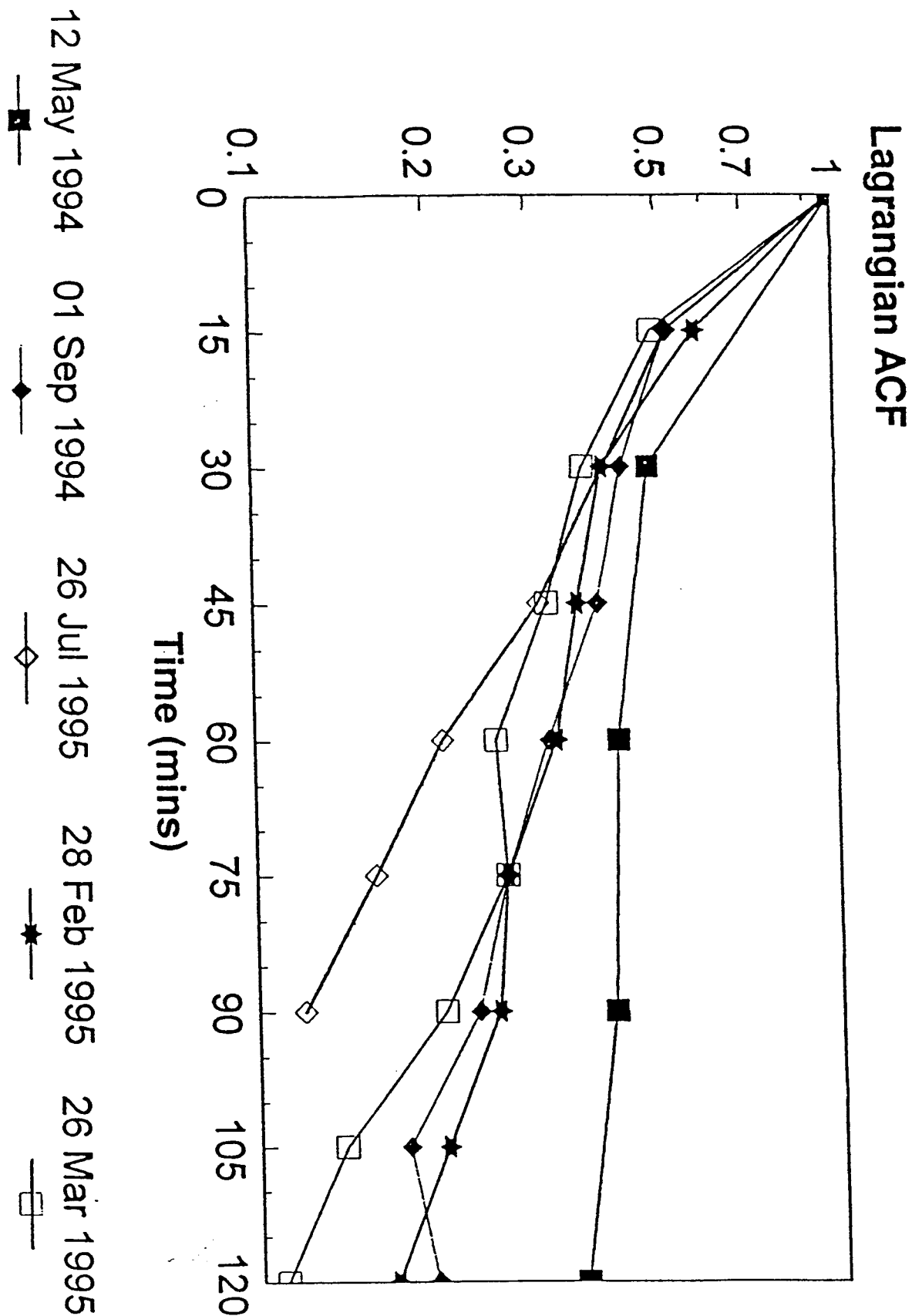


Figure 12 Lagrangian time autocorrelation functions: convective cases.

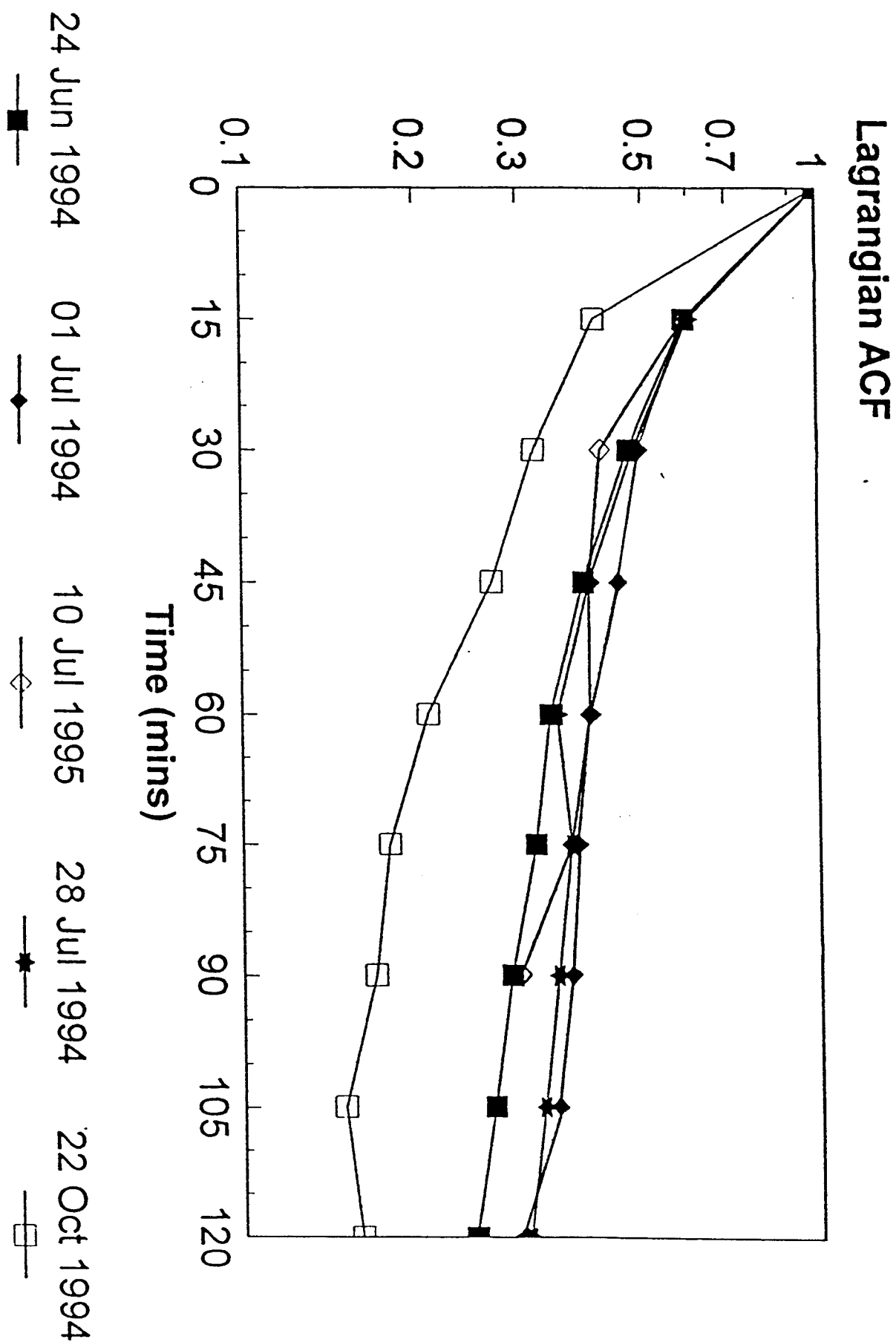


Figure 13 Lagrangian decorrelation time ( $T_L$ ) versus CAPE.

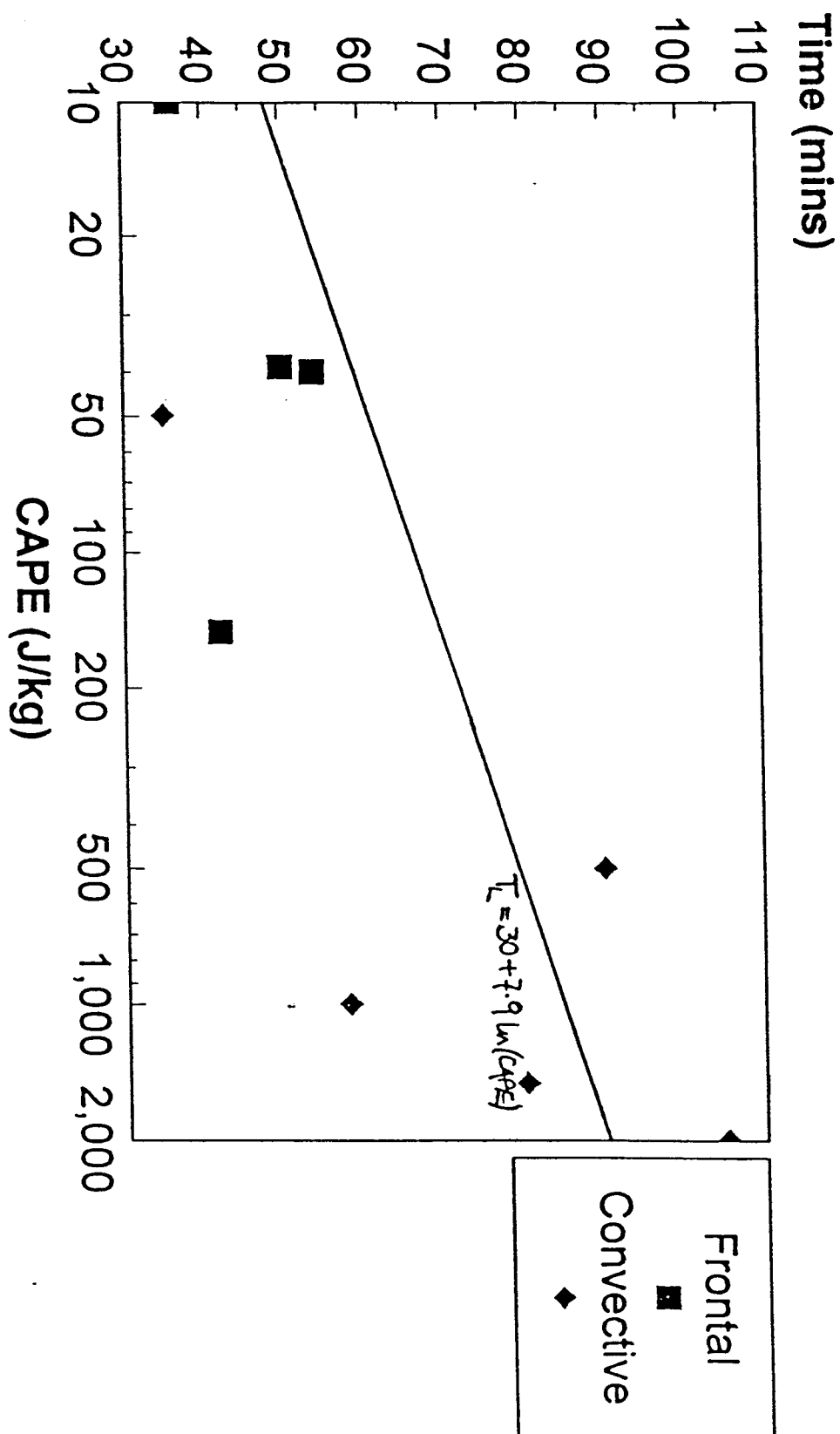


Figure 14 Lagrangian decorrelation time ( $T_L$ ) versus modified Richardson Number( $CAPE/H_R$ ).

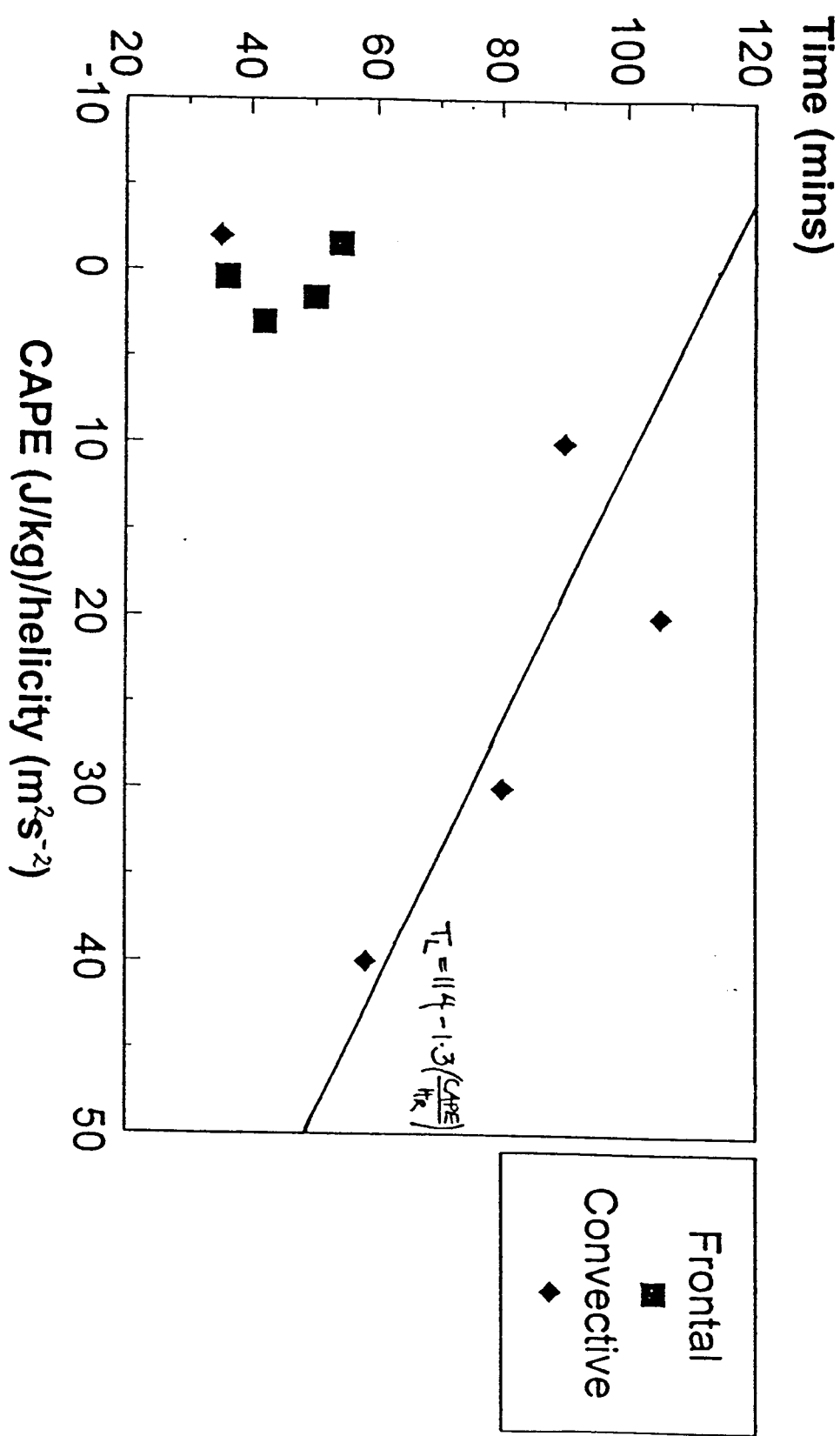
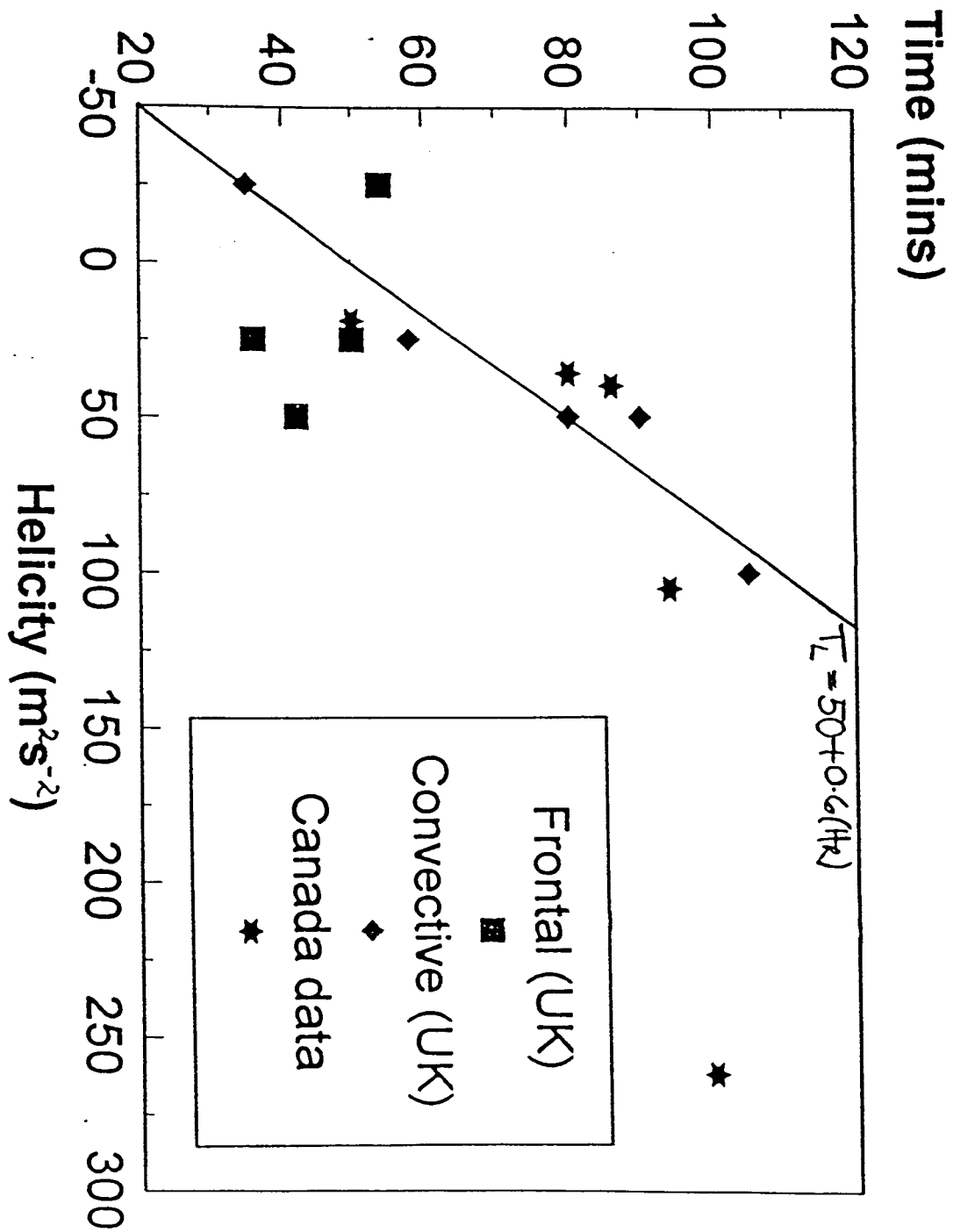
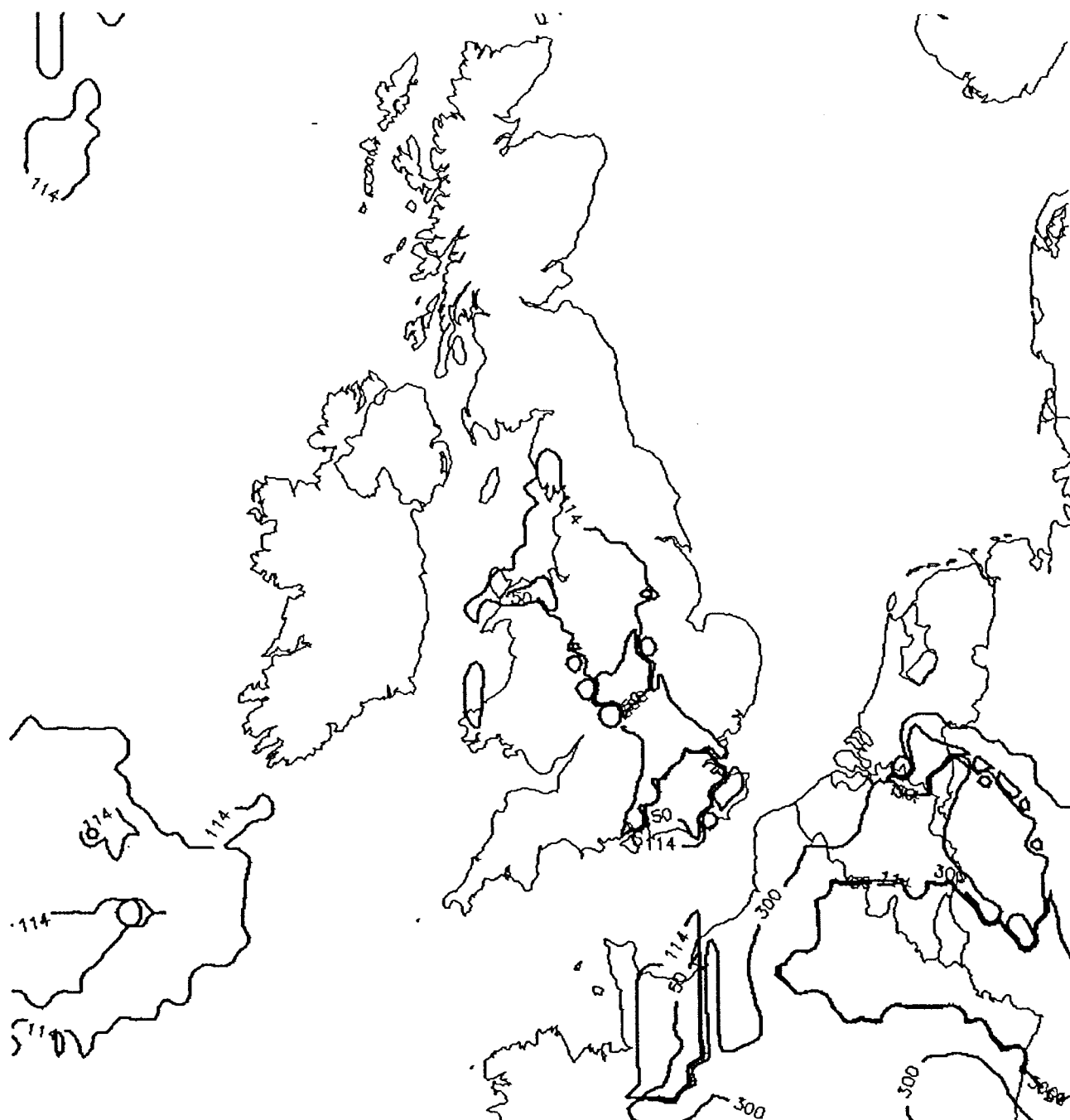


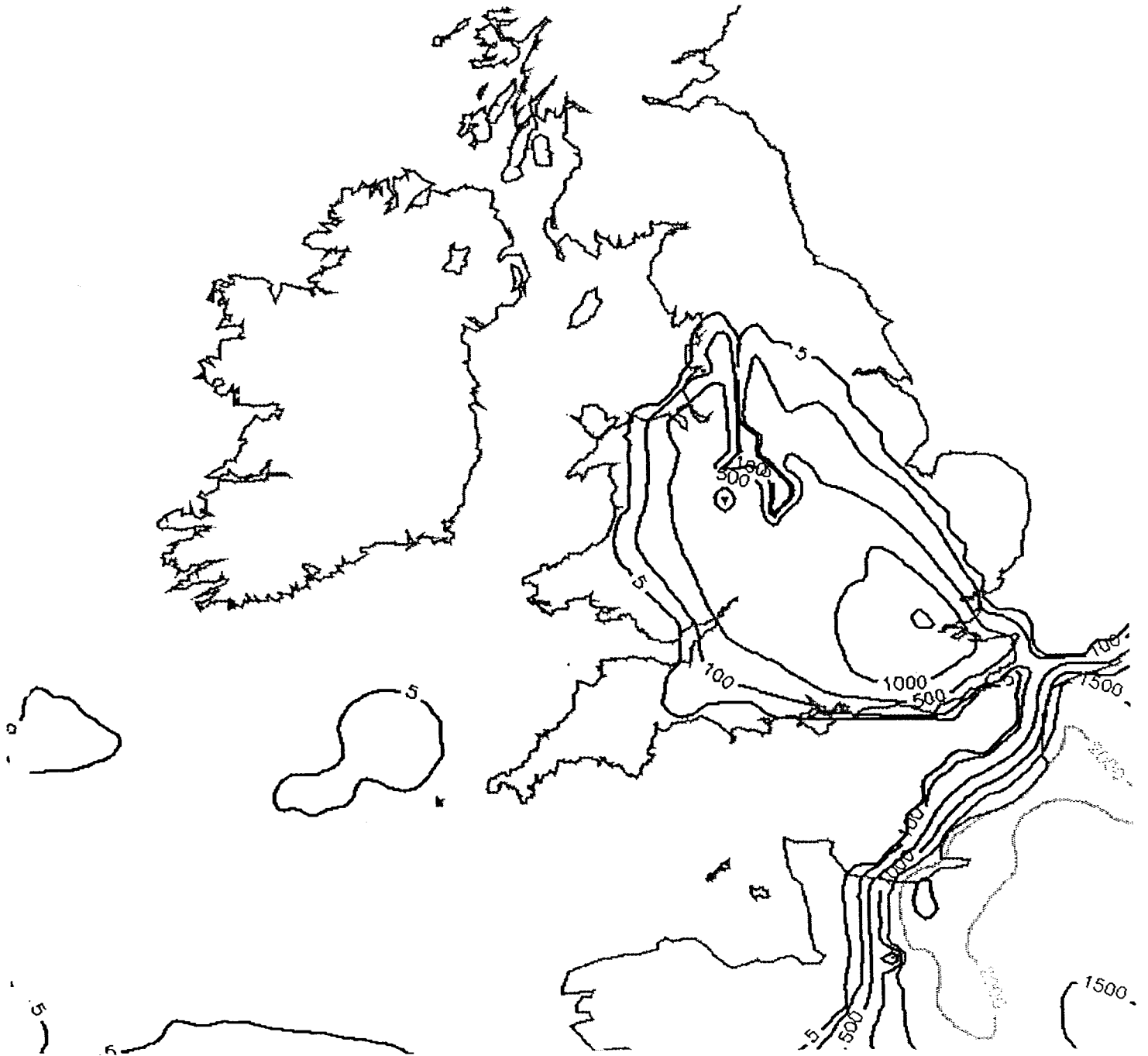
Figure 15 Least squares regression of Lagrangian decorrelation time ( $T_L$ ) and Helicity ( $H_R$ ) using both UK data (Rippon, 1995) and Canadian data (Zawadski *et al.*, 1994).



**Figure 16** Contour plot of forecast Lagrangian Decorrelation Time ( $T_L$ ) in minutes, 24 June 1994, DT 0600 GMT, VT 1800 GMT.



**Figure 17**      **Contour plot of forecast near surface CAPE, 24 June 1994,**  
**DT 0600 GMT, VT 1800 GMT.**





**Figure 18** Contour plot of forecast Helicity field for 24 June 1994, DT 0600 GMT, VT 1800 GMT.

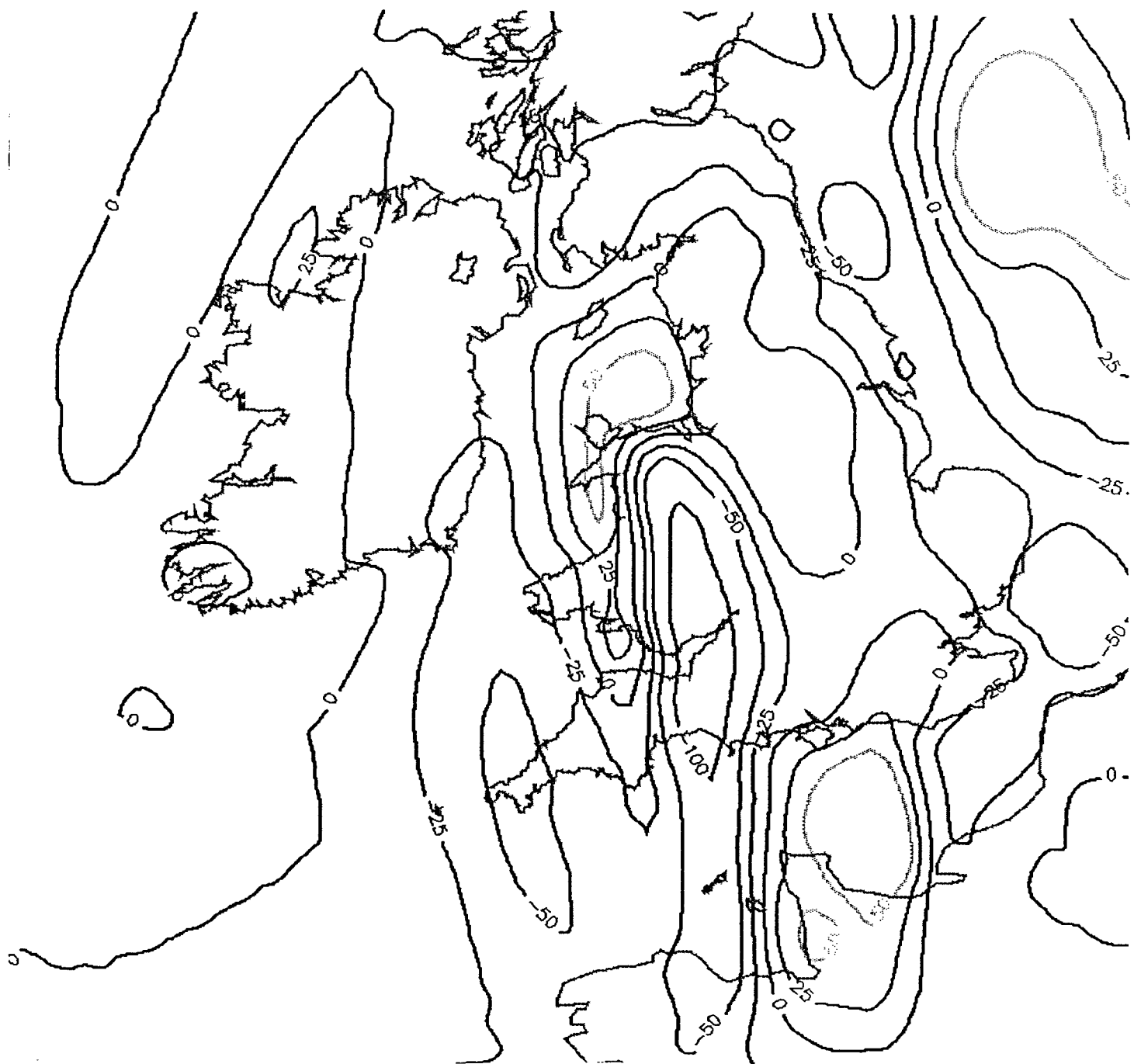
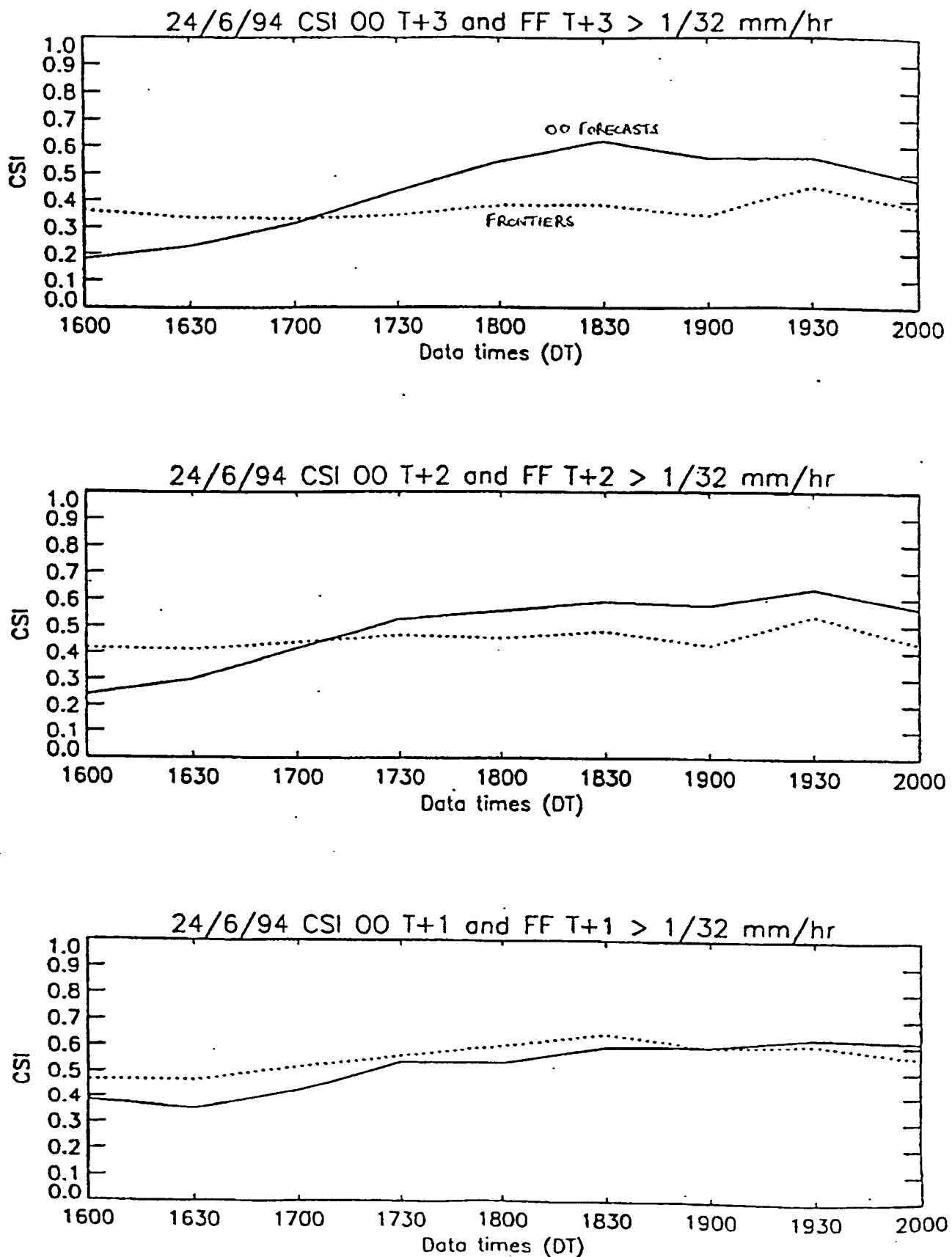
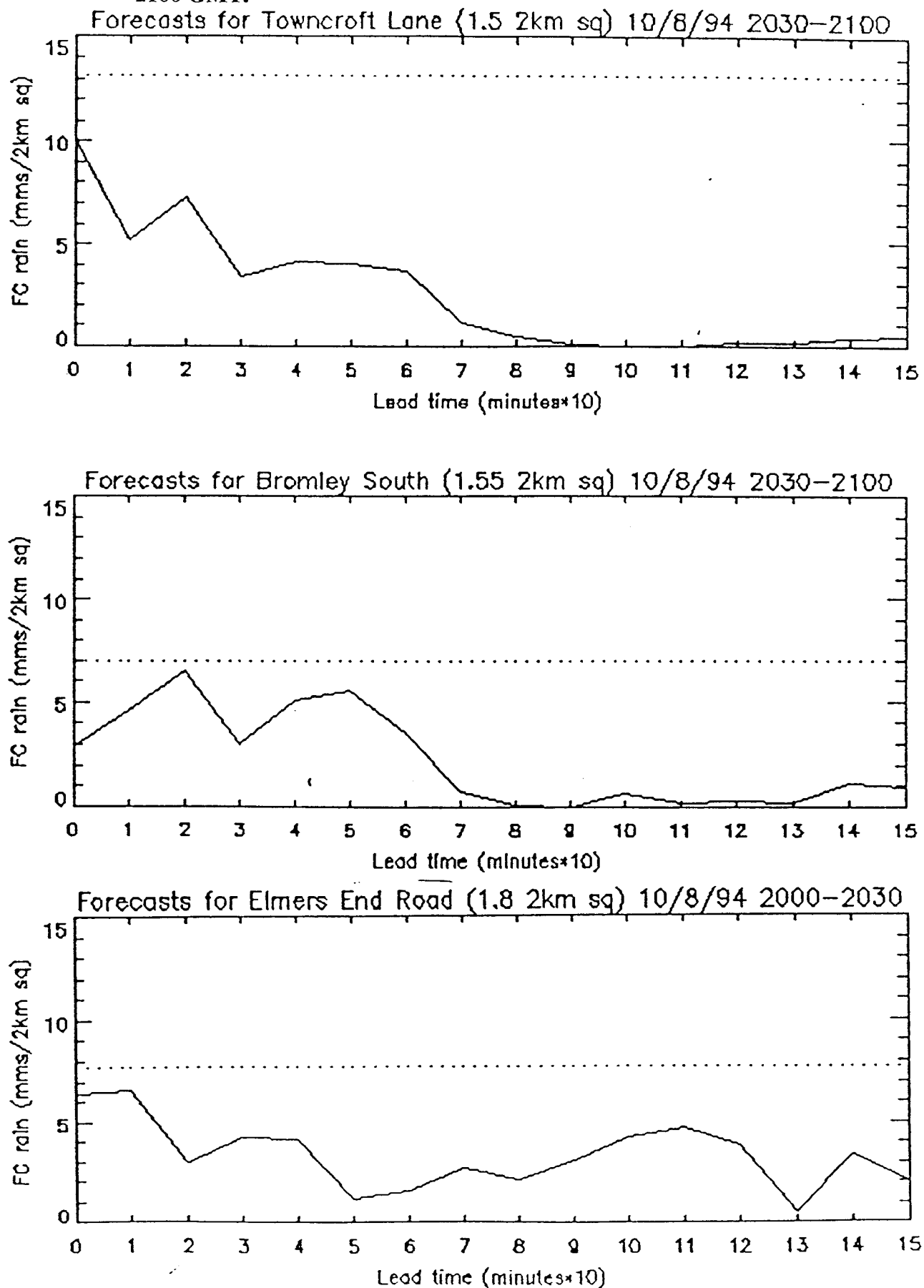


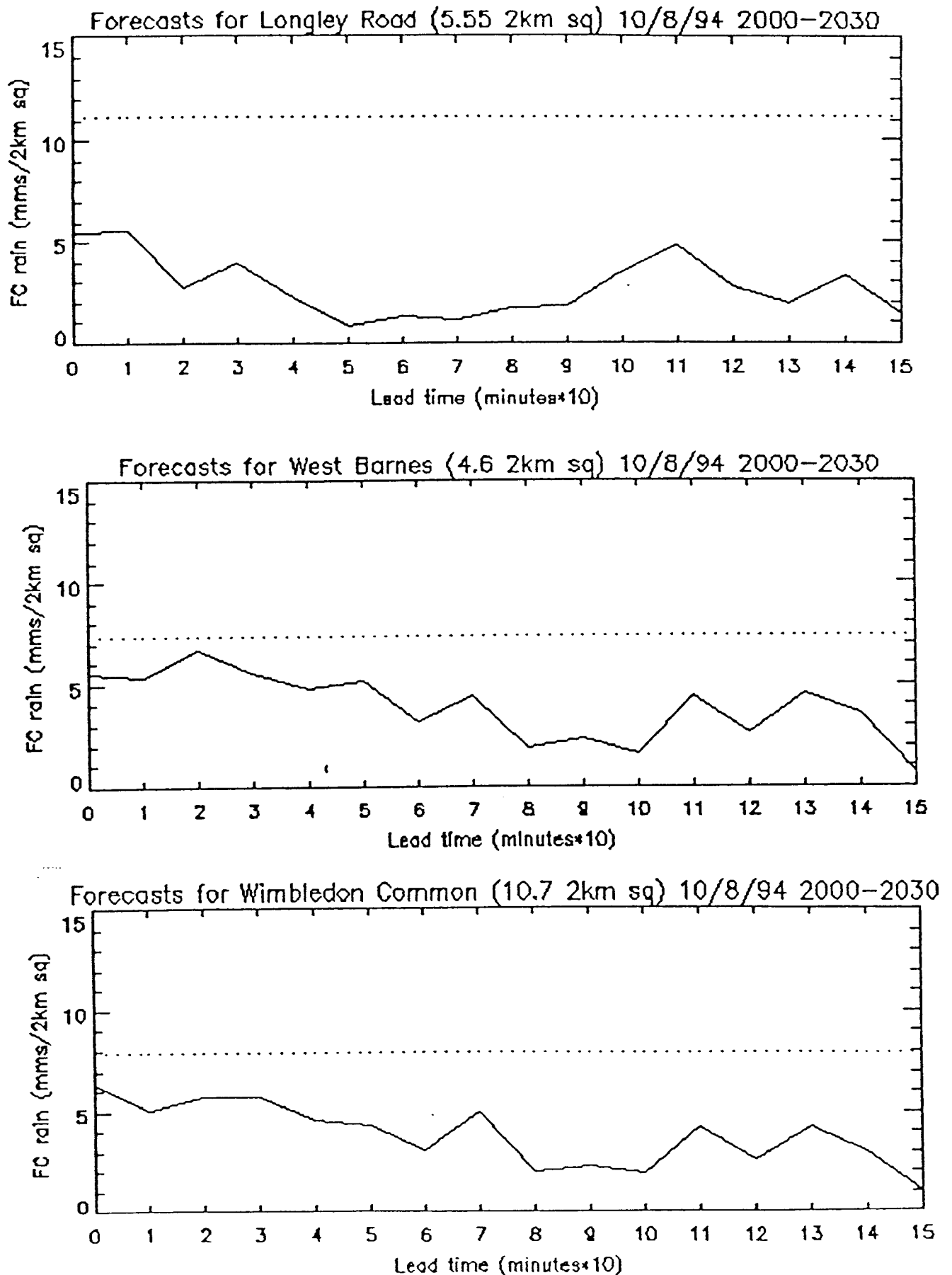
Figure 19 Critical Success Index (CSI) expressed as a function of model DT and lead time (T+1, T+2, and T+3 hours) on 24 June 1994: a comparison of the performance of FRONTIERS and the OOM.



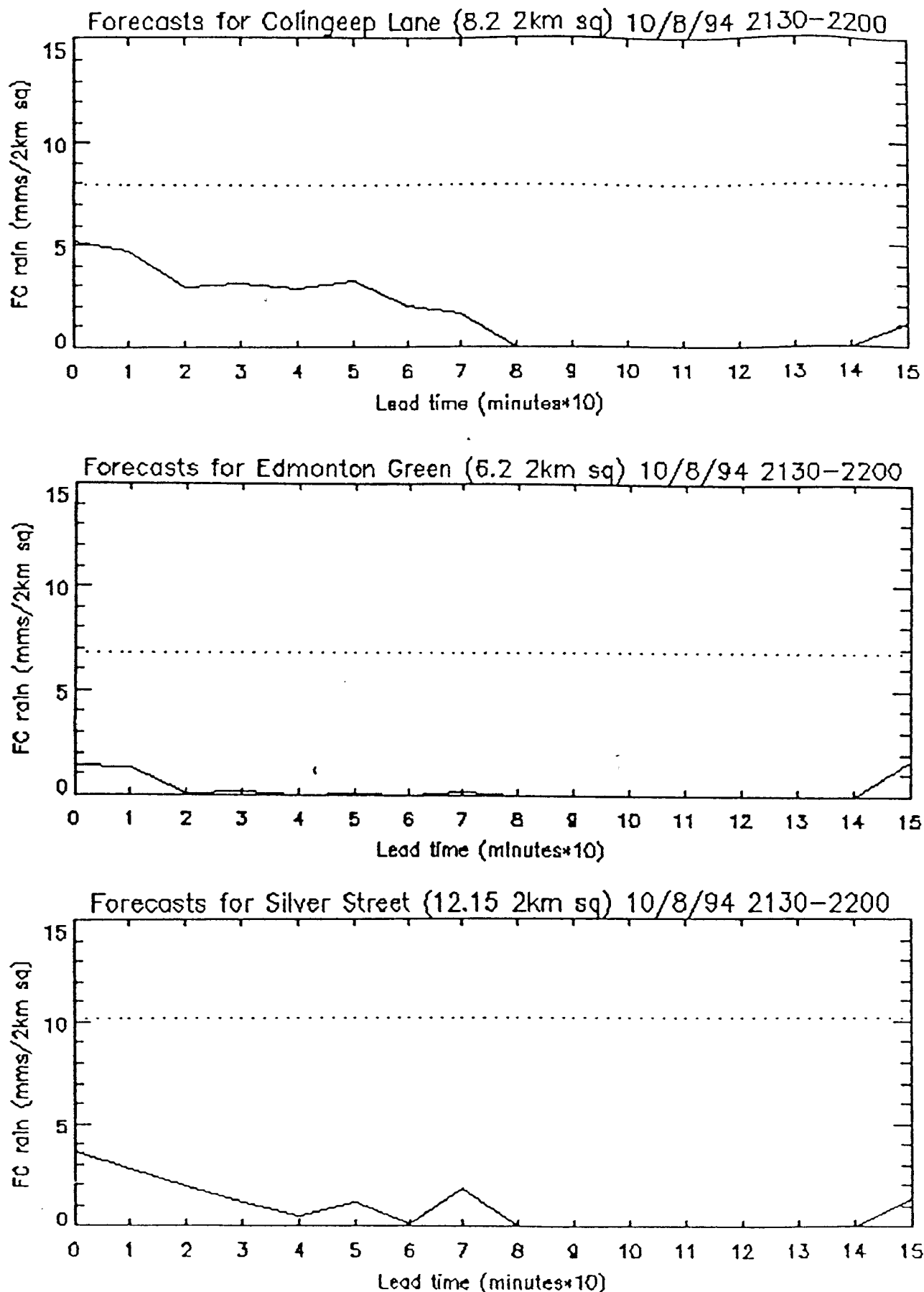
**Figure 20 OOM forecast validation: precipitation forecasts for Towncroft Lane, Bromley South and Elmers End Road, 10 August 1994, 2030 GMT–2100 GMT.**



**Figure 21 OOM forecast validation: precipitation forecasts for Langley Road, West Barnes and Wimbledon Common, 10 August 1994, 2000 GMT–2030 GMT.**



**Figure 22 OOM forecast validation: precipitation forecasts for Colindeep Lane, Edmonton Green and Silver Street, 10 August 1994, 2130 GMT–2200 GMT.**



**Figure 23 OOM forecast validation: precipitation forecasts for Towncroft Lane, Bromley South and Elmers End Road, 11 August 1994, 0800 GMT–0900 GMT.**

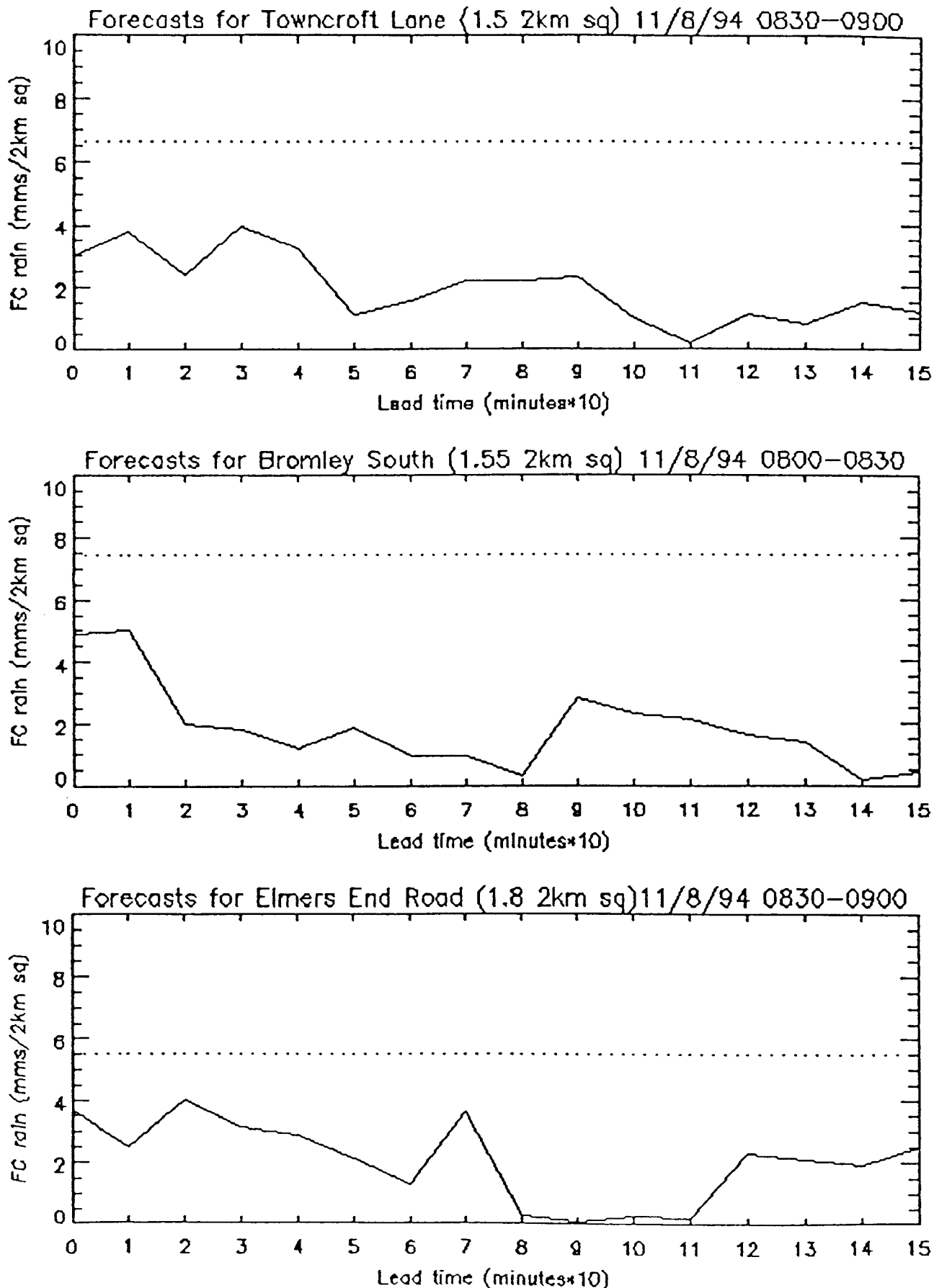


Figure 24 OOM forecast mean errors, standard deviation of errors and RMSE for all high rain events, 10-11 August 1994.

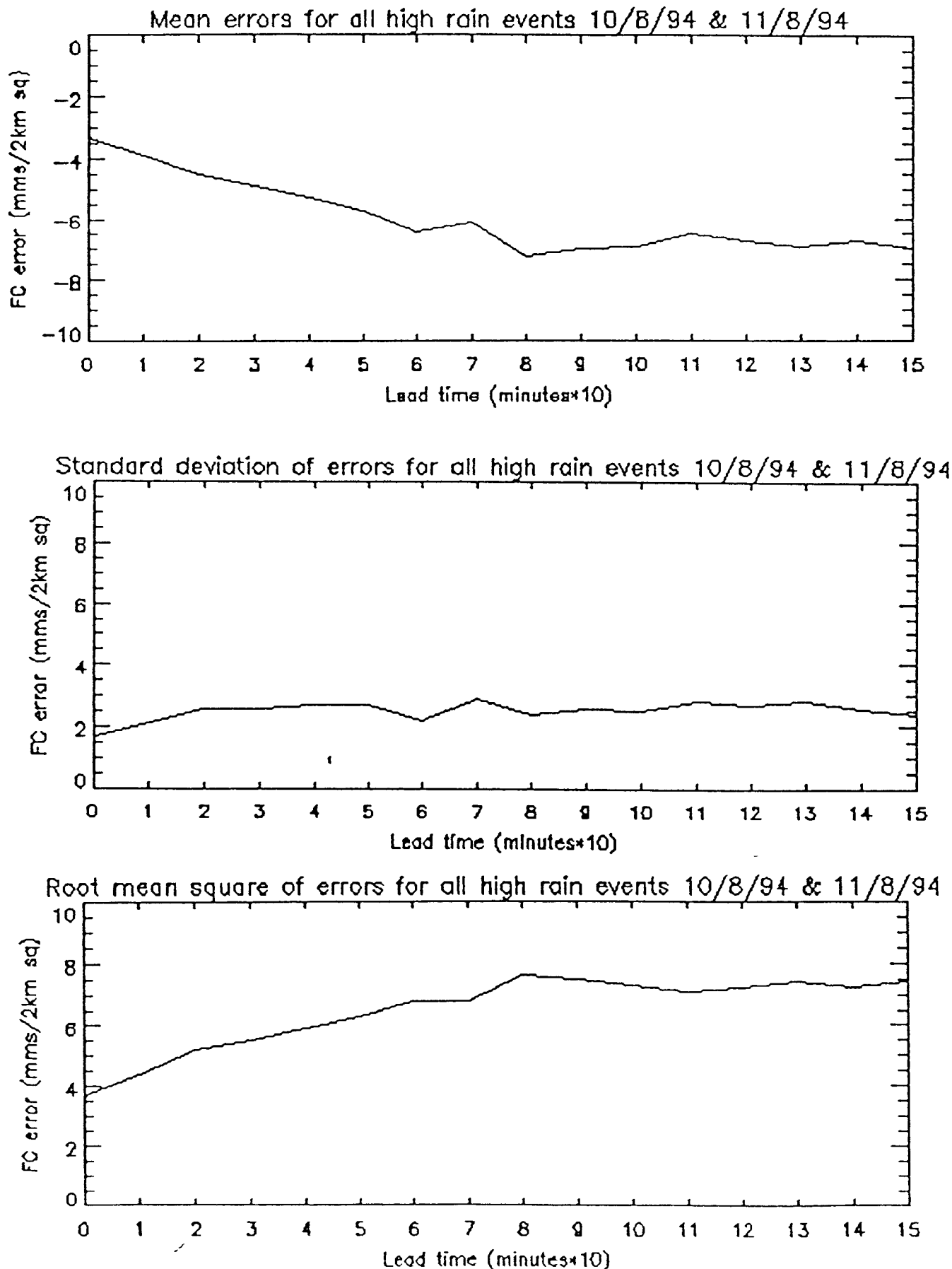
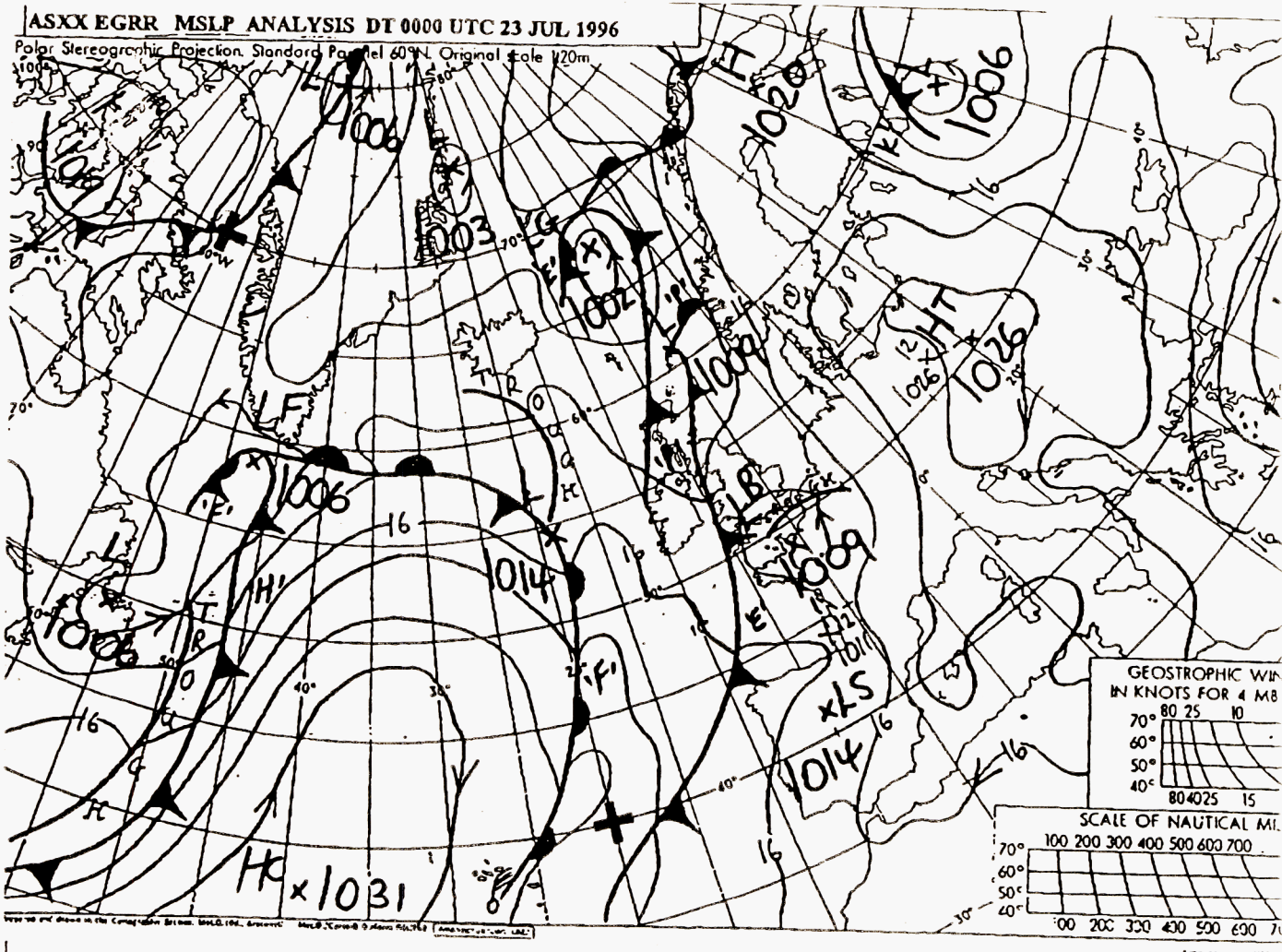


Figure 25





**Figure 26(a) Chenies 2 km surface beam image sequence for the period 0300 GMT to 0420 GMT, 23 July 1996.**

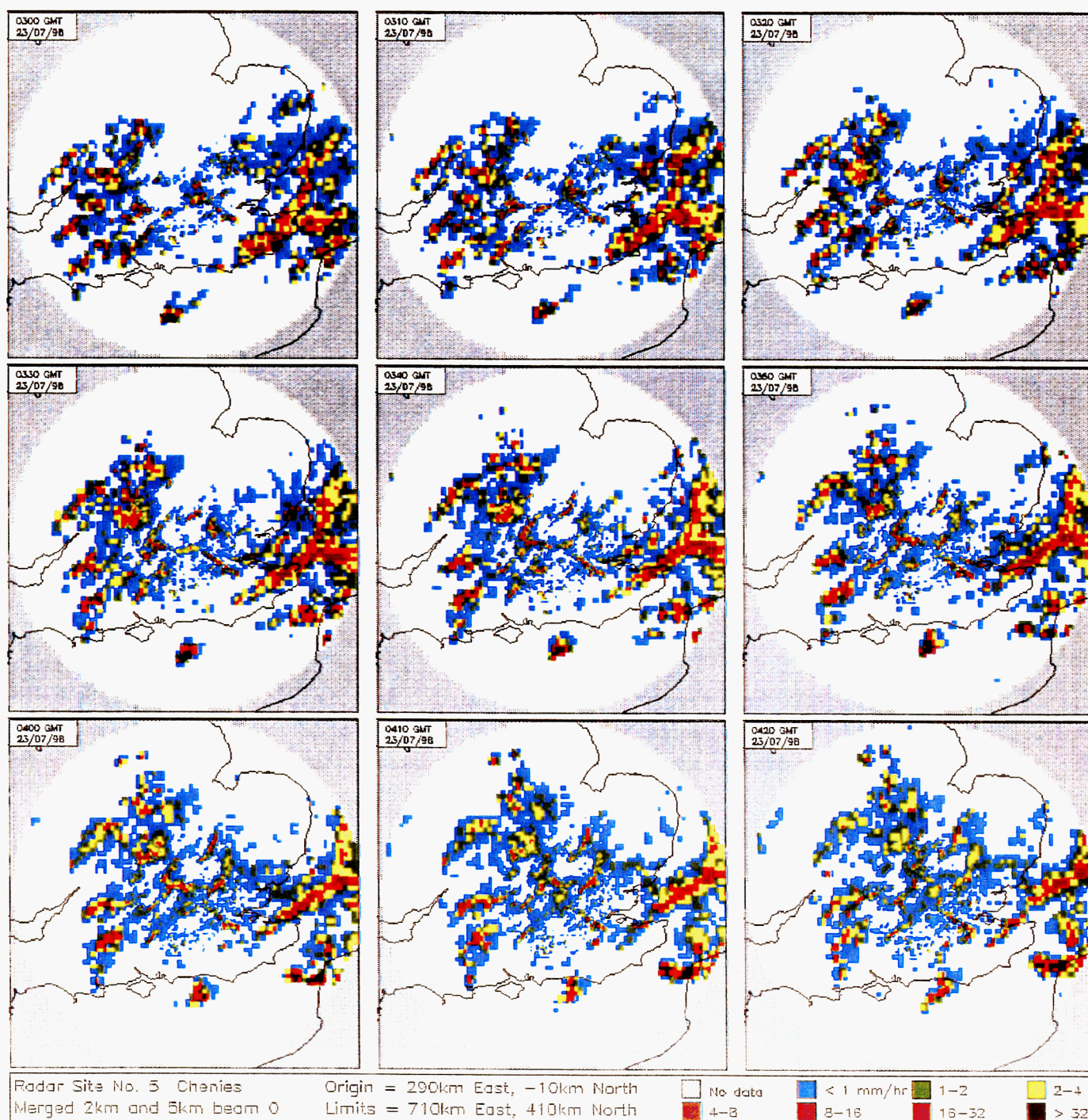




Figure 26(b) Chenies 2 km surface beam image sequence for the period 0430 GMT to 0550 GMT, 23 July 1996.

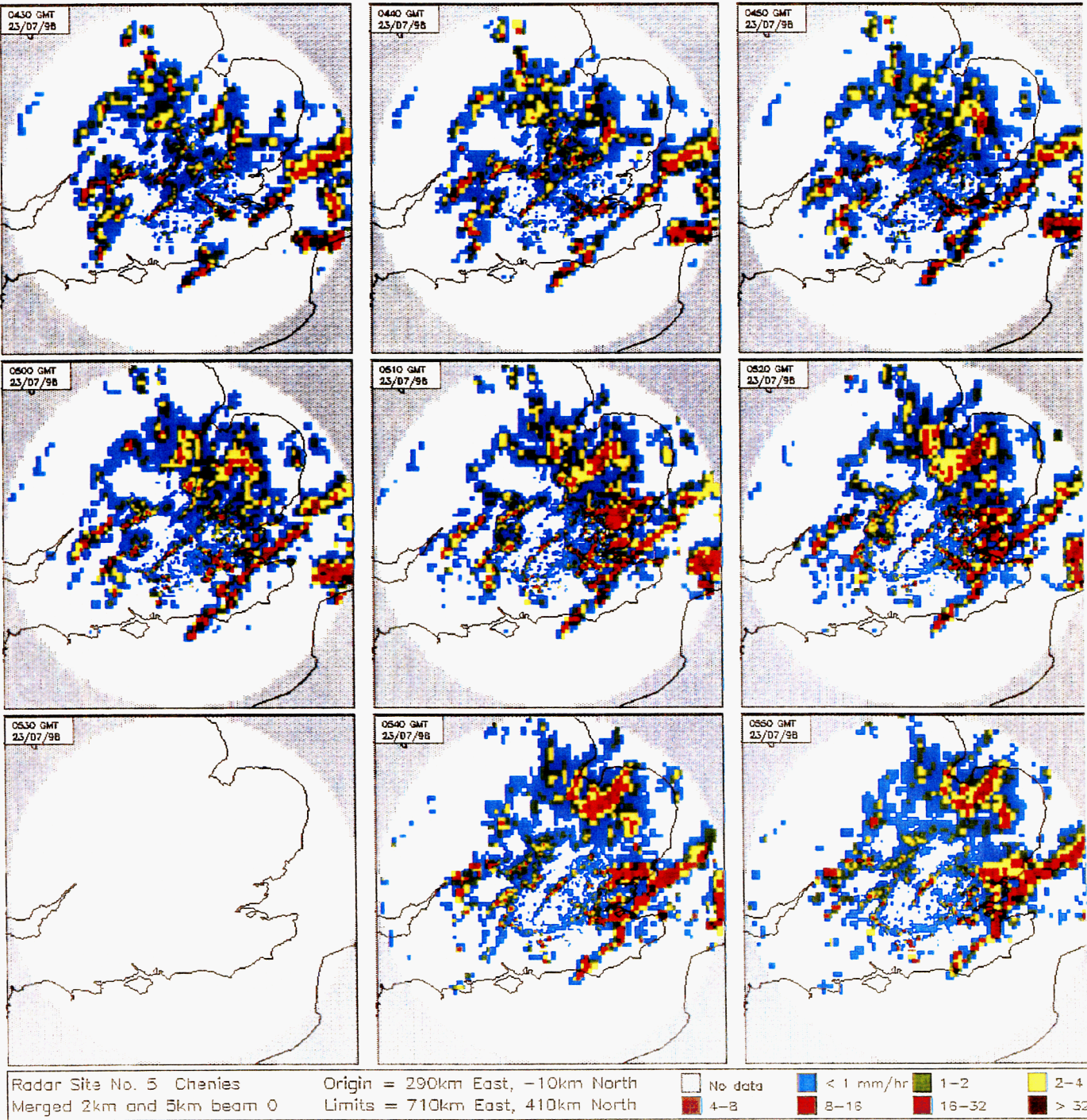
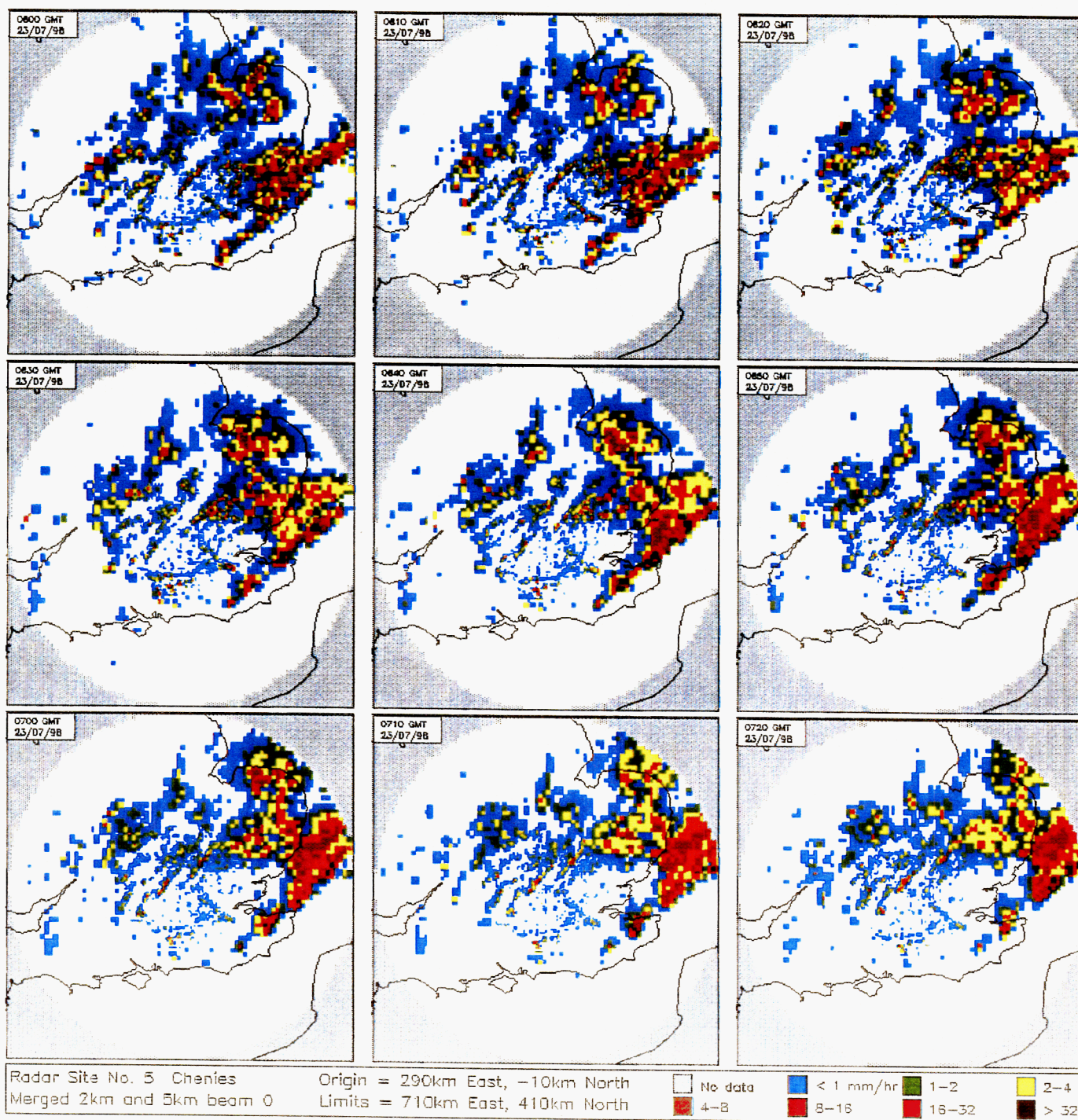


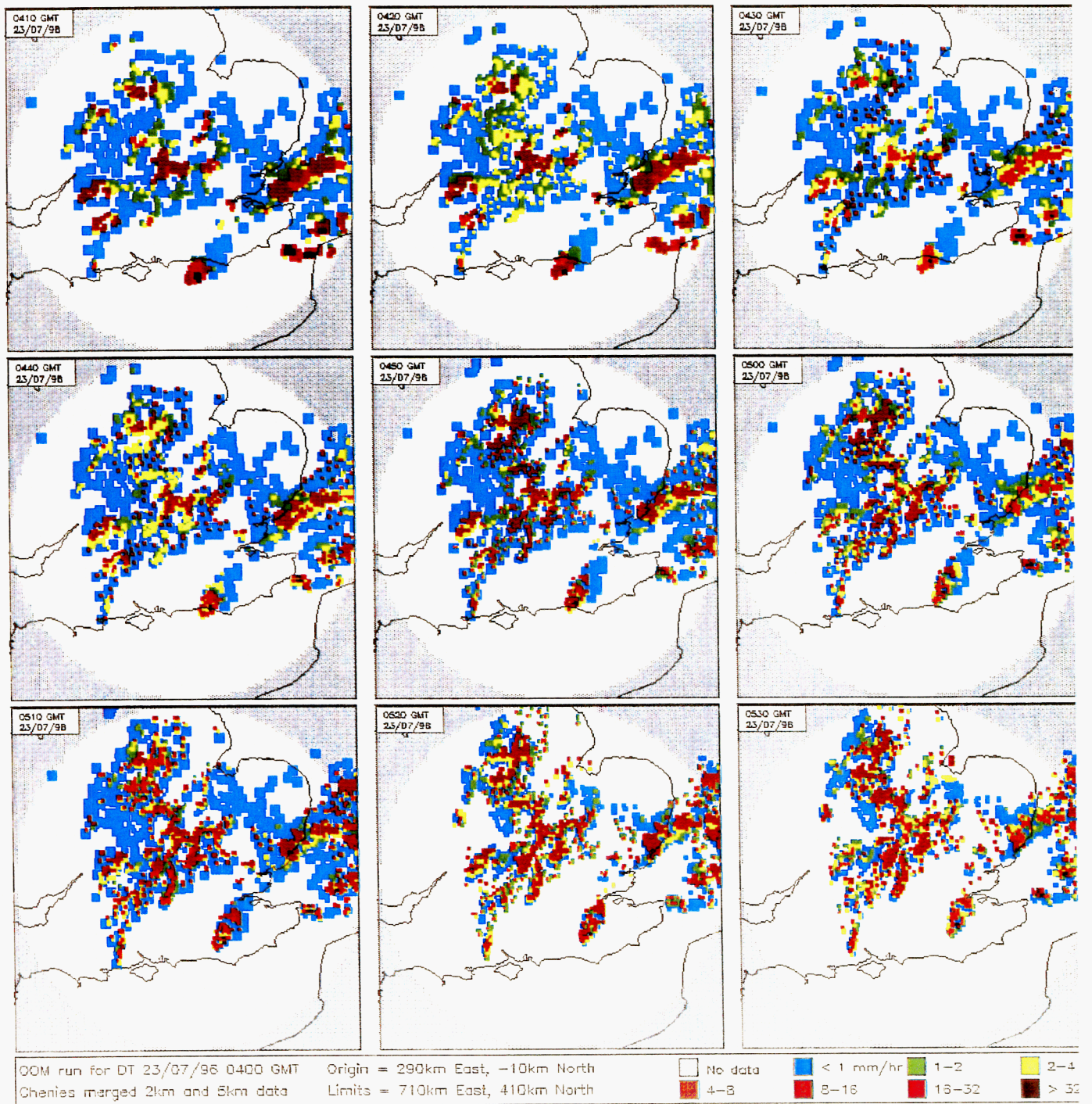


Figure 26(c) Chenies 2 km surface beam image sequence for the period 0600 GMT to 0720 GMT, 23 July 1996.



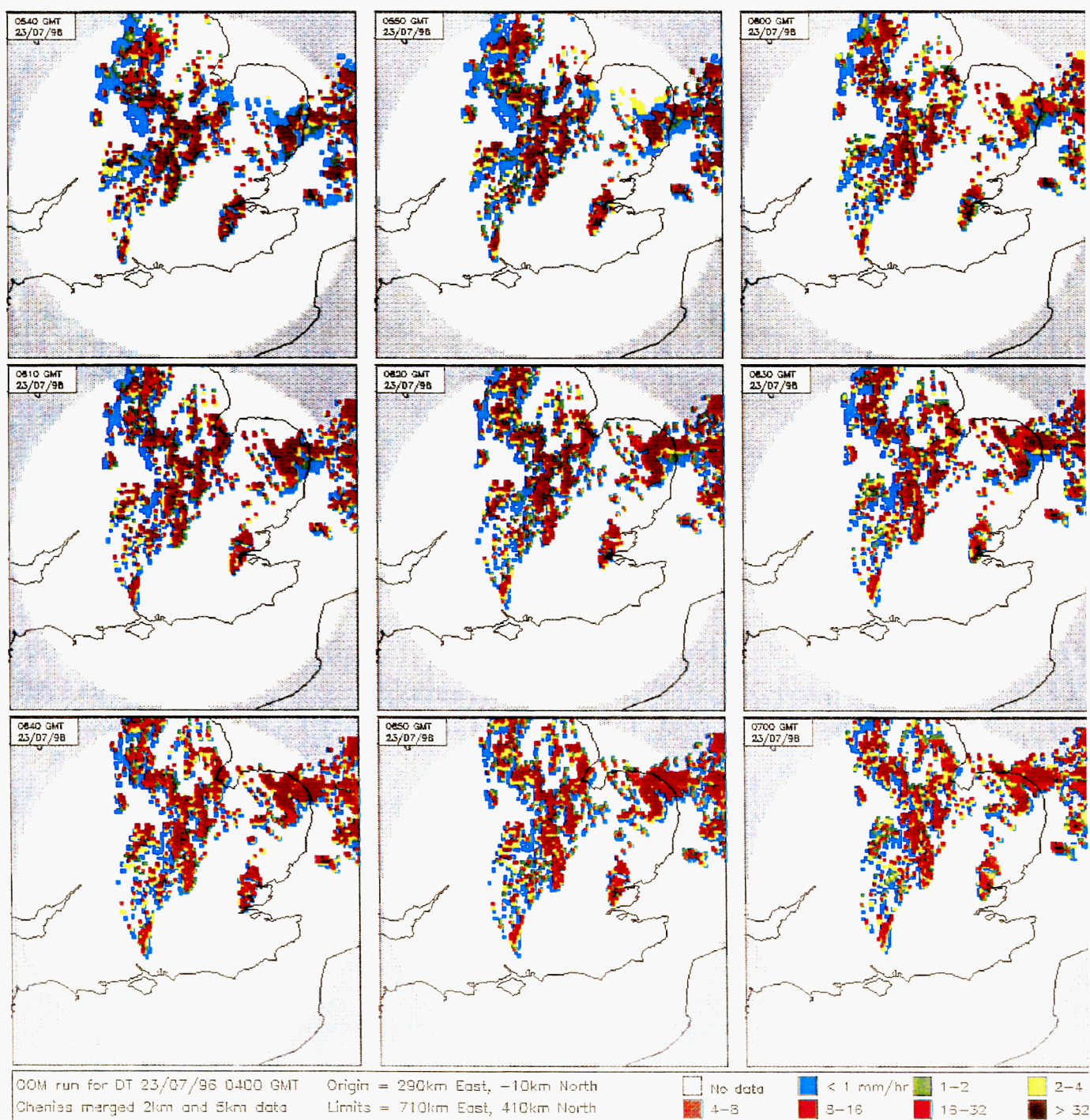


**Figure 27(a) OOM precipitation forecasts for DT 0400 GMT, VT 0410 GMT to 0530 GMT, 23 July 1996.**





**Figure 27(b) OOM precipitation forecasts for DT 0400 GMT, VT 0540 GMT to 0700 GMT, 23 July 1996.**



**Figure 28** Nimrod precipitation forecast sequence for DT 0400 GMT, 23 July 1996.

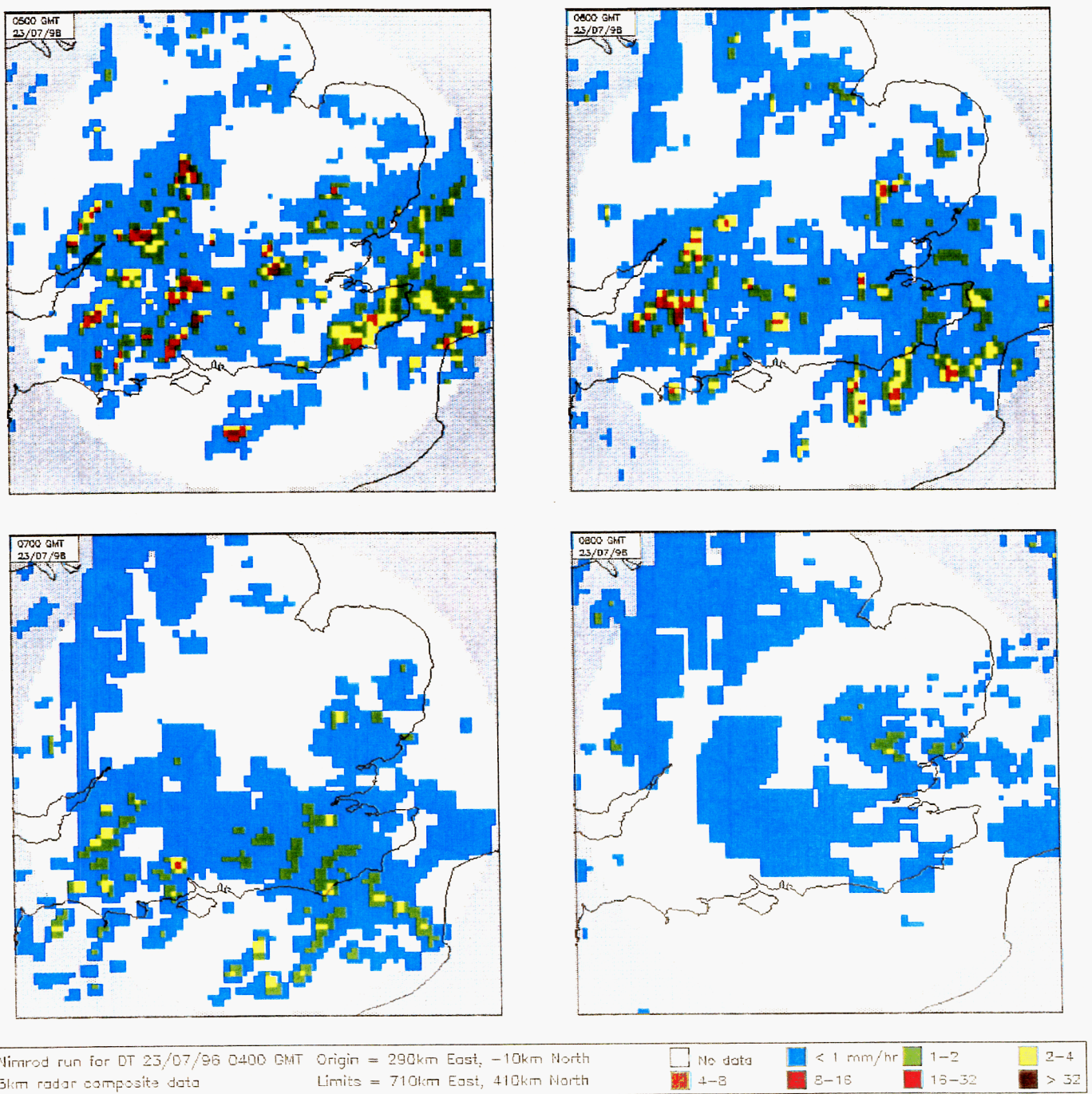
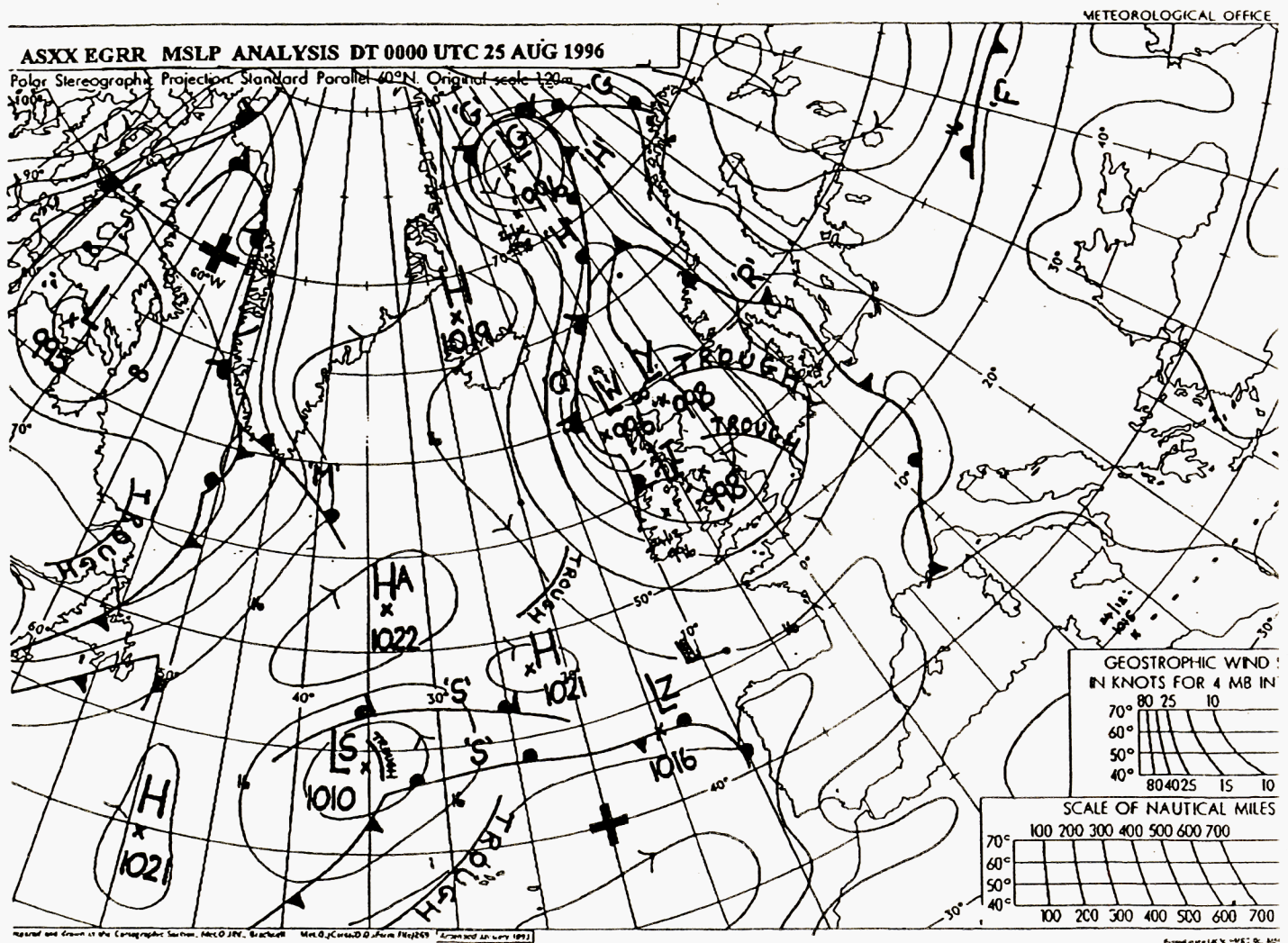
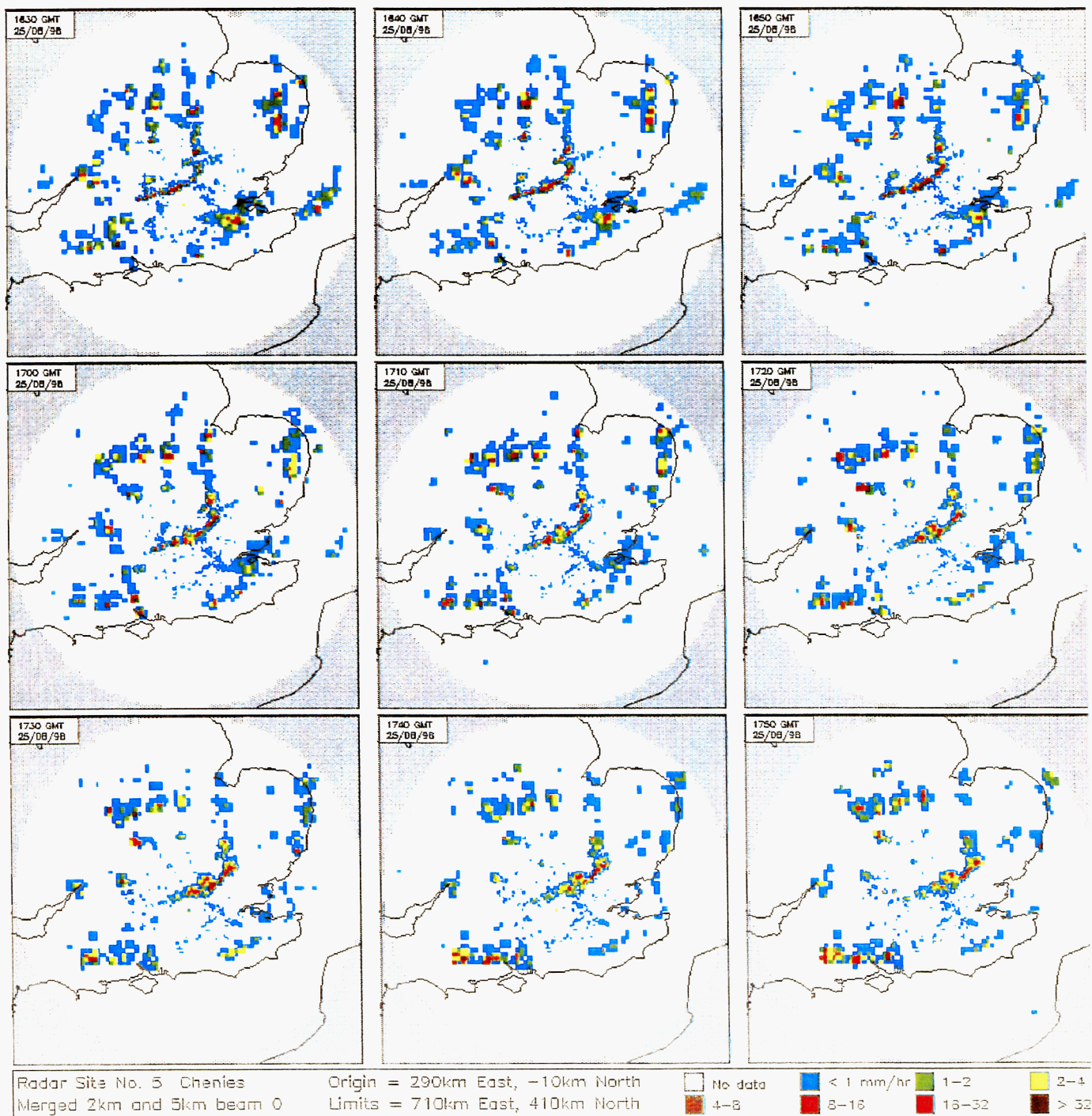




Figure 29 Surface analysis for 0000 GMT, 25 August 1996.

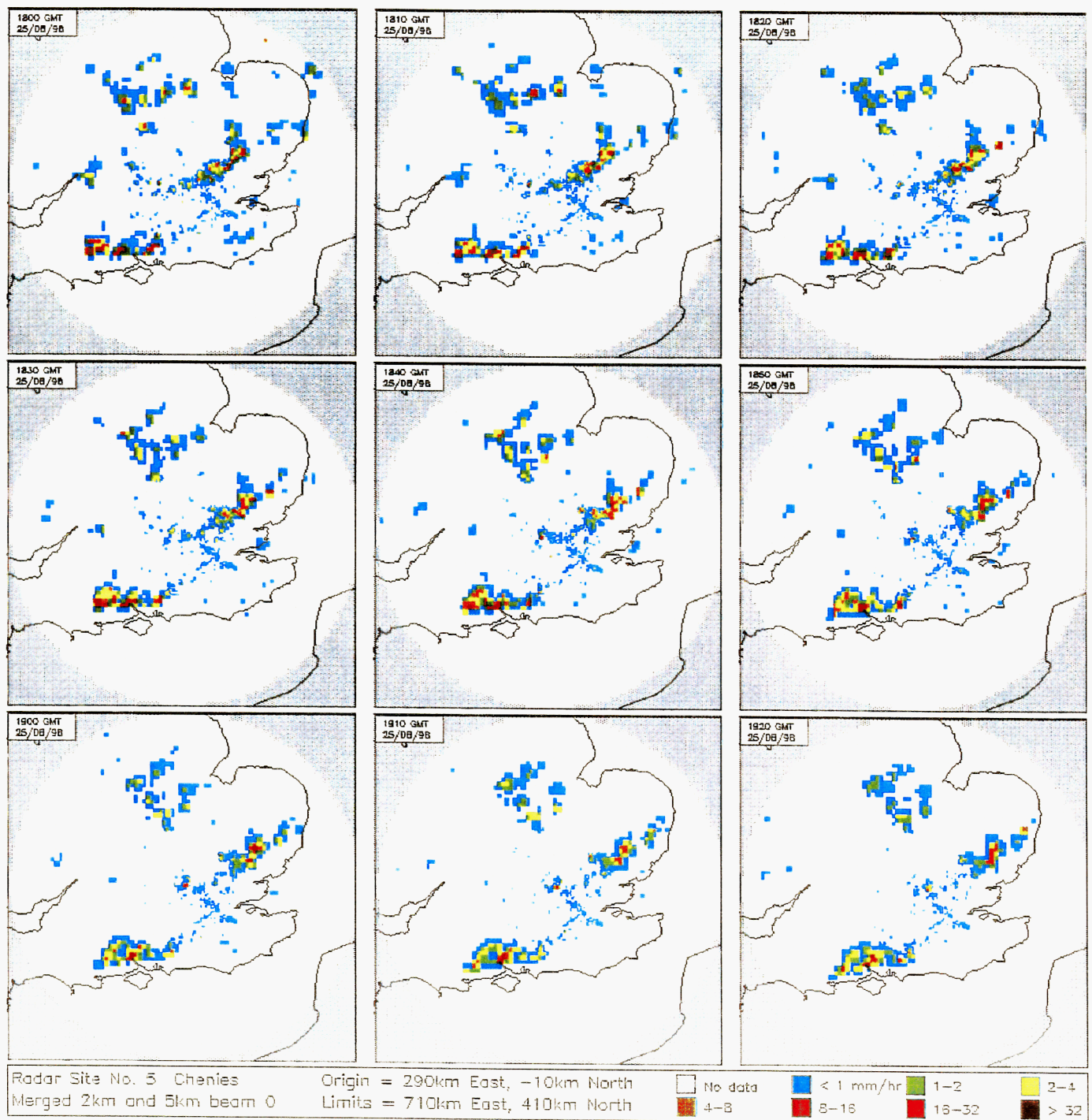


**Figure 30(a) Chenies 2 km surface beam image sequence for the period 1630 GMT to 1750 GMT, 25 August 1996.**

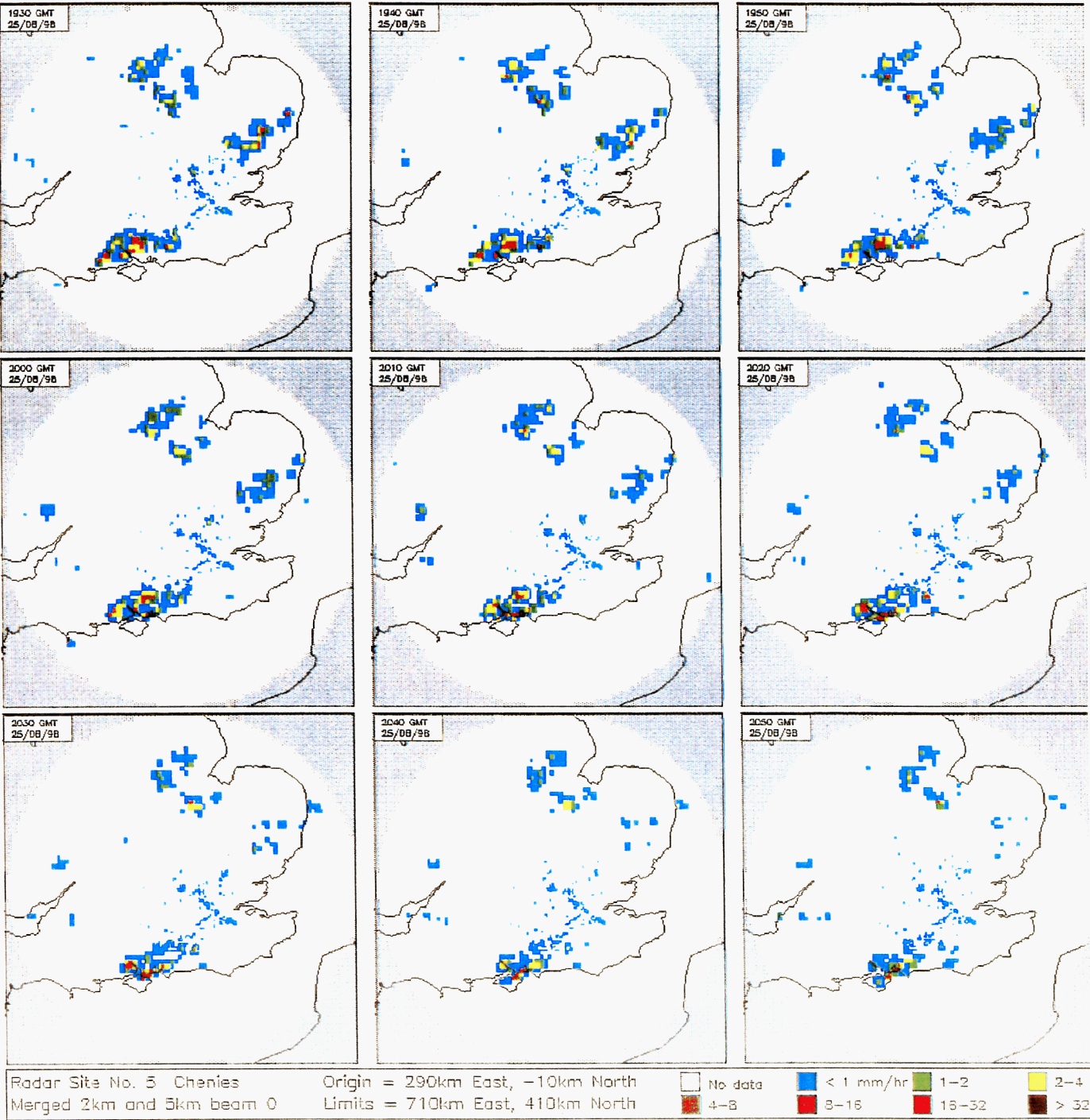




**Figure 30(b) Chenies 2 km surface beam image sequence for the period 1800 GMT to 1920 GMT, 25 August 1996.**

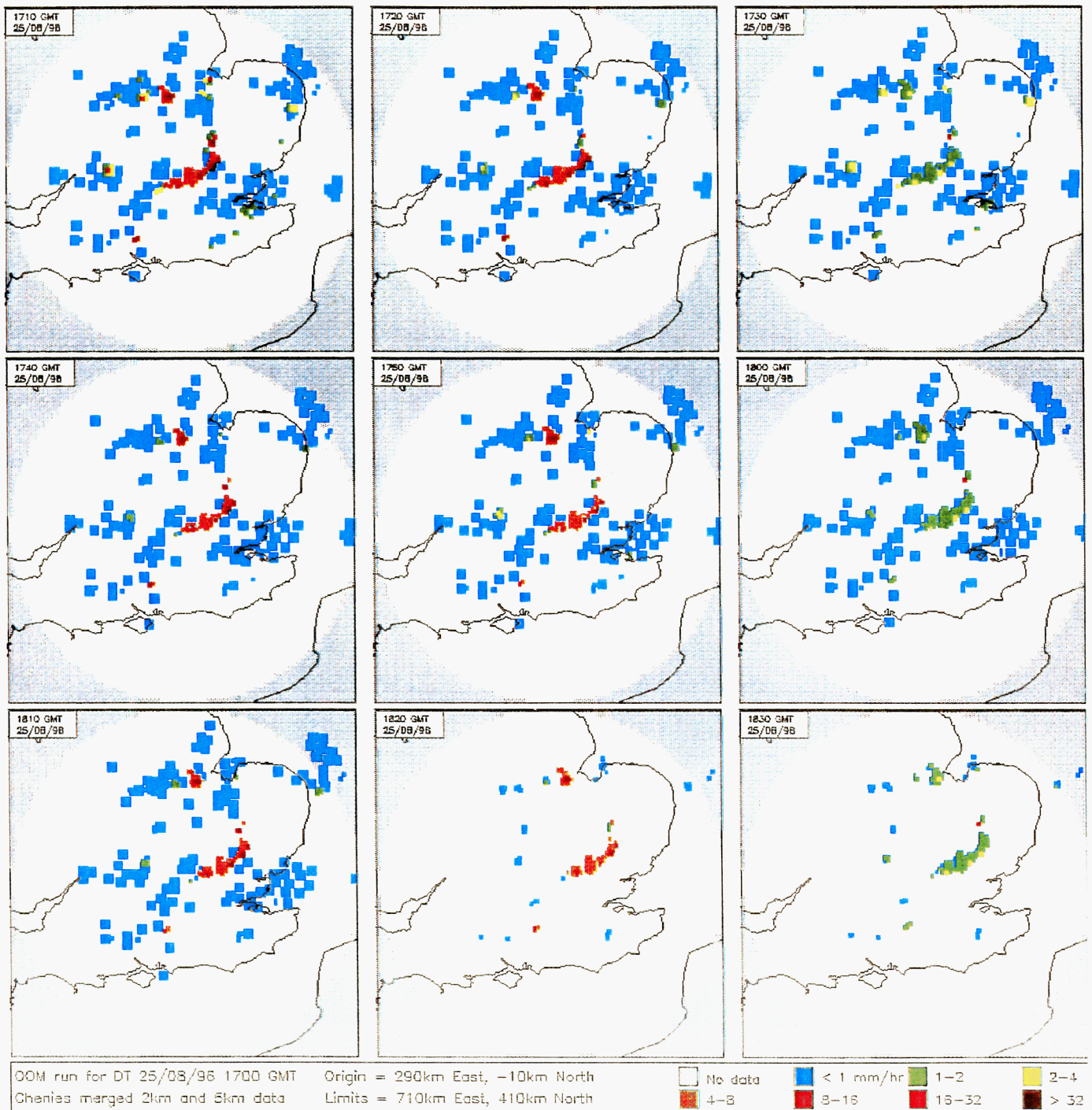


**Figure 30(c) Chenies 2 km surface beam image sequence for the period 1930 GMT to 2050 GMT, 25 August 1996.**





**Figure 31(a) OOM precipitation forecasts for DT 1700 GMT, VT 1710 GMT to 1830 GMT, 25 August 1996.**



**Figure 31(b) OOM precipitation forecasts for DT 1700 GMT, VT 1840 GMT to 2000 GMT, 25 August 1996.**

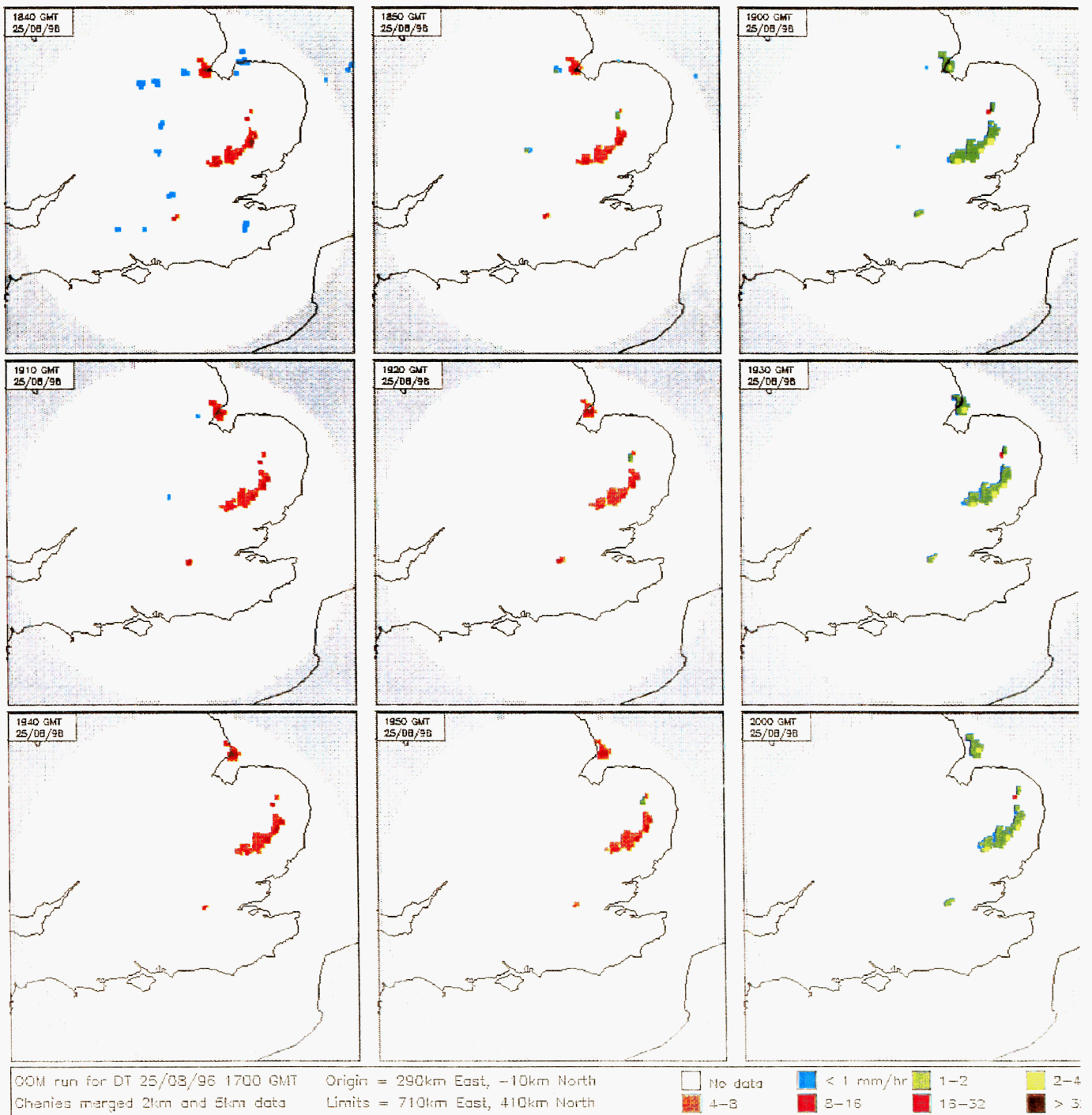
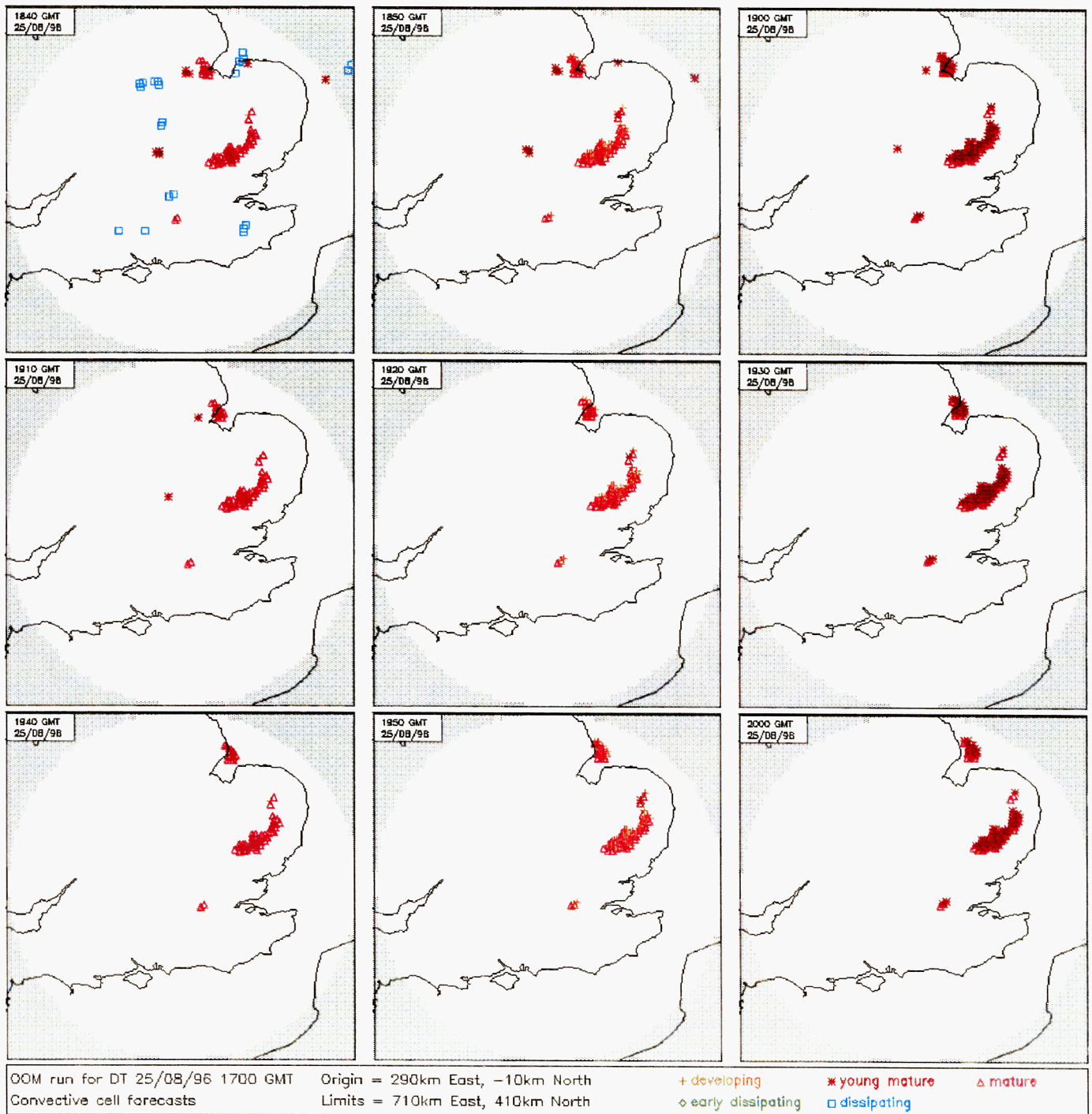




Figure 32(a) OOM cell forecasts for DT 1700 GMT, VT 1710 GMT to 1830 GMT, 25 August 1996.



**Figure 32(b) OOM cell forecasts for DT 1700 GMT, VT 1840 GMT to 2000 GMT, 25 August 1996.**





**Figure 33**      **Nimrod precipitation forecast sequence for DT 1700 GMT, 25 August 1996.**

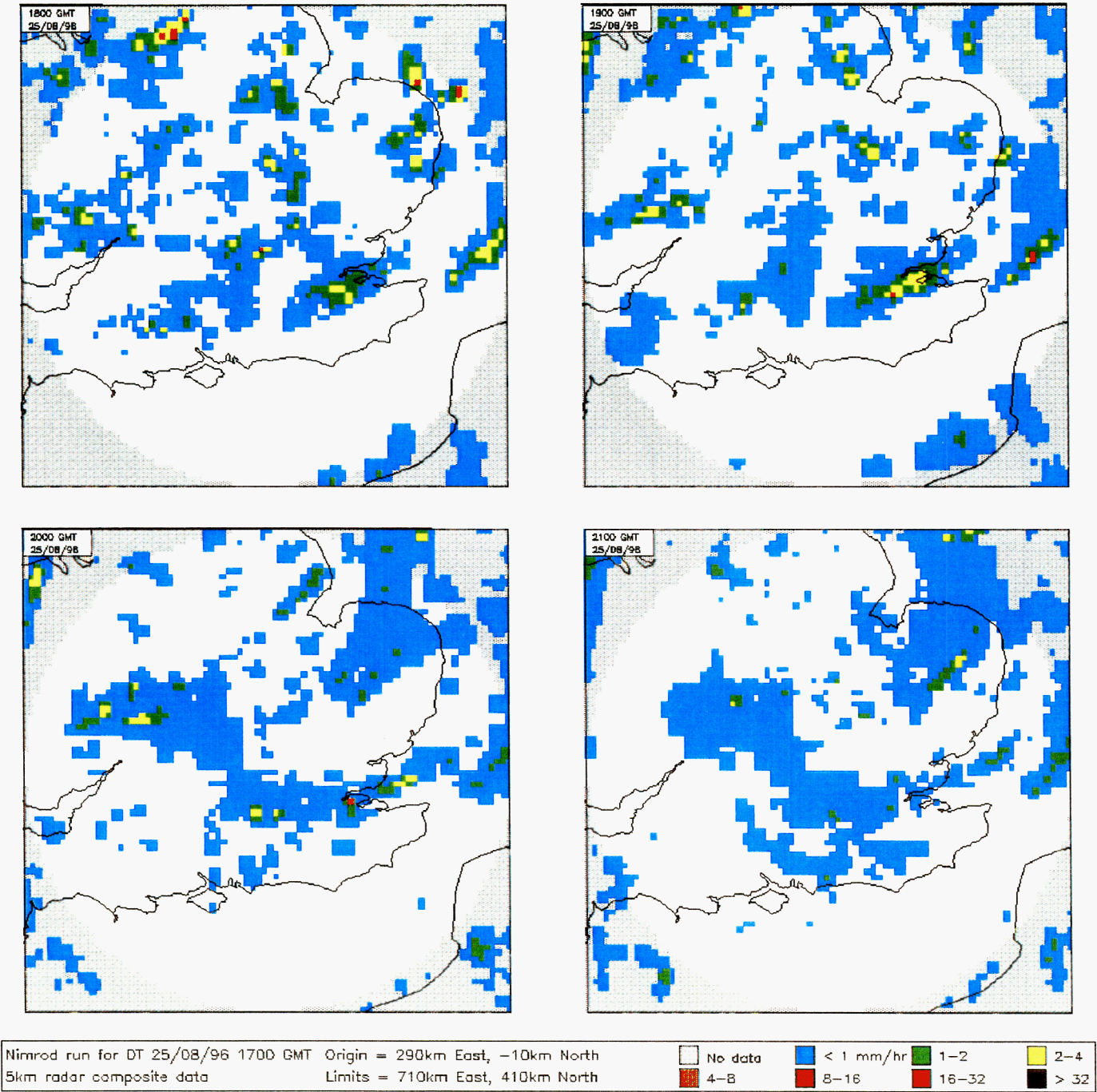
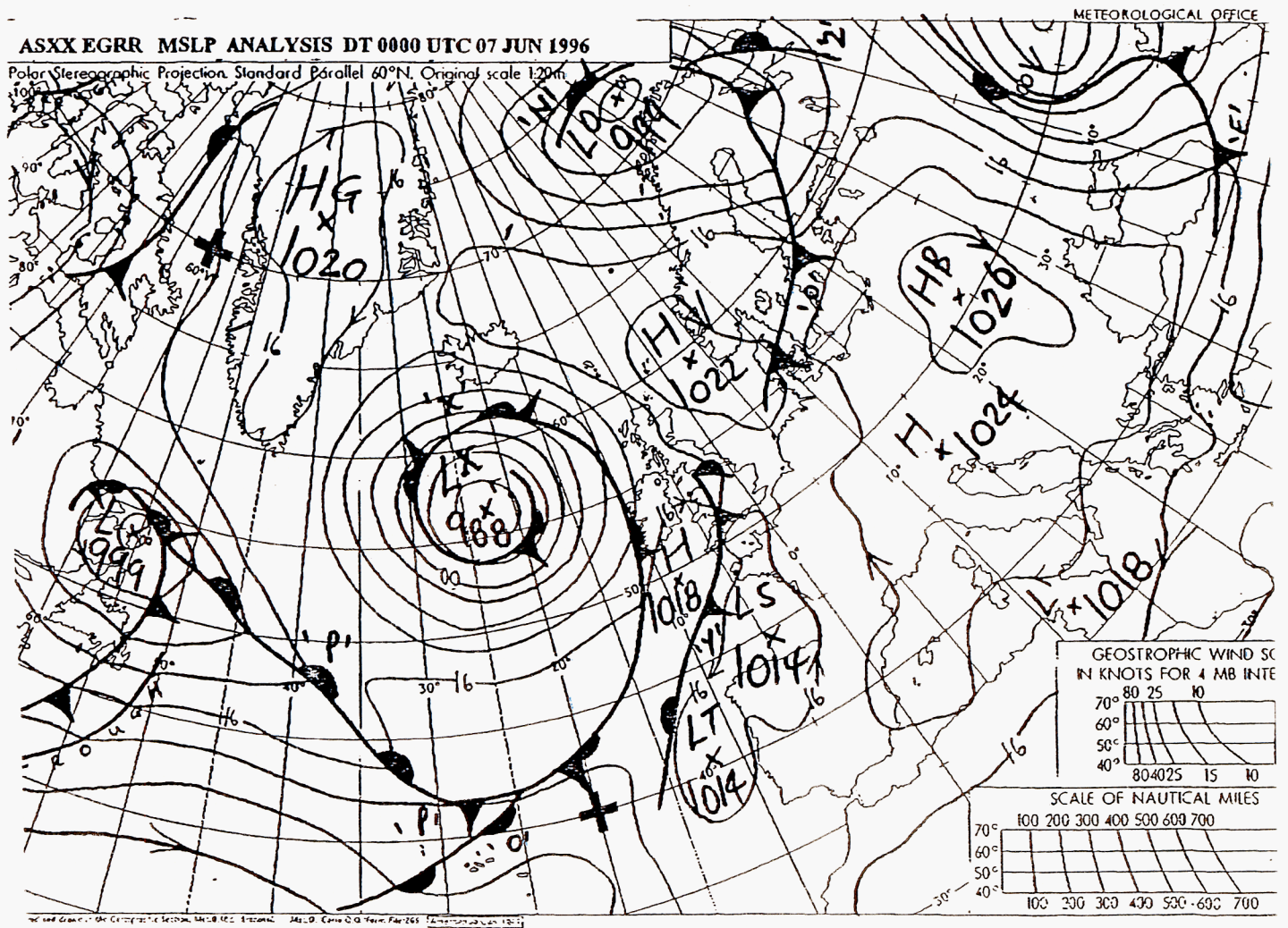


Figure 34 Surface analysis for 0000 GMT, 7 June 1996.





**Figure 35(a) Chenies 2 km surface beam image sequence for the period 1630 GMT to 1750 GMT, 7 June 1996.**

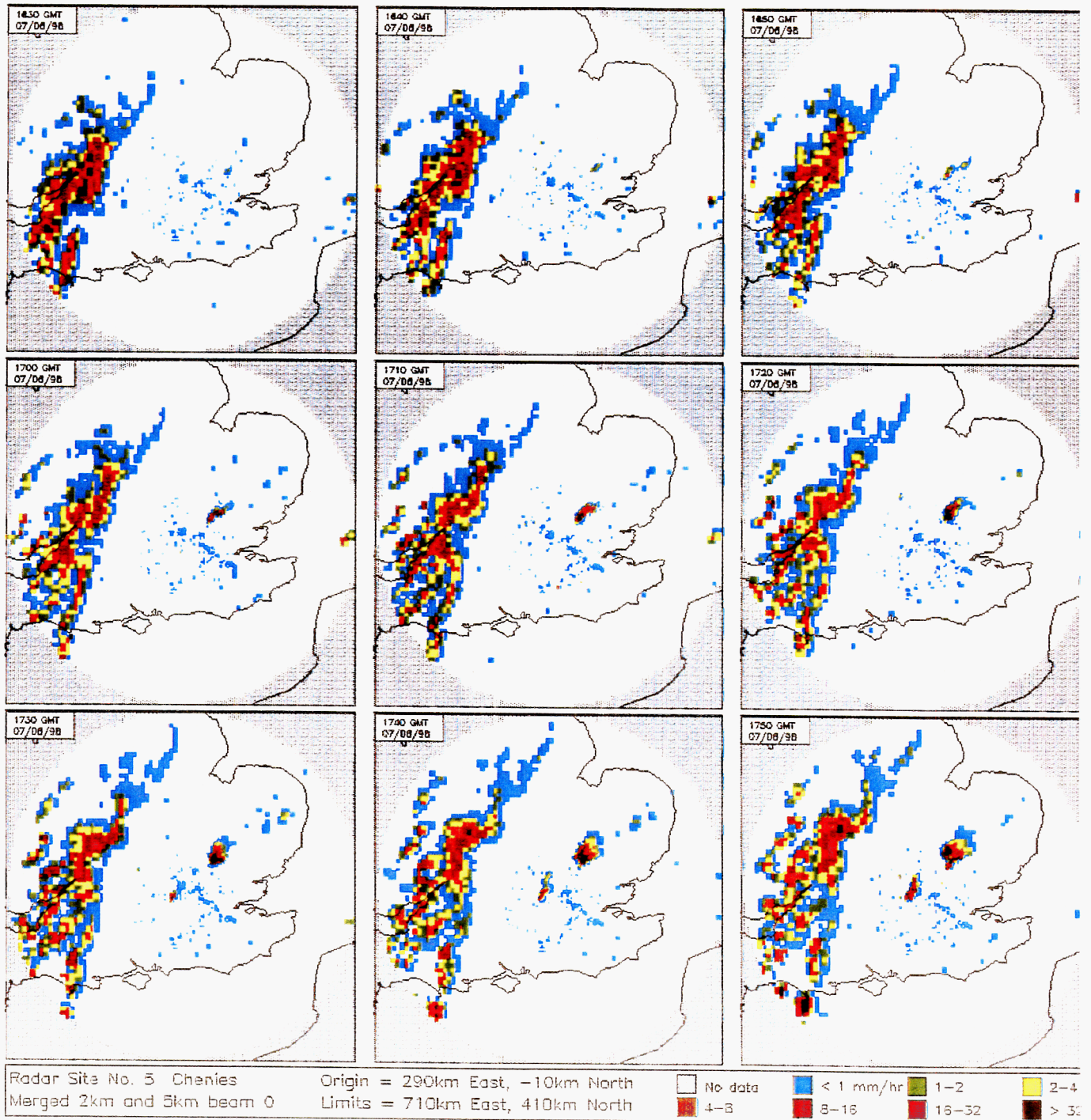
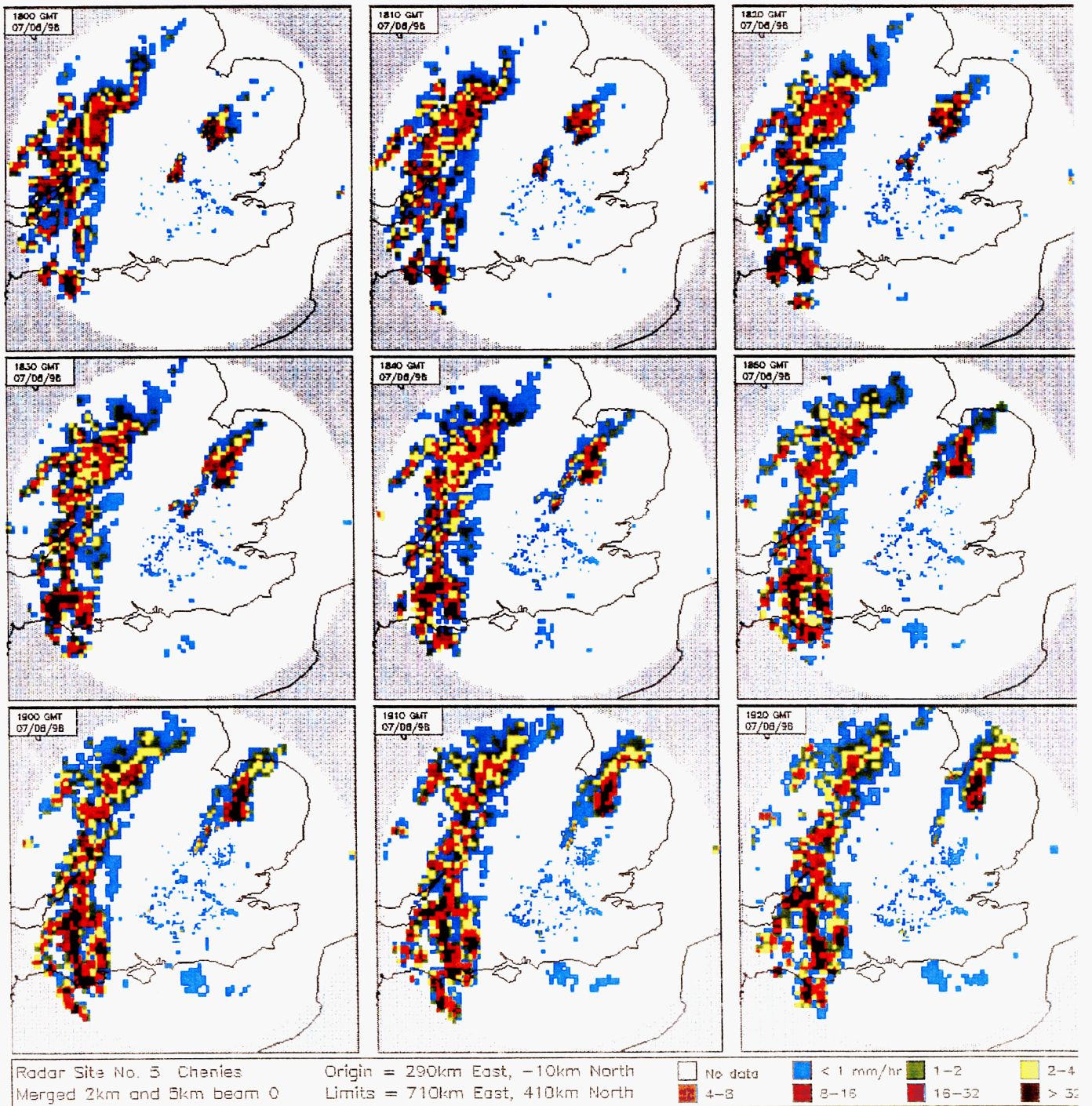


Figure 35(b) Chenies 2 km surface beam image sequence for the period 1800 GMT to 1920 GMT, 7 June 1996.





**Figure 35(c) Chenies 2 km surface beam image sequence for the period 1930 GMT to 2050 GMT, 7 June 1996.**

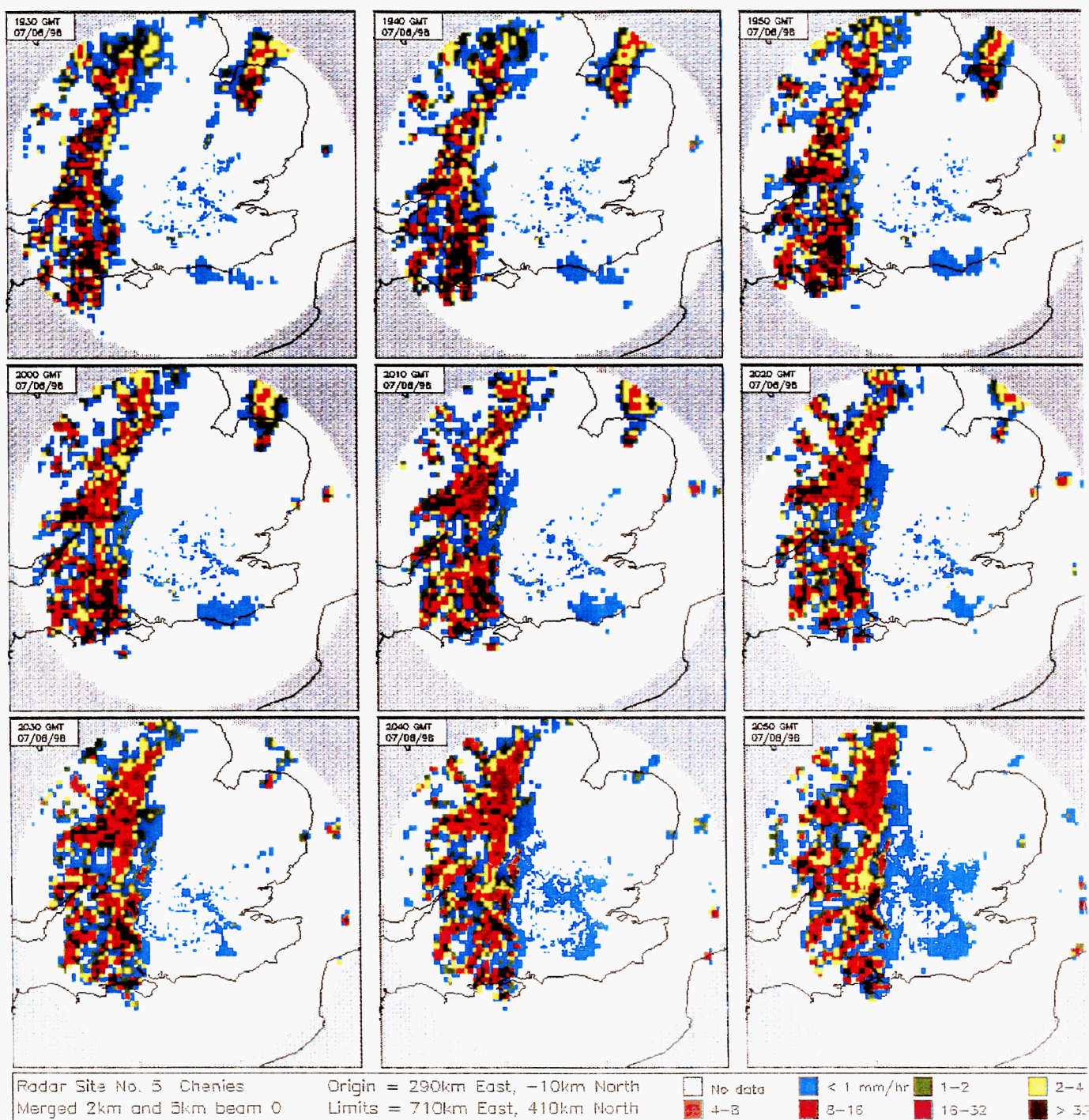


Figure 36(a) OOM cell forecasts for DT 1650 GMT, VT 1700 GMT to 1820 GMT,  
7 June 1996.

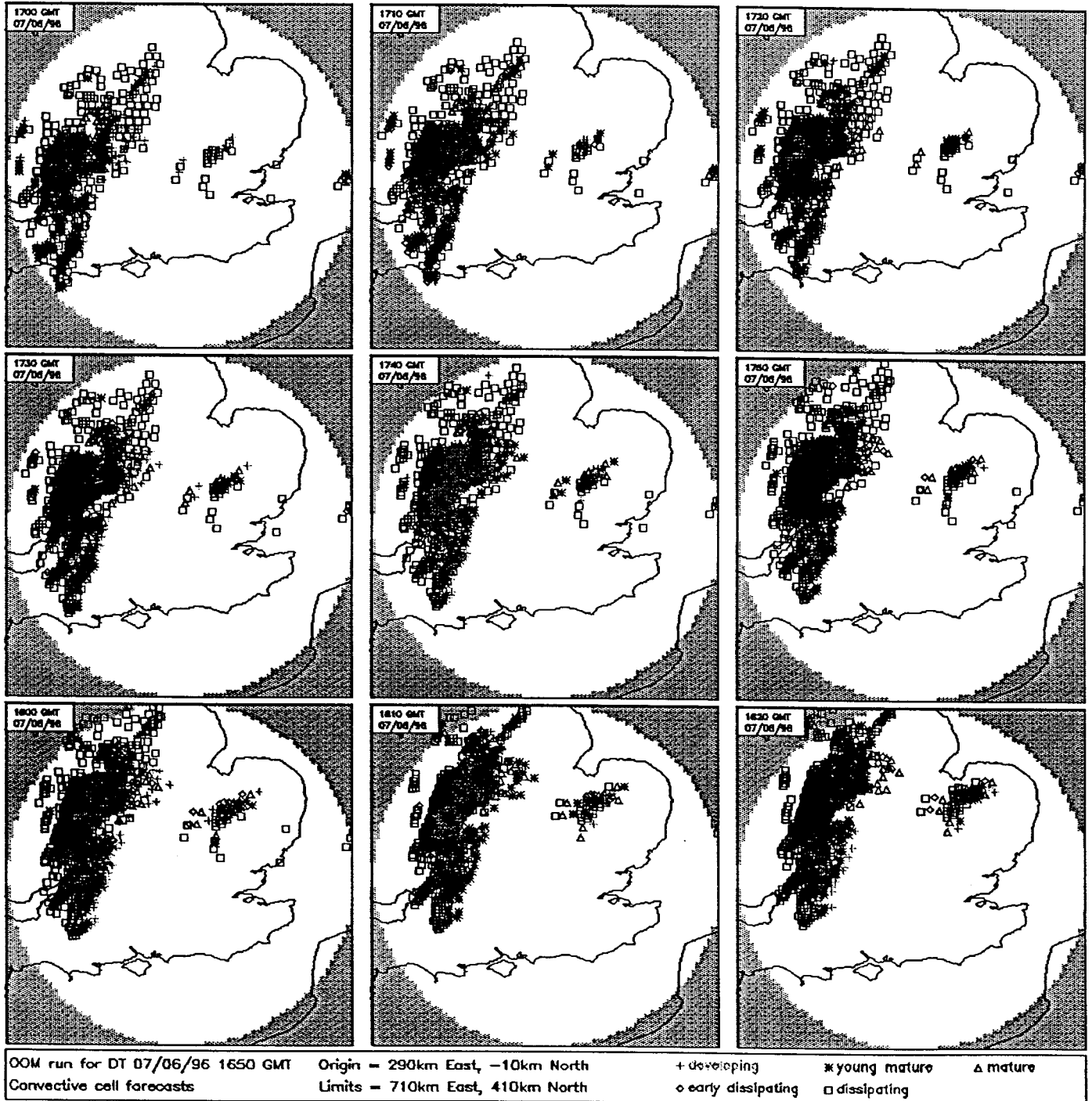
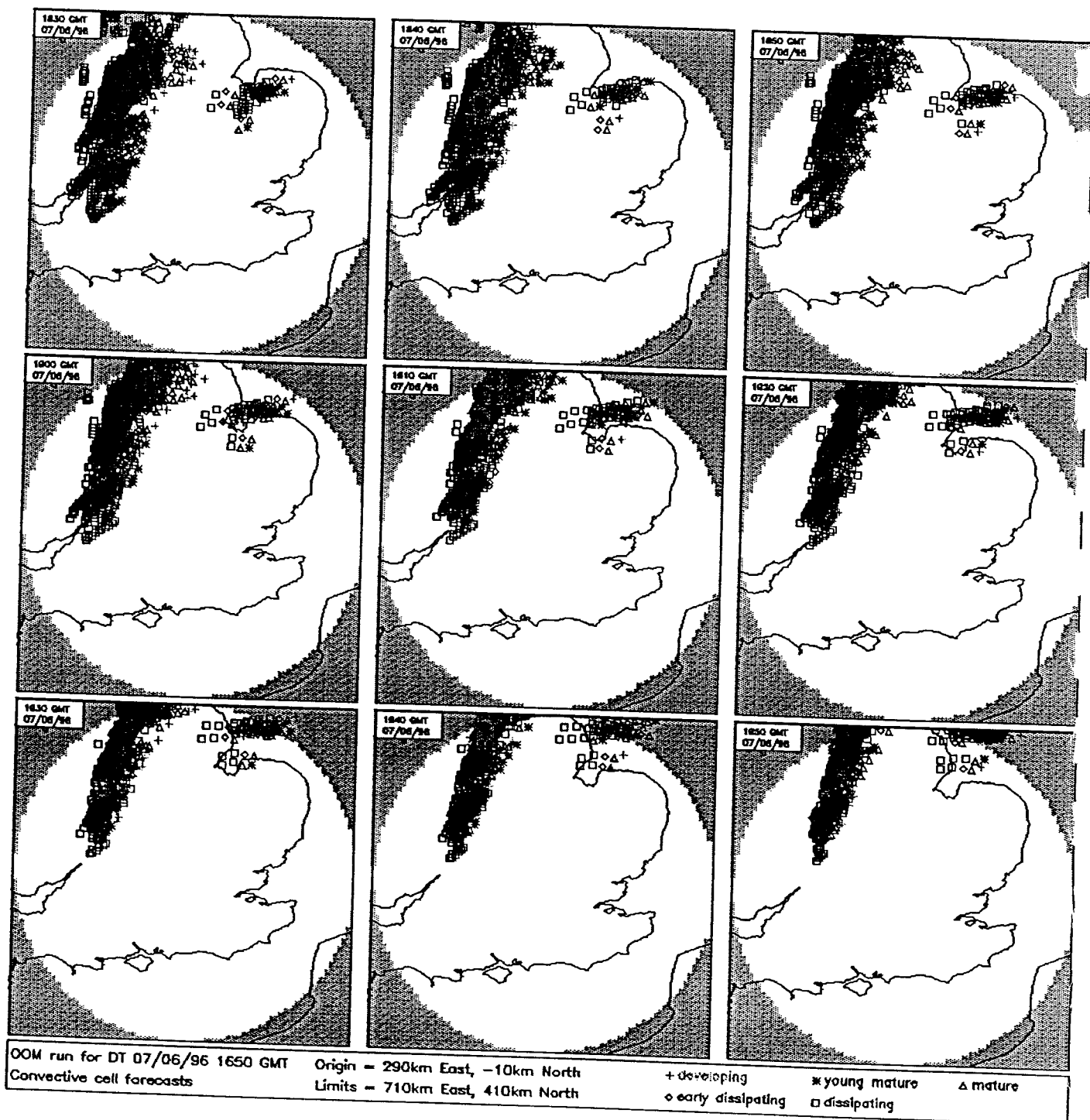


Figure 36(b) OOM cell forecasts for DT 1650 GMT, VT 1830 GMT to 1950 GMT,  
7 June 1996.





**Figure 37(a) OOM precipitation forecasts for DT 1650 GMT, VT 1700 GMT to 1820 GMT, 7 June 1996.**

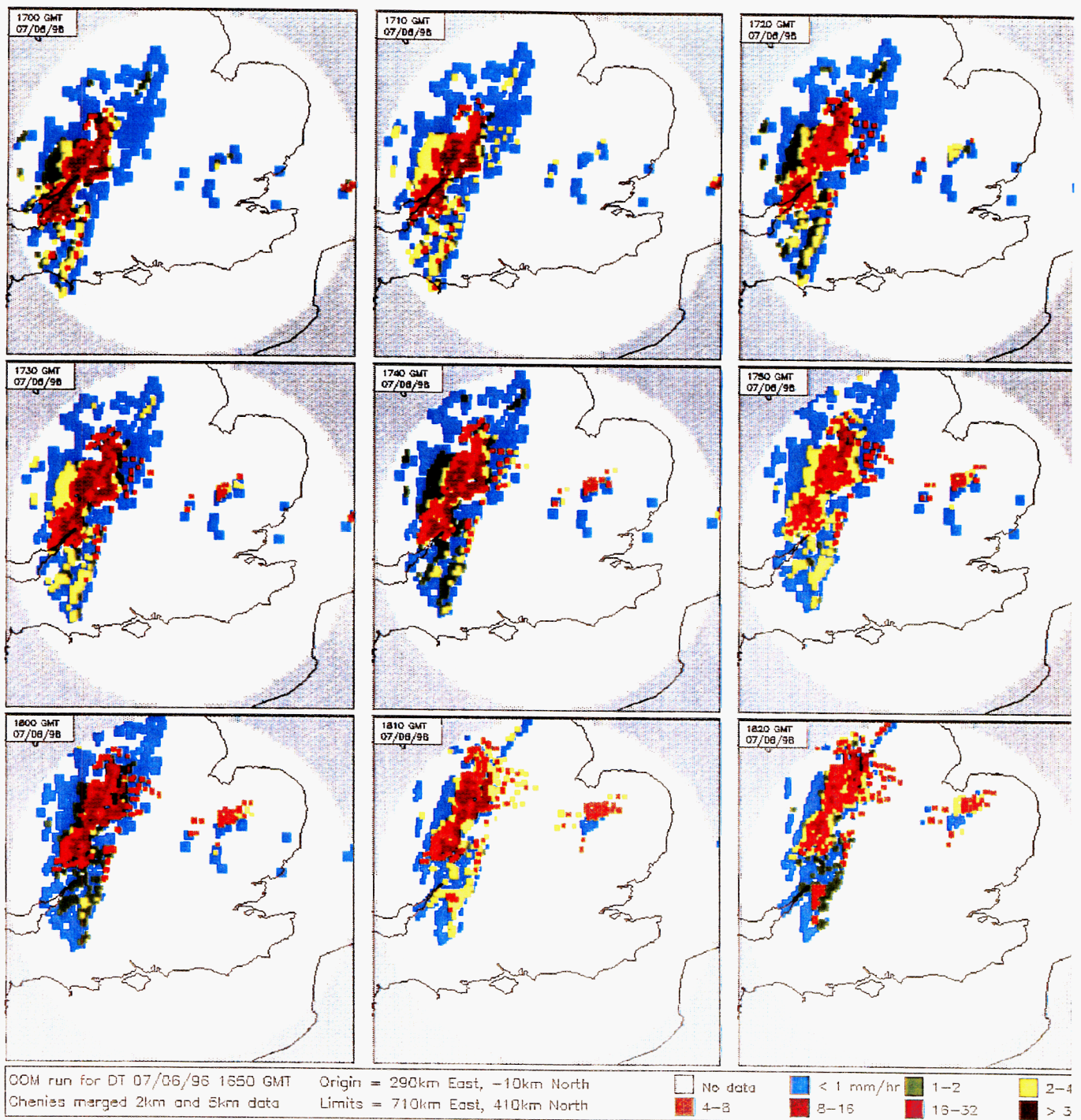
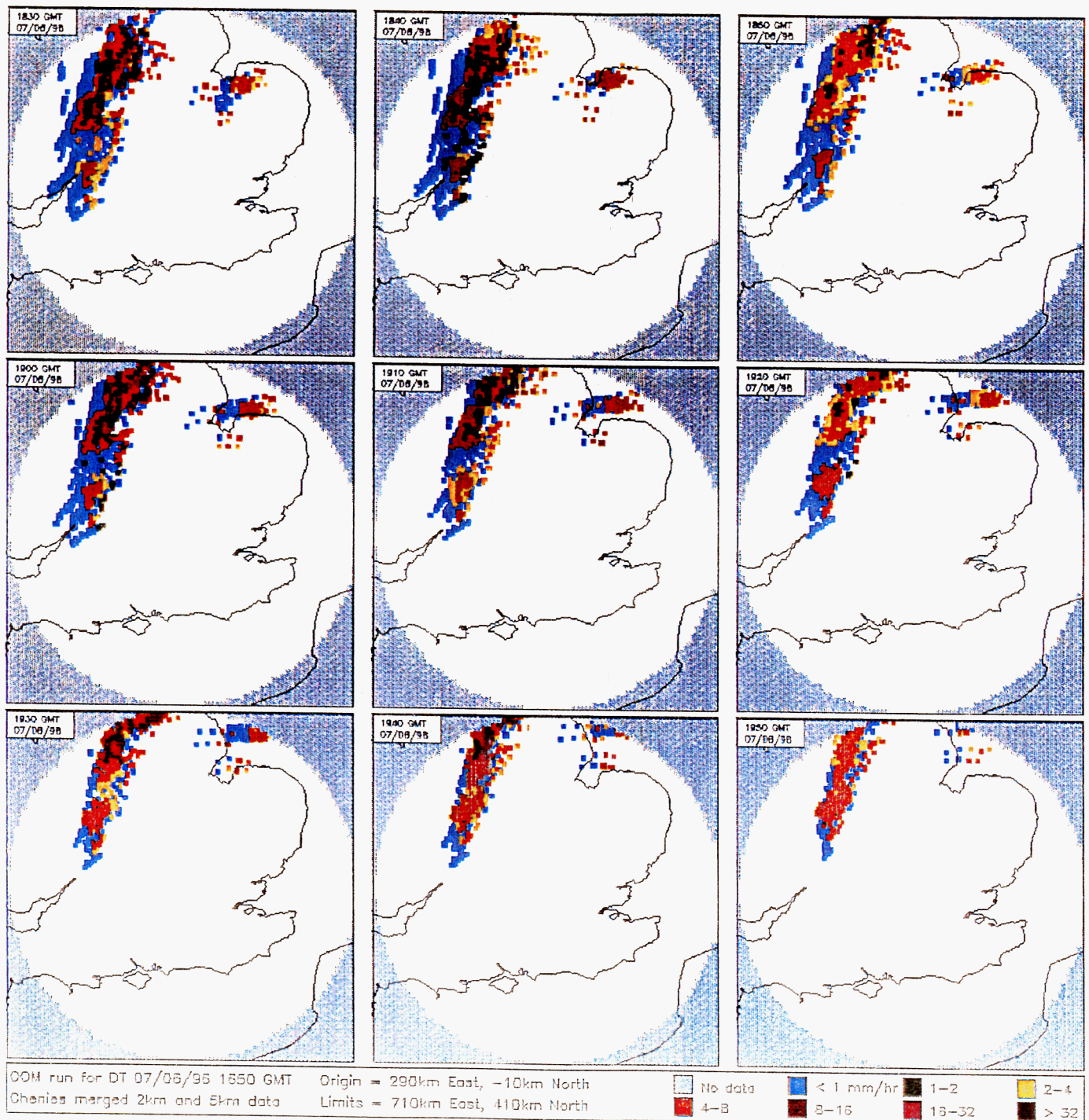
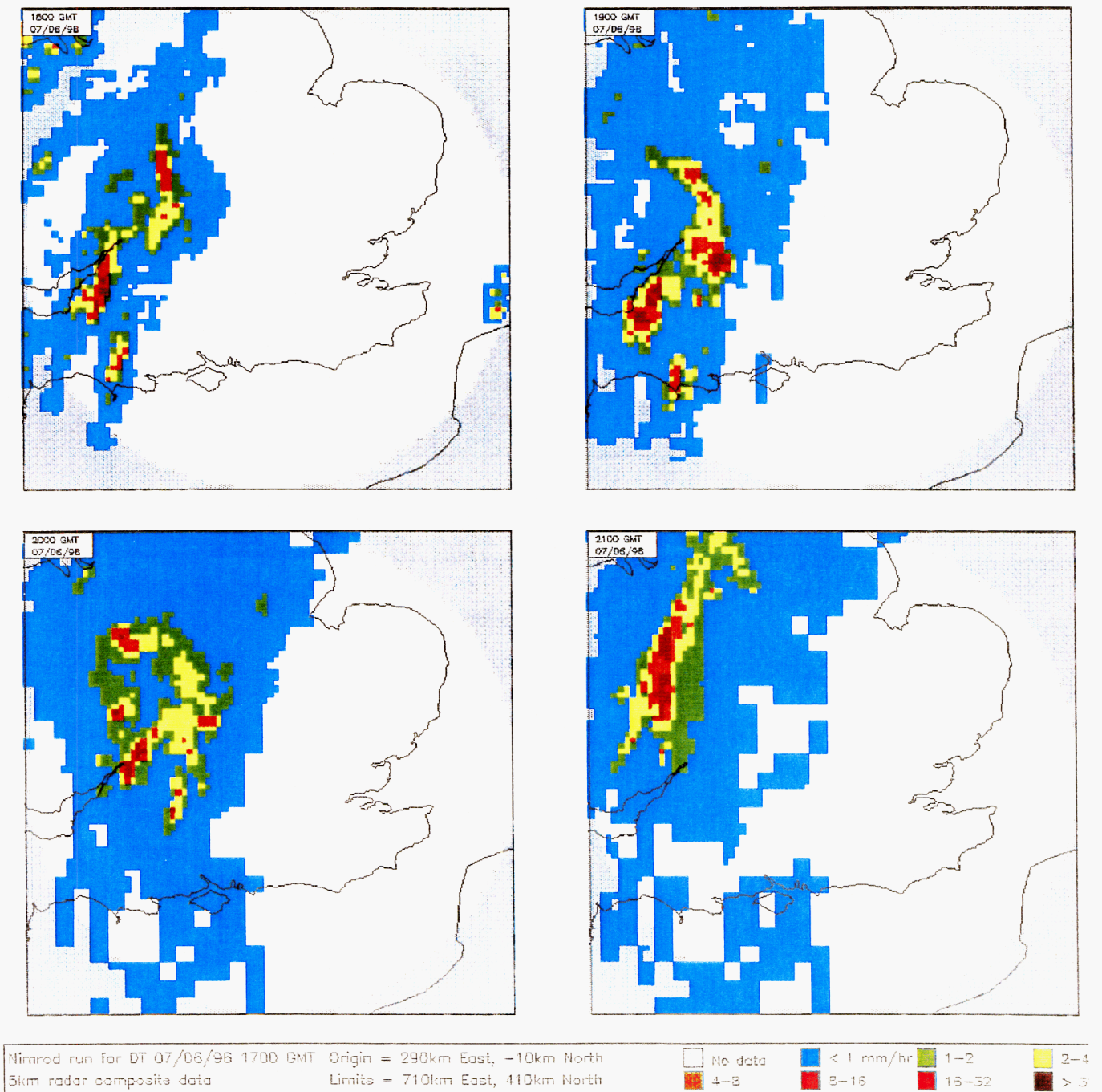


Figure 37(b) OOM precipitation forecasts for DT 1650 GMT, VT 1830 GMT to 1950 GMT, 7 June 1996.



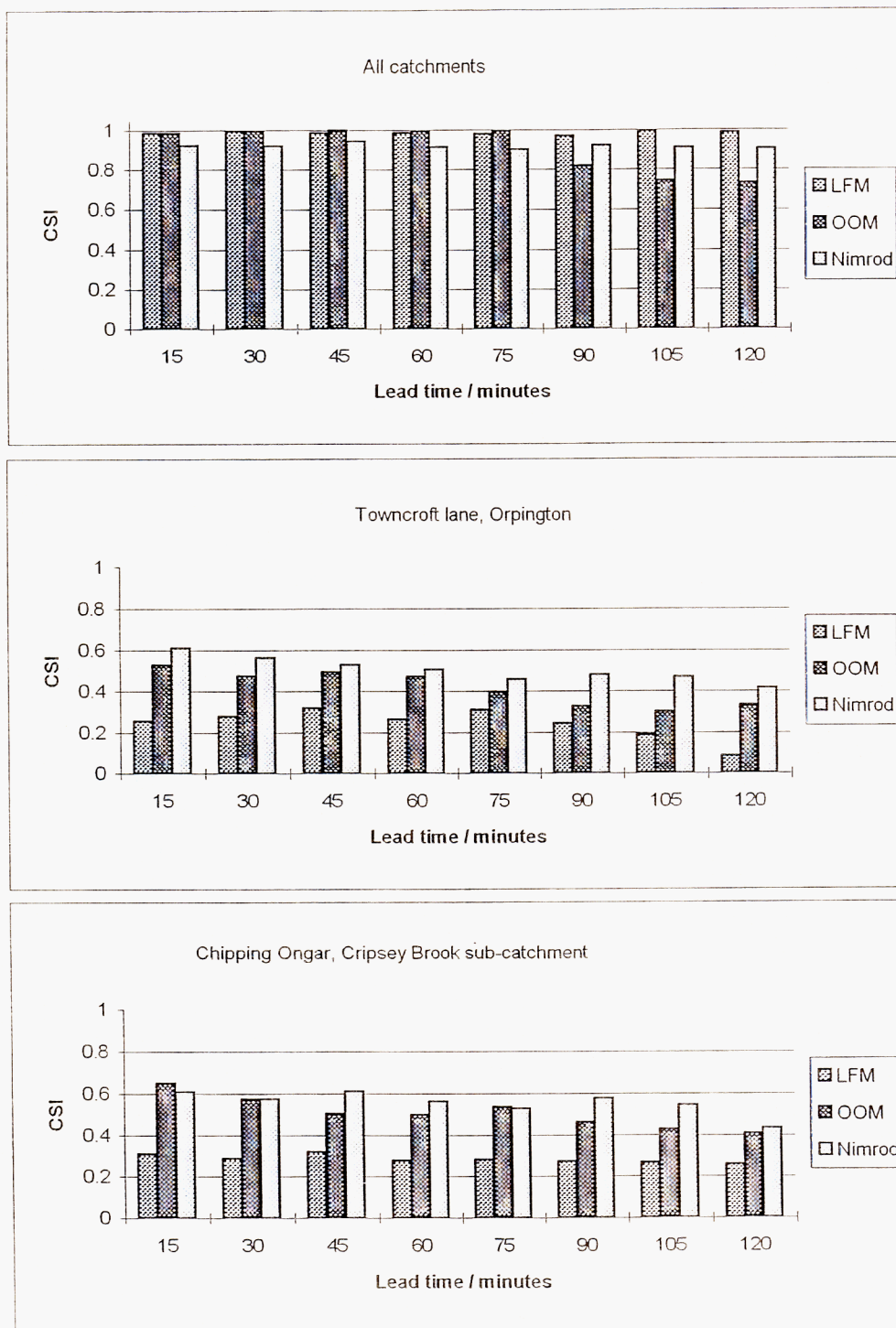


**Figure 38 Nimrod precipitation forecast sequence for DT 1700 GMT, 7 June 1996.**

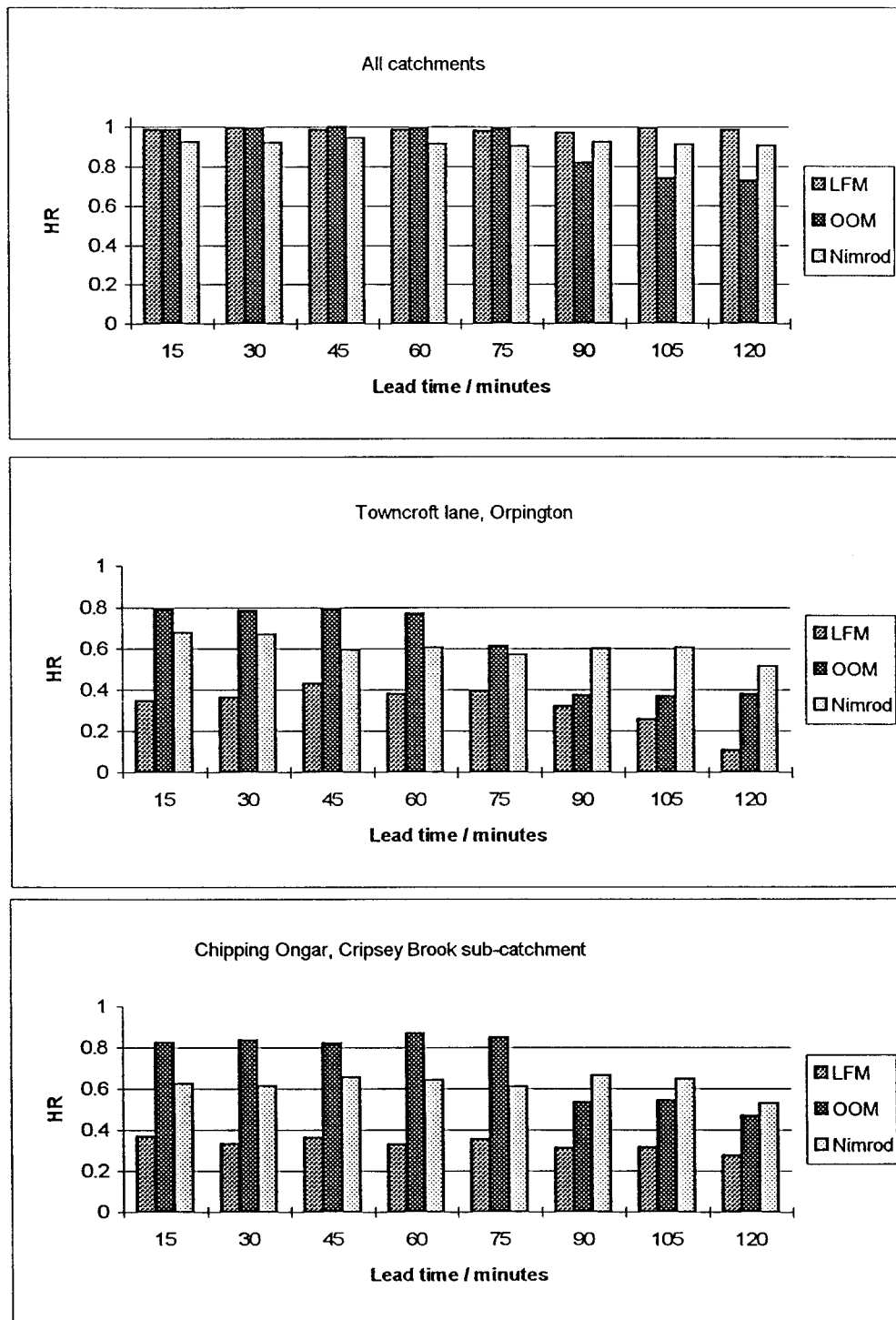




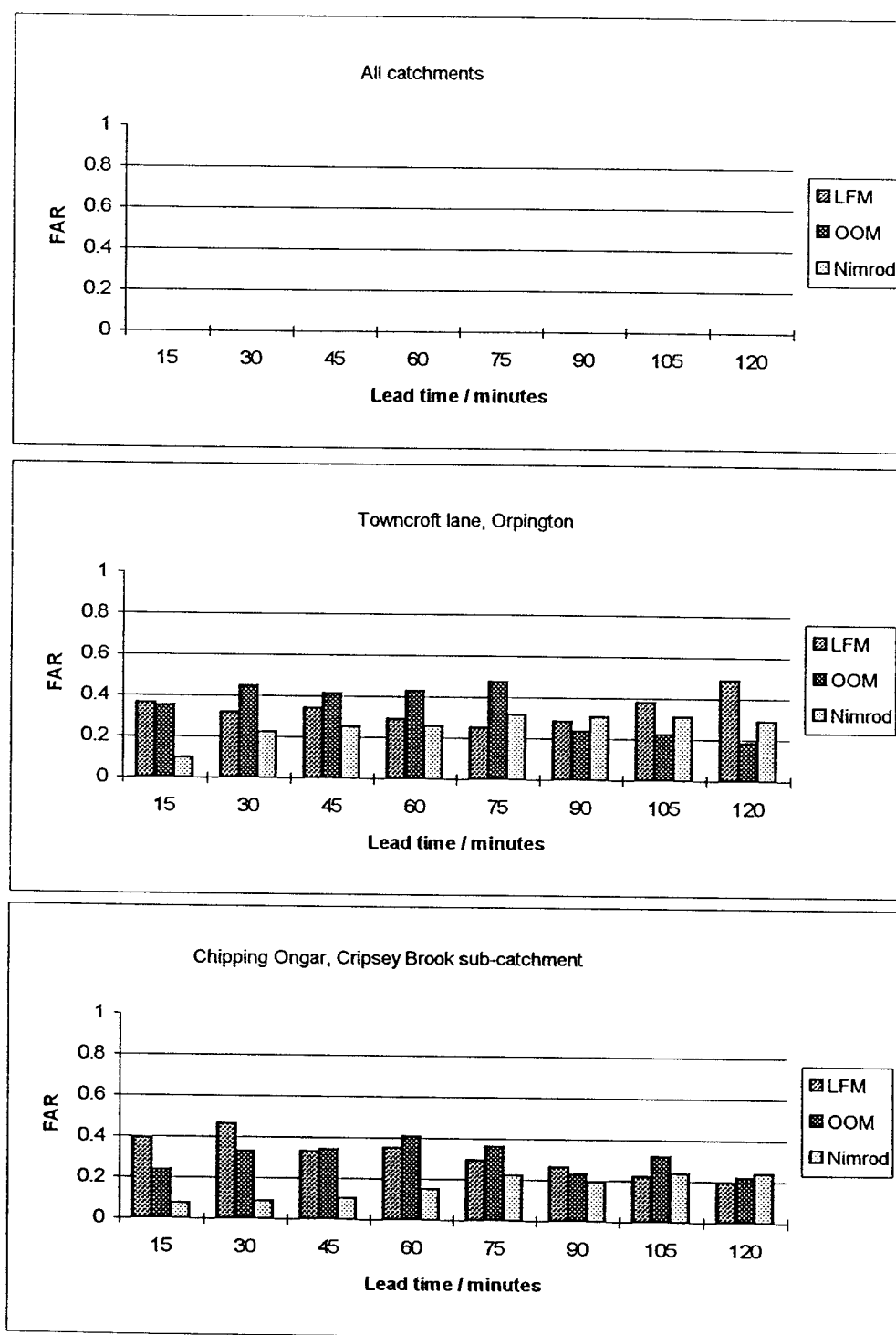
**Figure 39** Comparative performance of 15 minute accumulation forecasts for the OOM, LFM and Nimrod: Catchment CSI as a function of catchment and forecast lead time.



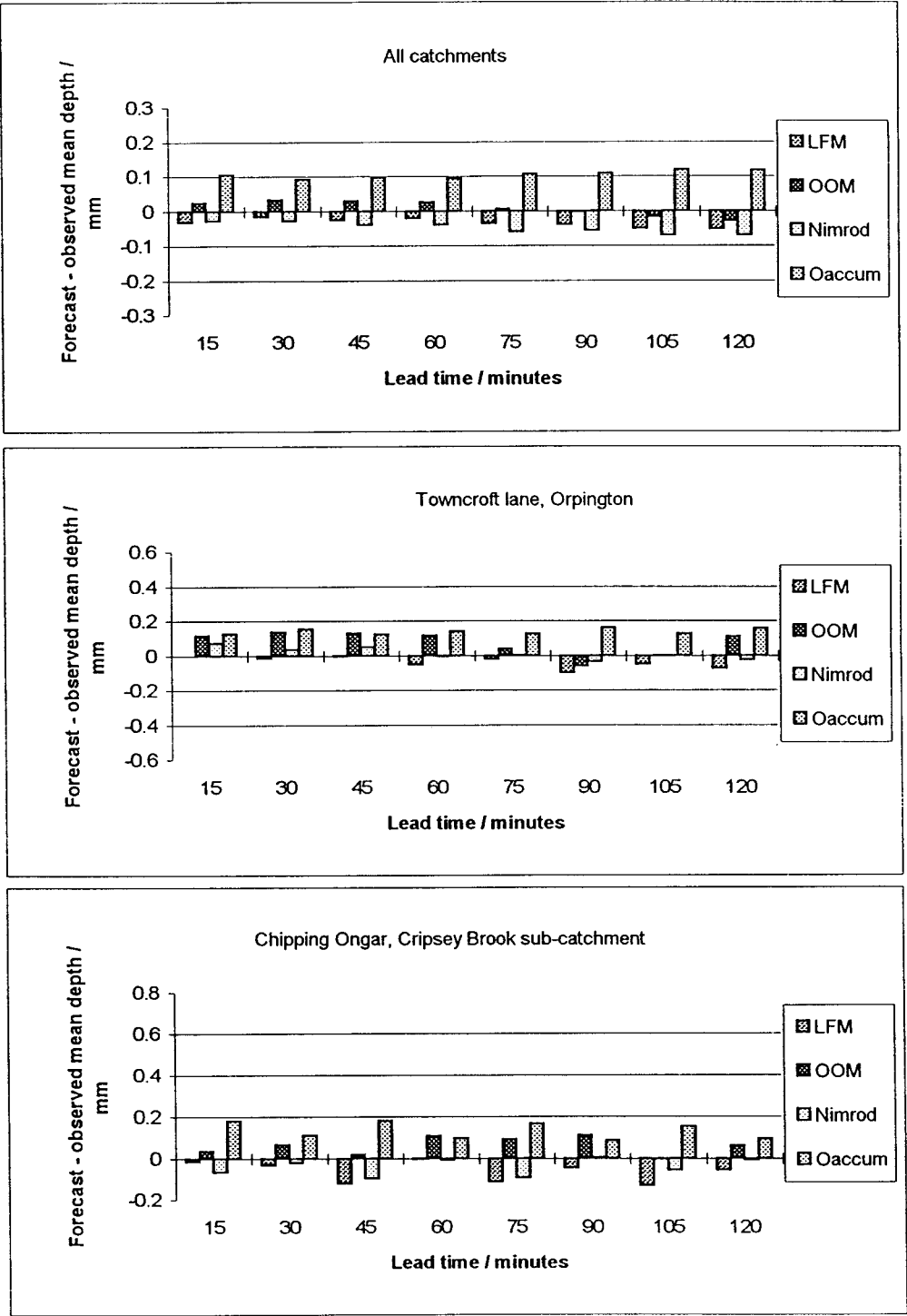
**Figure 40**      **Comparative performance of 15 minute accumulation forecasts for the OOM, LFM and Nimrod: Catchment HR as a function of catchment and forecast lead time.**



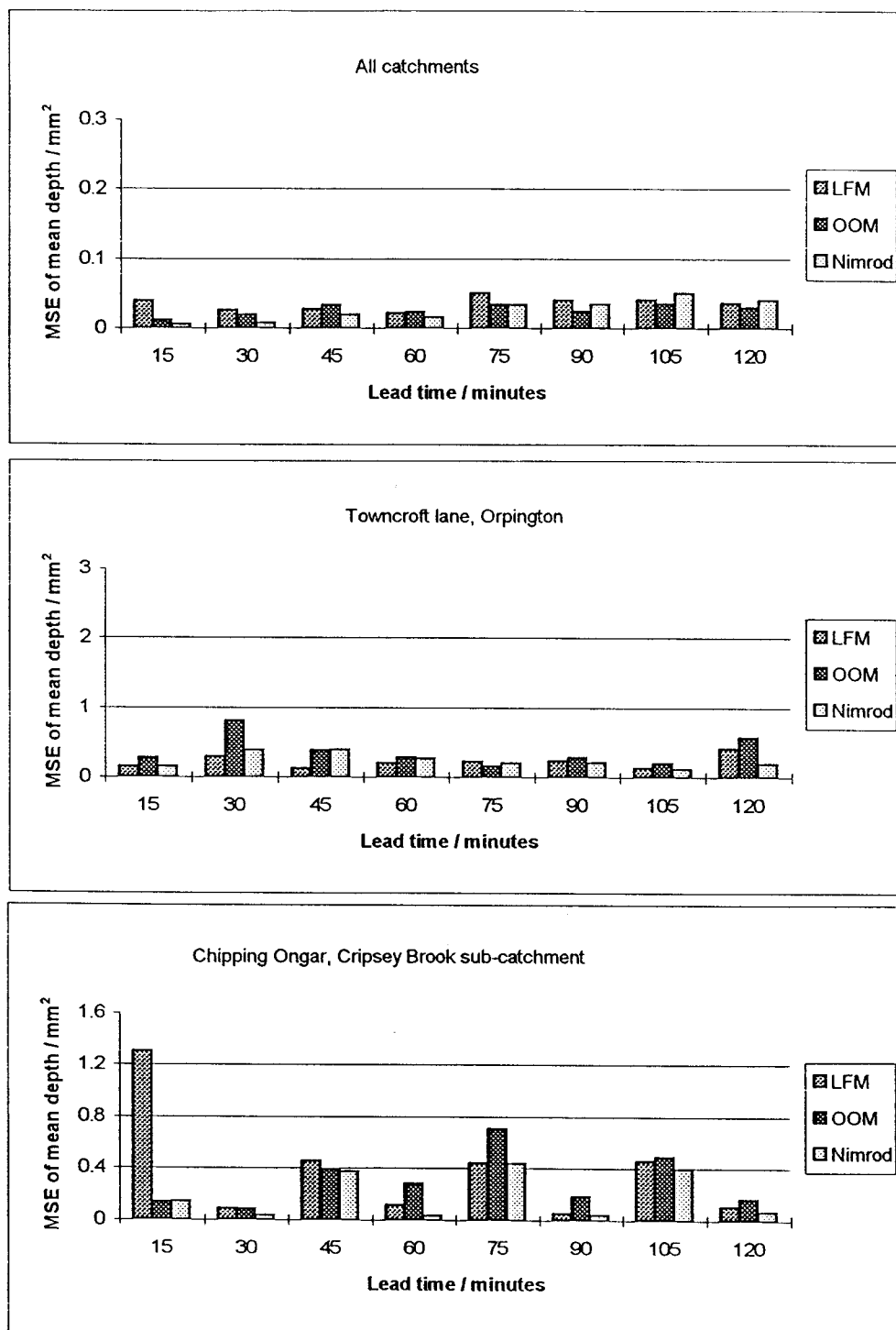
**Figure 41**      **Comparative performance of 15 minute accumulation forecasts for the OOM, LFM and Nimrod: Catchment FAR as a function of catchment and forecast lead time.**



**Figure 42**      **Comparative performance of 15 minute accumulation forecasts for the OOM, LFM and Nimrod: (Forecast - observed) catchment 15 minute accumulation as a function of catchment and forecast lead time.**



**Figure 43** Comparative performance of 15 minute accumulation forecasts for the OOM, LFM and Nimrod: MSE of 15 minute accumulation as a function of catchment and forecast lead time.



## APPENDIX A: THE OBJECT-ORIENTED MODEL

### A.1 Convective clouds and precipitation<sup>2</sup>

#### A.1.1 Cloud profiles

Consider a rising current of air originating at the Earth's surface. As the air parcel rises it cools adiabatically and moisture begins to condense on numerous microscopic condensation nuclei at a level that varies inversely with the moisture content of the parcel. This level is referred to as the condensation level and is a close approximation to the convective cloud base.

If the rising current remains warmer than its surroundings it will continue to ascend. During ascent, cloud particles typically numbering several hundred per cubic centimetre continue to be formed and grow. Since cloud condensate is distributed among many particles, their typical diameter is of the order of only a few microns (Mason, 1971). The smallness of the particles means they are carried upward with the rising current. As condensation continues the mass of condensate per unit volume increases. When the rising current reaches the higher part of the troposphere it has cooled considerably by adiabatic expansion and little moisture remains for further condensation. At higher altitudes cloud density usually diminishes with rising motion, since the cloud expands along with the air, and little new cloud can be created by condensation.

Figure A.1 shows a theoretical vertical profile of cloud density assuming a condensation level of 1 km at a temperature of 10°C in an ICAO standard atmosphere. This condensation level (cloud base) is typical for growing cumulus clouds during the summer months in the UK. Note that the diagram shows cloud droplet density increases rapidly below 3 km (-1°C) and reaches a maximum near 6 km (-22°C), then decreases higher up. This explains the very solid appearance of the growing top of a cumulonimbus cloud prior to glaciation.

#### A.1.2 Precipitation profiles

Precipitation forms from clouds that consist of droplets having a variety of sizes, chemical components and fall-speeds. If the variety is large then some droplets tend to grow at the expense of others which evaporate. At temperatures below -10°C ice particles will grow by deposition of vapour. Occasionally contacts arising from the relative motions of the droplets results in fusion. These processes initially produce a few large particles which then fall through the cloud and grow further by accretion of other cloud droplets. Precipitation is first formed somewhere near the dense middle of the cloud (see Figure A.1). The precipitation particles fall and descend to the ground unless the updraft exceeds a few metres per second. The cloud particles continue to form and rise in the updraft. However, they now start to deplete in number by their contacts with precipitation. This means that the precipitation grows during its descent to the ground, while the cloud becomes thinner.

Eventually, precipitation forms near to, or at the top of the cloud layer and develops at the expense of cloud on its way downwards. For small precipitation particles this process of gathering cloud droplets is quite efficient, therefore the rate of precipitation development at

---

<sup>2</sup> after Hand (1996)

each height depends on the rate of cloud formation at that height. Figure A.1 shows that cloud formation is fastest in the lower part of the cloud so it is typical that the most rapid development of precipitation takes place in the lower part of the updraft. However, this is an over-simplification when updraft speeds considerably exceed fall-speeds. In these cases of strong convection, particles may be recycled through the cloud so that it takes longer for the precipitation to descend to the ground, and when it does the particles are bigger.

In thunderstorms, updrafts can be very strong. In these clouds both precipitation particles and cloud droplets are carried upwards to near the top of the updraft column. When precipitation formation begins there is a larger amount of cloud to change to precipitation than in weaker convective clouds, and therefore a larger amount of precipitation in the upper part of the column, where it is very effective in reducing the amount of cloud by accretion. The precipitation cannot descend to the ground in the updraft region but may be transported horizontally to descend in adjacent downdrafts where it is often subject to large losses by evaporation. As the thunderstorm starts to decay, the updraft is replaced by a gentle downdraft throughout the cloud and precipitation production decreases and finally stops. This decay usually proceeds from the top of the cloud downwards as cloud droplets high up are not replaced.

The above is of necessity a simplified description of the precipitation producing processes. More detailed descriptions, can be found in Kessler (1975) and Young (1993), especially Chapters 9 and 10.

### **A.1.3 Cell stage descriptions**

Current operational UK radars operating at C-band wavelengths are unable to detect targets with diameters less than about 100  $\mu\text{m}$  (drizzle droplets). The scheme employed to identify convective cell stage will therefore only pick out convective cells containing precipitation-sized particles. The following cell stage classification is used which is very similar to that used in Hand and Conway (1995), hereafter known as HC.

- d** Large towering cumulus or cumulonimbus without anvil cirrus that is producing precipitation that evaporates before reaching the ground.
- m** Young and growing cumulonimbus cloud that is giving precipitation at the ground.
- M** Fully mature cumulonimbus cloud with pronounced cirrus anvil and well developed updrafts and downdrafts. Often giving heavy precipitation ( $> 10 \text{ mm h}^{-1}$ ) at the surface.
- E** Weakening cumulonimbus cloud or less intense cell giving mainly moderate precipitation at the surface ( $2 \text{ to } 10 \text{ mm h}^{-1}$ ).
- D** Cell in a dissipating stage with downdrafts eventually predominating throughout the cloud giving mainly light precipitation at the surface.

For each cell stage, idealised vertical radar reflectivity profiles have been calculated for 2 km resolution radar data and are shown in Figure A.2. The profiles are consistent with the discussions in Sections A.1.1 and A.1.2, and also with the radar observations of the growth of

a cumulonimbus cloud made in north-east Colorado on 12 July 1993 (Henry, 1995). The salient features of the graphs are:

- (i) a reflectivity maximum in the updraft region of growing cells, with small or no return below cloud base (d and m);
- (ii) the strong vertical gradient of radar reflectivity in the lower half of young cumulonimbus clouds (m);
- (iii) as the cumulonimbus cloud develops the value of the maximum reflectivity increases and occurs progressively lower down the cloud (M);
- (iv) the reflectivity maximum continues to descend and decrease as the cell weakens (E and D).

The main characteristics used for classifying the various cell stages are listed in Table A.1.

**Table A.1. Values of main attributes used for classifying cell stage.**

Cell type	Surface precipitation rate (mm h <sup>-1</sup> )	Maximum radar reflectivity (mm h <sup>-1</sup> )	Location of maximum reflectivity	Expected cell diameter (km)
d	0	<1	Top 1/2 of cloud	2
m	<10	<10 and >1	Top 1/2 of cloud	4
M	>0	>10	Usually mid-cloud	6
E	>0	<10 and >2	Bottom 1/2 of cloud	8
D	<2	<2	Bottom 1/2 of cloud	10

#### A.1.4 Identification

Each radar site over the UK transmits data from 4 beams at elevations, and with beam widths, similar to those of the London (Chenies) radar shown in Figure A.3. Near to the radar site all the beams intersect the atmosphere close to the ground. However, at longer ranges more information becomes available from higher up in the atmosphere. In the identification scheme allowance is made for the fact that a cell observed by radar will appear different according to how far it is from the site. Ideally one would have radar data with high vertical resolution extending through the troposphere in order to identify all the salient features picked out in Section A.1.3. Unfortunately, this is not possible operationally in the UK at present, so vertical profiles are extracted at each radar pixel by interpolating between beams where appropriate.

Thus, in Figure A.3, the rainfall rate at heights 1 and 2 is set to that returned by beam 0. Height 3 is an average of beam 0 and beam 1. Height 4 is set to that of beam 1. Height 5 is an average of beams 2 and 1. Rainfall at heights 6 and 7 are taken from beam 2 and 8, 9, 10 from beam 3. Given the wide beam width and the linear interpolation required to obtain these vertical rainfall rate profiles, one cannot observe the strong vertical gradients expected in developing cumulonimbus clouds. However, it is possible to identify broad vertical distributions of rainfall intensity.

In the analysis procedure the expected convective cloud base is determined from the Mesoscale Model (MM) output. Any pixel vertical rainfall profile which gives a return above cloud base but none below is flagged as likely to belong to a 'd' cell. Pixels where the rainfall rate exceeds 10 mm h<sup>-1</sup> anywhere in the profile are flagged as belonging to a 'M' cell. Pixels where the rainfall rate is low below cloud base and in the lower part of the cloud, but is high higher up



are set to 'm'. Any pixels with moderate intensities throughout the profile are set to 'E' and those with low intensities near the ground decreasing to near zero in the upper part of the cloud are set to 'D'. This procedure works fine except for pixels close to the radar site where all the information is from near the surface, and for pixels further than about 100 km from the radar site where usually no information will be available below cloud base. In these cases a best estimate is made from the rainfall rates available.

At this point in the procedure each precipitating radar pixel has been flagged as possibly belonging to a particular cell type. The expected horizontal dimensions of each cell type must now be taken into account. For example, in HC it is stated that a mature cell may occupy an area of 25 km<sup>2</sup> or more, which is at least seven 2 km pixels. To account for this, square groups of pixels are examined in turn, the number in the group depending on the expected size of the cell, viz.; 'd' = 1; 'm' = 4; 'M' = 9; 'E' = 16; 'D' = 25. Within each group each pixel is assigned a numerical value depending on the cell type it is likely to belong to, if any. For a group to be identified as a particular cell then the numerical sum of each of the pixel values must lie within a pre-defined range. This allows for a fully mature cell, for example, to contain regions of light and heavy or even no precipitation. Also, pixels identified as belonging to a 'd' cell could, in the final analysis, become the anvil region of a fully mature cell. In examining the groups of pixels, 'M' cells are identified first, followed by 'm', 'E', 'D' and 'd'. This ensures that no 'M' and 'm' cells are missed. Once a pixel has been identified as belonging to a particular cell then that pixel is not used again.

Having identified the cell objects from the radar data, other attributes similar to those listed in HC are assigned values. The cell precipitation rate has 3 components; the average of all the surface beam pixels belonging to the cell, the maximum rate and the minimum rate within the cell. The cloud base is taken from the MM. The cloud top is determined using Meteosat IR data (if available) or the average value of previous analyses according to cell type. The velocity of each cell is determined from the MM wind at a level corresponding to the cloud base + 1/3 depth. A development potential attribute is defined by comparing previous cell analyses made 10 and 20 minutes earlier with backward advected versions of the current one. The development potential is used in the analysis to determine areas where strong convection is taking place and multicell development can be expected to occur, and also where convection is less vigorous and therefore can be expected to produce less rain. Development potential is also used in the forecast process and is thus defined:

- 1 = unknown (used for 'd' cells);
- 0 = weak (cell will quickly reach dissipating 'D' stage);
- 1 = moderate (will initiate further moderate development and then dissipate);
- 2 = strong, gives heavy rain and triggers further strong development;
- 3 = cell about to initiate a new (daughter) cell or, in the case of (E), did so in previous stage;
- 4 = a cell which has initiated a new cell but has not changed its stage yet.

## A.2 Producing the forecast<sup>3</sup>

### A.2.1 Overview of forecast process

Forecasts up to 3 hours ahead are produced by advecting analysed cells with their steering velocity, which is updated after each 10 minute timestep. Cell stage is adjusted at the end of each timestep according to a life-cycle which is dependent upon the development potential of the cell. Other attributes are also changed where necessary to maintain consistency with the cell stage. The change of rainfall rate also depends on the life-cycle of the cell. Very old cells ( $> 2$  hours) are removed from the process and new ‘daughter’ cells are produced. ‘Daughters’ inherit the development potential of their parents immediately prior to birth (1 or 2). A mechanism for new cells to develop in regions of high near-surface convergence or high low-level relative vorticity is also present. It is possible for new cells to be created in this way at every timestep using divergence and vorticity field information from the MM forecast.

### A.2.2 Growth and decay of cells

The prescribed life-cycles of all cells are illustrated in Figure A.4. It can be seen that developing cells (d) have a potential of either -1, 1, or 2. Analysed cells (T+0) are always given a potential of -1. A potential of 0 is impossible for a ‘d’ cell since weak mature cells (potential 0) are not allowed to produce daughters. Potentials of 1 and 2 are reserved for daughter cells. All developing cells with a potential of -1 are removed after one forecast timestep. Others change to young mature (m) preserving their potential, but changing their other attributes. Young mature (m) cells with a potential of 0 ( $m_0$ ) change to dissipating (D) with potential 0 ( $D_0$ ). The  $m_1$  cells change to  $m_3$  and  $m_2$  to  $M_2$ . The  $m_3$  cells change to  $E_1$  and produce a daughter cell ( $d_1$ ). Similarly,  $M_3$  cells develop a daughter ( $d_2$ ) and change to  $M_4$ . Also,  $E_2$  cells change to  $E_3$ . Other E cells change to dissipating. Note that the diagram shows that young cells with a potential of 2 go through more stages to dissipation than those with potential 1. This models what one would expect in reality with stronger more vigorous cells lasting longer than weaker ones. Dissipating cells are not allowed to decay completely until they are 2 hours old, at which point they are removed. However, the length of time spent in the dissipating stage does depend on the cell potential in the maturing stages. Weak cells reach the dissipating stage faster than stronger ones.

After the stages and potentials of all the cells have been changed, the cloud base, cloud top height (CTH), and cloud top temperature (CTT) are set to average values according to cell stage at T+0. The rainfall rate for each cell is adjusted according to a weighted average of the rate in the previous stage and the mean value for the current cell type in the analysis. The weights vary depending on where in the life-cycle a particular cell is. The general ethos of the scheme is to carry forward into the forecast as much information as possible from the analysis of individual objects. This is achieved through daughter cell generation. As the forecast progresses, a stage will be reached when only strongly developing cells (potential = 2) will produce daughters and the frequency of  $D_0$  and  $D_1$  cells able to trigger new cells will diminish. This means that the latter stages of the forecasts should emphasize the more intense convective regions.

---

<sup>3</sup> after Hand (1996)

### A.2.3 Initiation of new cells

Fully mature ( $M_3$ ) cells, and young mature ( $m_3$ ) cells with a precipitation rate greater than  $1.0 \text{ mm h}^{-1}$ , are allowed to initiate new cells (daughters) at the end of each timestep. That is, after cells have been advected and all attributes have been updated. The initiation procedure is summarized in Figure A.5. Level B, which is taken to be the outflow level (cloud top - 1/3 cloud depth), is determined for each cell. The MM forecast wind corresponding to this level is calculated and the cell velocity ( $V_a$ ) is subtracted from this to give the cell-relative outflow velocity. This velocity is the wind shear between levels A and B which, when multiplied by the age of the cell, gives the horizontal displacement of B from A. The horizontal component of this displacement is the length L. The shear within the cell is assumed to vary with height. In Figure A.5 the shear between X' and A is less than that between A and B. This will often be the case in severe convective situations in the UK.

The downdraught is displaced from the centre of the base of the cell by the distance L. This forces the origin of the downdraught to be somewhere near the middle of the cloud. Without direct measurement of vertical motion within convective clouds, this is a reasonable working approximation. The important point here is that the downdraught is displaced by an amount depending on the vertical wind shear in the middle of the cloud. On striking the ground the downdraught spreads out in all directions as a low-level density current below cloud base. The cell relative inflow vector is calculated using MM winds for the nearest model level below cloud base. A daughter cell is created at a point 1 km from the downdraught in the direction which directly opposes the relative inflow. This region is where the convergence between the spreading density current and the inflow is greatest. The 1 km distance is arbitrary, but ensures that in cases of almost vertical cloud growth, the new cell is not created directly underneath the parent cell.

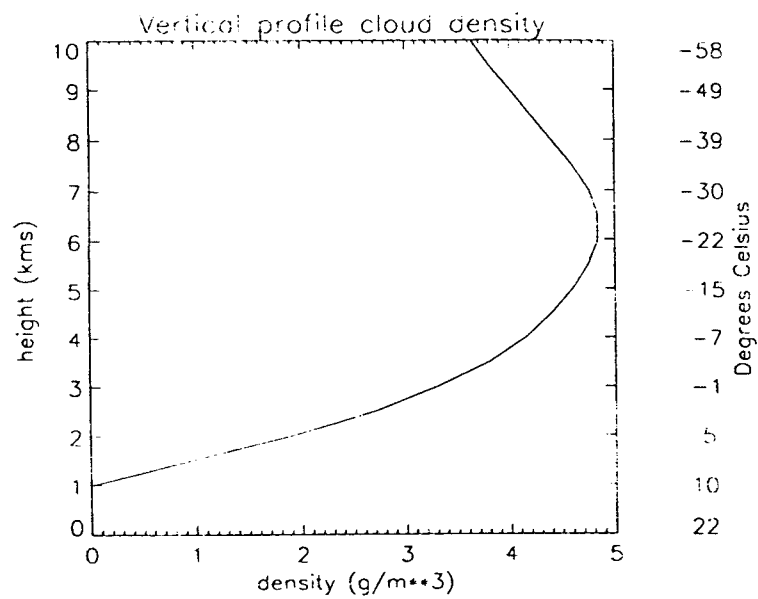
The daughter cell stage is set to 'd' with corresponding default values for other attributes. Its development potential is then set to that of the parent cell and its velocity from interpolated MM winds. Cloud base, CTT and CTH are set from the current statistical averages for 'd' cells. As well as creating new cells by convergence of the spreading gust front with the inflow to the cell, there is a mechanism to create new cells within regions of low-level convergence forecast by the MM. At the end of each timestep, the MM forecast divergence at level 3 (currently  $\sim 100 \text{ m}$ ) and the relative vorticity at level 11 (currently  $\sim 1400 \text{ m}$ ) are examined at grid points containing a dissipating cell with a potential of either 1 or 0.

If either the MM divergence is  $< -7.5 \times 10^{-5}$  per second (significant convergence) or the relative vorticity is  $> 10^{-4}$  per second then a new cell ( $d_2$ ) is created at the dissipating cell position. After creation, the new cell is advected for 10 minutes with its steering velocity. This is to simulate the time taken for it to grow and to move it away from the dissipating cell. The potential of the dissipating cell is then changed to 4 to prevent it from triggering further new cell development. Dissipating cells with a potential of 2 are not used in this process since they would have already triggered new cells by the 'daughter' mechanism when they were mature.

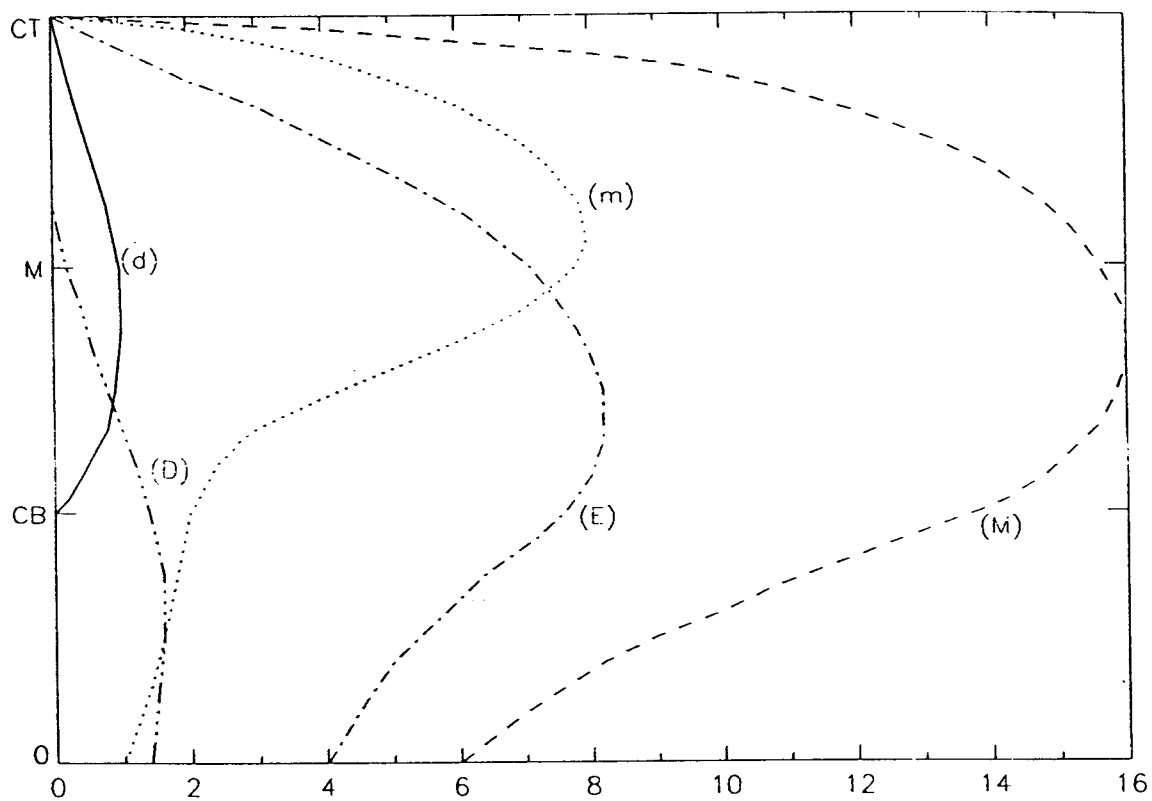
The threshold values for the divergence and vorticity can be adjusted. However, the values given above have proven optimal so far. Low-level convergence can, in potentially unstable situations, provide the trigger for new convection; the presence of moisture (rain) from a dissipating cell makes this process more certain. Low-level convergence can be very localised, often being generated by topography and temperature differentials (for example, sea breezes)

both of which can be well predicted by the MM. Broader scale forcing is provided by the positive relative vorticity. Strictly one should be considering the change of vorticity over time, since it is this which is related to divergence. However, a snapshot of relative vorticity does give a good indication of where there is possible upward motion. The threshold value can be expected to be exceeded in sharp troughs and near low centres in the lower troposphere which provide good triggers for releasing instability.

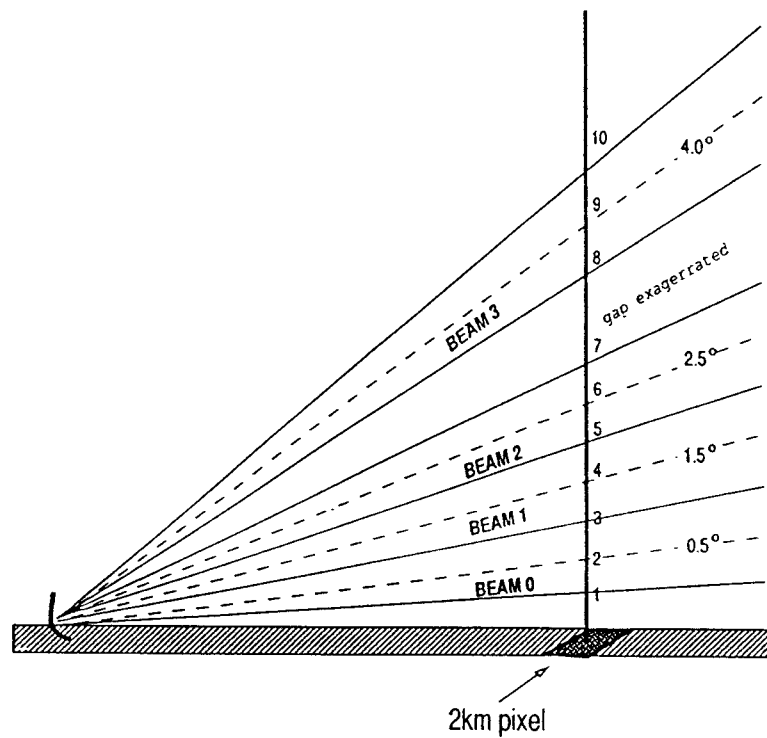
**Figure A.1.** Theoretical vertical profile of adiabatic cloud density, without any mixing of ambient air, for a cloud base at 1 km with a temperature of 10°C in an ICAO standard atmosphere environment. The density is plotted in  $\text{g m}^{-3}$  and the ordinates give height in kilometres and temperatures in degrees C.



**Figure A.2.** Idealised vertical radar reflectivity profiles expressed in  $\text{mm h}^{-1}$  for the cell stages identified in the OOM. CB = cloud base, ML = mid-cloud level, CT = cloud top. The solid line is the profile for developing (d) cells, dotted for young mature (m), dashed for fully mature (M), dash-dotted for early dissipating (E), and dash-double-dotted for dissipating (D).

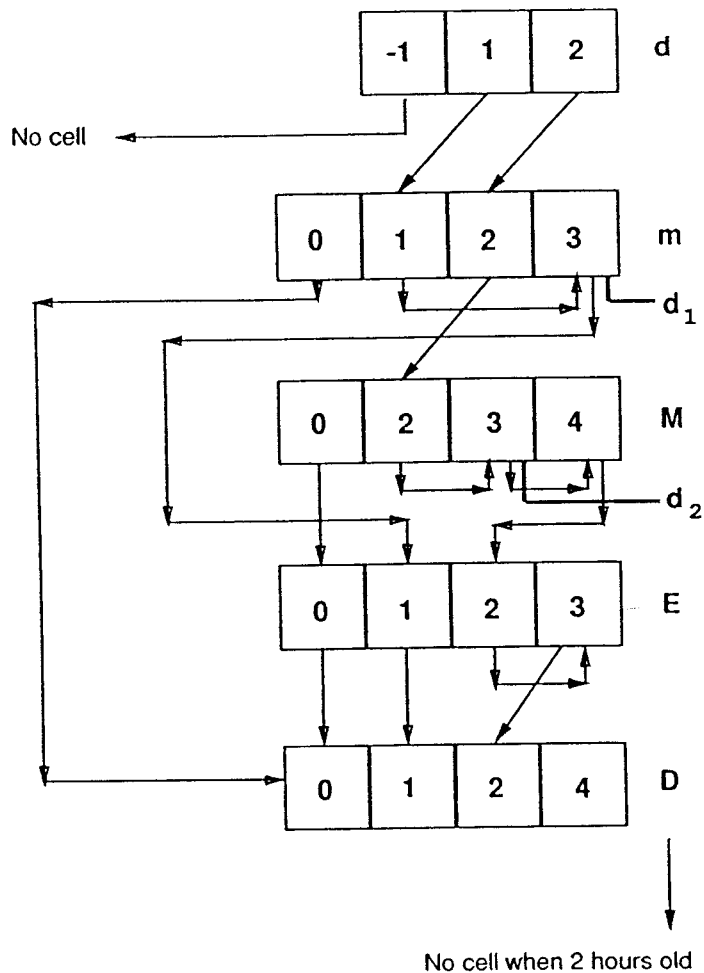


**Figure A.3.** Schematic showing the four elevations of the beams available in the Chenies radar. Beam elevations are 0.5, 1.5, 2.5 and 4.0 degrees. The mid-point of each beam is shown as a dashed line and the numbers 1 to 10 indicate levels at which radar rainfall data are determined.

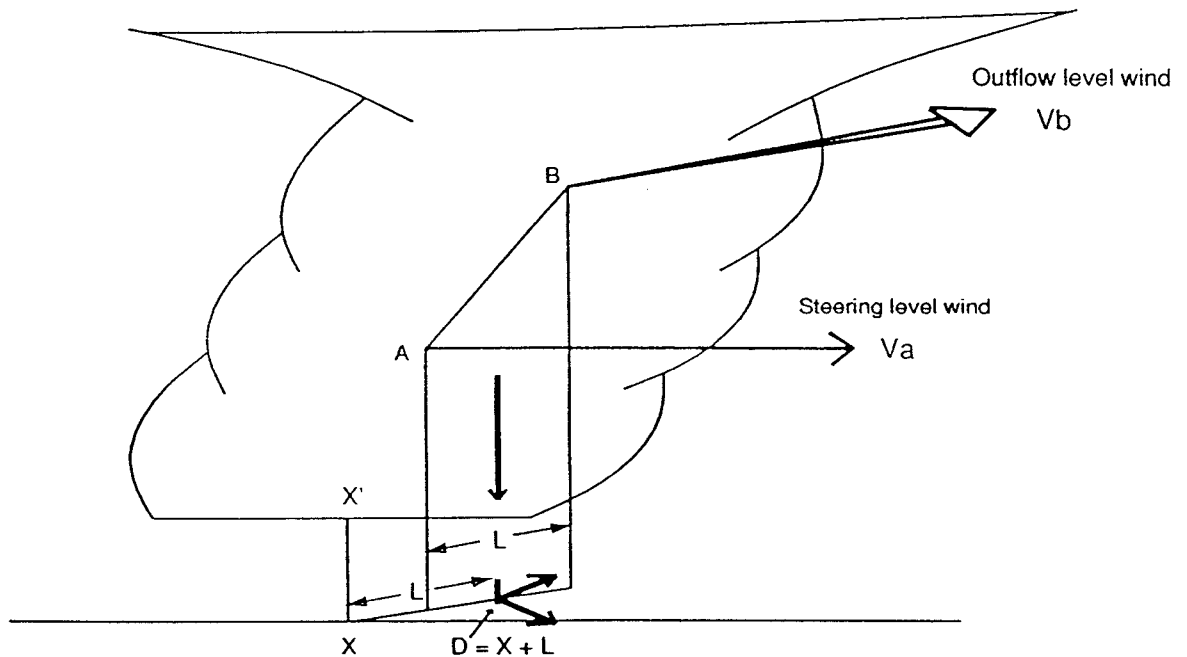




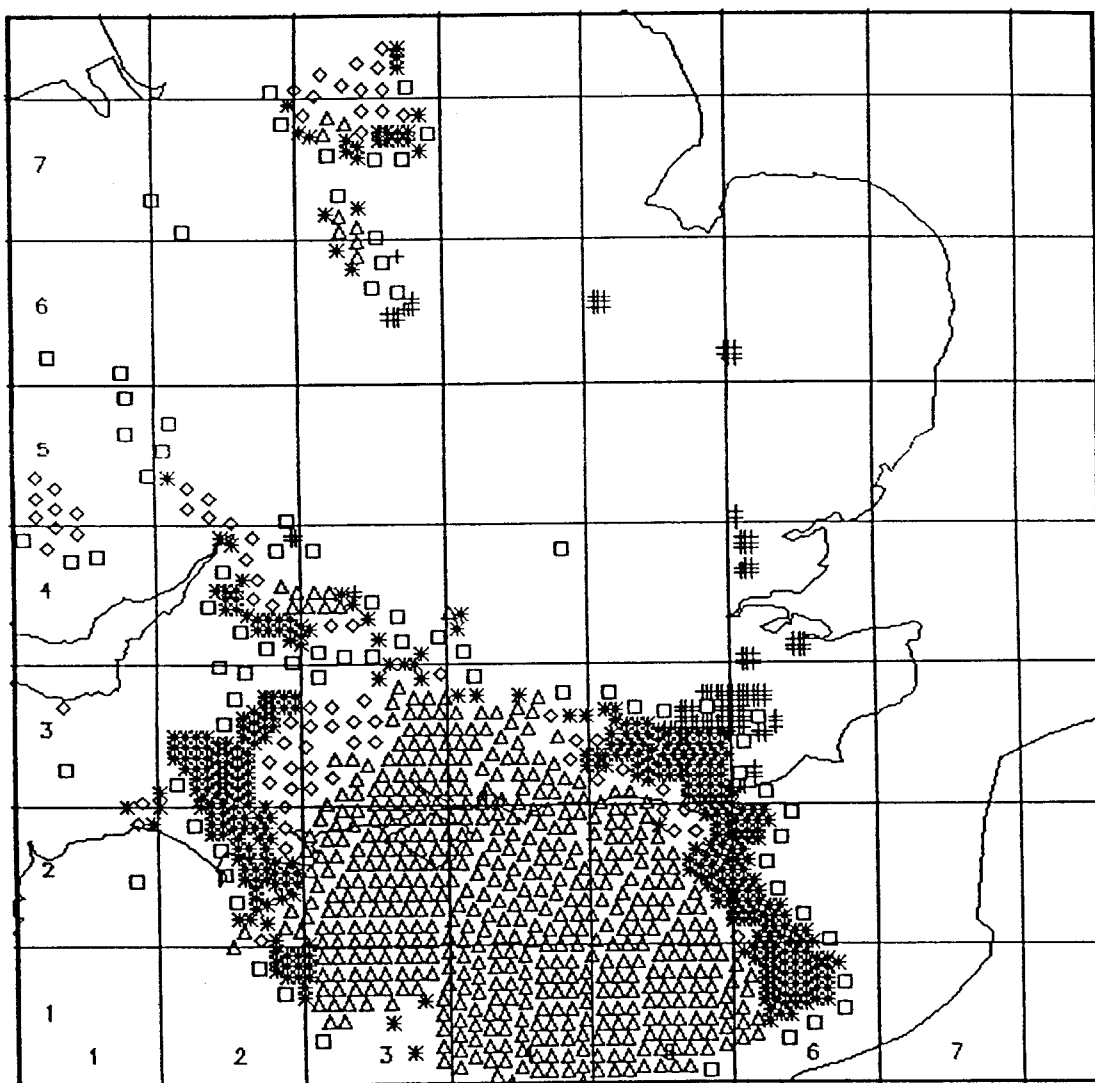
**Figure A.4.** Diagram showing the change of cell stage at each 10 minute timestep of the OOM. Each row of boxes represents a cell stage with each box indicating a possible value for the current cell potential (see text). The arrows show the allowed changes in cell stage. The bold lines indicate when new (daughter) cells are created at the end of a timestep.



**Figure A.5.** Schematic diagram illustrating how the downdraught is modelled in the OOM. The slope of the line AB is estimated by subtracting the cell velocity (steering level wind)  $V_a$  from the outflow velocity at level B,  $V_b$ , and then multiplying this relative velocity by the age of the cell to give the distance  $L$ . Level B is at cloud top - 1/3 cloud depth. The downdraught is displaced from the point X directly beneath the middle of the cloud  $X'$  by the distance  $X + L$  in the direction pointed to by the shear vector  $V_b - V_a$ .



**Figure A.6. Analysis of convective cells at 1800 GMT 24 June 94 using the OOM. A cross indicates a cell in stage d (developing), asterisk - stage m (young mature), triangle - stage M (fully mature), diamond - stage E (early dissipating), square - stage D (dissipating). The big squares are an arbitrary grid used for reference.**



## **APPENDIX B: Comparative model performance statistics for all cases of non-frontal convection during the summer trial of 1996**

### **B.1 Explanation of the layout of Tables B.1., B.2., and B.3.**

Tables B.1., B.2., and B.3. contain 2 km and sub-catchment resolution performance statistics for the LFM, Nimrod and OOM respectively.

From left to right in the tables of 2 km resolution performance statistics are: the date (all days of non-frontal convection during the summer of 1996), the sub-catchment number (sub-catchment 0 refers to an amalgamation of the 19 sub-catchment areas in Table 7), sub-catchment name, model lead time (in minutes), mean CSI, standard deviation of CSI, HR, standard deviation of HR, FAR, standard deviation of FAR, MSE, standard deviation of MSE, the MSE error components,  $U_b$ , and standard deviation of  $U_b$ ,  $U_r$ , and standard deviation of  $U_r$ ,  $U_d$  and standard deviation of  $U_d$ , and finally, the number of model runs that contribute to the mean statistics presented in the preceding alternate columns.

From left to right in the tables of sub-catchment resolution performance statistics are: the date (all days of non-frontal convection during the summer of 1996), the sub-catchment number (sub-catchment 0 refers to an amalgamation of the 19 sub-catchment areas in Table 7), sub-catchment name, model lead time (in minutes), mean observed 15 minute accumulation (as an average depth over the sub-catchment area), mean forecast 15 minute accumulation (again, as an average depth over the sub-catchment area), the forecast bias (the average of [forecast 15 minute accumulation - observed 15 minute accumulation]), the standard deviation of forecast bias, the sub-catchment CSI, HR, FAR, and MSE, the sub-catchment MSE error components,  $U_b$ ,  $U_r$  and  $U_d$ , and finally, the number of model runs that contribute to the mean statistics presented in the preceding columns. The values shown in the sub-catchment CSI, HR, FAR, MSE,  $U_b$ ,  $U_r$ , and  $U_d$  columns are not accompanied by standard deviations: they are single values representing average performance over all model runs and all days with non-frontal convective precipitation.

**Table B.1. LFM 2 km resolution performance statistics**

Date	Catch number	Catchment Name	Lead time min.	GSI 2km pixel	SD GSI 2km pixel	HR 2km pixel	SD HR 2km pixel	FAR 2km pixel	SD FAR 2km pixel	MSE mm <sup>2</sup>	SD MSE mm <sup>2</sup>	Ub 2km pixel	SD Ub 2km pixel	Ur 2km pixel	SD Ur 2km pixel	Ud 2km pixel	SD Ud 2km pixel	Runs LFM
All cases	0	All catchments	15	0.08	0.09	0.06	0.08	0.37	0.23	1.19	2.88	0.12	0.12	0.43	0.31	0.44	0.27	142
All cases	0	All catchments	30	0.07	0.08	0.06	0.07	0.39	0.22	1.09	2.30	0.11	0.10	0.48	0.32	0.40	0.28	139
All cases	0	All catchments	45	0.09	0.10	0.07	0.08	0.36	0.20	1.16	2.86	0.10	0.10	0.46	0.31	0.43	0.27	139
All cases	0	All catchments	60	0.08	0.08	0.06	0.07	0.34	0.20	0.75	1.21	0.11	0.10	0.48	0.32	0.42	0.29	138
All cases	0	All catchments	75	0.08	0.09	0.06	0.08	0.33	0.22	1.18	2.68	0.12	0.10	0.42	0.29	0.46	0.28	141
All cases	0	All catchments	90	0.07	0.08	0.05	0.07	0.36	0.23	1.10	1.94	0.12	0.10	0.42	0.31	0.45	0.28	132
All cases	0	All catchments	105	0.07	0.08	0.05	0.07	0.34	0.21	1.32	2.83	0.13	0.11	0.38	0.32	0.49	0.29	136
All cases	0	All catchments	120	0.06	0.07	0.04	0.06	0.43	0.23	1.17	1.85	0.14	0.11	0.39	0.31	0.47	0.28	126
All cases	1	Mimshall Brook	15	0.05	0.11	0.04	0.10	0.18	0.28	0.18	0.49	0.47	0.24	0.24	0.30	0.28	0.19	142
All cases	1	Mimshall Brook	30	0.04	0.08	0.03	0.07	0.23	0.31	0.30	0.69	0.43	0.26	0.32	0.34	0.25	0.20	139
All cases	1	Mimshall Brook	45	0.03	0.08	0.04	0.08	0.19	0.29	0.24	0.72	0.44	0.25	0.28	0.30	0.28	0.21	139
All cases	1	Mimshall Brook	60	0.05	0.11	0.05	0.11	0.22	0.30	0.31	0.92	0.37	0.24	0.37	0.30	0.26	0.22	138
All cases	1	Mimshall Brook	75	0.03	0.08	0.03	0.07	0.17	0.26	0.90	4.22	0.42	0.22	0.29	0.27	0.28	0.20	141
All cases	1	Mimshall Brook	90	0.04	0.10	0.03	0.08	0.18	0.26	0.76	3.05	0.40	0.23	0.30	0.28	0.30	0.20	132
All cases	1	Mimshall Brook	105	0.04	0.08	0.03	0.07	0.17	0.29	0.98	3.80	0.44	0.22	0.27	0.28	0.28	0.19	136
All cases	1	Mimshall Brook	120	0.02	0.06	0.02	0.05	0.24	0.32	1.42	4.67	0.42	0.21	0.31	0.31	0.27	0.20	126
All cases	2	Towncroft lane, Orpington	15	0.07	0.17	0.07	0.18	0.20	0.28	0.41	1.44	0.62	0.27	0.14	0.19	0.12	0.14	89
All cases	2	Towncroft lane, Orpington	30	0.05	0.12	0.06	0.14	0.24	0.33	0.36	0.86	0.59	0.32	0.10	0.16	0.09	0.12	86
All cases	2	Towncroft lane, Orpington	45	0.08	0.18	0.08	0.18	0.23	0.29	0.16	0.43	0.58	0.33	0.14	0.19	0.13	0.17	88
All cases	2	Towncroft lane, Orpington	60	0.05	0.13	0.06	0.14	0.30	0.31	0.24	0.57	0.58	0.35	0.11	0.16	0.09	0.12	83
All cases	2	Towncroft lane, Orpington	75	0.09	0.19	0.09	0.19	0.17	0.22	0.28	0.81	0.56	0.30	0.13	0.18	0.14	0.18	77
All cases	2	Towncroft lane, Orpington	90	0.07	0.17	0.07	0.18	0.19	0.28	0.29	0.72	0.54	0.37	0.10	0.17	0.11	0.13	77
All cases	2	Towncroft lane, Orpington	105	0.06	0.15	0.07	0.15	0.13	0.21	0.19	0.45	0.61	0.28	0.08	0.11	0.19	0.21	74
All cases	2	Towncroft lane, Orpington	120	0.03	0.09	0.05	0.15	0.09	0.23	0.52	1.68	0.59	0.38	0.02	0.05	0.12	0.14	69
All cases	3	Elmers End Road	15	0.04	0.13	0.05	0.14	0.14	0.24	1.32	7.09	0.45	0.32	0.11	0.20	0.17	0.18	142
All cases	3	Elmers End Road	30	0.07	0.16	0.07	0.17	0.13	0.25	0.37	1.06	0.45	0.35	0.11	0.20	0.17	0.20	139
All cases	3	Elmers End Road	45	0.06	0.15	0.07	0.15	0.14	0.24	1.25	6.82	0.43	0.31	0.10	0.17	0.17	0.18	139
All cases	3	Elmers End Road	60	0.06	0.15	0.05	0.14	0.13	0.24	0.36	1.24	0.41	0.35	0.10	0.17	0.18	0.20	138
All cases	3	Elmers End Road	75	0.04	0.13	0.04	0.13	0.08	0.18	1.30	6.87	0.42	0.32	0.08	0.13	0.19	0.19	141
All cases	3	Elmers End Road	90	0.02	0.07	0.03	0.08	0.07	0.19	0.34	1.12	0.44	0.33	0.07	0.14	0.21	0.20	132
All cases	3	Elmers End Road	105	0.03	0.09	0.03	0.11	0.08	0.16	1.55	7.20	0.44	0.30	0.07	0.14	0.19	0.17	136
All cases	3	Elmers End Road	120	0.01	0.04	0.01	0.04	0.05	0.12	0.31	0.95	0.44	0.32	0.04	0.10	0.22	0.19	126
All cases	4	Longley Road Recorder	15	0.04	0.10	0.05	0.10	0.22	0.34	0.91	4.05	0.36	0.29	0.23	0.25	0.31	0.21	142
All cases	4	Longley Road Recorder	30	0.05	0.12	0.05	0.11	0.19	0.28	0.90	2.95	0.38	0.30	0.23	0.23	0.29	0.23	139
All cases	4	Longley Road Recorder	45	0.06	0.12	0.07	0.12	0.20	0.31	0.82	3.93	0.36	0.31	0.23	0.27	0.20	0.20	139
All cases	4	Longley Road Recorder	60	0.05	0.10	0.05	0.10	0.20	0.32	1.07	3.85	0.36	0.30	0.26	0.31	0.20	0.22	138
All cases	4	Longley Road Recorder	75	0.04	0.11	0.04	0.10	0.18	0.30	0.85	3.85	0.33	0.28	0.31	0.34	0.20	0.22	141
All cases	4	Longley Road Recorder	90	0.04	0.08	0.04	0.09	0.20	0.34	0.89	2.91	0.37	0.30	0.23	0.29	0.22	0.22	132
All cases	4	Longley Road Recorder	105	0.04	0.10	0.04	0.09	0.20	0.33	2.25	8.44	0.36	0.27	0.29	0.32	0.21	0.21	136
All cases	4	Longley Road Recorder	120	0.02	0.07	0.02	0.06	0.18	0.32	1.68	5.22	0.37	0.30	0.22	0.31	0.24	0.22	126
All cases	5	West Barnes Lane	15	0.04	0.10	0.05	0.10	0.22	0.34	0.91	4.05	0.39	0.29	0.23	0.23	0.29	0.21	142
All cases	5	West Barnes Lane	30	0.05	0.12	0.05	0.11	0.19	0.28	0.90	2.95	0.38	0.30	0.25	0.31	0.21	0.23	139
All cases	5	West Barnes Lane	45	0.06	0.12	0.07	0.12	0.20	0.31	0.82	3.93	0.36	0.31	0.23	0.27	0.20	0.20	139
All cases	5	West Barnes Lane	60	0.05	0.10	0.05	0.10	0.20	0.32	1.07	3.85	0.36	0.30	0.26	0.31	0.20	0.22	138
All cases	5	West Barnes Lane	75	0.04	0.11	0.04	0.10	0.18	0.30	0.85	3.85	0.33	0.28	0.31	0.34	0.20	0.22	141

**Table B.1. LFM 2 km resolution performance statistics contd.**

Date	Catch number	Catchment Name	Lead time min.	CSI 2km pixel	SD CSI 2km pixel	HR 2km pixel	SD HR 2km pixel	FAR 2km pixel	SD FAR 2km pixel	MSE mm <sup>2</sup>	SD MSE mm <sup>2</sup>	Ub 2km pixel	SD Ub 2km pixel	Ur 2km pixel	SD Ur 2km pixel	Ud 2km pixel	SD Ud 2km pixel	Runs LFM
All cases	5	West Barnes Lane	90	0.04	0.08	0.04	0.09	0.20	0.34	0.89	2.91	0.37	0.30	0.23	0.29	0.22	0.22	132
All cases	5	West Barnes Lane	105	0.04	0.10	0.04	0.09	0.20	0.33	2.25	8.44	0.35	0.27	0.22	0.31	0.24	0.21	136
All cases	5	West Barnes Lane	120	0.02	0.07	0.02	0.06	0.18	0.32	1.68	5.22	0.37	0.30	0.22	0.31	0.24	0.22	126
All cases	6	Wimbleton Common	15	0.08	0.12	0.07	0.12	0.19	0.28	1.79	6.84	0.42	0.28	0.30	0.30	0.26	0.22	139
All cases	6	Wimbleton Common	30	0.08	0.12	0.07	0.11	0.18	0.27	0.75	3.21	0.40	0.26	0.31	0.32	0.25	0.21	136
All cases	6	Wimbleton Common	45	0.08	0.12	0.07	0.12	0.21	0.30	1.83	6.78	0.41	0.29	0.32	0.32	0.25	0.21	136
All cases	6	Wimbleton Common	60	0.09	0.16	0.08	0.15	0.18	0.29	0.82	3.13	0.42	0.29	0.31	0.33	0.24	0.21	138
All cases	6	Wimbleton Common	75	0.08	0.14	0.07	0.14	0.18	0.27	2.17	6.61	0.43	0.27	0.31	0.32	0.24	0.19	137
All cases	6	Wimbleton Common	90	0.07	0.14	0.06	0.13	0.21	0.29	2.39	9.09	0.37	0.25	0.36	0.32	0.24	0.21	132
All cases	6	Wimbleton Common	105	0.09	0.18	0.07	0.16	0.18	0.30	2.95	7.85	0.41	0.27	0.30	0.32	0.25	0.20	136
All cases	6	Wimbleton Common	120	0.07	0.16	0.06	0.14	0.22	0.31	2.47	8.08	0.44	0.26	0.28	0.33	0.26	0.21	125
All cases	7	Yeading West	15	0.02	0.06	0.02	0.07	0.20	0.30	0.69	2.36	0.43	0.31	0.22	0.25	0.13	0.19	110
All cases	7	Yeading West	30	0.03	0.07	0.03	0.07	0.20	0.27	1.37	6.66	0.44	0.29	0.27	0.27	0.13	0.19	109
All cases	7	Yeading West	45	0.03	0.10	0.03	0.11	0.20	0.29	1.48	1.65	0.52	0.28	0.27	0.27	0.13	0.20	120
All cases	7	Yeading West	60	0.01	0.06	0.01	0.06	0.21	0.30	0.42	1.47	0.48	0.28	0.29	0.27	0.13	0.18	114
All cases	7	Yeading West	75	0.04	0.09	0.04	0.09	0.22	0.30	0.59	2.54	0.49	0.26	0.28	0.27	0.13	0.17	113
All cases	7	Yeading West	90	0.03	0.11	0.04	0.11	0.18	0.28	0.76	2.66	0.42	0.30	0.24	0.27	0.14	0.17	109
All cases	7	Yeading West	105	0.04	0.10	0.04	0.10	0.24	0.30	0.56	2.34	0.46	0.26	0.31	0.25	0.12	0.17	118
All cases	7	Yeading West	120	0.03	0.08	0.03	0.07	0.30	0.37	0.43	1.17	0.47	0.28	0.28	0.28	0.14	0.20	106
All cases	8	Yeading East	15	0.02	0.06	0.02	0.06	0.19	0.32	0.99	3.24	0.45	0.31	0.17	0.25	0.11	0.17	96
All cases	8	Yeading East	30	0.02	0.07	0.02	0.05	0.15	0.29	3.45	18.66	0.48	0.31	0.20	0.27	0.10	0.15	102
All cases	8	Yeading East	45	0.02	0.08	0.02	0.08	0.17	0.30	0.81	2.70	0.53	0.35	0.18	0.23	0.09	0.15	116
All cases	8	Yeading East	60	0.02	0.08	0.02	0.08	0.15	0.27	0.59	1.21	0.50	0.35	0.21	0.26	0.10	0.15	108
All cases	8	Yeading East	75	0.03	0.10	0.03	0.10	0.19	0.27	0.72	2.58	0.46	0.33	0.23	0.28	0.09	0.14	111
All cases	8	Yeading East	90	0.04	0.13	0.04	0.14	0.18	0.32	1.03	4.10	0.45	0.34	0.22	0.29	0.10	0.14	101
All cases	8	Yeading East	105	0.04	0.11	0.03	0.10	0.19	0.30	0.44	1.33	0.48	0.33	0.23	0.28	0.08	0.14	110
All cases	8	Yeading East	120	0.03	0.09	0.03	0.09	0.25	0.38	0.27	0.92	0.52	0.32	0.17	0.22	0.12	0.17	100
All cases	9	Colindale Lane	15	0.03	0.08	0.03	0.08	0.16	0.27	0.84	4.11	0.65	0.26	0.17	0.27	0.18	0.16	142
All cases	9	Colindale Lane	30	0.02	0.05	0.02	0.06	0.16	0.27	0.72	2.58	0.60	0.26	0.21	0.30	0.20	0.16	139
All cases	9	Colindale Lane	45	0.02	0.04	0.02	0.04	0.17	0.26	1.60	8.33	0.56	0.28	0.24	0.28	0.20	0.18	139
All cases	9	Colindale Lane	60	0.03	0.08	0.03	0.07	0.17	0.30	0.37	1.11	0.44	0.30	0.34	0.32	0.22	0.18	138
All cases	9	Colindale Lane	75	0.02	0.06	0.02	0.07	0.16	0.27	0.22	0.79	0.52	0.27	0.27	0.28	0.22	0.18	141
All cases	9	Colindale Lane	90	0.03	0.09	0.03	0.07	0.17	0.29	0.44	1.35	0.54	0.26	0.24	0.28	0.22	0.17	132
All cases	9	Colindale Lane	105	0.02	0.05	0.02	0.05	0.15	0.25	0.29	0.83	0.56	0.26	0.24	0.25	0.20	0.16	136
All cases	9	Colindale Lane	120	0.03	0.08	0.03	0.07	0.20	0.32	0.72	1.83	0.53	0.27	0.28	0.31	0.19	0.15	126
All cases	10	Chipping Ongar	15	0.06	0.11	0.06	0.11	0.14	0.25	2.05	8.16	0.48	0.30	0.15	0.23	0.26	0.25	96
All cases	10	Chipping Ongar	30	0.05	0.10	0.06	0.11	0.20	0.28	0.20	0.40	0.45	0.26	0.15	0.18	0.25	0.25	90
All cases	10	Chipping Ongar	45	0.05	0.10	0.05	0.09	0.15	0.24	0.69	2.06	0.47	0.29	0.13	0.19	0.26	0.27	90
All cases	10	Chipping Ongar	60	0.05	0.11	0.05	0.11	0.18	0.27	0.24	0.53	0.46	0.28	0.16	0.20	0.25	0.25	86
All cases	10	Chipping Ongar	75	0.04	0.09	0.05	0.11	0.18	0.28	0.69	2.07	0.44	0.28	0.14	0.19	0.28	0.28	85
All cases	10	Chipping Ongar	90	0.05	0.11	0.05	0.11	0.17	0.27	0.15	0.28	0.44	0.27	0.15	0.19	0.31	0.26	80
All cases	10	Chipping Ongar	105	0.04	0.09	0.05	0.09	0.14	0.24	0.71	2.10	0.42	0.30	0.13	0.19	0.29	0.26	82
All cases	10	Chipping Ongar	120	0.04	0.11	0.04	0.10	0.15	0.25	0.22	0.55	0.44	0.28	0.12	0.19	0.31	0.25	73
All cases	11	Sewardstone Road	15	0.07	0.13	0.07	0.13	0.16	0.29	0.19	0.41	0.46	0.28	0.15	0.20	0.24	0.25	93
All cases	11	Sewardstone Road	30	0.08	0.13	0.08	0.13	0.16	0.28	0.15	0.42	0.43	0.29	0.15	0.21	0.22	0.22	88

**Table B.1. LFM 2 km resolution performance statistics contd.**

Date	Catch number	Catchment Name	Lead time min.	CSI 2km pixel	SD CSI 2km pixel	HR 2km pixel	SD HR 2km pixel	FAR 2km pixel	SD FAR 2km pixel	MSE mm <sup>2</sup>	SD MSE mm <sup>2</sup>	Up 2km pixel	SD Up 2km pixel	Ur 2km pixel	SD Ur 2km pixel	Ud 2km pixel	SD Ud 2km pixel	Runs LFM
All cases	11	Sewardstone Road	45	0.07	0.14	0.06	0.14	0.15	0.26	0.23	0.50	0.47	0.28	0.14	0.21	0.21	0.23	92
All cases	11	Sewardstone Road	60	0.05	0.13	0.05	0.13	0.12	0.26	0.12	0.35	0.44	0.31	0.13	0.20	0.22	0.22	89
All cases	11	Sewardstone Road	75	0.04	0.11	0.03	0.11	0.12	0.24	0.21	0.48	0.48	0.30	0.12	0.17	0.24	0.23	86
All cases	11	Sewardstone Road	90	0.04	0.11	0.05	0.12	0.10	0.20	0.18	0.64	0.40	0.30	0.09	0.17	0.25	0.23	82
All cases	11	Sewardstone Road	105	0.04	0.11	0.04	0.10	0.09	0.20	0.18	0.43	0.41	0.32	0.11	0.19	0.28	0.26	84
All cases	11	Sewardstone Road	120	0.04	0.11	0.05	0.13	0.08	0.17	0.71	3.32	0.45	0.28	0.07	0.17	0.29	0.22	76
All cases	12	Luton Hoo	15	0.08	0.18	0.10	0.19	0.24	0.30	0.94	3.41	0.40	0.29	0.27	0.28	0.21	0.26	114
All cases	12	Luton Hoo	30	0.06	0.14	0.07	0.16	0.24	0.29	0.75	1.92	0.41	0.28	0.25	0.26	0.23	0.26	104
All cases	12	Luton Hoo	45	0.08	0.17	0.07	0.15	0.17	0.26	0.50	1.45	0.39	0.28	0.23	0.29	0.24	0.28	110
All cases	12	Luton Hoo	60	0.04	0.08	0.04	0.10	0.19	0.24	0.65	1.64	0.43	0.29	0.26	0.28	0.21	0.23	115
All cases	12	Luton Hoo	75	0.04	0.11	0.05	0.12	0.18	0.26	0.91	2.72	0.42	0.29	0.22	0.26	0.22	0.23	124
All cases	12	Luton Hoo	90	0.04	0.09	0.04	0.12	0.23	0.28	2.34	7.51	0.38	0.24	0.29	0.25	0.27	0.25	103
All cases	12	Luton Hoo	105	0.03	0.08	0.04	0.10	0.21	0.25	1.35	4.72	0.39	0.27	0.21	0.21	0.25	0.24	112
All cases	12	Luton Hoo	120	0.04	0.08	0.04	0.09	0.26	0.31	1.41	4.41	0.38	0.26	0.26	0.26	0.26	0.27	95
All cases	13	Gypsy Lane	15	0.06	0.15	0.06	0.15	0.12	0.22	0.83	2.17	0.54	0.28	0.15	0.23	0.24	0.23	94
All cases	13	Gypsy Lane	30	0.06	0.13	0.05	0.13	0.13	0.25	1.33	4.69	0.48	0.27	0.16	0.25	0.25	0.22	92
All cases	13	Gypsy Lane	45	0.06	0.14	0.06	0.14	0.15	0.28	0.71	1.73	0.48	0.29	0.17	0.23	0.27	0.26	84
All cases	13	Gypsy Lane	60	0.07	0.15	0.06	0.15	0.17	0.30	1.29	5.04	0.49	0.30	0.14	0.23	0.28	0.25	88
All cases	13	Gypsy Lane	75	0.08	0.17	0.09	0.17	0.18	0.30	1.07	5.28	0.45	0.27	0.15	0.21	0.24	0.24	82
All cases	13	Gypsy Lane	90	0.12	0.22	0.11	0.21	0.15	0.25	1.46	5.28	0.45	0.28	0.16	0.24	0.30	0.25	80
All cases	13	Gypsy Lane	105	0.05	0.13	0.06	0.13	0.13	0.24	0.82	1.72	0.52	0.28	0.09	0.15	0.27	0.26	79
All cases	13	Gypsy Lane	120	0.06	0.13	0.06	0.13	0.16	0.25	1.51	5.38	0.52	0.26	0.10	0.18	0.30	0.23	78
All cases	14	Albany Park	15	0.07	0.13	0.07	0.12	0.24	0.35	0.20	0.68	0.51	0.31	0.20	0.25	0.21	0.22	107
All cases	14	Albany Park	30	0.05	0.12	0.06	0.11	0.28	0.37	0.29	0.73	0.42	0.31	0.24	0.30	0.17	0.23	111
All cases	14	Albany Park	45	0.04	0.10	0.05	0.11	0.27	0.36	0.30	0.89	0.49	0.30	0.23	0.26	0.19	0.24	112
All cases	14	Albany Park	60	0.04	0.11	0.04	0.10	0.23	0.31	0.46	1.41	0.43	0.32	0.25	0.28	0.17	0.23	118
All cases	14	Albany Park	75	0.05	0.11	0.04	0.09	0.21	0.35	0.99	4.80	0.43	0.33	0.21	0.27	0.21	0.20	111
All cases	14	Albany Park	90	0.03	0.10	0.03	0.09	0.20	0.33	0.42	1.44	0.40	0.29	0.21	0.28	0.22	0.21	108
All cases	14	Albany Park	105	0.04	0.11	0.03	0.09	0.23	0.32	0.26	0.58	0.49	0.30	0.18	0.23	0.24	0.21	106
All cases	14	Albany Park	120	0.03	0.09	0.03	0.08	0.20	0.33	0.67	1.68	0.42	0.31	0.16	0.27	0.23	0.23	104
All cases	15	Edmonton Green	15	0.05	0.13	0.06	0.12	0.27	0.35	0.27	0.68	0.47	0.30	0.23	0.26	0.17	0.21	93
All cases	15	Edmonton Green	30	0.03	0.08	0.03	0.08	0.29	0.38	0.23	0.65	0.44	0.32	0.22	0.26	0.16	0.23	101
All cases	15	Edmonton Green	45	0.05	0.13	0.05	0.11	0.27	0.35	0.40	1.21	0.47	0.31	0.23	0.25	0.17	0.22	105
All cases	15	Edmonton Green	60	0.03	0.08	0.03	0.07	0.26	0.33	0.70	7.77	0.44	0.32	0.19	0.25	0.17	0.20	108
All cases	15	Edmonton Green	75	0.04	0.14	0.02	0.08	0.18	0.32	1.63	7.41	0.42	0.32	0.18	0.25	0.17	0.20	103
All cases	15	Edmonton Green	90	0.03	0.08	0.03	0.07	0.24	0.37	0.18	0.54	0.47	0.33	0.18	0.26	0.20	0.23	103
All cases	15	Edmonton Green	105	0.02	0.07	0.02	0.07	0.21	0.36	0.39	1.39	0.48	0.33	0.16	0.23	0.17	0.20	109
All cases	15	Edmonton Green	120	0.02	0.07	0.02	0.06	0.22	0.35	0.31	0.88	0.46	0.31	0.13	0.21	0.22	0.23	97
All cases	16	Silver Street	15	0.05	0.09	0.03	0.06	0.25	0.34	0.78	3.17	0.45	0.29	0.26	0.29	0.21	0.22	125
All cases	16	Silver Street	30	0.02	0.07	0.02	0.06	0.27	0.36	2.20	10.92	0.45	0.27	0.31	0.30	0.21	0.23	122
All cases	16	Silver Street	45	0.04	0.09	0.03	0.06	0.24	0.30	0.86	4.07	0.42	0.27	0.32	0.32	0.22	0.24	124
All cases	16	Silver Street	60	0.03	0.07	0.02	0.06	0.25	0.30	0.55	1.87	0.44	0.30	0.30	0.29	0.18	0.21	130
All cases	16	Silver Street	75	0.03	0.07	0.02	0.07	0.23	0.31	0.56	2.38	0.39	0.28	0.36	0.33	0.18	0.22	136
All cases	16	Silver Street	90	0.03	0.08	0.02	0.05	0.20	0.30	0.27	0.98	0.42	0.25	0.31	0.32	0.23	0.24	125
All cases	16	Silver Street	105	0.02	0.06	0.02	0.06	0.21	0.31	0.33	1.24	0.46	0.28	0.29	0.31	0.21	0.22	130



Table B.1. LFM 2 km resolution performance statistics contd.

Date	Catch number	Catchment Name	Lead time min.	CSI 2km pixel	SD CSI 2km pixel	HR 2km pixel	SD HR 2km pixel	FAR 2km pixel	SD FAR 2km pixel	MSE mm <sup>2</sup>	SD MSE mm <sup>2</sup>	Ub 2km pixel	SD Ub 2km pixel	Ur 2km pixel	SD Ur 2km pixel	Ud 2km pixel	SD Ud 2km pixel	Runs LFM
All cases	16	Silver Street	120	0.02	0.05	0.01	0.04	0.25	0.33	0.46	1.72	0.46	0.29	0.26	0.28	0.23	0.24	119
All cases	17	Bretons Farm	15	0.02	0.05	0.02	0.05	0.11	0.19	0.30	1.25	0.36	0.29	0.16	0.26	0.23	0.22	141
All cases	17	Bretons Farm	30	0.03	0.06	0.02	0.05	0.11	0.22	0.21	0.90	0.35	0.28	0.16	0.25	0.22	0.23	135
All cases	17	Bretons Farm	45	0.04	0.09	0.04	0.09	0.10	0.18	0.29	1.22	0.36	0.31	0.13	0.21	0.23	0.21	138
All cases	17	Bretons Farm	60	0.03	0.08	0.03	0.08	0.09	0.20	0.34	1.15	0.36	0.31	0.10	0.17	0.22	0.23	134
All cases	17	Bretons Farm	75	0.04	0.09	0.04	0.10	0.10	0.18	0.30	1.23	0.37	0.31	0.09	0.17	0.23	0.23	140
All cases	17	Bretons Farm	90	0.03	0.07	0.03	0.07	0.12	0.22	0.24	0.93	0.35	0.30	0.12	0.19	0.24	0.24	128
All cases	17	Bretons Farm	105	0.03	0.07	0.03	0.08	0.08	0.17	0.33	1.28	0.36	0.32	0.07	0.19	0.23	0.21	135
All cases	17	Bretons Farm	120	0.02	0.06	0.03	0.07	0.07	0.18	0.22	0.93	0.36	0.30	0.12	0.16	0.26	0.24	122
All cases	18	Gaynes Park	15	0.03	0.10	0.03	0.11	0.14	0.25	0.66	2.19	0.41	0.30	0.16	0.23	0.26	0.25	119
All cases	18	Gaynes Park	30	0.03	0.08	0.03	0.08	0.12	0.24	0.48	1.63	0.44	0.30	0.15	0.24	0.25	0.23	118
All cases	18	Gaynes Park	45	0.04	0.11	0.04	0.11	0.11	0.24	0.63	2.21	0.47	0.31	0.08	0.18	0.26	0.25	119
All cases	18	Gaynes Park	60	0.05	0.12	0.05	0.13	0.11	0.21	0.66	2.12	0.46	0.32	0.08	0.15	0.26	0.25	116
All cases	18	Gaynes Park	75	0.04	0.10	0.05	0.11	0.10	0.21	0.60	2.11	0.42	0.33	0.09	0.17	0.26	0.25	120
All cases	18	Gaynes Park	90	0.05	0.12	0.05	0.12	0.13	0.24	0.60	1.97	0.41	0.30	0.10	0.18	0.27	0.26	109
All cases	18	Gaynes Park	105	0.04	0.10	0.05	0.12	0.12	0.22	0.48	1.39	0.40	0.34	0.13	0.18	0.25	0.26	117
All cases	18	Gaynes Park	120	0.04	0.09	0.04	0.10	0.09	0.20	0.61	1.98	0.39	0.31	0.09	0.18	0.27	0.25	105
All cases	19	Bromley South Recorder	15	0.09	0.19	0.09	0.20	0.11	0.22	0.57	1.19	0.69	0.25	0.11	0.18	0.19	0.18	142
All cases	19	Bromley South Recorder	30	0.07	0.17	0.08	0.20	0.14	0.22	0.47	1.81	0.72	0.23	0.11	0.18	0.17	0.16	139
All cases	19	Bromley South Recorder	45	0.09	0.18	0.10	0.19	0.12	0.20	0.43	1.07	0.70	0.25	0.10	0.17	0.20	0.20	139
All cases	19	Bromley South Recorder	60	0.09	0.20	0.09	0.20	0.13	0.22	0.51	1.21	0.73	0.24	0.09	0.16	0.18	0.18	138
All cases	19	Bromley South Recorder	75	0.08	0.18	0.08	0.17	0.08	0.13	0.49	1.18	0.73	0.24	0.09	0.15	0.18	0.16	141
All cases	19	Bromley South Recorder	90	0.05	0.13	0.05	0.14	0.06	0.12	0.67	1.78	0.73	0.24	0.07	0.15	0.20	0.19	132
All cases	19	Bromley South Recorder	105	0.04	0.14	0.04	0.15	0.07	0.16	0.42	0.98	0.73	0.23	0.09	0.18	0.18	0.16	136
All cases	19	Bromley South Recorder	120	0.04	0.12	0.04	0.12	0.03	0.10	0.56	1.41	0.76	0.21	0.06	0.13	0.19	0.16	126

**Table B.1. LFM catchment resolution performance statistics**

Date	Catch number	Catchment Name	Lead time min.	Observed depth / mm	Forecast depth / mm	F-O depth / mm	SD (F-O) depth / mm	CSI catchment	HR catchment	FAR catchment	MSE catchment	Ub catchment	Ur catchment	Ud catchment	Runs LFM
All cases	0	All catchments	15	0.11	0.07	-0.03	0.15	0.99	0.99	0.00	0.04	0.08	0.35	0.57	142
All cases	0	All catchments	30	0.09	0.08	-0.02	0.13	0.99	0.99	0.00	0.03	0.07	0.43	0.50	139
All cases	0	All catchments	45	0.10	0.07	-0.03	0.13	0.99	0.99	0.00	0.03	0.11	0.31	0.58	139
All cases	0	All catchments	60	0.09	0.07	-0.02	0.12	0.99	0.99	0.00	0.02	0.10	0.37	0.53	138
All cases	0	All catchments	75	0.11	0.07	-0.04	0.16	0.98	0.98	0.00	0.05	0.12	0.30	0.58	141
All cases	0	All catchments	90	0.11	0.07	-0.04	0.15	0.97	0.97	0.00	0.04	0.16	0.33	0.50	132
All cases	0	All catchments	105	0.12	0.07	-0.05	0.15	0.99	0.99	0.00	0.04	0.19	0.25	0.55	136
All cases	0	All catchments	120	0.12	0.06	-0.05	0.14	0.98	0.98	0.00	0.04	0.20	0.26	0.54	126
All cases	1	Mimshall Brook	15	0.08	0.08	-0.01	0.25	0.55	0.55	0.00	0.10	0.13	0.38	0.49	142
All cases	1	Mimshall Brook	30	0.06	0.11	0.06	0.29	0.61	0.61	0.00	0.11	0.08	0.71	0.22	139
All cases	1	Mimshall Brook	45	0.07	0.09	0.01	0.26	0.66	0.66	0.00	0.10	0.08	0.61	0.31	139
All cases	1	Mimshall Brook	60	0.08	0.09	0.01	0.28	0.76	0.76	0.00	0.10	0.08	0.48	0.44	138
All cases	1	Mimshall Brook	75	0.13	0.08	-0.05	0.49	0.71	0.71	0.00	0.43	0.06	0.51	0.44	141
All cases	1	Mimshall Brook	90	0.12	0.07	-0.05	0.41	0.66	0.66	0.00	0.36	0.09	0.43	0.48	132
All cases	1	Mimshall Brook	105	0.15	0.08	-0.07	0.48	0.62	0.62	0.00	0.49	0.10	0.41	0.49	136
All cases	1	Mimshall Brook	120	0.13	0.12	-0.02	0.52	0.63	0.63	0.00	0.50	0.10	0.56	0.34	126
All cases	2	Towncroft lane, Oprington	15	0.11	0.11	0.00	0.35	0.26	0.35	0.36	0.15	0.16	0.42	0.43	89
All cases	2	Towncroft lane, Oprington	30	0.15	0.14	-0.02	0.50	0.28	0.36	0.32	0.30	0.13	0.48	0.39	86
All cases	2	Towncroft lane, Oprington	45	0.12	0.11	-0.01	0.30	0.32	0.43	0.34	0.12	0.20	0.32	0.48	88
All cases	2	Towncroft lane, Oprington	60	0.14	0.09	-0.06	0.37	0.26	0.38	0.29	0.20	0.18	0.38	0.45	83
All cases	2	Towncroft lane, Oprington	75	0.13	0.11	-0.03	0.43	0.31	0.39	0.25	0.23	0.16	0.46	0.38	77
All cases	2	Towncroft lane, Oprington	90	0.17	0.07	-0.10	0.39	0.25	0.32	0.29	0.23	0.22	0.31	0.47	77
All cases	2	Towncroft lane, Oprington	105	0.14	0.09	-0.05	0.34	0.19	0.26	0.38	0.14	0.15	0.27	0.57	74
All cases	2	Towncroft lane, Oprington	120	0.17	0.09	-0.08	0.53	0.09	0.11	0.49	0.41	0.16	0.44	0.38	69
All cases	3	Elmers End Road	15	0.16	0.08	-0.08	0.63	0.35	0.35	0.00	0.79	0.12	0.31	0.57	142
All cases	3	Elmers End Road	30	0.14	0.09	-0.05	0.46	0.29	0.29	0.00	0.29	0.09	0.40	0.51	139
All cases	3	Elmers End Road	45	0.15	0.07	-0.08	0.56	0.29	0.29	0.00	0.74	0.12	0.28	0.60	139
All cases	3	Elmers End Road	60	0.13	0.09	-0.04	0.48	0.28	0.28	0.00	0.30	0.09	0.45	0.46	138
All cases	3	Elmers End Road	75	0.16	0.06	-0.10	0.58	0.25	0.25	0.00	0.78	0.11	0.24	0.65	141
All cases	3	Elmers End Road	90	0.15	0.04	-0.11	0.44	0.18	0.18	0.00	0.27	0.13	0.26	0.61	132
All cases	3	Elmers End Road	105	0.17	0.06	-0.11	0.63	0.17	0.17	0.00	1.01	0.12	0.28	0.60	136
All cases	3	Elmers End Road	120	0.16	0.02	-0.14	0.38	0.11	0.11	0.00	0.25	0.18	0.17	0.65	126
All cases	4	Longley Road Recorder	15	0.15	0.07	-0.08	0.45	0.54	0.54	0.00	0.36	0.09	0.34	0.56	142
All cases	4	Longley Road Recorder	30	0.17	0.09	-0.08	0.56	0.58	0.58	0.00	0.61	0.11	0.32	0.57	139
All cases	4	Longley Road Recorder	45	0.13	0.07	-0.06	0.44	0.54	0.54	0.00	0.34	0.11	0.21	0.68	139
All cases	4	Longley Road Recorder	60	0.16	0.09	-0.08	0.59	0.57	0.57	0.00	0.62	0.08	0.35	0.58	138
All cases	4	Longley Road Recorder	75	0.13	0.06	-0.07	0.41	0.55	0.55	0.00	0.34	0.09	0.21	0.71	141
All cases	4	Longley Road Recorder	90	0.19	0.05	-0.14	0.53	0.55	0.55	0.00	0.59	0.09	0.33	0.58	132
All cases	4	Longley Road Recorder	105	0.15	0.10	-0.06	0.54	0.57	0.57	0.00	0.64	0.05	0.32	0.64	136
All cases	4	Longley Road Recorder	120	0.20	0.08	-0.12	0.58	0.48	0.48	0.00	0.76	0.08	0.35	0.56	126
All cases	5	West Barnes Lane	15	0.15	0.07	-0.08	0.45	0.54	0.54	0.00	0.36	0.09	0.34	0.56	142
All cases	5	West Barnes Lane	30	0.17	0.09	-0.08	0.56	0.58	0.58	0.00	0.61	0.11	0.32	0.57	139
All cases	5	West Barnes Lane	45	0.13	0.07	-0.06	0.44	0.54	0.54	0.00	0.34	0.11	0.21	0.68	139
All cases	5	West Barnes Lane	60	0.16	0.09	-0.08	0.59	0.57	0.57	0.00	0.62	0.08	0.35	0.58	138
All cases	5	West Barnes Lane	75	0.13	0.06	-0.07	0.41	0.55	0.55	0.00	0.34	0.09	0.21	0.71	141

**Table B.1. LFM catchment resolution performance statistics contd.**

Date	Catch number	Catchment Name	Lead time min.	Observed depth / mm	Forecast depth / mm	F-O depth / mm	SD (F-O) depth / mm	CSI catchment	HR catchment	FAR catchment	MSE catchment	Up catchment	Ur catchment	Ud catchment	Runs LFM
All cases	5	West Barnes Lane	90	0.19	0.05	-0.14	0.53	0.55	0.55	0.00	0.59	0.09	0.33	0.59	132
All cases	5	West Barnes Lane	105	0.15	0.10	-0.06	0.54	0.57	0.57	0.00	0.64	0.05	0.32	0.64	136
All cases	5	West Barnes Lane	120	0.20	0.08	-0.12	0.58	0.48	0.48	0.00	0.76	0.08	0.35	0.56	126
All cases	6	Wimbleton Common	15	0.23	0.05	-0.18	0.69	0.72	0.73	0.01	1.14	0.08	0.23	0.69	139
All cases	6	Wimbleton Common	30	0.15	0.05	-0.10	0.42	0.74	0.74	0.01	0.35	0.06	0.24	0.70	136
All cases	6	Wimbleton Common	45	0.23	0.08	-0.15	0.71	0.68	0.68	0.01	1.15	0.13	0.22	0.65	136
All cases	6	Wimbleton Common	60	0.16	0.07	-0.08	0.42	0.62	0.63	0.02	0.33	0.07	0.28	0.65	138
All cases	6	Wimbleton Common	75	0.26	0.10	-0.16	0.72	0.70	0.70	0.00	1.26	0.08	0.28	0.64	137
All cases	6	Wimbleton Common	90	0.17	0.17	0.00	0.65	0.71	0.72	0.01	0.89	0.06	0.52	0.42	132
All cases	6	Wimbleton Common	105	0.26	0.18	-0.08	0.77	0.67	0.68	0.03	1.51	0.04	0.25	0.71	136
All cases	6	Wimbleton Common	120	0.18	0.17	-0.01	0.60	0.54	0.54	0.01	0.72	0.06	0.43	0.51	125
All cases	7	Yeading West	15	0.06	0.13	0.07	0.40	0.42	0.49	0.36	0.28	0.08	0.64	0.28	110
All cases	7	Yeading West	30	0.05	0.16	0.11	0.51	0.47	0.57	0.32	0.46	0.08	0.71	0.21	109
All cases	7	Yeading West	45	0.05	0.10	0.04	0.30	0.55	0.78	0.33	0.18	0.11	0.45	0.43	120
All cases	7	Yeading West	60	0.08	0.07	-0.01	0.33	0.57	0.76	0.30	0.17	0.10	0.38	0.52	114
All cases	7	Yeading West	75	0.12	0.08	-0.04	0.47	0.48	0.61	0.30	0.41	0.10	0.51	0.40	113
All cases	7	Yeading West	90	0.11	0.14	0.03	0.47	0.40	0.50	0.36	0.30	0.07	0.55	0.38	109
All cases	7	Yeading West	105	0.12	0.08	-0.04	0.43	0.49	0.68	0.37	0.39	0.11	0.34	0.54	118
All cases	7	Yeading West	120	0.11	0.07	-0.04	0.37	0.53	0.70	0.29	0.22	0.07	0.44	0.49	106
All cases	8	Yeading East	15	0.09	0.17	0.09	0.60	0.43	0.44	0.21	0.56	0.06	0.72	0.23	96
All cases	8	Yeading East	30	0.06	0.21	0.15	1.03	0.42	0.46	0.34	2.51	0.07	0.68	0.25	102
All cases	8	Yeading East	45	0.07	0.12	0.04	0.44	0.44	0.59	0.34	0.40	0.09	0.47	0.43	116
All cases	8	Yeading East	60	0.07	0.07	0.00	0.34	0.42	0.49	0.37	0.16	0.10	0.40	0.50	108
All cases	8	Yeading East	75	0.13	0.06	-0.07	0.49	0.41	0.47	0.30	0.43	0.10	0.34	0.56	111
All cases	8	Yeading East	90	0.10	0.17	0.07	0.54	0.36	0.43	0.32	0.52	0.05	0.44	0.51	101
All cases	8	Yeading East	105	0.13	0.12	-0.02	0.43	0.45	0.57	0.33	0.32	0.08	0.30	0.62	110
All cases	8	Yeading East	120	0.10	0.07	-0.03	0.33	0.34	0.38	0.38	0.17	0.05	0.40	0.55	100
All cases	9	Colindale Lane	15	0.06	0.14	0.08	0.44	0.43	0.43	0.00	0.36	0.15	0.70	0.15	142
All cases	9	Colindale Lane	30	0.08	0.10	0.03	0.40	0.47	0.47	0.00	0.27	0.05	0.69	0.26	139
All cases	9	Colindale Lane	45	0.05	0.16	0.11	0.57	0.59	0.59	0.00	0.68	0.08	0.73	0.19	139
All cases	9	Colindale Lane	60	0.10	0.07	-0.02	0.33	0.73	0.73	0.00	0.16	0.05	0.53	0.42	138
All cases	9	Colindale Lane	75	0.07	0.07	0.00	0.28	0.61	0.61	0.00	0.12	0.07	0.45	0.47	141
All cases	9	Colindale Lane	90	0.12	0.06	-0.06	0.37	0.59	0.59	0.00	0.21	0.10	0.42	0.48	132
All cases	9	Colindale Lane	105	0.08	0.09	0.00	0.36	0.63	0.63	0.00	0.16	0.12	0.54	0.34	136
All cases	9	Colindale Lane	120	0.13	0.13	0.00	0.50	0.57	0.57	0.00	0.37	0.07	0.62	0.31	126
All cases	10	Chipping Ongar	15	0.16	0.15	-0.02	0.81	0.31	0.37	0.39	1.30	0.09	0.42	0.49	96
All cases	10	Chipping Ongar	30	0.10	0.07	-0.04	0.26	0.28	0.33	0.47	0.09	0.10	0.43	0.47	90
All cases	10	Chipping Ongar	45	0.17	0.05	-0.12	0.45	0.32	0.36	0.33	0.46	0.08	0.23	0.68	86
All cases	10	Chipping Ongar	60	0.10	0.09	-0.01	0.30	0.28	0.35	0.35	0.12	0.07	0.52	0.40	86
All cases	10	Chipping Ongar	75	0.17	0.05	-0.12	0.41	0.28	0.35	0.30	0.44	0.09	0.19	0.71	85
All cases	10	Chipping Ongar	90	0.09	0.04	-0.05	0.18	0.27	0.31	0.26	0.06	0.11	0.31	0.57	80
All cases	10	Chipping Ongar	105	0.17	0.03	-0.13	0.40	0.27	0.32	0.22	0.46	0.12	0.26	0.62	82
All cases	10	Chipping Ongar	120	0.11	0.05	-0.06	0.26	0.26	0.28	0.20	0.11	0.20	0.35	0.44	73
All cases	11	Sewardstone Road	15	0.11	0.05	-0.06	0.23	0.34	0.37	0.35	0.07	0.11	0.32	0.58	93
All cases	11	Sewardstone Road	30	0.10	0.06	-0.04	0.22	0.31	0.33	0.21	0.07	0.09	0.30	0.61	88

**Table B.1. LFM catchment resolution performance statistics contd.**

Date	Catch number	Catchment Name	Lead time min.	Observed depth / mm	Forecast depth / mm	F-O depth / mm	SD (F-O) depth / mm	CSI catchment	HR catchment	FAR catchment	MSE catchment	Ub catchment	Ur catchment	Ud catchment	Runs
All cases	11	Sewardstone Road	45	0.11	0.08	-0.03	0.26	0.29	0.33	0.28	0.10	0.12	0.38	0.50	92
All cases	11	Sewardstone Road	60	0.09	0.04	-0.05	0.20	0.30	0.33	0.17	0.05	0.10	0.33	0.57	89
All cases	11	Sewardstone Road	75	0.11	0.04	-0.07	0.23	0.30	0.33	0.15	0.08	0.15	0.33	0.52	86
All cases	11	Sewardstone Road	90	0.09	0.03	-0.07	0.21	0.26	0.28	0.14	0.06	0.14	0.33	0.53	82
All cases	11	Sewardstone Road	105	0.11	0.03	-0.08	0.20	0.26	0.27	0.15	0.07	0.20	0.21	0.60	84
All cases	11	Sewardstone Road	120	0.11	0.09	-0.02	0.55	0.18	0.19	0.04	0.51	0.16	0.38	0.46	76
All cases	12	Luton Hoo	15	0.14	0.15	0.02	0.48	0.61	0.68	0.16	0.44	0.04	0.17	0.79	114
All cases	12	Luton Hoo	30	0.11	0.17	0.05	0.39	0.54	0.64	0.24	0.21	0.10	0.45	0.45	104
All cases	12	Luton Hoo	45	0.08	0.14	0.06	0.35	0.52	0.58	0.19	0.17	0.08	0.62	0.30	110
All cases	12	Luton Hoo	60	0.09	0.13	0.04	0.37	0.49	0.66	0.33	0.26	0.19	0.41	0.40	115
All cases	12	Luton Hoo	75	0.07	0.15	0.08	0.45	0.48	0.64	0.26	0.49	0.16	0.48	0.36	124
All cases	12	Luton Hoo	90	0.13	0.21	0.08	0.77	0.59	0.75	0.25	1.26	0.10	0.55	0.34	103
All cases	12	Luton Hoo	105	0.14	0.12	-0.02	0.58	0.50	0.56	0.26	0.72	0.08	0.46	0.46	112
All cases	12	Luton Hoo	120	0.16	0.11	-0.04	0.53	0.47	0.56	0.33	0.44	0.10	0.43	0.47	95
All cases	13	Gypsy Lane	15	0.25	0.08	-0.17	0.49	0.34	0.41	0.32	0.41	0.18	0.42	0.38	94
All cases	13	Gypsy Lane	30	0.31	0.06	-0.26	0.65	0.35	0.41	0.29	0.78	0.16	0.22	0.59	92
All cases	13	Gypsy Lane	45	0.27	0.05	-0.22	0.42	0.42	0.46	0.23	0.34	0.22	0.20	0.59	84
All cases	13	Gypsy Lane	60	0.31	0.07	-0.24	0.72	0.32	0.36	0.22	0.80	0.14	0.28	0.57	88
All cases	13	Gypsy Lane	75	0.27	0.13	-0.14	0.62	0.34	0.37	0.22	0.53	0.15	0.44	0.40	82
All cases	13	Gypsy Lane	90	0.33	0.07	-0.26	0.71	0.38	0.40	0.17	0.87	0.16	0.17	0.65	80
All cases	13	Gypsy Lane	105	0.28	0.06	-0.22	0.44	0.32	0.34	0.18	0.38	0.21	0.24	0.55	79
All cases	13	Gypsy Lane	120	0.35	0.05	-0.30	0.72	0.28	0.31	0.18	0.90	0.19	0.16	0.64	78
All cases	14	Albany Park	15	0.08	0.06	-0.02	0.21	0.39	0.50	0.35	0.06	0.06	0.41	0.53	107
All cases	14	Albany Park	30	0.07	0.10	0.03	0.27	0.47	0.54	0.26	0.09	0.07	0.64	0.29	111
All cases	14	Albany Park	45	0.06	0.07	0.01	0.18	0.42	0.53	0.39	0.04	0.07	0.62	0.31	112
All cases	14	Albany Park	60	0.06	0.09	0.03	0.28	0.47	0.59	0.28	0.16	0.13	0.51	0.37	118
All cases	14	Albany Park	75	0.08	0.10	0.02	0.47	0.43	0.51	0.32	0.49	0.11	0.60	0.29	111
All cases	14	Albany Park	90	0.11	0.04	-0.07	0.27	0.46	0.54	0.18	0.13	0.13	0.33	0.54	108
All cases	14	Albany Park	105	0.10	0.04	-0.06	0.24	0.41	0.45	0.30	0.11	0.17	0.26	0.57	106
All cases	14	Albany Park	120	0.11	0.05	-0.07	0.28	0.38	0.44	0.20	0.15	0.16	0.28	0.56	104
All cases	15	Edmonton Green	15	0.10	0.07	-0.03	0.28	0.45	0.50	0.31	0.10	0.10	0.43	0.47	93
All cases	15	Edmonton Green	30	0.07	0.07	0.00	0.24	0.43	0.54	0.37	0.07	0.07	0.44	0.49	101
All cases	15	Edmonton Green	45	0.09	0.06	-0.03	0.24	0.43	0.54	0.38	0.08	0.10	0.46	0.44	105
All cases	15	Edmonton Green	60	0.07	0.09	0.02	0.26	0.38	0.54	0.39	0.12	0.12	0.39	0.48	108
All cases	15	Edmonton Green	75	0.09	0.11	0.03	0.56	0.41	0.54	0.38	0.61	0.09	0.63	0.28	108
All cases	15	Edmonton Green	90	0.08	0.03	-0.05	0.20	0.33	0.43	0.41	0.05	0.11	0.22	0.68	103
All cases	15	Edmonton Green	105	0.10	0.06	-0.04	0.34	0.34	0.41	0.42	0.22	0.12	0.38	0.50	109
All cases	15	Edmonton Green	120	0.09	0.03	-0.06	0.20	0.28	0.36	0.42	0.06	0.13	0.33	0.55	97
All cases	16	Silver Street	15	0.08	0.09	0.01	0.25	0.53	0.53	0.08	0.09	0.02	0.61	0.36	125
All cases	16	Silver Street	30	0.07	0.12	0.05	0.40	0.60	0.61	0.11	0.26	0.06	0.65	0.29	122
All cases	16	Silver Street	45	0.08	0.07	0.00	0.31	0.66	0.68	0.06	0.15	0.05	0.63	0.32	124
All cases	16	Silver Street	60	0.06	0.07	0.01	0.21	0.60	0.65	0.14	0.07	0.08	0.34	0.58	130
All cases	16	Silver Street	75	0.07	0.06	-0.01	0.26	0.65	0.74	0.13	0.11	0.06	0.57	0.37	136
All cases	16	Silver Street	90	0.07	0.04	-0.03	0.20	0.61	0.69	0.10	0.05	0.06	0.36	0.58	125
All cases	16	Silver Street	105	0.09	0.05	-0.04	0.27	0.58	0.62	0.14	0.13	0.07	0.41	0.53	130

**Table B.1. LFM catchment resolution performance statistics contd.**

Date	Catch number	Catchment Name	Lead time min.	Observed depth / mm	Forecast depth / mm	F-O depth / mm	SD (F-O) depth / mm	CSI catchment	HR catchment	FAR catchment	MSE catchment	Ub catchment	Ur catchment	Ud catchment	Runs LFM
All cases	16	Silver Street	120	0.08	0.04	-0.03	0.24	0.54	0.57	0.15	0.07	0.08	0.12	0.24	0.48 115.6
All cases	17	Bretons Farm	15	0.08	0.03	-0.05	0.26	0.38	0.38	0.00	0.11	0.12	0.24	0.63 141.1	
All cases	17	Bretons Farm	30	0.07	0.02	-0.06	0.19	0.33	0.33	0.00	0.06	0.10	0.08	0.82 135.5	
All cases	17	Bretons Farm	45	0.08	0.03	-0.05	0.23	0.25	0.25	0.00	0.09	0.13	0.27	0.61 136.9	
All cases	17	Bretons Farm	60	0.07	0.06	-0.01	0.27	0.22	0.22	0.00	0.15	0.07	0.24	0.68 134.9	
All cases	17	Bretons Farm	75	0.08	0.05	-0.03	0.27	0.24	0.24	0.00	0.12	0.12	0.31	0.57 140.3	
All cases	17	Bretons Farm	90	0.06	0.04	-0.02	0.20	0.25	0.25	0.00	0.06	0.06	0.28	0.66 128.8	
All cases	17	Bretons Farm	105	0.08	0.04	-0.04	0.28	0.29	0.29	0.00	0.15	0.13	0.27	0.60 135.5	
All cases	17	Bretons Farm	120	0.07	0.01	-0.06	0.19	0.16	0.16	0.00	0.06	0.11	0.20	0.70 122.2	
All cases	18	Gaynes Park	15	0.15	0.04	-0.11	0.32	0.38	0.38	0.10	0.15	0.15	0.19	0.66 122.2	
All cases	18	Gaynes Park	30	0.13	0.02	-0.11	0.32	0.35	0.36	0.12	0.15	0.14	0.09	0.77 118.8	
All cases	18	Gaynes Park	45	0.15	0.02	-0.12	0.32	0.31	0.31	0.08	0.16	0.17	0.12	0.71 119.9	
All cases	18	Gaynes Park	60	0.14	0.07	-0.07	0.40	0.22	0.23	0.11	0.23	0.09	0.24	0.67 116.8	
All cases	18	Gaynes Park	75	0.14	0.04	-0.11	0.29	0.28	0.28	0.02	0.13	0.15	0.12	0.73 120.3	
All cases	18	Gaynes Park	90	0.13	0.05	-0.07	0.34	0.25	0.25	0.09	0.15	0.08	0.26	0.66 109.9	
All cases	18	Gaynes Park	105	0.13	0.05	-0.08	0.31	0.31	0.32	0.06	0.14	0.12	0.31	0.57 117.7	
All cases	18	Gaynes Park	120	0.14	0.02	-0.12	0.33	0.23	0.23	0.06	0.17	0.15	0.12	0.73 105.6	
All cases	19	Bromley South Recorder	15	0.22	0.08	-0.14	0.38	0.32	0.32	0.00	0.29	0.21	0.36	0.43 142.1	
All cases	19	Bromley South Recorder	30	0.25	0.07	-0.18	0.47	0.31	0.31	0.00	0.42	0.19	0.33	0.48 139.9	
All cases	19	Bromley South Recorder	45	0.21	0.07	-0.14	0.35	0.34	0.34	0.00	0.26	0.22	0.35	0.43 139.9	
All cases	19	Bromley South Recorder	60	0.22	0.06	-0.15	0.37	0.29	0.29	0.00	0.29	0.20	0.31	0.49 138.3	
All cases	19	Bromley South Recorder	75	0.21	0.05	-0.16	0.37	0.28	0.28	0.00	0.27	0.24	0.39	0.37 141.1	
All cases	19	Bromley South Recorder	90	0.25	0.02	-0.22	0.45	0.21	0.21	0.00	0.42	0.23	0.17	0.60 132.1	
All cases	19	Bromley South Recorder	105	0.20	0.06	-0.14	0.37	0.20	0.20	0.00	0.23	0.23	0.27	0.49 136.9	
All cases	19	Bromley South Recorder	120	0.24	0.05	-0.19	0.36	0.13	0.13	0.00	0.27	0.29	0.10	0.60 126.9	

**Table B.2. Nimrod 2 km resolution performance statistics**

Date	Catch number	Catchment Name	Lead time min.	CSI 2km pixel	SD CSI 2km pixel	HR 2km pixel	SD HR 2km pixel	FAR 2km pixel	SD FAR 2km pixel	MSE mm <sup>2</sup>	SD MSE mm <sup>2</sup>	Ub 2km pixel	SD Ub 2km pixel	Ur 2km pixel	SD Ur 2km pixel	Ud 2km pixel	SD Ud 2km pixel	Runs Nimrod
All cases	0	All catchments	15	0.41	0.24	0.26	0.20	0.17	0.13	0.46	1.35	0.13	0.12	0.14	0.18	0.73	0.20	142
All cases	0	All catchments	30	0.34	0.24	0.24	0.20	0.23	0.19	0.41	0.81	0.14	0.14	0.20	0.21	0.66	0.23	139
All cases	0	All catchments	45	0.30	0.22	0.22	0.18	0.24	0.18	0.59	1.46	0.12	0.12	0.21	0.24	0.67	0.23	139
All cases	0	All catchments	60	0.24	0.22	0.18	0.17	0.28	0.21	0.48	1.00	0.15	0.15	0.23	0.25	0.62	0.25	138
All cases	0	All catchments	75	0.20	0.20	0.17	0.18	0.29	0.23	0.66	1.81	0.16	0.13	0.21	0.23	0.63	0.23	141
All cases	0	All catchments	90	0.18	0.18	0.15	0.16	0.33	0.24	0.46	0.79	0.17	0.14	0.22	0.24	0.61	0.24	132
All cases	0	All catchments	105	0.16	0.17	0.14	0.16	0.36	0.26	0.62	1.28	0.17	0.14	0.22	0.24	0.60	0.24	136
All cases	0	All catchments	120	0.12	0.13	0.12	0.14	0.37	0.26	0.48	0.79	0.17	0.15	0.22	0.24	0.60	0.25	126
All cases	1	Mimshall Brook	15	0.19	0.28	0.15	0.24	0.07	0.15	0.04	0.14	0.45	0.22	0.13	0.20	0.42	0.21	142
All cases	1	Mimshall Brook	30	0.15	0.23	0.13	0.22	0.11	0.21	0.12	0.57	0.49	0.23	0.14	0.22	0.37	0.21	139
All cases	1	Mimshall Brook	45	0.16	0.27	0.13	0.24	0.09	0.15	0.13	0.57	0.44	0.23	0.19	0.23	0.37	0.22	139
All cases	1	Mimshall Brook	60	0.11	0.22	0.11	0.21	0.13	0.23	0.16	0.62	0.49	0.23	0.16	0.24	0.35	0.20	138
All cases	1	Mimshall Brook	75	0.13	0.25	0.12	0.23	0.11	0.20	0.66	3.50	0.50	0.22	0.14	0.20	0.36	0.21	141
All cases	1	Mimshall Brook	90	0.10	0.21	0.11	0.21	0.18	0.23	0.60	2.90	0.48	0.22	0.17	0.20	0.35	0.19	132
All cases	1	Mimshall Brook	105	0.11	0.22	0.10	0.20	0.16	0.24	0.74	3.59	0.54	0.22	0.12	0.18	0.34	0.20	136
All cases	1	Mimshall Brook	120	0.07	0.15	0.07	0.15	0.15	0.24	0.66	3.03	0.55	0.21	0.10	0.16	0.35	0.18	126
All cases	2	Towncroft lane, Orpington	15	0.30	0.32	0.29	0.32	0.17	0.22	0.20	0.61	0.52	0.31	0.16	0.21	0.14	0.19	77
All cases	2	Towncroft lane, Orpington	30	0.23	0.32	0.25	0.34	0.23	0.33	0.48	1.41	0.43	0.35	0.20	0.24	0.09	0.14	84
All cases	2	Towncroft lane, Orpington	45	0.26	0.32	0.23	0.30	0.19	0.29	0.52	2.10	0.53	0.31	0.13	0.17	0.17	0.23	78
All cases	2	Towncroft lane, Orpington	60	0.18	0.28	0.19	0.29	0.18	0.28	0.33	1.01	0.47	0.33	0.20	0.24	0.11	0.18	80
All cases	2	Towncroft lane, Orpington	75	0.19	0.28	0.19	0.29	0.22	0.38	0.24	0.72	0.58	0.34	0.15	0.23	0.14	0.19	82
All cases	2	Towncroft lane, Orpington	90	0.15	0.28	0.19	0.31	0.21	0.32	0.27	0.65	0.60	0.37	0.13	0.18	0.09	0.13	85
All cases	2	Towncroft lane, Orpington	105	0.16	0.28	0.17	0.28	0.20	0.31	0.15	0.39	0.55	0.32	0.16	0.23	0.14	0.19	84
All cases	2	Towncroft lane, Orpington	120	0.10	0.22	0.13	0.25	0.25	0.35	0.25	0.60	0.58	0.35	0.13	0.19	0.12	0.17	82
All cases	3	Elmers End Road	15	0.18	0.29	0.17	0.27	0.12	0.21	0.81	4.02	0.32	0.33	0.20	0.25	0.21	0.22	142
All cases	3	Elmers End Road	30	0.17	0.29	0.17	0.30	0.12	0.24	0.34	1.60	0.33	0.33	0.13	0.19	0.22	0.24	139
All cases	3	Elmers End Road	45	0.15	0.26	0.14	0.25	0.12	0.25	1.17	6.57	0.37	0.29	0.15	0.23	0.21	0.21	139
All cases	3	Elmers End Road	60	0.13	0.27	0.13	0.26	0.13	0.27	0.20	0.73	0.40	0.36	0.12	0.20	0.20	0.22	138
All cases	3	Elmers End Road	75	0.10	0.23	0.10	0.23	0.16	0.30	1.16	6.32	0.42	0.32	0.16	0.25	0.18	0.20	141
All cases	3	Elmers End Road	90	0.11	0.23	0.11	0.24	0.10	0.25	0.23	0.81	0.44	0.34	0.14	0.25	0.22	0.23	132
All cases	3	Elmers End Road	105	0.09	0.21	0.10	0.21	0.18	0.31	1.01	5.37	0.45	0.34	0.12	0.23	0.18	0.19	136
All cases	3	Elmers End Road	120	0.09	0.19	0.09	0.19	0.14	0.28	0.29	0.92	0.41	0.36	0.12	0.20	0.21	0.23	126
All cases	4	Longley Road Recorder	15	0.16	0.28	0.15	0.26	0.13	0.23	0.78	2.99	0.32	0.30	0.15	0.23	0.31	0.27	142
All cases	4	Longley Road Recorder	30	0.17	0.30	0.16	0.30	0.13	0.26	0.45	1.93	0.33	0.33	0.14	0.23	0.31	0.28	139
All cases	4	Longley Road Recorder	45	0.14	0.27	0.13	0.25	0.14	0.27	0.73	3.64	0.37	0.31	0.12	0.19	0.26	0.24	139
All cases	4	Longley Road Recorder	60	0.12	0.25	0.12	0.25	0.14	0.27	0.67	2.67	0.41	0.34	0.11	0.19	0.27	0.26	138
All cases	4	Longley Road Recorder	75	0.09	0.20	0.09	0.21	0.17	0.30	0.72	3.48	0.41	0.31	0.14	0.24	0.25	0.22	141
All cases	4	Longley Road Recorder	90	0.10	0.22	0.10	0.21	0.13	0.28	0.61	2.14	0.40	0.31	0.13	0.23	0.26	0.24	132
All cases	4	Longley Road Recorder	105	0.09	0.20	0.09	0.21	0.17	0.29	0.70	3.02	0.41	0.33	0.12	0.21	0.22	0.21	136
All cases	4	Longley Road Recorder	120	0.07	0.15	0.08	0.16	0.15	0.28	0.83	3.07	0.45	0.33	0.09	0.15	0.28	0.25	126
All cases	5	West Barnes Lane	15	0.16	0.28	0.15	0.26	0.13	0.23	0.78	2.99	0.32	0.30	0.15	0.23	0.31	0.27	142
All cases	5	West Barnes Lane	30	0.17	0.30	0.16	0.30	0.13	0.26	0.45	1.93	0.33	0.33	0.14	0.23	0.31	0.29	139
All cases	5	West Barnes Lane	45	0.14	0.27	0.13	0.25	0.14	0.27	0.73	3.64	0.37	0.31	0.12	0.19	0.26	0.24	139
All cases	5	West Barnes Lane	60	0.12	0.25	0.12	0.25	0.14	0.27	0.67	2.67	0.41	0.34	0.11	0.19	0.27	0.26	138
All cases	5	West Barnes Lane	75	0.09	0.20	0.09	0.21	0.17	0.30	0.72	3.48	0.41	0.31	0.14	0.24	0.25	0.22	141

Table B.2. Nimrod 2 km resolution performance statistics contd.

Date	Catch number	Catchment Name	Lead time min.	CSI 2km pixel	SD CSI 2km pixel	HR 2km pixel	SD HR 2km pixel	FAR 2km pixel	SD FAR 2km pixel	MSE mm <sup>2</sup>	SD MSE mm <sup>2</sup>	Ub 2km pixel	SD Ub 2km pixel	Ur 2km pixel	SD Ur 2km pixel	Ud 2km pixel	SD Ud 2km pixel	Runs Nimrod
All cases	5	West Barnes Lane	90	0.10	0.22	0.10	0.21	0.13	0.28	0.61	2.14	0.40	0.31	0.13	0.23	0.26	0.24	132
All cases	5	West Barnes Lane	105	0.09	0.20	0.09	0.21	0.17	0.28	0.70	3.02	0.41	0.33	0.12	0.21	0.22	0.21	136
All cases	5	West Barnes Lane	120	0.07	0.15	0.08	0.16	0.15	0.28	0.83	3.07	0.45	0.33	0.09	0.15	0.28	0.25	126
All cases	6	Wimbleton Common	15	0.24	0.31	0.21	0.28	0.08	0.15	0.64	2.23	0.45	0.29	0.10	0.18	0.39	0.26	139
All cases	6	Wimbleton Common	30	0.20	0.30	0.17	0.26	0.09	0.18	0.67	3.14	0.50	0.30	0.10	0.17	0.35	0.26	135
All cases	6	Wimbleton Common	45	0.18	0.25	0.16	0.24	0.12	0.22	1.71	6.62	0.48	0.29	0.13	0.20	0.34	0.23	135
All cases	6	Wimbleton Common	60	0.12	0.23	0.12	0.22	0.12	0.23	0.79	3.16	0.52	0.28	0.12	0.20	0.31	0.25	136
All cases	6	Wimbleton Common	75	0.13	0.22	0.12	0.21	0.11	0.21	1.82	6.63	0.52	0.28	0.13	0.19	0.31	0.23	137
All cases	6	Wimbleton Common	90	0.11	0.21	0.10	0.20	0.14	0.25	0.84	3.28	0.53	0.28	0.13	0.20	0.30	0.23	131
All cases	6	Wimbleton Common	105	0.09	0.18	0.08	0.18	0.12	0.26	1.92	6.79	0.53	0.29	0.14	0.23	0.30	0.23	134
All cases	6	Wimbleton Common	120	0.06	0.16	0.07	0.16	0.15	0.25	0.90	3.53	0.54	0.27	0.11	0.21	0.32	0.22	124
All cases	7	Yeading West	15	0.17	0.28	0.14	0.26	0.10	0.19	0.07	0.29	0.26	0.29	0.16	0.24	0.21	0.27	90
All cases	7	Yeading West	30	0.14	0.25	0.11	0.21	0.15	0.26	0.08	0.34	0.34	0.35	0.15	0.22	0.15	0.22	92
All cases	7	Yeading West	45	0.12	0.20	0.09	0.17	0.19	0.27	0.10	0.37	0.37	0.29	0.15	0.18	0.16	0.21	93
All cases	7	Yeading West	60	0.10	0.17	0.09	0.17	0.17	0.27	0.22	0.90	0.41	0.38	0.15	0.20	0.14	0.20	97
All cases	7	Yeading West	75	0.07	0.14	0.06	0.14	0.17	0.26	0.62	2.89	0.43	0.29	0.10	0.15	0.14	0.19	95
All cases	7	Yeading West	90	0.04	0.10	0.04	0.10	0.21	0.29	0.32	1.05	0.48	0.35	0.11	0.16	0.15	0.21	93
All cases	7	Yeading West	105	0.04	0.11	0.04	0.11	0.18	0.25	0.56	2.66	0.55	0.34	0.10	0.14	0.13	0.17	95
All cases	7	Yeading West	120	0.05	0.11	0.05	0.11	0.17	0.24	0.31	1.02	0.50	0.36	0.09	0.14	0.15	0.20	97
All cases	8	Yeading East	15	0.16	0.30	0.14	0.27	0.13	0.24	0.13	0.72	0.26	0.29	0.18	0.26	0.13	0.20	89
All cases	8	Yeading East	30	0.14	0.26	0.12	0.25	0.15	0.27	0.12	0.59	0.31	0.33	0.15	0.21	0.11	0.17	87
All cases	8	Yeading East	45	0.13	0.23	0.10	0.22	0.18	0.28	0.16	0.74	0.38	0.32	0.16	0.23	0.10	0.17	93
All cases	8	Yeading East	60	0.10	0.18	0.09	0.19	0.18	0.30	0.15	0.68	0.38	0.35	0.13	0.20	0.09	0.16	92
All cases	8	Yeading East	75	0.07	0.17	0.06	0.16	0.22	0.34	0.49	2.06	0.42	0.34	0.13	0.20	0.09	0.15	93
All cases	8	Yeading East	90	0.05	0.12	0.05	0.11	0.19	0.30	0.21	0.77	0.44	0.34	0.10	0.17	0.09	0.17	88
All cases	8	Yeading East	105	0.04	0.13	0.03	0.12	0.20	0.30	0.50	2.09	0.50	0.39	0.13	0.20	0.10	0.16	96
All cases	8	Yeading East	120	0.05	0.14	0.05	0.12	0.19	0.25	0.22	0.79	0.48	0.34	0.11	0.17	0.15	0.22	85
All cases	9	Colindeep Lane	15	0.10	0.21	0.09	0.20	0.06	0.14	0.02	0.08	0.62	0.27	0.10	0.20	0.26	0.19	142
All cases	9	Colindeep Lane	30	0.10	0.20	0.09	0.19	0.07	0.18	0.13	0.50	0.65	0.24	0.10	0.17	0.25	0.19	139
All cases	9	Colindeep Lane	45	0.10	0.20	0.09	0.19	0.09	0.19	0.08	0.29	0.64	0.26	0.11	0.18	0.24	0.21	139
All cases	9	Colindeep Lane	60	0.09	0.17	0.08	0.17	0.11	0.21	0.23	0.86	0.63	0.27	0.15	0.24	0.22	0.16	138
All cases	9	Colindeep Lane	75	0.07	0.16	0.07	0.16	0.12	0.23	0.08	0.30	0.66	0.23	0.11	0.18	0.23	0.19	141
All cases	9	Colindeep Lane	90	0.05	0.12	0.06	0.13	0.15	0.26	0.30	0.95	0.68	0.22	0.10	0.15	0.23	0.17	132
All cases	9	Colindeep Lane	105	0.05	0.13	0.05	0.13	0.15	0.27	0.11	0.35	0.67	0.27	0.11	0.20	0.22	0.17	136
All cases	9	Colindeep Lane	120	0.05	0.13	0.05	0.13	0.16	0.27	0.32	1.01	0.68	0.24	0.09	0.18	0.23	0.17	126
All cases	10	Chipping Ongar	15	0.26	0.30	0.25	0.30	0.17	0.22	0.41	1.30	0.35	0.31	0.16	0.21	0.33	0.29	83
All cases	10	Chipping Ongar	30	0.23	0.28	0.23	0.29	0.19	0.26	0.63	1.93	0.43	0.31	0.18	0.21	0.27	0.29	82
All cases	10	Chipping Ongar	45	0.22	0.30	0.22	0.29	0.19	0.26	0.11	1.22	0.47	0.29	0.15	0.16	0.27	0.27	83
All cases	10	Chipping Ongar	60	0.19	0.27	0.19	0.26	0.23	0.29	0.11	0.99	0.50	0.34	0.15	0.19	0.28	0.31	87
All cases	10	Chipping Ongar	75	0.15	0.23	0.15	0.23	0.22	0.32	0.67	2.09	0.50	0.31	0.17	0.22	0.30	0.27	85
All cases	10	Chipping Ongar	90	0.11	0.19	0.13	0.21	0.25	0.34	0.10	0.23	0.49	0.31	0.17	0.22	0.30	0.27	89
All cases	10	Chipping Ongar	105	0.13	0.19	0.13	0.20	0.26	0.34	0.62	1.95	0.51	0.29	0.15	0.19	0.26	0.28	89
All cases	10	Chipping Ongar	120	0.11	0.19	0.12	0.20	0.28	0.31	0.14	0.33	0.51	0.31	0.13	0.18	0.29	0.27	84
All cases	11	Sewardstone Road	15	0.24	0.30	0.21	0.29	0.14	0.21	0.09	0.22	0.34	0.33	0.18	0.24	0.28	0.28	89
All cases	11	Sewardstone Road	30	0.21	0.29	0.19	0.28	0.12	0.20	0.09	0.25	0.36	0.31	0.13	0.18	0.28	0.32	89



**Table B.2. Nimrod 2 km resolution performance statistics contd.**

Date	Catch number	Catchment Name	Lead time min.	CSI 2km pixel	SD CSI 2km pixel	HR 2km pixel	SD HR 2km pixel	FAR 2km pixel	SD FAR 2km pixel	MSE 2km pixel	SD MSE 2km pixel	UB 2km pixel	SD UB 2km pixel	Ur 2km pixel	SD Ur 2km pixel	Ud 2km pixel	SD Ud 2km pixel	Runs Nimrod
All cases	11	Sewardstone Road	45	0.17	0.27	0.16	0.25	0.17	0.27	0.17	0.39	0.42	0.36	0.18	0.23	0.23	0.27	96
All cases	11	Sewardstone Road	60	0.15	0.23	0.15	0.23	0.19	0.29	0.13	0.42	0.43	0.31	0.19	0.24	0.21	0.25	95
All cases	11	Sewardstone Road	75	0.13	0.23	0.13	0.22	0.18	0.28	0.13	0.51	0.49	0.34	0.16	0.21	0.25	0.28	93
All cases	11	Sewardstone Road	90	0.14	0.23	0.14	0.21	0.25	0.32	0.13	0.39	0.43	0.31	0.19	0.25	0.23	0.26	90
All cases	11	Sewardstone Road	105	0.11	0.21	0.10	0.20	0.24	0.31	0.17	0.40	0.51	0.30	0.16	0.22	0.22	0.25	96
All cases	11	Sewardstone Road	120	0.12	0.21	0.14	0.21	0.27	0.32	0.13	0.36	0.54	0.29	0.15	0.20	0.23	0.24	90
All cases	12	Luton Hoo	15	0.23	0.31	0.21	0.30	0.13	0.18	0.40	1.76	0.28	0.30	0.15	0.21	0.36	0.31	103
All cases	12	Luton Hoo	30	0.21	0.27	0.22	0.29	0.21	0.26	0.24	0.64	0.34	0.31	0.17	0.21	0.34	0.32	89
All cases	12	Luton Hoo	45	0.17	0.25	0.17	0.25	0.19	0.26	0.11	0.24	0.31	0.29	0.17	0.21	0.30	0.30	98
All cases	12	Luton Hoo	60	0.16	0.20	0.15	0.22	0.19	0.24	0.20	0.46	0.35	0.32	0.14	0.19	0.29	0.28	88
All cases	12	Luton Hoo	75	0.11	0.17	0.10	0.17	0.14	0.22	0.11	0.23	0.40	0.32	0.11	0.16	0.28	0.28	101
All cases	12	Luton Hoo	90	0.11	0.19	0.10	0.19	0.18	0.29	0.49	1.72	0.40	0.33	0.14	0.20	0.34	0.29	87
All cases	12	Luton Hoo	105	0.09	0.17	0.09	0.17	0.15	0.23	0.77	3.64	0.41	0.32	0.11	0.17	0.30	0.25	101
All cases	12	Luton Hoo	120	0.09	0.19	0.09	0.19	0.15	0.26	0.62	1.89	0.40	0.28	0.11	0.16	0.33	0.27	83
All cases	13	Gypsy Lane	15	0.40	0.38	0.37	0.37	0.18	0.27	0.39	1.08	0.34	0.29	0.12	0.17	0.41	0.32	82
All cases	13	Gypsy Lane	30	0.33	0.36	0.31	0.35	0.15	0.25	1.09	4.07	0.43	0.31	0.13	0.17	0.35	0.28	82
All cases	13	Gypsy Lane	45	0.28	0.36	0.28	0.35	0.16	0.27	0.65	1.59	0.43	0.32	0.15	0.19	0.28	0.31	79
All cases	13	Gypsy Lane	60	0.24	0.34	0.25	0.35	0.15	0.24	1.26	5.01	0.48	0.31	0.11	0.17	0.32	0.26	82
All cases	13	Gypsy Lane	75	0.24	0.33	0.25	0.34	0.21	0.30	0.94	1.89	0.47	0.30	0.12	0.20	0.28	0.28	81
All cases	13	Gypsy Lane	90	0.22	0.32	0.23	0.32	0.19	0.31	1.56	5.12	0.52	0.30	0.16	0.23	0.28	0.26	83
All cases	13	Gypsy Lane	105	0.20	0.28	0.21	0.29	0.27	0.34	0.80	1.72	0.54	0.32	0.11	0.16	0.24	0.25	84
All cases	13	Gypsy Lane	120	0.21	0.27	0.22	0.28	0.23	0.30	1.33	5.07	0.54	0.31	0.13	0.17	0.28	0.26	83
All cases	14	Albany Park	15	0.25	0.31	0.22	0.29	0.13	0.20	0.05	0.11	0.40	0.34	0.11	0.18	0.36	0.32	89
All cases	14	Albany Park	30	0.21	0.29	0.19	0.27	0.16	0.25	0.13	0.35	0.37	0.29	0.14	0.19	0.26	0.27	94
All cases	14	Albany Park	45	0.19	0.27	0.18	0.26	0.14	0.23	0.19	0.76	0.46	0.34	0.12	0.17	0.28	0.30	92
All cases	14	Albany Park	60	0.16	0.27	0.15	0.26	0.16	0.24	0.18	0.59	0.36	0.32	0.16	0.21	0.22	0.27	99
All cases	14	Albany Park	75	0.15	0.22	0.12	0.21	0.21	0.28	0.12	0.29	0.45	0.38	0.18	0.20	0.23	0.25	83
All cases	14	Albany Park	90	0.12	0.21	0.12	0.20	0.22	0.27	0.28	1.03	0.38	0.35	0.17	0.21	0.23	0.28	96
All cases	14	Albany Park	105	0.13	0.21	0.13	0.22	0.25	0.31	0.16	0.46	0.47	0.36	0.17	0.21	0.24	0.23	94
All cases	14	Albany Park	120	0.10	0.19	0.09	0.17	0.23	0.35	0.31	1.07	0.45	0.34	0.12	0.17	0.23	0.26	96
All cases	15	Edmonton Green	15	0.21	0.32	0.19	0.30	0.12	0.22	0.07	0.17	0.38	0.34	0.12	0.17	0.28	0.28	85
All cases	15	Edmonton Green	30	0.18	0.28	0.16	0.27	0.19	0.28	0.18	0.65	0.37	0.34	0.15	0.21	0.26	0.29	87
All cases	15	Edmonton Green	45	0.16	0.25	0.14	0.25	0.14	0.26	0.17	0.55	0.44	0.34	0.12	0.18	0.21	0.26	85
All cases	15	Edmonton Green	60	0.14	0.23	0.12	0.22	0.17	0.25	0.18	0.61	0.40	0.32	0.10	0.15	0.28	0.27	85
All cases	15	Edmonton Green	75	0.12	0.23	0.11	0.22	0.20	0.32	0.10	0.22	0.47	0.35	0.13	0.16	0.18	0.22	95
All cases	15	Edmonton Green	90	0.10	0.19	0.10	0.19	0.24	0.34	0.14	0.48	0.51	0.33	0.11	0.16	0.22	0.24	91
All cases	15	Edmonton Green	105	0.10	0.19	0.09	0.19	0.21	0.31	0.12	0.29	0.48	0.35	0.14	0.20	0.17	0.22	93
All cases	15	Edmonton Green	120	0.08	0.17	0.07	0.17	0.22	0.34	0.18	0.54	0.51	0.37	0.12	0.18	0.21	0.24	88
All cases	16	Silver Street	15	0.15	0.25	0.12	0.23	0.13	0.23	0.05	0.16	0.44	0.33	0.18	0.23	0.30	0.29	123
All cases	16	Silver Street	30	0.15	0.25	0.12	0.22	0.16	0.25	0.20	0.82	0.40	0.33	0.22	0.28	0.30	0.30	117
All cases	16	Silver Street	45	0.10	0.20	0.10	0.19	0.17	0.28	0.11	0.33	0.45	0.33	0.18	0.22	0.25	0.24	124
All cases	16	Silver Street	60	0.11	0.21	0.09	0.18	0.17	0.25	0.19	0.83	0.47	0.31	0.17	0.22	0.25	0.25	119
All cases	16	Silver Street	75	0.10	0.19	0.09	0.18	0.19	0.30	0.09	0.23	0.52	0.32	0.16	0.20	0.21	0.22	123
All cases	16	Silver Street	90	0.09	0.19	0.09	0.17	0.20	0.28	0.16	0.69	0.51	0.33	0.15	0.19	0.24	0.25	118
All cases	16	Silver Street	105	0.08	0.16	0.07	0.15	0.24	0.32	0.12	0.32	0.52	0.33	0.17	0.23	0.22	0.22	121

**Table B.2. Nimrod 2 km resolution performance statistics contd.**

Date	Catch number	Catchment Name	Lead time min.	CSI	SD CSI	HR	SD HR	FAR	SD FAR	MSE	SD MSE	Ub	SD Ub	Ur	SD Ur	Ud	SD Ud	Runs
All cases	16	Silver Street	120	0.07	0.15	0.06	0.14	0.22	0.29	0.20	0.82	0.55	0.31	0.16	0.19	0.24	0.24	111
All cases	17	Bretons Farm	15	0.14	0.23	0.12	0.21	0.11	0.21	0.14	0.56	0.29	0.30	0.13	0.21	0.28	0.30	142
All cases	17	Bretons Farm	30	0.11	0.20	0.10	0.19	0.16	0.25	0.18	0.77	0.35	0.33	0.19	0.25	0.22	0.26	136
All cases	17	Bretons Farm	45	0.10	0.18	0.10	0.18	0.16	0.24	0.25	1.08	0.36	0.34	0.21	0.29	0.20	0.23	139
All cases	17	Bretons Farm	60	0.07	0.15	0.07	0.13	0.17	0.25	0.20	0.87	0.39	0.32	0.17	0.25	0.21	0.24	136
All cases	17	Bretons Farm	75	0.08	0.16	0.08	0.16	0.17	0.29	0.25	1.16	0.38	0.33	0.15	0.23	0.20	0.23	141
All cases	17	Bretons Farm	90	0.07	0.15	0.07	0.14	0.17	0.27	0.18	0.83	0.42	0.33	0.15	0.23	0.21	0.24	131
All cases	17	Bretons Farm	105	0.07	0.15	0.07	0.15	0.18	0.29	0.27	1.19	0.40	0.32	0.16	0.22	0.21	0.23	136
All cases	17	Bretons Farm	120	0.05	0.10	0.06	0.10	0.25	0.33	0.23	0.95	0.41	0.32	0.17	0.24	0.23	0.25	125
All cases	18	Gaynes Park	15	0.20	0.29	0.18	0.28	0.10	0.24	0.41	1.49	0.34	0.33	0.12	0.18	0.32	0.28	120
All cases	18	Gaynes Park	30	0.17	0.27	0.15	0.23	0.16	0.24	0.34	1.07	0.42	0.33	0.12	0.20	0.25	0.27	118
All cases	18	Gaynes Park	45	0.13	0.23	0.13	0.23	0.16	0.25	0.60	2.16	0.45	0.33	0.15	0.21	0.22	0.25	120
All cases	18	Gaynes Park	60	0.10	0.19	0.11	0.19	0.15	0.23	0.61	2.04	0.45	0.32	0.12	0.19	0.23	0.24	116
All cases	18	Gaynes Park	75	0.10	0.18	0.10	0.18	0.16	0.26	0.62	2.26	0.47	0.32	0.13	0.18	0.24	0.27	122
All cases	18	Gaynes Park	90	0.09	0.18	0.10	0.19	0.19	0.25	0.59	2.01	0.47	0.32	0.14	0.18	0.24	0.26	113
All cases	18	Gaynes Park	105	0.09	0.18	0.10	0.18	0.20	0.28	0.54	1.87	0.44	0.36	0.12	0.19	0.24	0.28	118
All cases	18	Gaynes Park	120	0.07	0.16	0.08	0.16	0.24	0.34	0.63	2.06	0.49	0.32	0.14	0.18	0.24	0.26	112
All cases	19	Bromley South Recorder	15	0.21	0.29	0.21	0.30	0.06	0.12	0.44	0.94	0.66	0.29	0.06	0.14	0.28	0.24	142
All cases	19	Bromley South Recorder	30	0.17	0.29	0.18	0.31	0.10	0.23	0.82	2.04	0.70	0.30	0.08	0.17	0.23	0.26	139
All cases	19	Bromley South Recorder	45	0.17	0.31	0.17	0.31	0.07	0.18	0.66	1.78	0.68	0.27	0.05	0.11	0.27	0.24	139
All cases	19	Bromley South Recorder	60	0.14	0.25	0.16	0.27	0.06	0.14	0.50	1.31	0.72	0.28	0.06	0.11	0.23	0.24	141
All cases	19	Bromley South Recorder	75	0.15	0.27	0.17	0.31	0.09	0.20	0.44	1.05	0.70	0.30	0.06	0.16	0.24	0.24	138
All cases	19	Bromley South Recorder	90	0.11	0.22	0.13	0.25	0.11	0.24	0.59	1.63	0.69	0.28	0.07	0.15	0.24	0.24	132
All cases	19	Bromley South Recorder	105	0.12	0.23	0.14	0.26	0.11	0.22	0.35	0.93	0.69	0.28	0.07	0.15	0.24	0.24	136
All cases	19	Bromley South Recorder	120	0.13	0.25	0.15	0.28	0.13	0.24	0.56	1.38	0.71	0.27	0.07	0.16	0.22	0.19	126

**Table B.2. Nimrod catchment resolution performance statistics**

Date	Catch number	Catchment Name	Lead time min.	Observed depth / mm	Forecast depth / mm	F-O depth / mm	SD (F-O) depth / mm	CSI catchment	HR catchment	FAR catchment	MSE catchment	Ub catchment	Ur catchment	UD catchment	Runs Nimrod
All cases	0	All catchments	15	0.11	0.08	-0.03	0.06	0.92	0.92	0.00	0.01	0.25	0.13	0.62	142
All cases	0	All catchments	30	0.09	0.06	-0.03	0.07	0.92	0.92	0.00	0.01	0.20	0.15	0.65	139
All cases	0	All catchments	45	0.10	0.06	-0.04	0.10	0.94	0.94	0.00	0.02	0.21	0.10	0.69	139
All cases	0	All catchments	60	0.09	0.05	-0.04	0.09	0.91	0.91	0.00	0.02	0.20	0.14	0.66	138
All cases	0	All catchments	75	0.11	0.05	-0.06	0.12	0.90	0.90	0.00	0.03	0.23	0.11	0.68	141
All cases	0	All catchments	90	0.11	0.05	-0.06	0.12	0.92	0.92	0.00	0.03	0.26	0.12	0.62	132
All cases	0	All catchments	105	0.12	0.05	-0.07	0.14	0.91	0.91	0.00	0.05	0.27	0.09	0.64	136
All cases	0	All catchments	120	0.12	0.05	-0.07	0.13	0.90	0.90	0.00	0.04	0.27	0.20	0.53	126
All cases	1	Mimshall Brook	15	0.08	0.07	-0.01	0.08	0.46	0.46	0.00	0.01	0.23	0.29	0.48	142
All cases	1	Mimshall Brook	30	0.06	0.08	0.02	0.19	0.43	0.43	0.00	0.08	0.17	0.54	0.29	139
All cases	1	Mimshall Brook	45	0.07	0.08	0.00	0.20	0.53	0.53	0.00	0.08	0.17	0.36	0.47	139
All cases	1	Mimshall Brook	60	0.08	0.06	-0.02	0.19	0.46	0.46	0.00	0.06	0.15	0.22	0.62	138
All cases	1	Mimshall Brook	75	0.13	0.05	-0.07	0.37	0.47	0.47	0.00	0.33	0.17	0.21	0.62	141
All cases	1	Mimshall Brook	90	0.12	0.05	-0.08	0.32	0.46	0.46	0.00	0.30	0.18	0.24	0.58	132
All cases	1	Mimshall Brook	105	0.15	0.04	-0.10	0.40	0.44	0.44	0.00	0.40	0.21	0.15	0.65	136
All cases	1	Mimshall Brook	120	0.13	0.05	-0.09	0.37	0.44	0.44	0.00	0.34	0.25	0.14	0.61	126
All cases	2	Towncroft lane, Orlington	15	0.13	0.20	0.07	0.27	0.61	0.68	0.10	0.15	0.17	0.39	0.45	77
All cases	2	Towncroft lane, Orlington	30	0.15	0.19	0.04	0.46	0.56	0.67	0.22	0.39	0.12	0.51	0.37	84
All cases	2	Towncroft lane, Orlington	45	0.12	0.17	0.05	0.43	0.53	0.60	0.25	0.40	0.14	0.51	0.35	78
All cases	2	Towncroft lane, Orlington	60	0.14	0.13	-0.01	0.40	0.51	0.61	0.28	0.27	0.06	0.46	0.48	80
All cases	2	Towncroft lane, Orlington	75	0.12	0.13	0.00	0.35	0.46	0.57	0.32	0.20	0.06	0.42	0.52	82
All cases	2	Towncroft lane, Orlington	90	0.16	0.12	-0.04	0.38	0.48	0.60	0.31	0.22	0.10	0.40	0.50	85
All cases	2	Towncroft lane, Orlington	105	0.13	0.12	0.00	0.30	0.47	0.61	0.31	0.12	0.05	0.39	0.57	84
All cases	2	Towncroft lane, Orlington	120	0.16	0.13	-0.03	0.36	0.41	0.52	0.28	0.20	0.12	0.39	0.49	82
All cases	3	Elmers End Road	15	0.16	0.12	-0.04	0.32	0.53	0.53	0.00	0.23	0.10	0.15	0.75	142
All cases	3	Elmers End Road	30	0.14	0.12	-0.03	0.36	0.50	0.50	0.00	0.22	0.08	0.38	0.54	139
All cases	3	Elmers End Road	45	0.15	0.05	-0.10	0.47	0.47	0.47	0.00	0.65	0.09	0.16	0.75	139
All cases	3	Elmers End Road	60	0.13	0.05	-0.08	0.30	0.45	0.45	0.00	0.16	0.09	0.12	0.79	138
All cases	3	Elmers End Road	75	0.16	0.04	-0.11	0.51	0.51	0.51	0.00	0.67	0.06	0.20	0.73	141
All cases	3	Elmers End Road	90	0.15	0.05	-0.10	0.34	0.48	0.48	0.00	0.19	0.09	0.23	0.67	132
All cases	3	Elmers End Road	105	0.17	0.06	-0.11	0.45	0.40	0.40	0.00	0.47	0.12	0.40	0.48	136
All cases	3	Elmers End Road	120	0.16	0.06	-0.10	0.37	0.42	0.42	0.00	0.23	0.11	0.26	0.63	126
All cases	4	Longley Road Recorder	15	0.15	0.14	0.00	0.39	0.56	0.56	0.00	0.38	0.11	0.44	0.45	142
All cases	4	Longley Road Recorder	30	0.17	0.09	-0.08	0.32	0.53	0.53	0.00	0.22	0.12	0.38	0.50	139
All cases	4	Longley Road Recorder	45	0.13	0.04	-0.09	0.33	0.47	0.47	0.00	0.27	0.09	0.37	0.53	139
All cases	4	Longley Road Recorder	60	0.16	0.05	-0.12	0.47	0.47	0.47	0.00	0.51	0.08	0.24	0.69	138
All cases	4	Longley Road Recorder	75	0.13	0.05	-0.09	0.36	0.50	0.50	0.00	0.24	0.09	0.26	0.65	141
All cases	4	Longley Road Recorder	90	0.19	0.06	-0.14	0.45	0.47	0.47	0.00	0.45	0.13	0.29	0.59	132
All cases	4	Longley Road Recorder	105	0.15	0.07	-0.09	0.30	0.42	0.42	0.00	0.16	0.11	0.19	0.70	136
All cases	4	Longley Road Recorder	120	0.20	0.04	-0.16	0.52	0.42	0.42	0.00	0.61	0.13	0.21	0.66	126
All cases	5	West Barnes Lane	15	0.15	0.14	0.00	0.39	0.56	0.56	0.00	0.38	0.11	0.44	0.45	142
All cases	5	West Barnes Lane	30	0.17	0.09	-0.08	0.32	0.53	0.53	0.00	0.22	0.12	0.38	0.50	139
All cases	5	West Barnes Lane	45	0.13	0.04	-0.09	0.33	0.47	0.47	0.00	0.27	0.09	0.37	0.53	139
All cases	5	West Barnes Lane	60	0.16	0.05	-0.12	0.47	0.47	0.47	0.00	0.51	0.08	0.24	0.69	138
All cases	5	West Barnes Lane	75	0.13	0.05	-0.09	0.36	0.50	0.50	0.00	0.24	0.09	0.26	0.65	141

**Table B.2. Nimrod catchment resolution performance statistics contd.**

Date	Catch number	Catchment Name	Lead time min.	Observed depth / mm	Forecast depth / mm	F-O depth / mm	SD (F-O) depth / mm	CSI catchment	HR catchment	FAR catchment	MSE catchment	Up catchment	Ur catchment	Ud catchment	Runs
All cases	5	West Barnes Lane	90	0.19	0.06	-0.14	0.45	0.47	0.47	0.00	0.45	0.13	0.29	0.59	132
All cases	5	West Barnes Lane	105	0.15	0.07	-0.09	0.30	0.42	0.42	0.00	0.16	0.11	0.19	0.70	136
All cases	5	West Barnes Lane	120	0.20	0.04	-0.16	0.52	0.42	0.42	0.00	0.61	0.13	0.21	0.66	126
All cases	6	Wimbleton Common	15	0.24	0.11	-0.12	0.39	0.54	0.54	0.00	0.34	0.15	0.50	0.36	138
All cases	6	Wimbleton Common	30	0.25	0.05	-0.10	0.36	0.52	0.52	0.00	0.31	0.10	0.23	0.65	135
All cases	6	Wimbleton Common	45	0.13	0.04	-0.18	0.62	0.48	0.48	0.00	1.11	0.16	0.18	0.66	135
All cases	6	Wimbleton Common	60	0.16	0.05	-0.11	0.38	0.49	0.49	0.00	0.32	0.12	0.15	0.74	136
All cases	6	Wimbleton Common	75	0.26	0.06	-0.20	0.67	0.51	0.51	0.00	1.13	0.11	0.12	0.77	137
All cases	6	Wimbleton Common	90	0.17	0.06	-0.11	0.39	0.49	0.49	0.00	0.32	0.09	0.25	0.65	131
All cases	6	Wimbleton Common	105	0.26	0.05	-0.21	0.68	0.48	0.48	0.00	1.17	0.11	0.17	0.72	134
All cases	6	Wimbleton Common	120	0.18	0.02	-0.15	0.43	0.43	0.43	0.00	0.41	0.11	0.21	0.68	124
All cases	7	Yeading West	15	0.07	0.06	-0.01	0.11	0.47	0.48	0.02	0.02	#VALUE!	#VALUE!	#VALUE!	90
All cases	7	Yeading West	30	0.05	0.05	0.00	0.12	0.44	0.48	0.09	0.02	0.10	0.22	0.65	92
All cases	7	Yeading West	45	0.07	0.05	-0.01	0.15	0.47	0.50	0.13	0.04	0.07	0.42	0.40	93
All cases	7	Yeading West	60	0.08	0.04	-0.04	0.25	0.41	0.47	0.17	0.12	0.11	0.18	0.70	97
All cases	7	Yeading West	75	0.13	0.03	-0.10	0.44	0.37	0.40	0.18	0.50	#VALUE!	#VALUE!	#VALUE!	95
All cases	7	Yeading West	90	0.11	0.04	-0.07	0.31	0.35	0.40	0.19	0.21	0.14	0.27	0.59	93
All cases	7	Yeading West	105	0.13	0.04	-0.09	0.43	0.37	0.40	0.27	0.45	0.18	0.40	0.42	95
All cases	7	Yeading West	120	0.12	0.04	-0.08	0.33	0.34	0.39	0.29	0.20	0.14	0.33	0.53	97
All cases	8	Yeading East	15	0.09	0.06	-0.03	0.20	0.49	0.49	0.00	0.07	0.05	0.41	0.49	89
All cases	8	Yeading East	30	0.07	0.05	-0.01	0.18	0.42	0.45	0.08	0.06	0.11	0.34	0.46	87
All cases	8	Yeading East	45	0.08	0.06	-0.02	0.21	0.46	0.49	0.09	0.09	0.09	0.20	0.60	93
All cases	8	Yeading East	60	0.07	0.05	-0.02	0.22	0.37	0.43	0.26	0.08	0.10	0.28	0.62	92
All cases	8	Yeading East	75	0.13	0.04	-0.09	0.44	0.39	0.42	0.11	0.42	0.07	0.32	0.52	93
All cases	8	Yeading East	90	0.10	0.04	-0.06	0.28	0.35	0.40	0.16	0.14	0.13	0.28	0.50	86
All cases	8	Yeading East	105	0.14	0.04	-0.10	0.45	0.35	0.38	0.24	0.44	0.14	0.37	0.49	96
All cases	8	Yeading East	120	0.11	0.04	-0.07	0.28	0.43	0.47	0.20	0.14	0.17	0.30	0.52	85
All cases	9	Colindeep Lane	15	0.06	0.05	-0.01	0.06	0.37	0.37	0.00	0.01	0.18	0.39	0.43	142
All cases	9	Colindeep Lane	30	0.08	0.05	-0.03	0.21	0.33	0.33	0.00	0.08	0.17	0.40	0.43	139
All cases	9	Colindeep Lane	45	0.05	0.05	0.00	0.15	0.35	0.35	0.00	0.05	0.18	0.31	0.51	139
All cases	9	Colindeep Lane	60	0.10	0.04	-0.05	0.26	0.41	0.41	0.00	0.12	0.20	0.31	0.49	138
All cases	9	Colindeep Lane	75	0.07	0.03	-0.04	0.16	0.35	0.35	0.00	0.06	0.17	0.15	0.68	141
All cases	9	Colindeep Lane	90	0.12	0.03	-0.08	0.30	0.37	0.37	0.00	0.18	0.19	0.24	0.57	132
All cases	9	Colindeep Lane	105	0.08	0.03	-0.05	0.19	0.38	0.38	0.00	0.08	0.14	0.28	0.58	136
All cases	9	Colindeep Lane	120	0.13	0.03	-0.09	0.31	0.38	0.38	0.00	0.19	0.22	0.22	0.56	126
All cases	10	Chipping Ongar	15	0.18	0.11	-0.07	0.25	0.61	0.62	0.08	0.14	0.11	0.44	0.41	83
All cases	10	Chipping Ongar	30	0.11	0.09	-0.02	0.17	0.57	0.61	0.09	0.04	0.10	0.39	0.46	82
All cases	10	Chipping Ongar	45	0.18	0.08	-0.10	0.40	0.61	0.66	0.10	0.36	0.11	0.28	0.61	84
All cases	10	Chipping Ongar	60	0.10	0.09	-0.01	0.16	0.56	0.64	0.15	0.04	0.08	0.32	0.57	83
All cases	10	Chipping Ongar	75	0.17	0.07	-0.10	0.39	0.53	0.61	0.22	0.44	0.09	0.31	0.59	87
All cases	10	Chipping Ongar	90	0.09	0.09	0.00	0.16	0.58	0.67	0.19	0.04	0.17	0.50	0.33	85
All cases	10	Chipping Ongar	105	0.15	0.09	-0.06	0.41	0.54	0.65	0.24	0.39	0.12	0.44	0.44	89
All cases	10	Chipping Ongar	120	0.09	0.08	-0.01	0.22	0.44	0.53	0.24	0.07	0.14	0.31	0.55	84
All cases	11	Sewardstone Road	15	0.12	0.08	-0.04	0.11	0.62	0.65	0.07	0.02	0.17	0.26	0.57	89
All cases	11	Sewardstone Road	30	0.09	0.07	-0.02	0.15	0.58	0.63	0.10	0.03	0.12	0.35	0.53	89

**Table B.2. Nimrod catchment resolution performance statistics contd.**

Date	Catch number	Catchment Name	Lead time min.	Observed depth / mm	Forecast depth / mm	F-O depth / mm	SD (F-O) depth / mm	CSI catchment	HR catchment	FAR catchment	MSE catchment	Ub catchment	Ur catchment	Ud catchment	Runs Nimrod
All cases	11	Sewardstone Road	45	0.11	0.08	-0.03	0.17	0.56	0.63	0.18	0.04	0.09	0.25	0.66	96
All cases	11	Sewardstone Road	80	0.08	0.08	0.00	0.21	0.59	0.66	0.19	0.06	0.05	0.47	0.48	96
All cases	11	Sewardstone Road	75	0.10	0.09	-0.01	0.24	0.56	0.63	0.19	0.08	0.10	0.40	0.50	93
All cases	11	Sewardstone Road	90	0.09	0.09	0.00	0.22	0.54	0.62	0.17	0.07	0.11	0.42	0.47	90
All cases	11	Sewardstone Road	105	0.11	0.07	-0.04	0.22	0.58	0.67	0.19	0.07	0.12	0.39	0.50	96
All cases	11	Sewardstone Road	120	0.10	0.06	-0.05	0.22	0.55	0.64	0.17	0.06	0.09	0.27	0.64	90
All cases	12	Luton Hoo	15	0.15	0.11	-0.05	0.25	0.57	0.58	0.03	0.12	0.05	0.43	0.50	103
All cases	12	Luton Hoo	30	0.13	0.11	-0.02	0.18	0.66	0.69	0.03	0.04	0.09	0.15	0.76	89
All cases	12	Luton Hoo	45	0.08	0.07	-0.02	0.13	0.59	0.60	0.01	0.02	0.09	0.42	0.47	98
All cases	12	Luton Hoo	60	0.10	0.06	-0.04	0.17	0.49	0.50	0.05	0.05	0.22	0.16	0.62	88
All cases	12	Luton Hoo	75	0.08	0.04	-0.04	0.14	0.45	0.46	0.03	0.03	0.16	0.20	0.64	101
All cases	12	Luton Hoo	90	0.14	0.05	-0.09	0.31	0.46	0.49	0.13	0.15	0.16	0.19	0.65	87
All cases	12	Luton Hoo	105	0.14	0.04	-0.10	0.43	0.39	0.41	0.15	0.41	0.15	0.18	0.67	101
All cases	12	Luton Hoo	120	0.17	0.04	-0.13	0.36	0.46	0.48	0.11	0.20	0.19	0.10	0.69	83
All cases	13	Gypsy Lane	15	0.27	0.18	-0.08	0.22	0.73	0.75	0.05	0.08	0.14	0.26	0.59	82
All cases	13	Gypsy Lane	30	0.33	0.16	-0.17	0.58	0.64	0.68	0.07	0.58	0.15	0.23	0.60	82
All cases	13	Gypsy Lane	45	0.28	0.17	-0.11	0.43	0.68	0.69	0.05	0.27	0.14	0.32	0.54	79
All cases	13	Gypsy Lane	60	0.33	0.17	-0.16	0.66	0.53	0.57	0.07	0.75	0.15	0.15	0.69	82
All cases	13	Gypsy Lane	75	0.29	0.18	-0.11	0.53	0.58	0.62	0.11	0.46	0.12	0.33	0.55	81
All cases	13	Gypsy Lane	90	0.33	0.21	-0.12	0.77	0.52	0.59	0.14	1.00	0.14	0.25	0.60	83
All cases	13	Gypsy Lane	105	0.26	0.16	-0.10	0.49	0.54	0.62	0.19	0.40	0.14	0.35	0.51	84
All cases	13	Gypsy Lane	120	0.32	0.13	-0.19	0.68	0.52	0.63	0.22	0.76	0.21	0.10	0.67	83
All cases	14	Albany Park	15	0.10	0.10	0.00	0.08	0.59	0.61	0.05	0.01	0.15	0.24	0.59	89
All cases	14	Albany Park	30	0.08	0.09	0.01	0.19	0.58	0.58	0.00	0.06	0.15	0.44	0.41	94
All cases	14	Albany Park	45	0.07	0.11	0.04	0.26	0.60	0.66	0.12	0.13	0.10	0.54	0.31	92
All cases	14	Albany Park	60	0.08	0.09	0.01	0.22	0.55	0.57	0.05	0.10	0.19	0.41	0.40	99
All cases	14	Albany Park	75	0.08	0.08	0.00	0.18	0.52	0.57	0.24	0.05	0.11	0.38	0.51	93
All cases	14	Albany Park	90	0.11	0.06	-0.05	0.25	0.54	0.56	0.13	0.12	0.12	0.26	0.62	98
All cases	14	Albany Park	105	0.10	0.06	-0.04	0.21	0.52	0.58	0.20	0.08	0.16	0.24	0.60	94
All cases	14	Albany Park	120	0.12	0.06	-0.05	0.29	0.50	0.52	0.13	0.15	0.13	0.31	0.56	96
All cases	15	Edmonton Green	15	0.11	0.09	-0.02	0.12	0.57	0.60	0.06	0.02	0.19	0.48	0.29	85
All cases	15	Edmonton Green	30	0.08	0.09	0.00	0.21	0.56	0.63	0.14	0.07	0.08	0.32	0.60	87
All cases	15	Edmonton Green	45	0.10	0.09	-0.01	0.25	0.51	0.55	0.15	0.10	0.10	0.37	0.50	85
All cases	15	Edmonton Green	60	0.08	0.07	-0.01	0.23	0.51	0.57	0.19	0.08	0.11	0.40	0.49	85
All cases	15	Edmonton Green	75	0.09	0.05	-0.04	0.17	0.45	0.52	0.32	0.05	0.11	0.14	0.75	95
All cases	15	Edmonton Green	90	0.09	0.05	-0.04	0.19	0.48	0.56	0.22	0.05	0.12	0.28	0.60	91
All cases	15	Edmonton Green	105	0.10	0.05	-0.05	0.20	0.46	0.52	0.31	0.07	0.15	0.31	0.54	93
All cases	15	Edmonton Green	120	0.10	0.07	-0.03	0.24	0.43	0.49	0.28	0.08	0.11	0.42	0.47	88
All cases	16	Silver Street	15	0.08	0.07	-0.01	0.10	0.60	0.60	0.01	0.02	0.12	0.57	0.30	123
All cases	16	Silver Street	30	0.07	0.06	0.00	0.17	0.63	0.63	0.00	0.05	0.04	0.32	0.65	117
All cases	16	Silver Street	45	0.08	0.06	-0.02	0.18	0.56	0.56	0.06	0.06	0.10	0.44	0.47	124
All cases	16	Silver Street	60	0.06	0.05	-0.01	0.18	0.53	0.54	0.10	0.05	0.09	0.26	0.65	119
All cases	16	Silver Street	75	0.08	0.04	-0.04	0.16	0.53	0.53	0.11	0.04	0.12	0.27	0.61	123
All cases	16	Silver Street	90	0.07	0.04	-0.03	0.16	0.53	0.55	0.10	0.04	0.09	0.40	0.51	118
All cases	16	Silver Street	105	0.09	0.04	-0.05	0.19	0.51	0.51	0.15	0.06	0.12	0.27	0.61	121

**Table B.2. Nimrod catchment resolution performance statistics contd.**

Date	Catch number	Catchment Name	Lead time min.	Observed depth / mm	Forecast depth / mm	F-O depth / mm	SD (F-O) depth / mm	CSI catchment	HR catchment	FAR catchment	MSE catchment	Ub catchment	Ur catchment	Ud catchment	Runs Nimrod
All cases	16	Silver Street	120	0.08	0.05	-0.03	0.20	0.48	0.48	0.15	0.05	0.07	0.38	0.55	111
All cases	17	Bretons Farm	15	0.08	0.05	-0.03	0.12	0.47	0.48	0.05	0.02	0.12	0.48	0.41	142
All cases	17	Bretons Farm	30	0.07	0.04	-0.03	0.17	0.55	0.55	0.02	0.05	0.09	0.22	0.69	136
All cases	17	Bretons Farm	45	0.08	0.04	-0.04	0.22	0.56	0.57	0.01	0.08	0.10	0.17	0.73	139
All cases	17	Bretons Farm	60	0.07	0.04	-0.03	0.19	0.55	0.55	0.05	0.06	0.08	0.30	0.62	136
All cases	17	Bretons Farm	75	0.08	0.04	-0.04	0.23	0.49	0.49	0.04	0.09	0.08	0.25	0.66	141
All cases	17	Bretons Farm	90	0.06	0.04	-0.02	0.17	0.50	0.50	0.08	0.04	0.09	0.24	0.67	131
All cases	17	Bretons Farm	105	0.08	0.04	-0.04	0.24	0.51	0.51	0.02	0.10	0.12	0.16	0.72	136
All cases	17	Bretons Farm	120	0.07	0.05	-0.03	0.22	0.54	0.54	0.09	0.07	0.08	0.27	0.65	125
All cases	18	Gaynes Park	15	0.15	0.09	-0.06	0.22	0.49	0.49	0.04	0.07	0.12	0.29	0.59	120
All cases	18	Gaynes Park	30	0.13	0.06	-0.07	0.26	0.48	0.50	0.06	0.09	0.12	0.26	0.62	118
All cases	18	Gaynes Park	45	0.15	0.05	-0.10	0.31	0.56	0.57	0.02	0.14	0.14	0.14	0.72	120
All cases	18	Gaynes Park	60	0.14	0.05	-0.09	0.35	0.49	0.50	0.02	0.17	0.13	0.06	0.81	116
All cases	18	Gaynes Park	75	0.14	0.05	-0.10	0.31	0.52	0.53	0.05	0.15	0.14	0.13	0.73	122
All cases	18	Gaynes Park	90	0.13	0.05	-0.08	0.32	0.49	0.50	0.18	0.15	0.09	0.15	0.77	113
All cases	18	Gaynes Park	105	0.13	0.05	-0.09	0.30	0.49	0.50	0.07	0.14	0.14	0.09	0.77	118
All cases	18	Gaynes Park	120	0.14	0.05	-0.09	0.35	0.56	0.59	0.08	0.17	0.12	0.09	0.78	112
All cases	19	Bromley South Recorder	15	0.22	0.13	-0.09	0.31	0.37	0.37	0.00	0.21	0.23	0.23	0.54	142
All cases	19	Bromley South Recorder	30	0.25	0.13	-0.12	0.53	0.40	0.40	0.00	0.55	0.11	0.37	0.52	139
All cases	19	Bromley South Recorder	45	0.21	0.10	-0.11	0.42	0.37	0.37	0.00	0.41	0.14	0.50	0.36	139
All cases	19	Bromley South Recorder	60	0.22	0.07	-0.15	0.36	0.33	0.33	0.00	0.30	0.18	0.13	0.69	138
All cases	19	Bromley South Recorder	75	0.21	0.07	-0.14	0.31	0.37	0.37	0.00	0.23	0.13	0.24	0.63	141
All cases	19	Bromley South Recorder	90	0.25	0.07	-0.17	0.42	0.42	0.42	0.00	0.35	0.13	0.25	0.62	132
All cases	19	Bromley South Recorder	105	0.20	0.07	-0.13	0.31	0.39	0.39	0.00	0.19	0.23	0.20	0.57	136
All cases	19	Bromley South Recorder	120	0.24	0.09	-0.15	0.41	0.37	0.37	0.00	0.30	0.17	0.29	0.54	126

**Table B.3. OOM 2 km resolution performance statistics**

Date	Catch number	Catchment Name	Lead time min.	CSI 2km pixel	SD CSI 2km pixel	HR 2km pixel	SD HR 2km pixel	FAR 2km pixel	SD FAR 2km pixel	MSE mm <sup>2</sup>	SD MSE mm <sup>2</sup>	Ub 2km pixel	SD Ub 2km pixel	Ur 2km pixel	SD Ur 2km pixel	Ud 2km pixel	SD Ud 2km pixel	Runs
All cases	0	All catchments	15	0.29	0.24	0.21	0.19	0.15	0.15	0.42	0.97	0.12	0.11	0.27	0.25	0.60	0.28	142
All cases	0	All catchments	30	0.24	0.22	0.18	0.18	0.17	0.16	0.40	0.69	0.14	0.12	0.33	0.26	0.53	0.31	139
All cases	0	All catchments	45	0.16	0.16	0.13	0.14	0.20	0.19	0.57	1.15	0.13	0.11	0.35	0.27	0.52	0.30	139
All cases	0	All catchments	60	0.13	0.15	0.12	0.13	0.21	0.19	0.49	0.73	0.14	0.13	0.35	0.24	0.51	0.30	138
All cases	0	All catchments	75	0.10	0.12	0.09	0.10	0.21	0.23	0.69	1.35	0.14	0.12	0.33	0.24	0.52	0.28	141
All cases	0	All catchments	90	0.10	0.11	0.09	0.10	0.38	0.34	0.71	1.08	0.20	0.16	0.31	0.29	0.48	0.27	132
All cases	0	All catchments	105	0.09	0.10	0.08	0.09	0.30	0.33	0.84	1.59	0.20	0.16	0.28	0.28	0.52	0.23	136
All cases	0	All catchments	120	0.08	0.10	0.07	0.09	0.33	0.32	0.65	0.97	0.20	0.17	0.23	0.23	0.56	0.25	126
All cases	1	Mimshall Brook	15	0.15	0.24	0.12	0.22	0.07	0.14	0.09	0.23	0.40	0.25	0.24	0.24	0.37	0.24	142
All cases	1	Mimshall Brook	30	0.11	0.21	0.10	0.20	0.09	0.15	0.21	0.92	0.42	0.28	0.30	0.28	0.28	0.22	139
All cases	1	Mimshall Brook	45	0.10	0.20	0.08	0.18	0.13	0.22	0.33	0.83	0.40	0.25	0.30	0.27	0.30	0.23	139
All cases	1	Mimshall Brook	60	0.07	0.15	0.07	0.15	0.16	0.23	0.34	0.92	0.46	0.27	0.23	0.26	0.31	0.24	138
All cases	1	Mimshall Brook	75	0.04	0.12	0.04	0.12	0.13	0.23	0.69	3.50	0.49	0.25	0.18	0.25	0.32	0.24	141
All cases	1	Mimshall Brook	90	0.04	0.12	0.04	0.12	0.14	0.24	0.66	2.97	0.55	0.18	0.14	0.22	0.32	0.18	132
All cases	1	Mimshall Brook	105	0.03	0.10	0.04	0.11	0.12	0.24	0.78	3.61	0.55	0.17	0.12	0.20	0.33	0.18	136
All cases	1	Mimshall Brook	120	0.02	0.07	0.02	0.07	0.12	0.23	0.69	3.04	0.55	0.17	0.10	0.18	0.35	0.17	126
All cases	2	Towncroft lane, Orpington	15	0.18	0.30	0.17	0.29	0.11	0.21	0.33	0.71	0.65	0.34	0.12	0.21	0.16	0.26	102
All cases	2	Towncroft lane, Orpington	30	0.14	0.28	0.14	0.29	0.14	0.25	0.86	3.51	0.68	0.37	0.08	0.17	0.11	0.21	116
All cases	2	Towncroft lane, Orpington	45	0.11	0.23	0.11	0.23	0.18	0.32	0.47	1.44	0.71	0.32	0.12	0.19	0.12	0.20	109
All cases	2	Towncroft lane, Orpington	60	0.10	0.21	0.11	0.22	0.17	0.28	0.34	0.84	0.65	0.34	0.16	0.25	0.12	0.20	106
All cases	2	Towncroft lane, Orpington	75	0.10	0.21	0.10	0.19	0.16	0.32	0.25	0.61	0.67	0.33	0.11	0.21	0.14	0.23	98
All cases	2	Towncroft lane, Orpington	90	0.10	0.21	0.10	0.21	0.15	0.31	0.36	0.84	0.59	0.36	0.09	0.18	0.12	0.18	73
All cases	2	Towncroft lane, Orpington	105	0.09	0.19	0.09	0.19	0.12	0.24	0.25	0.52	0.60	0.33	0.09	0.17	0.18	0.21	73
All cases	2	Towncroft lane, Orpington	120	0.11	0.19	0.12	0.20	0.19	0.29	0.66	1.49	0.66	0.34	0.06	0.15	0.09	0.13	69
All cases	3	Elmers End Road	15	0.13	0.28	0.13	0.27	0.13	0.27	1.06	4.19	0.48	0.34	0.19	0.24	0.28	0.27	142
All cases	3	Elmers End Road	30	0.15	0.28	0.14	0.27	0.14	0.27	0.23	0.73	0.46	0.33	0.23	0.30	0.25	0.27	139
All cases	3	Elmers End Road	45	0.09	0.18	0.09	0.18	0.15	0.29	0.94	4.55	0.45	0.35	0.20	0.28	0.21	0.25	139
All cases	3	Elmers End Road	60	0.08	0.19	0.07	0.19	0.13	0.28	0.23	0.66	0.45	0.34	0.18	0.28	0.20	0.24	138
All cases	3	Elmers End Road	75	0.05	0.12	0.04	0.11	0.07	0.17	1.13	6.05	0.47	0.33	0.12	0.24	0.23	0.24	141
All cases	3	Elmers End Road	90	0.05	0.14	0.06	0.14	0.11	0.26	0.40	1.14	0.47	0.34	0.08	0.18	0.19	0.20	132
All cases	3	Elmers End Road	105	0.06	0.13	0.07	0.13	0.09	0.21	1.45	5.46	0.50	0.32	0.06	0.15	0.16	0.16	136
All cases	3	Elmers End Road	120	0.06	0.13	0.06	0.13	0.09	0.18	0.48	1.53	0.46	0.33	0.06	0.15	0.20	0.20	126
All cases	4	Longley Road Recorder	15	0.15	0.28	0.14	0.29	0.14	0.26	0.56	2.16	0.42	0.32	0.19	0.22	0.35	0.30	142
All cases	4	Longley Road Recorder	30	0.14	0.26	0.14	0.27	0.13	0.24	0.39	1.29	0.39	0.32	0.27	0.30	0.29	0.31	139
All cases	4	Longley Road Recorder	45	0.08	0.18	0.09	0.18	0.16	0.28	0.61	2.64	0.39	0.30	0.26	0.29	0.28	0.28	138
All cases	4	Longley Road Recorder	60	0.07	0.18	0.08	0.20	0.15	0.28	0.71	2.73	0.42	0.30	0.21	0.25	0.26	0.28	139
All cases	4	Longley Road Recorder	75	0.06	0.14	0.06	0.12	0.12	0.25	0.77	3.34	0.43	0.29	0.20	0.28	0.26	0.28	141
All cases	4	Longley Road Recorder	90	0.06	0.13	0.06	0.13	0.12	0.29	0.79	2.42	0.43	0.33	0.11	0.20	0.23	0.23	132
All cases	4	Longley Road Recorder	105	0.06	0.13	0.06	0.12	0.13	0.27	0.92	3.19	0.44	0.33	0.09	0.18	0.21	0.22	136
All cases	4	Longley Road Recorder	120	0.05	0.13	0.05	0.13	0.10	0.18	0.77	2.50	0.41	0.31	0.09	0.17	0.24	0.30	142
All cases	5	West Barnes Lane	15	0.15	0.28	0.14	0.29	0.14	0.26	0.56	2.16	0.42	0.32	0.19	0.22	0.35	0.30	126
All cases	5	West Barnes Lane	30	0.14	0.26	0.14	0.27	0.13	0.24	0.39	1.29	0.39	0.32	0.27	0.30	0.29	0.31	139
All cases	5	West Barnes Lane	45	0.08	0.18	0.09	0.18	0.16	0.28	0.61	2.64	0.39	0.30	0.26	0.29	0.26	0.25	139
All cases	5	West Barnes Lane	60	0.07	0.18	0.08	0.20	0.15	0.28	0.71	2.73	0.42	0.30	0.21	0.25	0.28	0.28	138
All cases	5	West Barnes Lane	75	0.06	0.14	0.06	0.12	0.12	0.25	0.77	3.34	0.43	0.29	0.20	0.28	0.26	0.28	141



**Table B.3. OOM 2 km resolution performance statistics contd.**

Date	Catch number	Catchment Name	Lead time min.	CSI 2km pixel	SD CSI 2km pixel	HR 2km pixel	SD HR 2km pixel	FAR 2km pixel	SD FAR 2km pixel	MSE mm <sup>2</sup>	SD MSE mm <sup>2</sup>	Ub 2km pixel	SD Ub 2km pixel	U <sub>r</sub> 2km pixel	SD U <sub>r</sub> 2km pixel	Ud 2km pixel	SD Ud 2km pixel	Runs OOM
All cases	5	West Barnes Lane	90	0.06	0.13	0.06	0.13	0.12	0.29	0.79	2.42	0.43	0.33	0.11	0.20	0.23	0.23	132
All cases	5	West Barnes Lane	105	0.06	0.13	0.06	0.12	0.13	0.27	0.92	3.19	0.44	0.33	0.09	0.18	0.21	0.22	136
All cases	5	West Barnes Lane	120	0.05	0.13	0.05	0.13	0.10	0.18	0.77	2.50	0.41	0.31	0.09	0.17	0.24	0.23	126
All cases	6	Wimbleton Common	15	0.16	0.25	0.14	0.24	0.12	0.23	0.82	2.91	0.40	0.30	0.26	0.27	0.31	0.28	141
All cases	6	Wimbleton Common	30	0.12	0.23	0.11	0.22	0.12	0.21	0.64	2.80	0.43	0.30	0.29	0.30	0.25	0.24	137
All cases	6	Wimbleton Common	45	0.09	0.19	0.09	0.18	0.14	0.27	1.66	6.33	0.43	0.29	0.29	0.28	0.26	0.24	137
All cases	6	Wimbleton Common	60	0.08	0.17	0.08	0.17	0.14	0.25	0.70	2.59	0.43	0.30	0.28	0.29	0.26	0.23	137
All cases	6	Wimbleton Common	75	0.07	0.17	0.07	0.15	0.09	0.23	1.45	4.49	0.49	0.30	0.18	0.26	0.30	0.24	139
All cases	6	Wimbleton Common	90	0.08	0.16	0.07	0.15	0.13	0.30	0.87	2.51	0.58	0.24	0.12	0.22	0.26	0.21	131
All cases	6	Wimbleton Common	105	0.06	0.12	0.06	0.12	0.10	0.22	1.49	4.08	0.59	0.24	0.11	0.19	0.27	0.19	134
All cases	6	Wimbleton Common	120	0.05	0.11	0.05	0.10	0.09	0.19	0.94	3.31	0.57	0.25	0.10	0.18	0.30	0.21	124
All cases	7	Yeading West	15	0.10	0.22	0.09	0.21	0.12	0.23	0.08	0.31	0.49	0.34	0.22	0.25	0.15	0.24	112
All cases	7	Yeading West	30	0.07	0.17	0.06	0.15	0.13	0.23	0.16	0.32	0.55	0.35	0.23	0.23	0.10	0.20	114
All cases	7	Yeading West	45	0.06	0.14	0.06	0.15	0.15	0.22	0.15	0.36	0.59	0.32	0.23	0.23	0.13	0.23	115
All cases	7	Yeading West	60	0.05	0.15	0.05	0.13	0.14	0.23	0.28	0.94	0.63	0.34	0.20	0.22	0.13	0.23	111
All cases	7	Yeading West	75	0.04	0.12	0.03	0.10	0.12	0.24	0.68	3.04	0.62	0.33	0.12	0.20	0.14	0.21	104
All cases	7	Yeading West	90	0.04	0.12	0.04	0.12	0.17	0.29	0.46	1.28	0.47	0.36	0.09	0.16	0.18	0.21	92
All cases	7	Yeading West	105	0.05	0.12	0.04	0.12	0.13	0.26	0.74	3.34	0.47	0.34	0.11	0.20	0.18	0.21	91
All cases	7	Yeading West	120	0.04	0.12	0.03	0.11	0.11	0.22	0.44	1.31	0.39	0.33	0.13	0.22	0.19	0.23	86
All cases	8	Yeading East	15	0.10	0.23	0.09	0.22	0.14	0.29	0.10	0.41	0.44	0.35	0.14	0.20	0.17	0.24	102
All cases	8	Yeading East	30	0.07	0.17	0.07	0.17	0.13	0.25	0.13	0.36	0.56	0.36	0.17	0.24	0.08	0.18	112
All cases	8	Yeading East	45	0.05	0.13	0.05	0.13	0.14	0.25	0.21	0.65	0.56	0.33	0.17	0.23	0.11	0.20	113
All cases	8	Yeading East	60	0.06	0.18	0.06	0.18	0.13	0.25	0.19	0.52	0.62	0.36	0.12	0.20	0.11	0.19	104
All cases	8	Yeading East	75	0.06	0.18	0.06	0.17	0.12	0.24	0.57	2.25	0.58	0.36	0.08	0.16	0.14	0.21	99
All cases	8	Yeading East	90	0.05	0.15	0.05	0.14	0.15	0.29	0.27	2.45	0.47	0.36	0.06	0.11	0.13	0.19	85
All cases	8	Yeading East	105	0.04	0.12	0.04	0.13	0.08	0.17	0.65	2.49	0.44	0.36	0.07	0.14	0.13	0.20	86
All cases	8	Yeading East	120	0.04	0.12	0.04	0.12	0.10	0.24	0.32	0.92	0.44	0.39	0.07	0.17	0.13	0.19	80
All cases	9	Collindale Lane	15	0.09	0.21	0.08	0.19	0.06	0.17	0.06	0.22	0.50	0.31	0.23	0.28	0.28	0.23	142
All cases	9	Collindale Lane	30	0.08	0.20	0.07	0.18	0.08	0.16	0.17	0.42	0.46	0.32	0.30	0.31	0.24	0.20	139
All cases	9	Collindale Lane	45	0.07	0.16	0.07	0.15	0.14	0.22	0.16	0.35	0.49	0.31	0.28	0.28	0.23	0.23	139
All cases	9	Collindale Lane	60	0.07	0.15	0.06	0.15	0.13	0.22	0.23	0.78	0.52	0.29	0.25	0.28	0.24	0.21	138
All cases	9	Collindale Lane	75	0.05	0.14	0.04	0.13	0.08	0.18	0.12	0.37	0.59	0.27	0.18	0.25	0.23	0.20	141
All cases	9	Collindale Lane	90	0.06	0.15	0.05	0.13	0.14	0.25	0.29	0.88	0.66	0.22	0.13	0.20	0.21	0.16	132
All cases	9	Collindale Lane	105	0.03	0.10	0.03	0.11	0.08	0.18	0.15	0.37	0.69	0.22	0.08	0.16	0.22	0.17	126
All cases	9	Collindale Lane	120	0.03	0.10	0.03	0.10	0.08	0.14	0.33	0.99	0.66	0.22	0.13	0.20	0.23	0.17	100
All cases	10	Chipping Ongar	15	0.17	0.28	0.15	0.25	0.12	0.24	0.36	1.03	0.45	0.34	0.22	0.24	0.23	0.23	110
All cases	10	Chipping Ongar	30	0.14	0.22	0.13	0.20	0.13	0.20	0.19	0.46	0.52	0.31	0.22	0.24	0.18	0.23	100
All cases	10	Chipping Ongar	45	0.08	0.17	0.09	0.17	0.13	0.25	0.62	1.72	0.55	0.30	0.20	0.25	0.17	0.21	115
All cases	10	Chipping Ongar	60	0.07	0.14	0.07	0.15	0.16	0.26	0.48	1.14	0.56	0.32	0.22	0.25	0.16	0.20	118
All cases	10	Chipping Ongar	75	0.06	0.14	0.07	0.14	0.21	0.32	0.99	2.94	0.59	0.34	0.15	0.20	0.20	0.25	110
All cases	10	Chipping Ongar	90	0.07	0.15	0.08	0.16	0.32	0.37	0.42	0.88	0.50	0.27	0.18	0.21	0.23	0.23	84
All cases	10	Chipping Ongar	105	0.06	0.15	0.07	0.15	0.26	0.34	0.81	2.33	0.50	0.31	0.16	0.21	0.23	0.23	91
All cases	10	Chipping Ongar	120	0.06	0.13	0.06	0.14	0.29	0.33	0.41	0.73	0.52	0.26	0.15	0.20	0.26	0.23	78
All cases	11	Sewardstone Road	15	0.14	0.25	0.13	0.23	0.10	0.19	0.18	0.43	0.52	0.33	0.18	0.22	0.19	0.24	115
All cases	11	Sewardstone Road	30	0.15	0.22	0.14	0.21	0.13	0.26	0.20	0.51	0.53	0.33	0.21	0.25	0.14	0.20	112

**Table B.3. OOM 2 km resolution performance statistics contd.**

Date	Catch number	Catchment Name	Lead time min.	CSI 2km pixel	SD CSI 2km pixel	HR 2km pixel	SD HR 2km pixel	FAR 2km pixel	SD FAR 2km pixel	MSE mm <sup>2</sup>	SD MSE mm <sup>2</sup>	Ub 2km pixel	SD Ub 2km pixel	U 2km pixel	SD U 2km pixel	Ud 2km pixel	SD Ud 2km pixel	Runs OOM
All cases	11	Sewardstone Road	45	0.09	0.16	0.08	0.16	0.14	0.23	0.35	0.74	0.59	0.33	0.20	0.22	0.15	0.22	121
All cases	11	Sewardstone Road	60	0.08	0.16	0.09	0.16	0.17	0.25	0.44	1.39	0.55	0.33	0.21	0.23	0.16	0.22	119
All cases	11	Sewardstone Road	75	0.07	0.17	0.07	0.15	0.23	0.32	0.68	2.35	0.57	0.34	0.19	0.23	0.16	0.22	112
All cases	11	Sewardstone Road	90	0.07	0.15	0.07	0.16	0.27	0.37	0.46	1.27	0.48	0.30	0.16	0.20	0.21	0.25	91
All cases	11	Sewardstone Road	105	0.06	0.12	0.06	0.12	0.24	0.34	0.43	0.75	0.48	0.33	0.15	0.22	0.22	0.25	92
All cases	11	Sewardstone Road	120	0.07	0.14	0.08	0.16	0.23	0.33	0.28	0.60	0.50	0.30	0.13	0.17	0.25	0.23	84
All cases	12	Luton Hoo	15	0.16	0.23	0.15	0.22	0.16	0.23	0.28	0.96	0.45	0.35	0.22	0.23	0.25	0.30	121
All cases	12	Luton Hoo	30	0.14	0.20	0.14	0.21	0.18	0.27	0.27	0.60	0.47	0.32	0.23	0.24	0.22	0.27	113
All cases	12	Luton Hoo	45	0.09	0.19	0.09	0.20	0.17	0.27	0.17	0.36	0.49	0.30	0.18	0.20	0.25	0.28	114
All cases	12	Luton Hoo	60	0.11	0.20	0.11	0.21	0.16	0.26	0.27	0.61	0.45	0.32	0.21	0.24	0.23	0.27	105
All cases	12	Luton Hoo	75	0.08	0.15	0.08	0.16	0.14	0.25	0.19	0.39	0.48	0.32	0.17	0.22	0.26	0.27	108
All cases	12	Luton Hoo	90	0.08	0.16	0.08	0.15	0.21	0.31	0.68	1.96	0.45	0.31	0.15	0.23	0.27	0.26	88
All cases	12	Luton Hoo	105	0.07	0.15	0.08	0.15	0.17	0.27	0.97	3.88	0.44	0.29	0.12	0.19	0.25	0.24	100
All cases	12	Luton Hoo	120	0.06	0.15	0.07	0.16	0.22	0.31	0.80	2.08	0.45	0.28	0.15	0.21	0.28	0.27	84
All cases	13	Gypsy Lane	15	0.23	0.31	0.23	0.31	0.13	0.25	0.64	1.41	0.45	0.28	0.16	0.20	0.27	0.27	85
All cases	13	Gypsy Lane	30	0.25	0.32	0.24	0.32	0.10	0.21	1.09	2.81	0.46	0.28	0.14	0.20	0.31	0.26	83
All cases	13	Gypsy Lane	45	0.13	0.23	0.13	0.23	0.13	0.21	0.77	1.93	0.52	0.34	0.11	0.16	0.22	0.23	93
All cases	13	Gypsy Lane	60	0.14	0.20	0.14	0.19	0.12	0.22	1.06	3.17	0.54	0.32	0.16	0.22	0.25	0.24	98
All cases	13	Gypsy Lane	75	0.14	0.20	0.14	0.20	0.21	0.33	1.22	2.84	0.51	0.30	0.16	0.22	0.23	0.23	87
All cases	13	Gypsy Lane	90	0.14	0.20	0.14	0.20	0.20	0.32	1.50	4.68	0.54	0.28	0.14	0.19	0.27	0.27	82
All cases	13	Gypsy Lane	105	0.11	0.17	0.10	0.17	0.15	0.26	0.90	1.81	0.49	0.33	0.13	0.20	0.25	0.27	84
All cases	13	Gypsy Lane	120	0.10	0.16	0.10	0.17	0.15	0.26	1.37	5.01	0.50	0.28	0.13	0.18	0.27	0.24	80
All cases	14	Albany Park	15	0.15	0.24	0.14	0.24	0.13	0.21	0.15	0.35	0.53	0.33	0.21	0.25	0.19	0.25	119
All cases	14	Albany Park	30	0.11	0.20	0.12	0.19	0.14	0.21	0.18	0.31	0.52	0.34	0.23	0.24	0.16	0.24	127
All cases	14	Albany Park	45	0.10	0.22	0.09	0.18	0.16	0.22	0.34	1.13	0.52	0.33	0.25	0.24	0.18	0.23	117
All cases	14	Albany Park	60	0.08	0.17	0.08	0.16	0.18	0.23	0.40	0.92	0.45	0.32	0.26	0.24	0.19	0.25	116
All cases	14	Albany Park	75	0.07	0.18	0.07	0.15	0.18	0.29	0.34	0.85	0.50	0.31	0.22	0.25	0.22	0.27	110
All cases	14	Albany Park	90	0.05	0.13	0.05	0.13	0.24	0.31	0.40	1.12	0.43	0.30	0.18	0.24	0.22	0.25	99
All cases	14	Albany Park	105	0.05	0.13	0.05	0.14	0.18	0.29	0.26	0.64	0.48	0.30	0.11	0.16	0.27	0.24	92
All cases	14	Albany Park	120	0.03	0.09	0.04	0.10	0.16	0.22	0.36	1.13	0.45	0.29	0.11	0.17	0.25	0.24	96
All cases	15	Edmonton Green	15	0.12	0.23	0.11	0.22	0.13	0.22	0.10	0.30	0.59	0.29	0.20	0.20	0.14	0.19	126
All cases	15	Edmonton Green	30	0.11	0.22	0.10	0.20	0.14	0.20	0.26	0.78	0.56	0.34	0.21	0.23	0.14	0.21	121
All cases	15	Edmonton Green	45	0.09	0.20	0.09	0.19	0.16	0.25	0.33	1.32	0.53	0.30	0.27	0.25	0.14	0.21	108
All cases	15	Edmonton Green	60	0.08	0.20	0.08	0.18	0.15	0.24	0.24	0.59	0.47	0.33	0.25	0.27	0.17	0.21	112
All cases	15	Edmonton Green	75	0.06	0.15	0.06	0.15	0.20	0.32	0.26	0.50	0.56	0.32	0.18	0.21	0.17	0.25	113
All cases	15	Edmonton Green	90	0.07	0.19	0.07	0.17	0.30	0.36	0.33	0.69	0.52	0.31	0.14	0.20	0.19	0.20	94
All cases	15	Edmonton Green	105	0.04	0.13	0.04	0.12	0.14	0.30	0.18	0.39	0.42	0.33	0.11	0.19	0.22	0.24	92
All cases	15	Edmonton Green	120	0.05	0.15	0.05	0.15	0.14	0.27	0.22	0.57	0.45	0.32	0.09	0.17	0.25	0.25	84
All cases	16	Silver Street	15	0.12	0.25	0.10	0.21	0.13	0.22	0.09	0.25	0.55	0.25	0.26	0.22	0.19	0.22	141
All cases	16	Silver Street	30	0.09	0.19	0.08	0.18	0.12	0.18	0.24	0.70	0.48	0.32	0.26	0.23	0.20	0.25	136
All cases	16	Silver Street	45	0.07	0.18	0.07	0.17	0.13	0.20	0.20	0.69	0.45	0.30	0.30	0.27	0.22	0.25	131
All cases	16	Silver Street	60	0.07	0.16	0.07	0.15	0.15	0.22	0.28	0.73	0.48	0.31	0.26	0.27	0.20	0.24	129
All cases	16	Silver Street	75	0.05	0.14	0.05	0.14	0.17	0.28	0.19	0.33	0.51	0.30	0.20	0.22	0.23	0.27	128
All cases	16	Silver Street	90	0.06	0.16	0.06	0.14	0.25	0.33	0.36	1.08	0.51	0.28	0.18	0.22	0.23	0.23	115
All cases	16	Silver Street	105	0.04	0.12	0.04	0.11	0.12	0.26	0.17	0.44	0.54	0.31	0.11	0.20	0.28	0.25	120

**Table B.3. OOM 2 km resolution performance statistics contd.**

Date	Catch number	Catchment Name	Lead time min.	CSI 2km pixel	SD CSI 2km pixel	HR 2km pixel	SD HR 2km pixel	FAR 2km pixel	SD FAR 2km pixel	MSE mm <sup>2</sup>	SD MSE mm <sup>2</sup>	Ub 2km pixel	SD Ub 2km pixel	Ur 2km pixel	SD Ur 2km pixel	Ud 2km pixel	SD Ud 2km pixel	Runs OOM
All cases	16	Silver Street	120	0.05	0.14	0.04	0.12	0.13	0.25	0.25	0.92	0.57	0.29	0.09	0.18	0.30	0.25	111
All cases	17	Bretons Farm	15	0.10	0.19	0.10	0.18	0.12	0.22	0.21	0.65	0.39	0.31	0.25	0.28	0.21	0.25	142
All cases	17	Bretons Farm	30	0.09	0.17	0.09	0.16	0.16	0.27	0.27	0.74	0.50	0.31	0.19	0.22	0.18	0.24	139
All cases	17	Bretons Farm	45	0.06	0.13	0.06	0.13	0.17	0.27	0.31	0.86	0.50	0.29	0.23	0.23	0.18	0.23	139
All cases	17	Bretons Farm	60	0.05	0.11	0.05	0.12	0.19	0.28	0.26	0.73	0.51	0.30	0.24	0.25	0.18	0.25	138
All cases	17	Bretons Farm	75	0.04	0.08	0.04	0.08	0.19	0.33	0.39	1.22	0.45	0.33	0.27	0.28	0.15	0.21	141
All cases	17	Bretons Farm	90	0.05	0.09	0.04	0.09	0.21	0.30	0.40	1.08	0.39	0.32	0.17	0.20	0.19	0.23	131
All cases	17	Bretons Farm	105	0.05	0.12	0.05	0.11	0.16	0.25	0.43	1.20	0.42	0.32	0.12	0.17	0.20	0.23	136
All cases	17	Bretons Farm	120	0.05	0.13	0.05	0.13	0.20	0.31	0.35	0.80	0.39	0.32	0.12	0.20	0.23	0.26	124
All cases	18	Gaynes Park	15	0.13	0.23	0.12	0.21	0.11	0.21	0.46	1.46	0.49	0.32	0.15	0.19	0.23	0.27	133
All cases	18	Gaynes Park	30	0.10	0.18	0.10	0.18	0.13	0.22	0.38	1.12	0.46	0.33	0.21	0.27	0.21	0.26	134
All cases	18	Gaynes Park	45	0.07	0.14	0.08	0.15	0.15	0.25	0.47	1.28	0.53	0.30	0.21	0.25	0.18	0.23	139
All cases	18	Gaynes Park	60	0.08	0.13	0.08	0.13	0.19	0.29	0.58	1.70	0.52	0.29	0.23	0.23	0.17	0.24	136
All cases	18	Gaynes Park	75	0.06	0.12	0.07	0.13	0.17	0.28	0.52	1.41	0.48	0.32	0.22	0.26	0.19	0.24	135
All cases	18	Gaynes Park	90	0.06	0.12	0.07	0.12	0.25	0.33	0.88	2.33	0.47	0.31	0.18	0.22	0.20	0.25	111
All cases	18	Gaynes Park	105	0.06	0.12	0.07	0.13	0.20	0.28	0.71	1.70	0.46	0.33	0.16	0.20	0.22	0.27	116
All cases	18	Gaynes Park	120	0.06	0.14	0.07	0.14	0.20	0.30	0.83	2.03	0.45	0.33	0.15	0.20	0.23	0.26	108
All cases	19	Bromley South Recorder	15	0.16	0.30	0.16	0.29	0.05	0.14	0.74	1.56	0.54	0.31	0.13	0.21	0.33	0.30	142
All cases	19	Bromley South Recorder	30	0.16	0.27	0.18	0.29	0.08	0.17	1.01	2.39	0.47	0.31	0.16	0.22	0.37	0.32	139
All cases	19	Bromley South Recorder	45	0.16	0.31	0.17	0.32	0.12	0.23	0.62	1.16	0.54	0.32	0.16	0.25	0.30	0.30	139
All cases	19	Bromley South Recorder	60	0.12	0.23	0.13	0.25	0.09	0.20	0.58	1.24	0.60	0.29	0.14	0.21	0.26	0.26	138
All cases	19	Bromley South Recorder	75	0.09	0.20	0.10	0.24	0.07	0.19	0.48	1.09	0.58	0.32	0.15	0.26	0.27	0.27	141
All cases	19	Bromley South Recorder	90	0.09	0.17	0.08	0.15	0.05	0.15	0.72	1.94	0.74	0.22	0.07	0.16	0.19	0.18	132
All cases	19	Bromley South Recorder	105	0.07	0.15	0.08	0.17	0.06	0.15	0.38	0.81	0.74	0.24	0.05	0.11	0.21	0.22	136
All cases	19	Bromley South Recorder	120	0.10	0.18	0.10	0.19	0.06	0.14	0.68	1.70	0.74	0.27	0.05	0.14	0.20	0.22	126

**Table B.3. OOM catchment resolution performance statistics**

Date	Catch number	Catchment Name	Lead time min.	Observed depth / mm	Forecast depth / mm	F-O depth / mm	SD (F-O) depth / mm	CSI catchment	HR catchment	FAR catchment	MSE catchment	Ub catchment	Ur catchment	Ud catchment	Runs OOM
All cases	0	All catchments	15	0.11	0.13	0.02	0.08	0.99	0.99	0.00	0.01	0.19	0.24	0.57	142
All cases	0	All catchments	30	0.09	0.13	0.03	0.10	0.99	0.99	0.00	0.02	0.18	0.37	0.45	139
All cases	0	All catchments	45	0.10	0.13	0.03	0.13	1.00	1.00	0.00	0.03	0.23	0.34	0.44	139
All cases	0	All catchments	60	0.09	0.12	0.03	0.11	0.99	0.99	0.00	0.02	0.23	0.32	0.45	138
All cases	0	All catchments	75	0.11	0.11	0.01	0.14	0.99	0.99	0.00	0.03	0.22	0.23	0.55	141
All cases	0	All catchments	90	0.11	0.10	0.00	0.12	0.82	0.82	0.00	0.02	0.18	0.32	0.51	132
All cases	0	All catchments	105	0.12	0.10	-0.02	0.14	0.74	0.74	0.00	0.04	0.18	0.24	0.58	136
All cases	0	All catchments	120	0.12	0.09	-0.03	0.12	0.73	0.73	0.00	0.03	0.25	0.16	0.59	126
All cases	1	Mimshall Brook	15	0.08	0.11	0.02	0.11	0.70	0.70	0.00	0.02	0.10	0.32	0.56	142
All cases	1	Mimshall Brook	30	0.06	0.12	0.06	0.23	0.76	0.76	0.00	0.13	0.14	0.52	0.34	139
All cases	1	Mimshall Brook	45	0.07	0.16	0.08	0.26	0.78	0.78	0.00	0.15	0.16	0.60	0.24	139
All cases	1	Mimshall Brook	60	0.08	0.14	0.06	0.30	0.71	0.71	0.00	0.14	0.10	0.52	0.38	138
All cases	1	Mimshall Brook	75	0.13	0.07	-0.05	0.41	0.60	0.60	0.00	0.36	0.08	0.35	0.58	141
All cases	1	Mimshall Brook	90	0.12	0.07	-0.05	0.40	0.34	0.34	0.00	0.34	0.19	0.38	0.43	132
All cases	1	Mimshall Brook	105	0.15	0.05	-0.09	0.43	0.29	0.29	0.00	0.42	0.21	0.27	0.52	136
All cases	1	Mimshall Brook	120	0.13	0.05	-0.09	0.38	0.27	0.27	0.00	0.36	0.28	0.11	0.62	126
All cases	2	Towncroft lane, Orpington	15	0.10	0.22	0.12	0.37	0.53	0.79	0.35	0.28	0.09	0.58	0.32	102
All cases	2	Towncroft lane, Orpington	30	0.11	0.25	0.14	0.66	0.47	0.79	0.45	0.81	0.16	0.67	0.17	116
All cases	2	Towncroft lane, Orpington	45	0.09	0.22	0.13	0.44	0.50	0.79	0.41	0.39	0.10	0.67	0.23	109
All cases	2	Towncroft lane, Orpington	60	0.11	0.23	0.12	0.39	0.47	0.77	0.43	0.29	0.16	0.60	0.24	106
All cases	2	Towncroft lane, Orpington	75	0.11	0.14	0.04	0.32	0.40	0.61	0.48	0.16	0.08	0.60	0.32	98
All cases	2	Towncroft lane, Orpington	90	0.18	0.11	-0.07	0.48	0.33	0.37	0.24	0.29	0.09	0.44	0.48	73
All cases	2	Towncroft lane, Orpington	105	0.14	0.14	0.00	0.37	0.30	0.37	0.23	0.20	0.08	0.38	0.54	73
All cases	2	Towncroft lane, Orpington	120	0.17	0.28	0.11	0.63	0.33	0.38	0.18	0.58	0.16	0.63	0.19	69
All cases	3	Elmers End Road	15	0.16	0.23	0.07	0.43	0.92	0.92	0.00	0.39	0.12	0.34	0.54	142
All cases	3	Elmers End Road	30	0.14	0.18	0.04	0.31	0.89	0.89	0.00	0.14	0.14	0.48	0.31	139
All cases	3	Elmers End Road	45	0.15	0.16	0.01	0.45	0.73	0.73	0.00	0.41	0.06	0.33	0.61	139
All cases	3	Elmers End Road	60	0.13	0.09	-0.04	0.33	0.68	0.68	0.00	0.16	0.05	0.39	0.57	139
All cases	3	Elmers End Road	75	0.16	0.05	-0.11	0.54	0.52	0.52	0.00	0.69	0.07	0.21	0.72	141
All cases	3	Elmers End Road	90	0.15	0.11	-0.05	0.40	0.30	0.30	0.00	0.25	0.09	0.31	0.60	132
All cases	3	Elmers End Road	105	0.17	0.19	0.02	0.60	0.25	0.25	0.00	0.36	0.07	0.33	0.59	136
All cases	3	Elmers End Road	120	0.16	0.13	-0.03	0.46	0.25	0.25	0.00	0.37	0.15	0.27	0.58	126
All cases	4	Longley Road Recorder	15	0.15	0.19	0.04	0.28	0.92	0.92	0.00	0.16	0.09	0.29	0.62	142
All cases	4	Longley Road Recorder	30	0.17	0.18	0.00	0.30	0.80	0.90	0.00	0.12	0.07	0.37	0.56	139
All cases	4	Longley Road Recorder	45	0.13	0.12	0.00	0.33	0.82	0.82	0.00	0.18	0.06	0.27	0.67	139
All cases	4	Longley Road Recorder	60	0.16	0.08	-0.08	0.49	0.75	0.75	0.00	0.52	0.08	0.36	0.56	138
All cases	4	Longley Road Recorder	75	0.13	0.10	-0.04	0.41	0.63	0.63	0.00	0.31	0.04	0.21	0.75	141
All cases	4	Longley Road Recorder	90	0.19	0.14	-0.06	0.51	0.33	0.33	0.00	0.50	0.09	0.30	0.61	132
All cases	4	Longley Road Recorder	105	0.15	0.18	0.02	0.35	0.28	0.29	0.00	0.22	0.09	0.23	0.68	136
All cases	5	West Barnes Lane	15	0.20	0.13	-0.07	0.46	0.92	0.92	0.00	0.43	0.21	0.04	0.74	126
All cases	5	West Barnes Lane	30	0.15	0.19	0.04	0.28	0.92	0.92	0.00	0.16	0.09	0.28	0.62	142
All cases	5	West Barnes Lane	45	0.17	0.18	0.00	0.30	0.90	0.90	0.00	0.12	0.07	0.37	0.56	139
All cases	5	West Barnes Lane	60	0.13	0.12	0.00	0.33	0.82	0.82	0.00	0.18	0.06	0.27	0.67	139
All cases	5	West Barnes Lane	75	0.16	0.08	-0.08	0.49	0.75	0.75	0.00	0.52	0.08	0.36	0.56	138
All cases	5	West Barnes Lane	90	0.13	0.10	-0.04	0.41	0.63	0.63	0.00	0.31	0.04	0.21	0.75	141
All cases	5	West Barnes Lane	105	0.19	0.14	-0.06	0.51	0.33	0.33	0.00	0.50	0.09	0.30	0.61	132
All cases	5	West Barnes Lane	120	0.15	0.13	-0.02	0.35	0.28	0.29	0.00	0.22	0.09	0.23	0.68	136
All cases	5	West Barnes Lane	15	0.15	0.19	0.04	0.28	0.92	0.92	0.00	0.16	0.09	0.28	0.62	142
All cases	5	West Barnes Lane	30	0.17	0.18	0.00	0.30	0.90	0.90	0.00	0.12	0.07	0.37	0.56	139
All cases	5	West Barnes Lane	45	0.13	0.12	0.00	0.33	0.82	0.82	0.00	0.18	0.06	0.27	0.67	139
All cases	5	West Barnes Lane	60	0.16	0.08	-0.08	0.49	0.75	0.75	0.00	0.52	0.08	0.36	0.56	138
All cases	5	West Barnes Lane	75	0.13	0.10	-0.04	0.41	0.63	0.63	0.00	0.31	0.04	0.21	0.75	141
All cases	5	West Barnes Lane	90	0.19	0.14	-0.06	0.51	0.33	0.33	0.00	0.50	0.09	0.30	0.61	132
All cases	5	West Barnes Lane	105	0.15	0.13	-0.02	0.35	0.28	0.29	0.00	0.22	0.09	0.23	0.68	136
All cases	5	West Barnes Lane	120	0.15	0.13	-0.02	0.35	0.28	0.29	0.00	0.22	0.09	0.23	0.68	136
All cases	5	West Barnes Lane	15	0.15	0.19	0.04	0.28	0.92	0.92	0.00	0.16	0.09	0.28	0.62	142
All cases	5	West Barnes Lane	30	0.17	0.18	0.00	0.30	0.90	0.90	0.00	0.12	0.07	0.37	0.56	139
All cases	5	West Barnes Lane	45	0.13	0.12	0.00	0.33	0.82	0.82	0.00	0.18	0.06	0.27	0.67	139
All cases	5	West Barnes Lane	60	0.16	0.08	-0.08	0.49	0.75	0.75	0.00	0.52	0.08	0.36	0.56	138
All cases	5	West Barnes Lane	75	0.13	0.10	-0.04	0.41	0.63	0.63	0.00	0.31	0.04	0.21	0.75	141
All cases	5	West Barnes Lane	90	0.19	0.14	-0.06	0.51	0.33	0.33	0.00	0.50	0.09	0.30	0.61	132
All cases	5	West Barnes Lane	105	0.15	0.13	-0.02	0.35	0.28	0.29	0.00	0.22	0.09	0.23	0.68	136
All cases	5	West Barnes Lane	120	0.15	0.13	-0.02	0.35	0.28	0.29	0.00	0.22	0.09	0.23	0.68	136
All cases	5	West Barnes Lane	15	0.15	0.19	0.04	0.28	0.92	0.92	0.00	0.16	0.09	0.28	0.62	142
All cases	5	West Barnes Lane	30	0.17	0.18	0.00	0.30	0.90	0.90	0.00	0.12	0.07	0.37	0.56	139
All cases	5	West Barnes Lane	45	0.13	0.12	0.00	0.33	0.82	0.82	0.00	0.18	0.06	0.27	0.67	139
All cases	5	West Barnes Lane	60	0.16	0.08	-0.08	0.49	0.75	0.75	0.00	0.52	0.08	0.36	0.56	138
All cases	5	West Barnes Lane	75	0.13	0.10	-0.04	0.41	0.63	0.63	0.00	0.31	0.04	0.21	0.75	141
All cases	5	West Barnes Lane	90	0.19	0.14	-0.06	0.51	0.33	0.33	0.00	0.50	0.09	0.30	0.61	132
All cases	5	West Barnes Lane	105	0.15	0.13	-0.02	0.35	0.28	0.29	0.00	0.22	0.09	0.23	0.68	136
All cases	5	West Barnes Lane	120	0.15	0.13	-0.02	0.35	0.28	0.29	0.00	0.22	0.09	0.23	0.68	136
All cases	5	West Barnes Lane	15	0.15	0.19	0.04	0.28	0.92	0.92	0.00	0.16	0.09	0.28	0.62	142
All cases	5	West Barnes Lane	30	0.17	0.18	0.00	0.30	0.90	0.90	0.00	0.12	0.07	0.37	0.56	139
All cases	5	West Barnes Lane	45	0.13	0.12	0.00	0.33	0.82	0.82	0.00	0.18	0.06	0.27	0.67	139
All cases	5	West Barnes Lane	60	0.16	0.08	-0.08	0.49	0.75	0.75	0.00	0.52	0.08	0.36	0.56	138
All cases	5	West Barnes Lane	75	0.13	0.10	-0.04	0.41	0.63	0.63	0.00	0.31	0.04	0.21	0.75	141
All cases	5	West Barnes Lane	90	0.19	0.14	-0.06	0.51	0.33	0.33	0.00	0.50	0.09	0.30	0.61	132
All cases	5	West Barnes Lane	105	0.15	0.13	-0.02	0.35	0.28	0.29	0.00	0.22	0.09	0.23	0.68	136
All cases	5	West Barnes Lane	120	0.15	0.13	-0.02	0.35	0.28	0.29	0.00	0.22	0.09	0.23	0.68	136
All cases	5	West Barnes Lane	15	0.15	0.19	0.04	0.28	0.92	0.92	0.00	0.16	0.09	0.28	0.62	142
All cases	5	West Barnes Lane	30	0.17	0.18	0.00	0.30	0.90	0.90	0.00	0.12	0.07	0.37	0.56	139
All cases	5	West Barnes Lane	45	0.13	0.12	0.00	0.33	0.82	0.82	0.00	0.18	0.06	0.27	0.67	139
All cases	5	West Barnes Lane	60	0.16	0.08	-0.08	0.49	0.75	0.75	0.00	0.52	0.08	0.36	0.56	138
All cases	5	West Barnes Lane	75	0.13	0.10	-0.04	0.41	0.63	0.63	0.00	0.31	0.04	0.21	0.75	141
All cases	5	West Barnes Lane	90	0.19	0.14	-0.06	0.51	0.33	0.33	0.00	0.50	0.09	0.30	0.61	132
All cases	5	West Barnes Lane	105	0.15	0.13	-0.02	0.35	0.28	0.29	0.00	0.22	0.09	0.23	0.68	136
All cases	5	West Barnes Lane	120	0.15	0.13	-0.02	0.35	0.28	0.29	0.00	0.22	0.09	0.23	0.68	136
All cases	5														

**Table B.3. OOM catchment resolution performance statistics contd.**

Date	Catch number	Catchment Name	Lead time min.	Observed depth / mm	Forecast depth / mm	F-O depth / mm	SD (F-O) depth / mm	CSI catchment	HR catchment	FAR catchment	MSE catchment	Ub catchment	Ur catchment	Ud catchment	Runs OOM
All cases	5	West Barnes Lane	90	0.19	0.14	-0.06	0.51	0.33	0.33	0.00	0.50	0.09	0.30	0.61	132
All cases	5	West Barnes Lane	105	0.15	0.18	0.02	0.35	0.29	0.29	0.00	0.22	0.09	0.23	0.68	136
All cases	5	West Barnes Lane	120	0.20	0.13	-0.07	0.46	0.27	0.27	0.00	0.43	0.21	0.04	0.74	126
All cases	6	Wimbleton Common	15	0.23	0.18	-0.05	0.33	0.87	0.88	0.03	0.21	0.09	0.39	0.52	141
All cases	6	Wimbleton Common	30	0.15	0.12	-0.03	0.38	0.81	0.82	0.02	0.23	0.07	0.42	0.50	137
All cases	6	Wimbleton Common	45	0.22	0.11	-0.12	0.65	0.74	0.75	0.03	1.01	0.10	0.29	0.62	137
All cases	6	Wimbleton Common	60	0.16	0.09	-0.06	0.35	0.74	0.75	0.01	0.24	0.06	0.26	0.68	137
All cases	6	Wimbleton Common	75	0.26	0.14	-0.11	0.56	0.60	0.61	0.02	0.64	0.09	0.25	0.67	139
All cases	6	Wimbleton Common	90	0.17	0.15	-0.02	0.39	0.34	0.34	0.00	0.28	0.09	0.27	0.64	131
All cases	6	Wimbleton Common	105	0.27	0.17	-0.10	0.52	0.28	0.28	0.00	0.55	0.14	0.06	0.80	134
All cases	6	Wimbleton Common	120	0.18	0.10	-0.08	0.40	0.26	0.26	0.00	0.30	0.16	0.13	0.70	124
All cases	7	Yeading West	15	0.06	0.09	0.03	0.12	0.64	0.80	0.25	0.02	0.12	0.44	0.45	112
All cases	7	Yeading West	30	0.05	0.11	0.07	0.18	0.61	0.80	0.28	0.07	0.15	0.37	0.47	114
All cases	7	Yeading West	45	0.06	0.12	0.06	0.22	0.63	0.80	0.30	0.06	0.18	0.52	0.30	115
All cases	7	Yeading West	60	0.08	0.11	0.03	0.29	0.54	0.69	0.30	0.12	0.10	0.34	0.55	111
All cases	7	Yeading West	75	0.13	0.10	-0.03	0.52	0.50	0.60	0.27	0.53	0.09	0.44	0.47	104
All cases	7	Yeading West	90	0.13	0.09	-0.03	0.40	0.28	0.32	0.25	0.28	0.10	0.40	0.51	92
All cases	7	Yeading West	105	0.16	0.07	-0.09	0.51	0.29	0.30	0.18	0.58	0.10	0.32	0.56	91
All cases	7	Yeading West	120	0.14	0.06	-0.08	0.40	0.34	0.36	0.06	0.28	0.10	0.17	0.74	86
All cases	8	Yeading East	15	0.08	0.10	0.02	0.15	0.62	0.72	0.16	0.03	0.05	0.09	0.84	102
All cases	8	Yeading East	30	0.06	0.10	0.04	0.19	0.48	0.65	0.33	0.07	0.12	0.32	0.56	112
All cases	8	Yeading East	45	0.08	0.11	0.04	0.30	0.58	0.77	0.26	0.12	0.12	0.43	0.45	113
All cases	8	Yeading East	60	0.07	0.14	0.06	0.28	0.52	0.66	0.28	0.12	0.11	0.43	0.46	104
All cases	8	Yeading East	75	0.14	0.11	-0.03	0.53	0.48	0.54	0.18	0.48	0.08	0.42	0.50	99
All cases	8	Yeading East	90	0.12	0.10	-0.02	0.36	0.24	0.25	0.25	0.18	0.06	0.39	0.53	85
All cases	8	Yeading East	105	0.17	0.08	-0.09	0.54	0.27	0.27	0.05	0.56	0.10	0.30	0.59	86
All cases	8	Yeading East	120	0.13	0.08	-0.05	0.38	0.24	0.24	0.07	0.22	0.08	0.25	0.68	80
All cases	9	Colindale Lane	15	0.06	0.08	0.03	0.14	0.64	0.64	0.00	0.03	0.07	0.74	0.19	142
All cases	9	Colindale Lane	30	0.08	0.10	0.02	0.20	0.70	0.70	0.00	0.07	0.04	0.48	0.48	139
All cases	9	Colindale Lane	45	0.05	0.13	0.08	0.21	0.72	0.72	0.00	0.09	0.17	0.60	0.23	139
All cases	9	Colindale Lane	60	0.10	0.09	0.00	0.24	0.67	0.67	0.00	0.08	0.06	0.33	0.61	138
All cases	9	Colindale Lane	75	0.07	0.07	0.00	0.21	0.50	0.50	0.00	0.07	0.16	0.39	0.45	141
All cases	9	Colindale Lane	90	0.12	0.06	-0.05	0.28	0.27	0.27	0.00	0.15	0.22	0.28	0.50	132
All cases	9	Colindale Lane	105	0.08	0.05	-0.03	0.22	0.24	0.24	0.00	0.09	0.23	0.35	0.41	136
All cases	9	Colindale Lane	120	0.13	0.04	-0.09	0.31	0.20	0.20	0.00	0.18	0.24	0.14	0.62	126
All cases	10	Chipping Ongar	15	0.16	0.19	0.03	0.31	0.65	0.83	0.24	0.14	0.19	0.45	0.36	100
All cases	10	Chipping Ongar	30	0.09	0.15	0.07	0.22	0.57	0.84	0.33	0.08	0.28	0.45	0.26	110
All cases	10	Chipping Ongar	45	0.14	0.15	0.02	0.40	0.50	0.82	0.34	0.39	0.25	0.39	0.36	115
All cases	10	Chipping Ongar	60	0.07	0.18	0.11	0.31	0.50	0.87	0.41	0.28	0.22	0.50	0.27	118
All cases	10	Chipping Ongar	75	0.13	0.22	0.09	0.59	0.54	0.85	0.36	0.71	0.21	0.44	0.34	110
All cases	10	Chipping Ongar	90	0.09	0.20	0.11	0.33	0.46	0.54	0.23	0.18	0.22	0.58	0.20	84
All cases	10	Chipping Ongar	105	0.15	0.14	-0.01	0.51	0.43	0.54	0.32	0.49	0.22	0.47	0.31	91
All cases	10	Chipping Ongar	120	0.10	0.17	0.06	0.30	0.41	0.47	0.22	0.17	0.26	0.34	0.40	78
All cases	11	Sewardstone Road	15	0.09	0.14	0.05	0.21	0.57	0.80	0.30	0.08	0.19	0.43	0.39	115
All cases	11	Sewardstone Road	30	0.08	0.14	0.07	0.21	0.56	0.81	0.31	0.10	0.24	0.36	0.40	112

**Table B.3. OOM catchment resolution performance statistics contd.**

Date	Catch number	Catchment Name	Lead time min.	Observed depth / mm	Forecast depth / mm	F-O depth / mm	SD (F-O) depth / mm	CSI catchment	HR catchment	FAR catchment	MSE catchment	Ub catchment	Ur catchment	Ud catchment	Runs
All cases	11	Sewardstone Road	45	0.08	0.16	0.08	0.28	0.57	0.87	0.34	0.17	0.21	0.37	0.42	121
All cases	11	Sewardstone Road	60	0.07	0.17	0.10	0.35	0.57	0.82	0.34	0.28	0.19	0.44	0.36	119
All cases	11	Sewardstone Road	75	0.09	0.20	0.12	0.49	0.58	0.82	0.32	0.50	0.13	0.51	0.36	112
All cases	11	Sewardstone Road	90	0.08	0.20	0.12	0.40	0.45	0.55	0.24	0.26	0.15	0.55	0.30	91
All cases	11	Sewardstone Road	105	0.10	0.18	0.07	0.34	0.41	0.47	0.25	0.22	0.22	0.45	0.33	92
All cases	11	Sewardstone Road	120	0.10	0.11	0.01	0.29	0.43	0.47	0.21	0.12	0.15	0.43	0.43	84
All cases	12	Luton Hoo	15	0.13	0.15	0.02	0.18	0.66	0.81	0.18	0.06	0.13	0.28	0.59	121
All cases	12	Luton Hoo	30	0.10	0.12	0.02	0.21	0.65	0.86	0.25	0.06	0.21	0.19	0.61	113
All cases	12	Luton Hoo	45	0.08	0.12	0.04	0.20	0.63	0.73	0.19	0.06	0.15	0.39	0.46	114
All cases	12	Luton Hoo	60	0.10	0.12	0.01	0.24	0.59	0.74	0.25	0.09	0.16	0.33	0.51	105
All cases	12	Luton Hoo	75	0.08	0.10	0.02	0.25	0.60	0.66	0.11	0.09	0.18	0.46	0.36	108
All cases	12	Luton Hoo	90	0.15	0.14	-0.01	0.40	0.45	0.49	0.13	0.25	0.17	0.30	0.53	88
All cases	12	Luton Hoo	105	0.15	0.14	-0.01	0.54	0.33	0.36	0.09	0.53	0.10	0.21	0.69	100
All cases	12	Luton Hoo	120	0.18	0.12	-0.05	0.42	0.40	0.44	0.12	0.27	0.17	0.34	0.49	84
All cases	13	Gypsy Lane	15	0.27	0.29	0.02	0.40	0.62	0.67	0.10	0.22	0.06	0.44	0.49	85
All cases	13	Gypsy Lane	30	0.35	0.28	-0.07	0.57	0.59	0.61	0.08	0.43	0.08	0.26	0.64	83
All cases	13	Gypsy Lane	45	0.24	0.23	-0.01	0.52	0.49	0.57	0.23	0.43	0.14	0.48	0.38	93
All cases	13	Gypsy Lane	60	0.28	0.20	-0.08	0.53	0.49	0.59	0.27	0.49	0.15	0.22	0.63	98
All cases	13	Gypsy Lane	75	0.27	0.31	0.03	0.63	0.52	0.61	0.18	0.69	0.11	0.51	0.37	87
All cases	13	Gypsy Lane	90	0.33	0.23	-0.10	0.72	0.41	0.47	0.18	0.78	0.13	0.24	0.63	82
All cases	13	Gypsy Lane	105	0.26	0.17	-0.09	0.54	0.40	0.45	0.31	0.42	0.15	0.42	0.42	84
All cases	13	Gypsy Lane	120	0.34	0.13	-0.21	0.70	0.40	0.45	0.31	0.78	0.19	0.11	0.68	80
All cases	14	Albany Park	15	0.08	0.14	0.06	0.18	0.57	0.82	0.31	0.06	0.14	0.50	0.36	119
All cases	14	Albany Park	30	0.06	0.14	0.08	0.20	0.61	0.86	0.27	0.10	0.18	0.47	0.35	127
All cases	14	Albany Park	45	0.06	0.15	0.09	0.27	0.61	0.85	0.31	0.16	0.15	0.59	0.27	117
All cases	14	Albany Park	60	0.07	0.16	0.09	0.30	0.67	0.82	0.20	0.18	0.15	0.60	0.25	116
All cases	14	Albany Park	75	0.08	0.16	0.09	0.34	0.61	0.83	0.26	0.17	0.15	0.59	0.26	110
All cases	14	Albany Park	90	0.12	0.10	-0.02	0.30	0.46	0.49	0.09	0.15	0.10	0.20	0.70	99
All cases	14	Albany Park	105	0.11	0.09	-0.03	0.31	0.37	0.41	0.15	0.13	0.07	0.43	0.49	92
All cases	14	Albany Park	120	0.12	0.06	-0.06	0.31	0.35	0.37	0.09	0.18	0.17	0.25	0.58	96
All cases	15	Edmonton Green	15	0.08	0.12	0.05	0.17	0.59	0.93	0.37	0.05	0.25	0.39	0.36	126
All cases	15	Edmonton Green	30	0.06	0.15	0.09	0.25	0.59	0.94	0.36	0.13	0.22	0.41	0.37	121
All cases	15	Edmonton Green	45	0.09	0.14	0.06	0.33	0.64	0.87	0.31	0.19	0.14	0.48	0.37	108
All cases	15	Edmonton Green	60	0.07	0.12	0.06	0.25	0.58	0.86	0.33	0.10	0.18	0.45	0.38	112
All cases	15	Edmonton Green	75	0.08	0.17	0.08	0.25	0.50	0.70	0.37	0.13	0.18	0.33	0.49	113
All cases	15	Edmonton Green	90	0.09	0.13	0.04	0.30	0.42	0.51	0.28	0.13	0.13	0.60	0.28	94
All cases	15	Edmonton Green	105	0.12	0.07	-0.05	0.26	0.29	0.33	0.26	0.09	0.11	0.37	0.52	82
All cases	15	Edmonton Green	120	0.11	0.08	-0.03	0.28	0.30	0.32	0.28	0.10	0.10	0.54	0.36	84
All cases	16	Silver Street	15	0.07	0.11	0.05	0.14	0.77	0.90	0.14	0.04	0.28	0.38	0.34	136
All cases	16	Silver Street	30	0.06	0.13	0.07	0.22	0.74	0.87	0.14	0.09	0.18	0.50	0.32	136
All cases	16	Silver Street	45	0.07	0.10	0.03	0.23	0.76	0.81	0.10	0.09	0.12	0.47	0.41	131
All cases	16	Silver Street	60	0.06	0.13	0.06	0.25	0.71	0.80	0.12	0.10	0.13	0.43	0.43	129
All cases	16	Silver Street	75	0.08	0.12	0.05	0.22	0.65	0.69	0.11	0.08	0.13	0.35	0.52	128
All cases	16	Silver Street	90	0.07	0.11	0.03	0.29	0.47	0.47	0.03	0.12	0.09	0.60	0.31	115
All cases	16	Silver Street	105	0.10	0.06	-0.03	0.25	0.33	0.34	0.07	0.08	0.11	0.34	0.55	120

**Table B.3. OOM catchment resolution performance statistics contd.**

Date	Catch number	Catchment Name	Lead time min.	Observed depth / mm	Forecast depth / mm	F-O depth / mm	SD (F-O) depth / mm	CSI catchment	HR catchment	FAR catchment	MSE catchment	Ub catchment	Ur catchment	Ud catchment	Runs
All cases	16	Silver Street	120	0.08	0.06	-0.03	0.23	0.31	0.31	0.10	0.07	0.08	0.42	0.50	111
All cases	17	Bretons Farm	15	0.08	0.12	0.03	0.16	0.69	0.70	0.01	0.05	0.17	0.37	0.46	142
All cases	17	Bretons Farm	30	0.07	0.13	0.06	0.22	0.72	0.74	0.03	0.09	0.17	0.38	0.45	139
All cases	17	Bretons Farm	45	0.08	0.14	0.06	0.25	0.81	0.81	0.01	0.11	0.19	0.33	0.47	139
All cases	17	Bretons Farm	60	0.07	0.14	0.07	0.23	0.82	0.85	0.03	0.08	0.15	0.45	0.41	138
All cases	17	Bretons Farm	75	0.08	0.11	0.03	0.31	0.78	0.79	0.01	0.17	0.12	0.41	0.47	141
All cases	17	Bretons Farm	90	0.06	0.12	0.07	0.28	0.42	0.42	0.13	0.15	0.09	0.46	0.45	131
All cases	17	Bretons Farm	105	0.08	0.13	0.05	0.28	0.37	0.38	0.04	0.16	0.15	0.34	0.52	136
All cases	17	Bretons Farm	120	0.07	0.14	0.07	0.26	0.36	0.36	0.14	0.14	0.10	0.38	0.52	124
All cases	18	Gaynes Park	15	0.14	0.13	-0.01	0.31	0.61	0.69	0.12	0.14	0.12	0.45	0.43	133
All cases	18	Gaynes Park	30	0.11	0.11	-0.01	0.27	0.60	0.72	0.18	0.11	0.14	0.25	0.62	134
All cases	18	Gaynes Park	45	0.13	0.15	0.02	0.30	0.63	0.78	0.17	0.16	0.27	0.23	0.50	139
All cases	18	Gaynes Park	60	0.12	0.14	0.03	0.32	0.64	0.79	0.19	0.15	0.14	0.36	0.49	136
All cases	18	Gaynes Park	75	0.13	0.13	0.00	0.33	0.68	0.78	0.13	0.17	0.15	0.44	0.41	135
All cases	18	Gaynes Park	90	0.12	0.14	0.02	0.46	0.45	0.48	0.06	0.30	0.09	0.42	0.50	111
All cases	18	Gaynes Park	105	0.13	0.15	0.02	0.41	0.47	0.47	0.08	0.28	0.15	0.32	0.54	116
All cases	18	Gaynes Park	120	0.14	0.18	0.04	0.44	0.44	0.46	0.15	0.30	0.15	0.38	0.48	108
All cases	19	Bromley South Recorder	15	0.22	0.17	-0.05	0.46	0.74	0.74	0.00	0.44	0.08	0.59	0.33	142
All cases	19	Bromley South Recorder	30	0.25	0.20	-0.06	0.60	0.83	0.83	0.00	0.60	0.05	0.62	0.33	139
All cases	19	Bromley South Recorder	45	0.21	0.17	-0.04	0.43	0.72	0.72	0.00	0.37	0.05	0.59	0.36	139
All cases	19	Bromley South Recorder	60	0.22	0.17	-0.04	0.43	0.68	0.68	0.00	0.35	0.06	0.62	0.31	138
All cases	19	Bromley South Recorder	75	0.21	0.08	-0.13	0.33	0.52	0.52	0.00	0.24	0.09	0.38	0.53	141
All cases	19	Bromley South Recorder	90	0.25	0.07	-0.18	0.50	0.27	0.27	0.00	0.44	0.20	0.23	0.57	132
All cases	19	Bromley South Recorder	105	0.20	0.10	-0.09	0.31	0.25	0.25	0.00	0.19	0.15	0.24	0.62	136
All cases	19	Bromley South Recorder	120	0.24	0.15	-0.08	0.50	0.25	0.25	0.00	0.37	0.08	0.57	0.35	126